INFORMAL ANNUAL REPORT NO. 1

PROJECT NO. B-159

AN INVESTIGATION OF THERMAL FORCE WITH PARTICULAR REFERENCE TO MATERIALS OF HIGH THERMAL CONDUCTIVITY

By

ANDREW McALISTER, THOMAS W. WILSON,
AND CLYDE ORR, JR.

RESEARCH GRANT NSF - G7051
NATIONAL SCIENCE FOUNDATION
WASHINGTON, D. C.

JANUARY 1, 1959 through DECEMBER 31, 1959

Engineering Experiment Station
Georgia Institute of Technology
Atlanta, Georgia

DEFINITION OF SYMBOLS

A	empirical constant appearing in slip-correction equation.
A_x	cross-sectional area of aerosol stream in precipitator, normal to direction of flow [$A = 2 \pi r L$]
a	particulate radius
B	empirical constant appearing in slip-correction equation
C	empirical constant appearing in slip-correction equation
D	particulate diameter
F	force
F_g	gravitational force
F_t	thermal force
g_c	conversion factor (gravitational constant)
k_m	thermal conductivity of aerosol carrier medium
k_p	thermal conductivity of particulate material (bulk conductivity)
L	precipitator plate separation
M	molecular weight of the aerosol carrier medium
P	pressure of the aerosol carrier medium
Q	volumetric flow rate of the aerosol
R	gas constant
r	radial distance
r_o	precipitator inlet radius
r_d	deposit radius
S	slip-correction factor
T	absolute temperature of aerosol carrier medium
ΔT	temperature difference between hot and cold precipitator plates
t	time
t_f	time required for particulate to move from precipitator inlet to cold plate surface
U	local (or point) fluid velocity
U_{avg}	average fluid velocity [$U_{avg} = Q/A_x$]
U_{max}	maximum fluid velocity

DEFINITION OF SYMBOLS (Continued)

V_r	horizontal velocity of particulate
V_y	vertical velocity of particulate
$\bar{v}$	mean molecular velocity of gas molecule
y	vertical distance measured from mid-plane of the precipitation region
$\mathbf{Z}$	mobility of particulate
λ	mean free path of aerosol carrier medium
μ	viscosity of aerosol carrier medium
ρ_p	particulate density

TABLE OF CONTENTS

This Report Contains 45 Pages.

LIST OF TABLES

I. SUMMARY

Current theory and recent experimental observations of thermal force phenomena are not in agreement, particularly with regard to the influence of the particulate thermal conductivity on the thermal force. The objective of the present study is to reconcile this disagreement and to develop a more thorough understanding of the force exerted on air-suspended particulates in a nonuniform temperature region.

Two types of experimental apparatus have been developed to facilitate this study. The first, a radial-flow thermal precipitator has been constructed and operational procedures and limits have been established. Sufficient measurements have been made on this apparatus to show that siginificant, reproducible data can be collected. The second type, a modified Millikan apparatus that permits the direct observation of particle behavior in a thermal gradient, has been constructed; but additional refinements must be made before reliable data can be obtained with it.

An extensive theoretical investigation of particle behavior based on radiometer force theory has been made. Theoretical values of the thermal force and of the corresponding deposit radii for a wide range of operating variables have been calculated using a program developed for the IBM-650 computer. These computed data have been plotted to show the hypothetical relationship of all variables. Resulting curves have been most useful in programming experimental work, in comparing experimental results, and in explaining some of the peculariities of thermal precipitator operation.

With the thermal precipitation apparatus, data have been obtained for both magnesium oxide and zinc aerosols. A really significant quantity of data has been recorded--only, however, for magnesium oxide particulates--and experimental thermal forces have been computed therefrom. For zinc particulates the limited data thus far collected are of qualitative significance only.

Observations upon the experimental results currently available might be summarized as follows: With magnesium oxide as the particulate material, the experimental inconsistencies are generally within $\pm$ 10 per cent of the mean observed value. The experimental thermal force at a pressure of one atmosphere appears to be about four to six times greater than the theoretical value. This factor seems to be somewhat dependent upon operating conditions and to be

particularly sensitive to pressure. With zinc as the particulate material, the experimental force appears to be much greater than the theoretical value; however, no quantitative statements can be made at this time.

More data are needed over a wider range of operating conditions before conclusive evaluations can be made. Future work will consist of expanding the collection of data for magnesium oxide, zinc and stearic acid particulates using present equipment and techniques. As time permits, other materials will be surveyed to provide a more comprehensive coverage of the effect of particulate physical properties. Experimental efforts will also be continued using the modified Millikan apparatus. Concurrent with the collection of experimental data, additional effort will be directed toward the determination of the correct particulate size to be used in the calculation of experimental forces. Presently, the particulate size can be estimated, but further experimental support is necessary for a more precise evaluation of results.

II. INTRODUCTION

Airborne particulates in a thermal gradient experience a force, the magnitude of which depends on a number of factors such as particulate size and thermal conductivity, physical properties of air, and thermal gradient. In certain types of experiments the magnitude of the forces and the influence of particulate thermal conducivity are not in accord with the currently accepted theory.

During the past few years, two experimental techniques for investigating these thermal force phenomena have been employed. One has involved the analysis of thermal precipitator deposition, while the second has utilized procedures and equipment similar to those of the Millikan oil drop experiment to study directly the behavior of a particulate under the influence of a thermal gradient. Previous results from the Millikan type experiments support the radiometer theory of Epstein[1] while the thermal precipitation analyses do not. A recent theoretical consideration of the so-called dust-free space phenomenon by Zernik[2] indicates that thermal forces in flowing systems should be greater than in nonflowing systems. Also, an experimental study by Schadt and Cadle[3] using a thermal precipitator technique shows that materials of relatively high thermal conductivity behave as if subjected to thermal forces considerably greater than would be predicted by rigorous theoretical considerations alone. This suggests that a correlation based on a diminished effective thermal conductivity for a particulate in a moving system might bring the thermal precipitator data into agreement with results from static systems that already support existing theories. In view of this possibility, a comprehensive study of thermal precipitator operations has been undertaken; the results of which are to be compared with those obtained from a Millikan-type experiment.

---

[1] P. Epstein, "Fur Theorie der Radiometers," Zeitschrift fur Physik 54, 537 (1929).

[2] W. Zernik, "The Dust-Free Space Surrounding Hot Bodies," British Journal of Applied Physics 8, 117 (1957).

[3] C. F. Schadt and R. D. Cadle, "Thermal Forces on Aerosol Particles in a Thermal Precipitator," Journal of Colloid Science 12, No. 4, 356 (1957).

Thus, the objective of the present study is to reconcile the disagreement between experimental results and theory and to develop a more complete understanding of thermal force phenomena.

This report, covering the accomplishments of the period from January 1, 1959 to January 1, 1960, presents apparatus design, preliminary experimental data, analytical studies, and future plans.

III. APPARATUS CONSTRUCTION AND OPERATION

Initial experiments in this investigation were performed with a thermal precipitator. While a number of geometric configurations may be employed in a precipitator, the operating principle is the same in all cases. Particulate matter is deposited on a surface which lies within the dust-free space of a relatively warmer one. Selected for use in the experimental phase of this study was a precipitator consisting of two horizontal circular plates, concentrically spaced so that the hot plate is directly above the cooler one. An aerosol (air laden with particulates) flows radially between the plates from an inlet in the center of the hot plate. Precipitators of this type have been investigated earlier in this laboratory[4, 5, 6] and are thought to be most appropriate for the study of thermal force phenomena.

Figure 1 is a half-section drawing showing general construction details. The precipitator consists essentially of an electrically heated hot plate spaced a known distance above a plate that is cooled by a water chest. Normally, a spacing of about 0.015 inch is used. The recess in the cold plate accommodates a thin glass plate, or disc, on which particulates deposit. This plate is removable so the deposit can be conveniently inspected and measured. When inserted, the glass is moistened with Kel-F 3 (fluorocarbon oil, M. W. Kellog Company) on its lower side to assure adequate thermal contact, and on its upper side, to insure retention of the impinged particles.

An experiment is initiated by bringing each plate in the thermal precipitator to a definite temperature. Dust-laden air is then metered at a constant flow rate through the inlet tube in the center. As the air flows radially outward between the plates, the particulates are deposited on the glass disc. A manifold around the periphery of the plates collects the discharged air and channels it through the exhaust tube. While the run is in progress the surface

---

[4] M. T. Gordon, "Thermal Precipitation Analyzed," Science 119, 816 (1954).

[5] C. Orr, Jr., M. T. Gordon, and M. C. Kordecki, "Thermal Precipitation for Sampling Air-Borne Microorganisms," Applied Microbiology 4, 116 (1956).

[6] C. Orr, Jr. and R. A. Martin, "A Precipitator for Continuous Aerosol Sampling," Review of Scientific Instruments 29, 129 (1958).

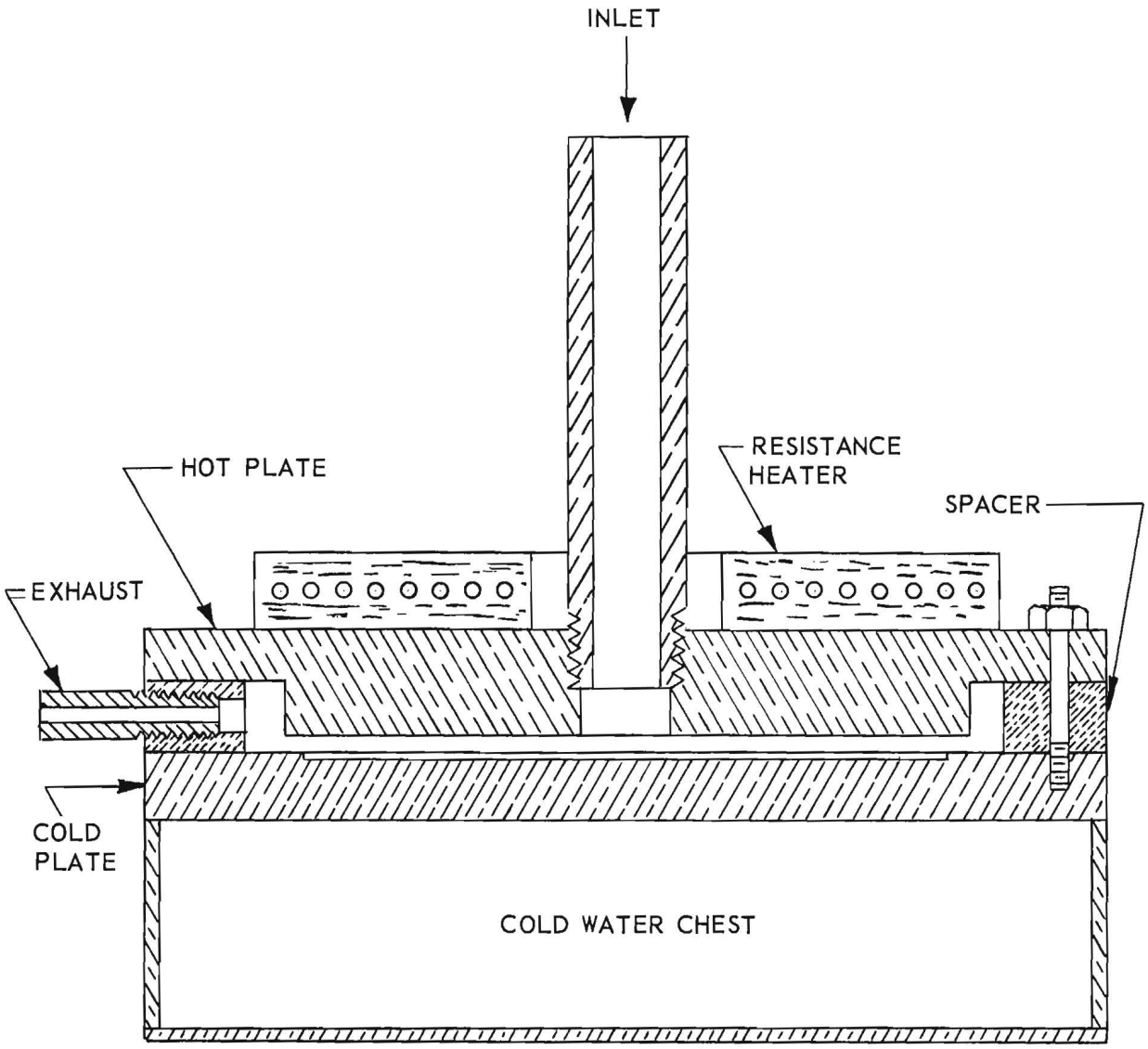

Figure 1. Thermal Precipitator Detail.

temperatures are monitored with thermocouples to assure constancy. Experimental results are computed from the maximum deposit width. This distance, measured radially from the point of particulate entry to the point of precipitation, is established by those particulates that travel the greatest distance.

As shown in Figure 2, particulates travelling this greatest distance must enter the precipitation zone near the heated surface and at the outer radius of the inlet. Particulates entering at other points are precipitated at shorter radii. This means that only the outer extremity of the deposits has significance and that results calculated for particulates precipitated within the deposits would be meaningless. To make optimum use of this feature, another precipitator was designed to restrict the variation in entrance conditions and thus produce a more useful deposit.

Figure 3 is a half-section drawing of the modified precipitator. Figure 4 is a photograph of the opened assembly. This precipitator is similar to the original except that the inlet stream is divided. One portion of the stream containing particulates enters around the side of the inlet value and emerges into the precipitation zone between the valve lip and the hot plate. A second portion of particulate-free air enters the precipitation zone from within the valve stem. This stream of air prevents the development of turbulence at the valve lip. By adjusting the micrometer, the valve lip is brought near the upper surface; thus all particulates are forced to enter the precipitation zone essentially at the same level. This, in theory at least, allows calculations to be made for particulates within the deposit. Experiments indicate it is possible to limit the particulate entrance to 0.002 inch from the upper surface. Present experiments, however, have been largely with the original design. It is anticipated that modified precipitation will be studied more thoroughly in future work.

Aside from the construction of a suitable thermal precipitator, much effort has been expended on the development of auxiliary equipment and the establishment of operating procedures. Preliminary investigations showed clearly that experimental results were particularly sensitive to the aerosol flow rates and that these rates were difficult to control and to measure under the conditions encountered. Therefore, a positive displacement mechanism was developed to control this flow adequately. Utilizing this mechanism, it was

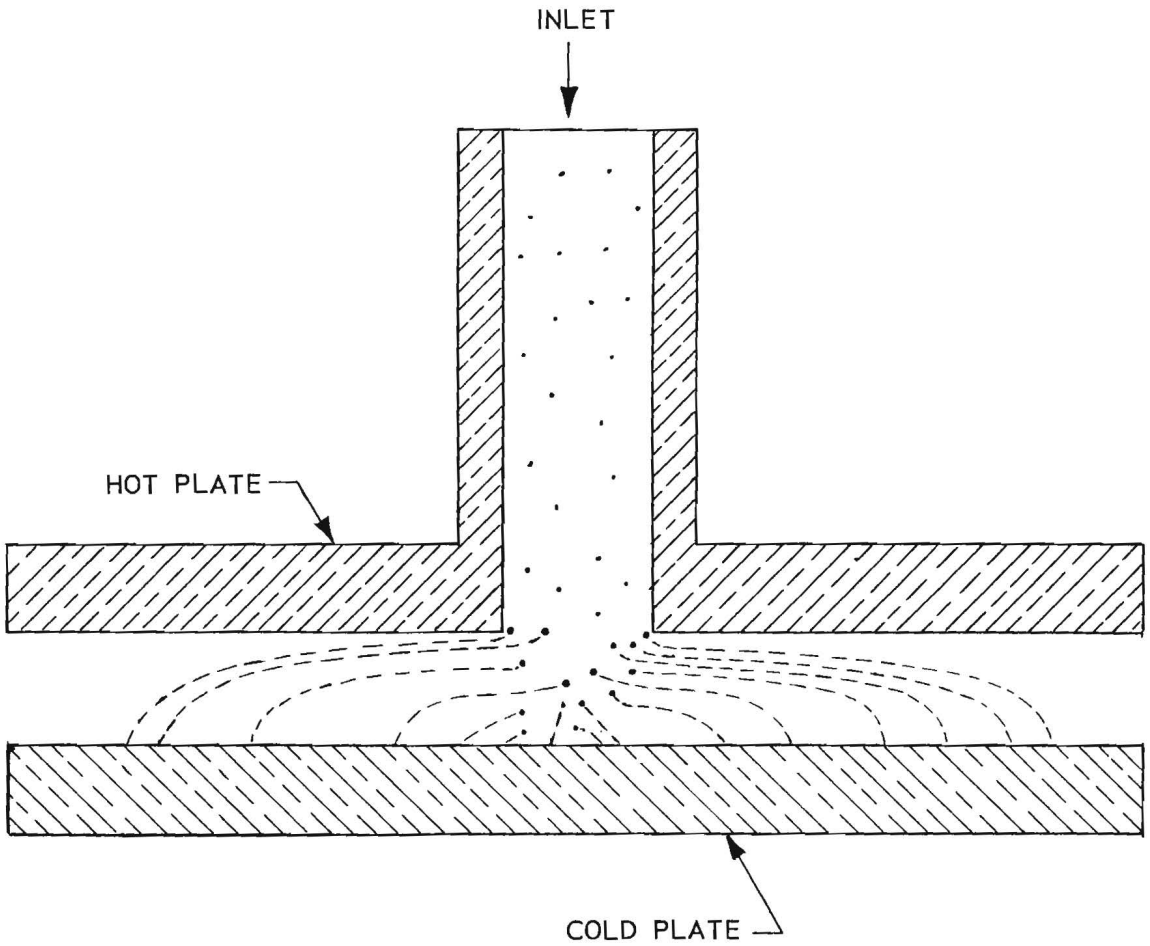

Figure 2. Schematic Diagram of Thermal Precipitator Showing Typical Particulate Paths.

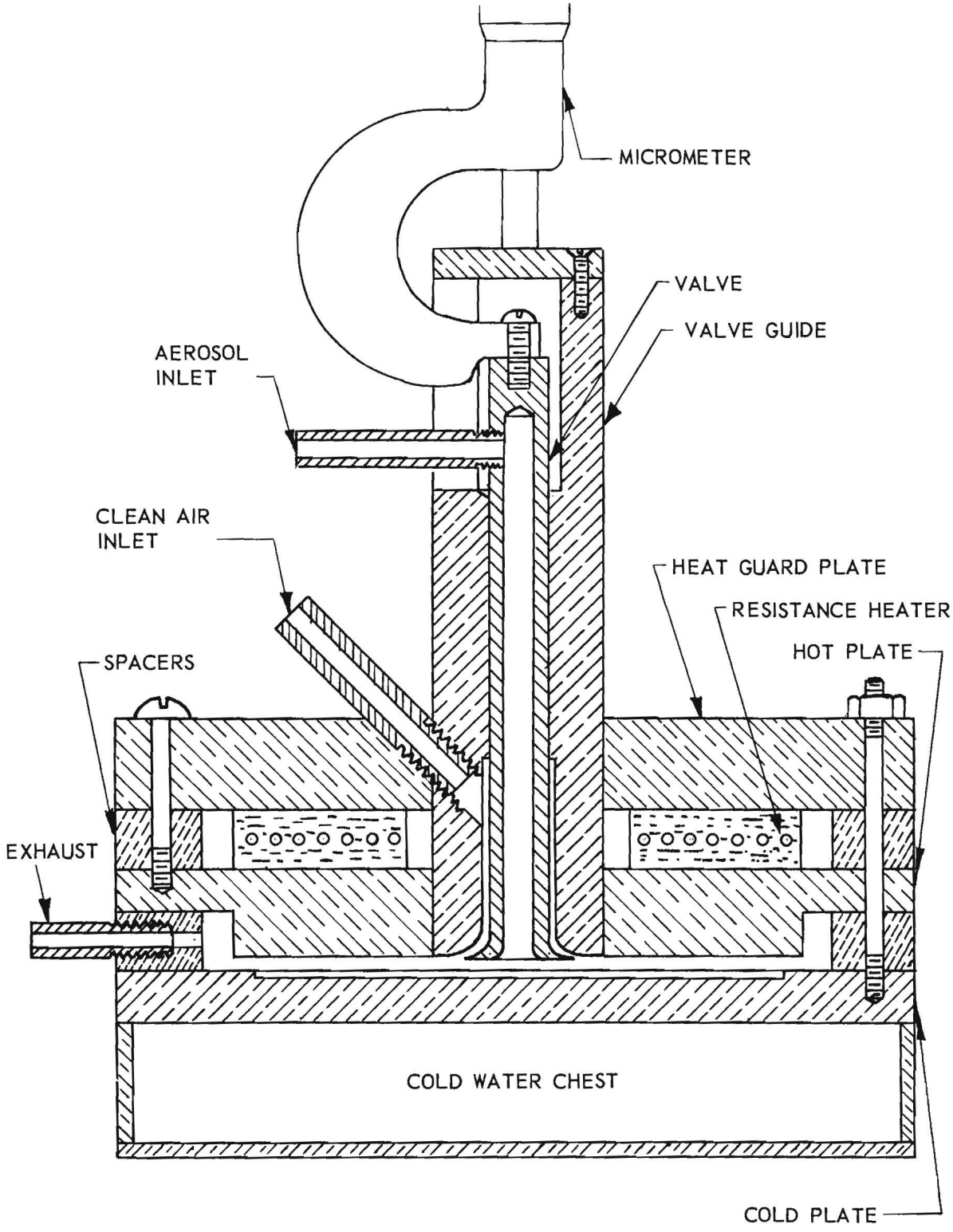

Figure 3. Modified Thermal Precipitator Detail.

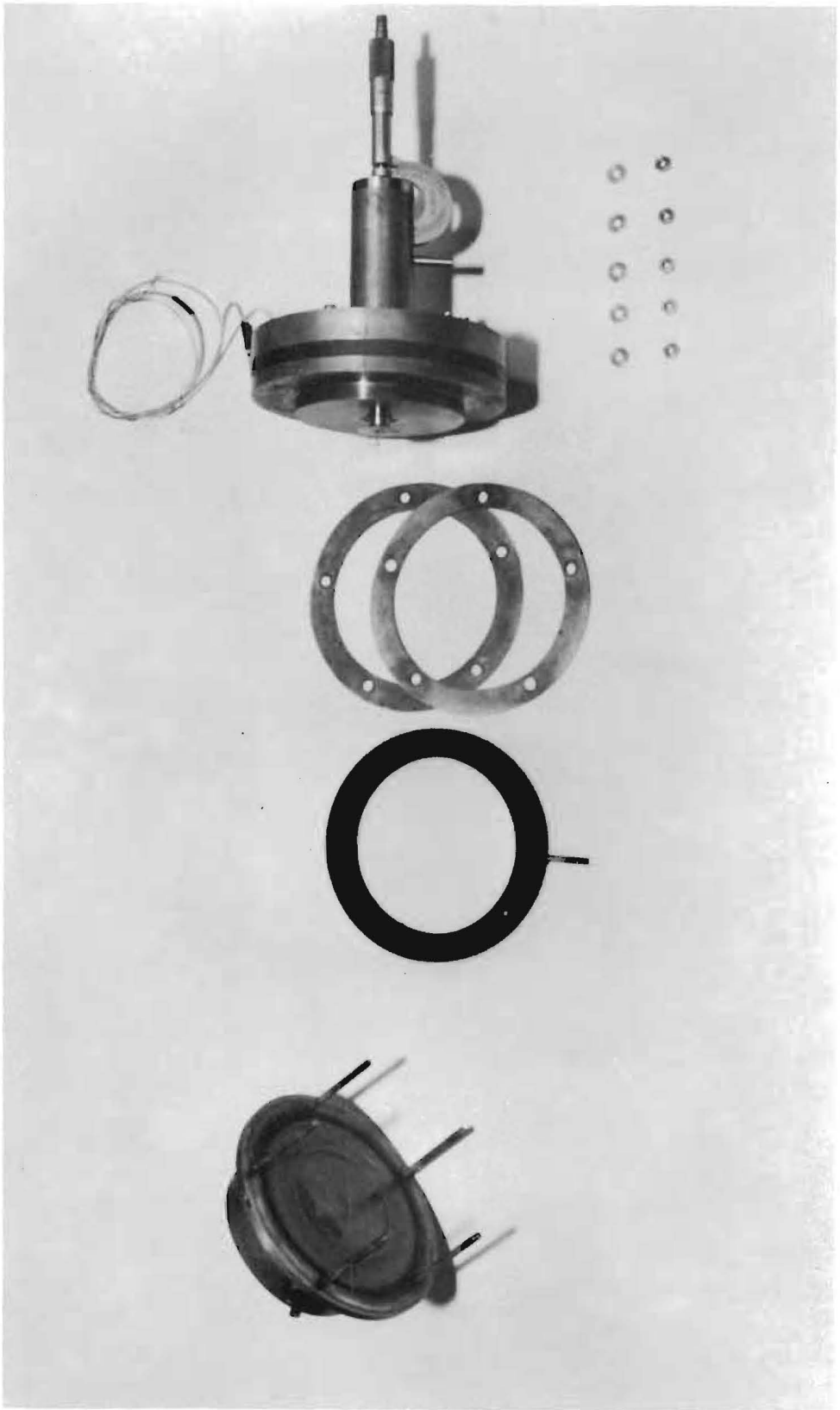

Figure 4. Modified Thermal Precipitator Partially Disassembled.

possible to maintain constant flow rates of a very low magnitude. The flow control system thus made possible a substantial improvement in the precision of experimental results.

While the thermal precipitator experiments were being made, a Millikan apparatus was also being adapted for the investigation of thermal force phenomena. Figure 5 is a photograph of the entire assembly, while Figure 6 is a detailed drawing of the main chamber. Particulate behavior in this apparatus is very similar to that occurring in the thermal precipitator. The distinguishing characteristic is that air in the Millikan apparatus is at rest while it is in motion in the thermal precipitator. Also, electric control makes it possible to study a given particulate repeatedly, thus making greater precision theoretically attainable.

The electrodes in this apparatus have been specially designed for determining thermal force as shown in Figure 7. Two cylindrical electrodes are arranged concentrically, one above the other. The upper one can be heated by a resistance coil while the lower one can be cooled by a small water jet. Thermocouples have been inserted near the inner surfaces of both for temperature measurement. Also, a centering electrode has been inserted in the surface of the lower electrode to prevent the loss of a particle while it is being studied. Both electrodes are encased in Bakelite shells which are rigidly mounted in a brass case. The complete assembly is suspended in the main chamber of the Millikan apparatus. A water bath shields the apparatus from ambient room temperature changes.

Particulates to be studied in this apparatus are passed through a corona discharge to give them an electric charge. In very dilute concentrations, they are then drawn into the main chamber. Here, the particles can be observed by dark field illumination. A single particulate is selected for study and kept suspended between the two parallel electrodes by an electric field. The mass is then determined by allowing the particulate to fall under the influence of gravity. After several such determinations, a thermal gradient is established and the experiment is repeated to evaluate the thermal force. A particulate may be studied as many times as desired by applying the proper electric field to raise the particulate after each fall.

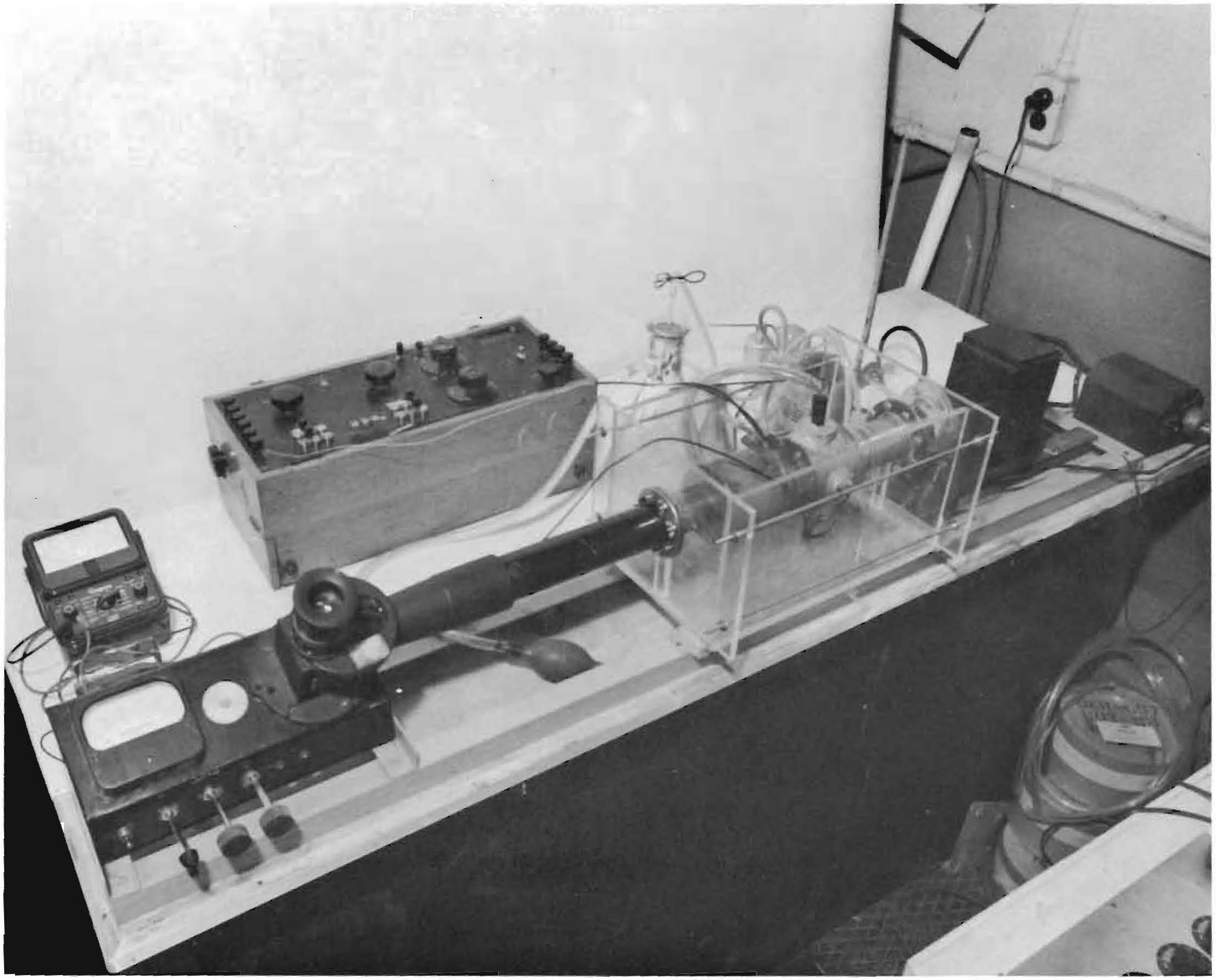

Figure 5. Georgia Tech Version of Millikan Apparatus.

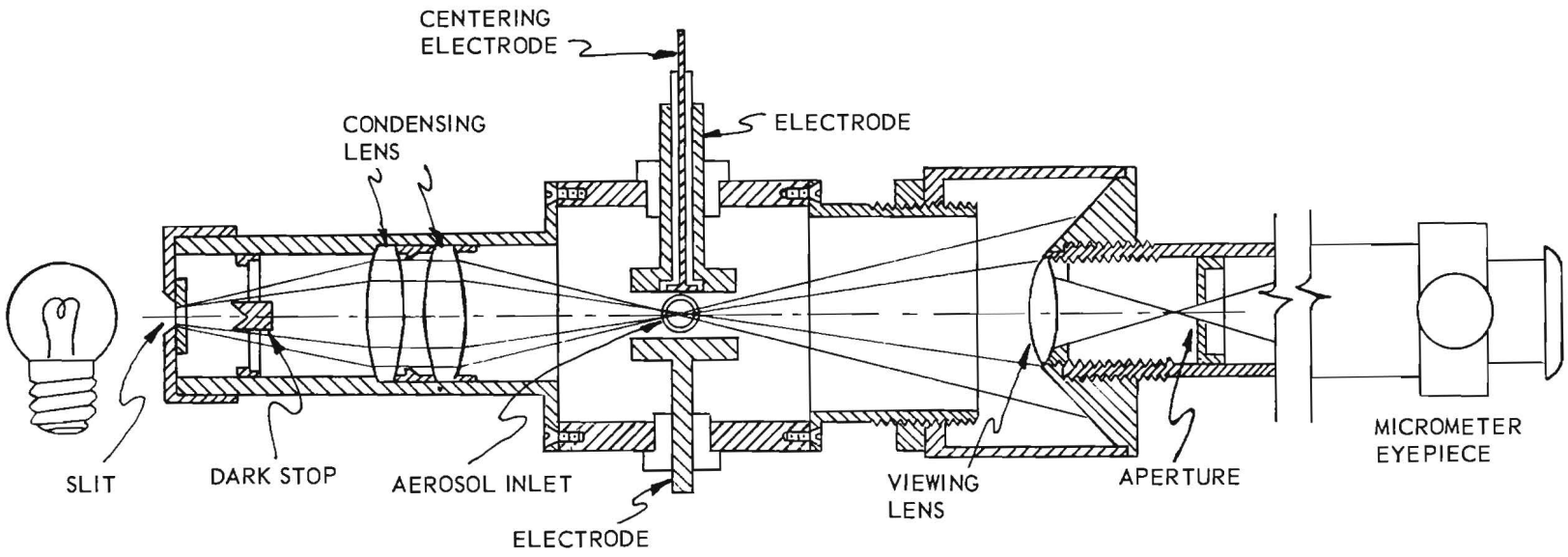

Figure 6. Central Cell of Georgia Tech Version of Millikan's Device Having Dark-Field Illumination.

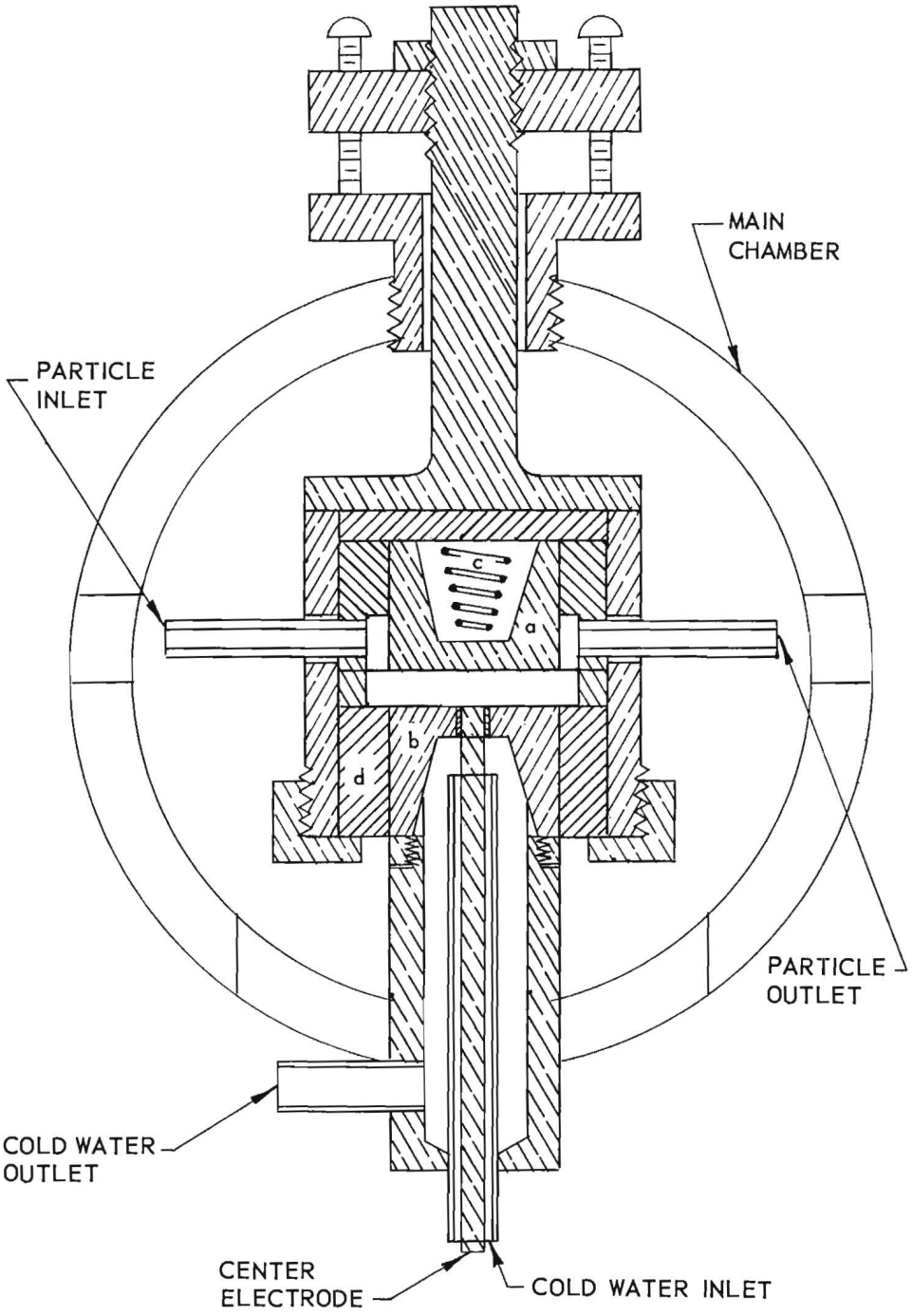

a – UPPER ELECTRODE
b – LOWER ELECTRODE
c – HEATER
d – BAKELITE INSULATION

Figure 7. Detail of Electrodes for Millikan Apparatus.

IV. CALCULATION OF EXPERIMENTAL THERMAL FORCE

Thermal force phenomena in thermal precipitation are deduced from the path a particulate describes in moving through the precipitation zone. As a particle falls under the influence of both gravitational and thermal forces, it is moved horizontally by the surrounding air stream. Hence the particulate path is a function of both vertical forces and the radial movement of the air in which the particulate is suspended. By the joint application of Stoke's law and principles of laminar fluid flow, the particulate behavior and the motivating forces can be resolved. This treatment is presented in the following derivations.

A. Calculation of the Velocity of a Particulate

Aerosol flow through a thermal precipitator must be laminar for analysis of results. This is ensured in the present study by the fact that the Reynolds number, being less than 100 for normal flow rates, is well below the critical value for turbulent flow. If the parabolic velocity profile for laminar flow between parallel plates is assumed not to be significantly altered by the thermal gradient, the following equations can be written:

$$U = U_{max} \left[1 - \left(\frac{4}{L^2}\right) y^2\right] \qquad (1)$$

and

$$U_{max} = \frac{3}{2} U_{avg} = \frac{3}{2}\left(\frac{Q}{A_x}\right) = \frac{3\,Q}{2\,(2\,\pi\,r\,L)}. \qquad (2)$$

Combining gives

$$U = \frac{3\,Q}{4\,\pi\,r\,L}\left[1 - \left(\frac{4}{L^2}\right) y^2\right]. \qquad (3)$$

At this point, it is necessary to determine the particulate velocity relative to the fluid velocity. It has been calculated that 10 micro seconds are required for a one-micron particulate in a flowing aerosol to be accelerated from rest to 90 per cent of the velocity of the passing air.* Hence, it

---

*This calculation was made by equating the particulate drag force to the inertial force: $(U - V_p)Z = \frac{\rho_p\,\pi\,D_p^3}{6}\,\frac{d\,V_p}{dt}$. Solution of this differential equation yields $t = \frac{\rho_p\,\pi\,D_p^3}{6\,Z}\,\ln\left[1 - (V_p/U)\right]$.

is quite adequate to assume that the particulate horizontal velocity, V_r, is equal to the local fluid velocity. Therfore

$$V_r = \frac{dr}{dt} = \frac{3\,Q}{4\,\pi\,r\,L}\left[1 - \left(\frac{4}{L^2}\right) y^2\right]$$

or

$$r\,dr = \frac{3\,Q}{r\,\pi\,L}\left[1 - \left(\frac{4}{L^2}\right) y^2\right]dt. \qquad (4)$$

The vertical coordinate of the particulate position, y, can be expressed as a function of time provided some assumption about the vertical particulate velocity is made. For the present, the vertical velocity is assumed to be constant. This assumption is not absolutely correct and in subsequent analysis the velocity will be allowed to change should experimental evidence indicate that such a change would be significant. After the assumption of a constant vertical velocity, V_y, it follows that

$$V_y = \frac{L}{t_f} \qquad (5)$$

and, from Figure 8,

$$y = \frac{L}{2} - V_y\,t. \qquad (6)$$

Substituting Equation 6 in Equation 4, and integrating between limits gives

$$\int_{r_o}^{r_d} r\,dr = \frac{3\,Q}{4\,\pi\,L}\int_{o}^{t_f}\left[1 - \left(\frac{4}{L^2}\right)\left(\frac{L}{2} - V_y\,t\right)^2\right]dt \qquad (7)$$

if the particle starts at r_o at time zero. Integration and simplification yields

$$t_f = \frac{\pi\,L}{Q}\left(r_d^2 - r_o^2\right) \qquad (8)$$

in which the precipitation time is a function of the plate spacing, aerosol flow rate, and the precipitation radius. Since, as given above,

$$V_y = \frac{L}{t_f}$$

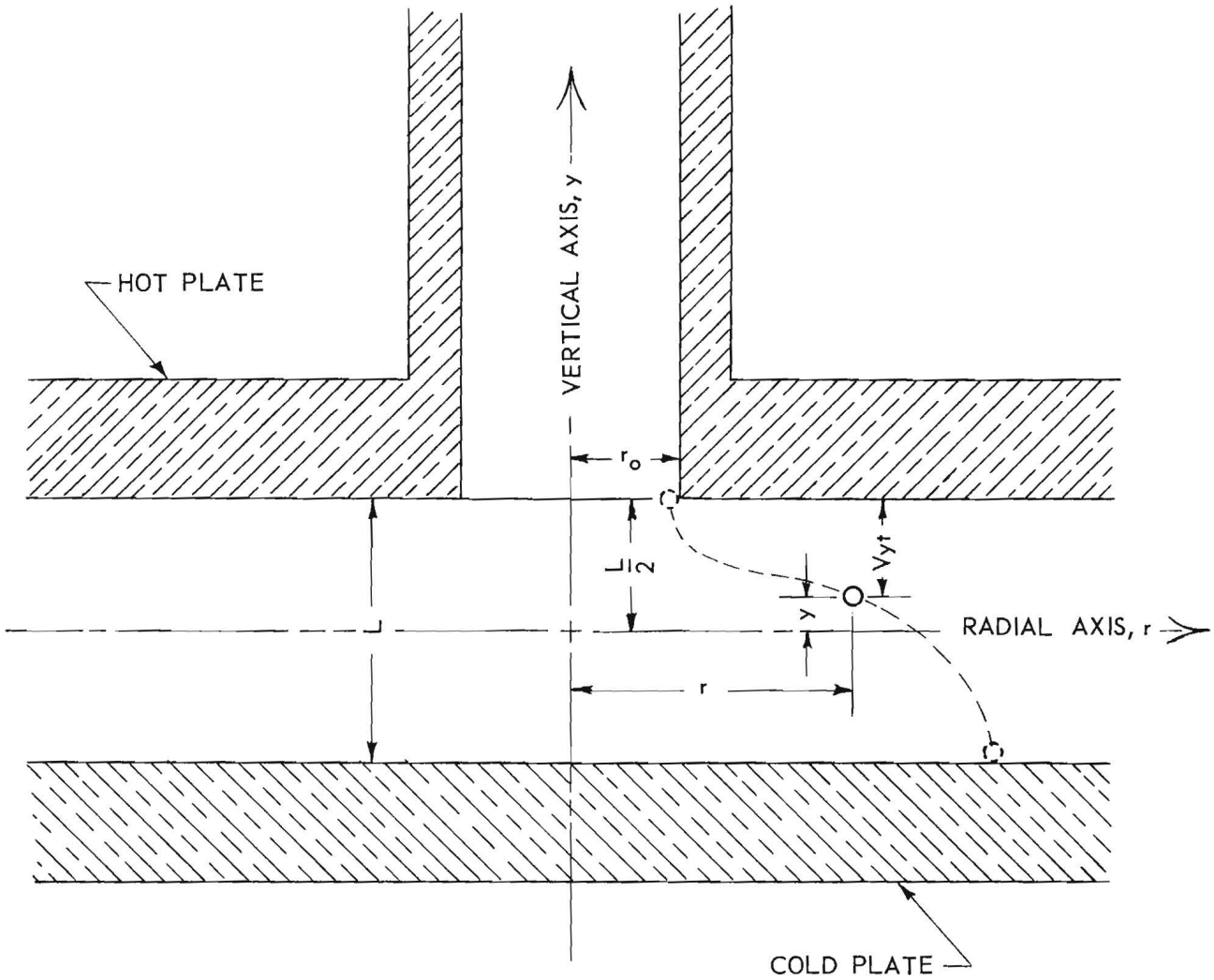

Figure 8. Coordinate System for Defining Particulate Trajectory.

it follows that

$$V_y = \frac{Q}{\pi (r_d^2 - r_o^2)} . \qquad (9)$$

B. Evaluation of Precipitation Forces

A particulate in a viscous medium moving under the influence of a constant force attains a steady velocity that is a measure of the force. Thus,

$$V = Z F, \qquad (10)$$

where Z, the mobility[7] of the particulate, depends on the material and shape of the particle, and on the medium. For a sphere in a homogeneous medium,

$$Z = \frac{1}{6 \pi \mu a} . \qquad (11)$$

This is a form of Stoke's law.[8] As the inhomogeneity of the medium becomes comparable in size with the particle, a slip factor[9, 10, 11] must be considered. Thus Equation 11 becomes

$$Z = \frac{\left[1 + \frac{\lambda}{a}\left(A + Be^{-C\frac{a}{\lambda}}\right)\right]}{6 \pi \mu a} \qquad (12)$$

in which $\left[1 + \frac{\lambda}{a}\left(A + Be^{-C\frac{a}{\lambda}}\right)\right]$ accounts for the slip of the particulate

---

[7] I. Mattauch, "Eine experimentelle Ermittlung des Widerstandsgesetzes kleiner Kugeln in Gases," Zeitschrift fur Physik 32, 439 (1925).

[8] R. A. Millikan, Electrons (+ and -), Protons, Photons, Neutrons, Mesotrons, and Cosmic Rays, The University of Chicago Press, Chicago (1935).

[9] E. Cunningham, "On The Velocity of Steady Fall of Spherical Particles Through Fluid Medium," Proceedings of The Royal Society 83A, 357 (1910).

[10] R. A. Millikan, "Coefficients of Slip in Gases and the Law of Reflection from the Surfaces of Solids and Liquids," Physical Review 21, 217 (1923).

[11] C. N. Davies, "Definitive Equations for the Fluid Resistance of Spheres," Proceedings of the Physical Society 57, 259 (1945).

between the gas molecules. By the combination of Equations 9, 10, and 12, the total precipitating force can be evaluated. Thus,

$$F = \frac{V}{Z} = \frac{6 \pi \mu a Q}{\pi \left(r_d^2 - r_o^2 \right) \left[1 + \frac{L}{a} \left(A + Be^{-C \frac{a}{L}} \right) \right]} \qquad (13)$$

where F is the sum of the gravitational and thermal forces. The gravitational force is merely the mass of the particulate times the gravitational acceleration constant, or

$$F_g = \frac{4}{3} \pi g_c a^3 \rho_p . \qquad (14)$$

Subtracting Equation 14 from Equation 13 gives as the expression for thermal force,

$$F_t = \frac{6 \mu a Q}{\left(r^2 - r_o^2 \right) \left[1 + \frac{\lambda}{a} \left(A + Be^{-C \frac{a}{\lambda}} \right) \right]} - \frac{4}{3} \pi g_c \rho_p A^3 . \qquad (15)$$

C. Mean Free Path of Air Molecules and Slip Factor Evaluation

For use in the previously developed equations, the mean free path for air molecules was computed from the relation,[12]

$$\lambda = \frac{\mu R T}{0.499 M P \bar{v}} , \qquad (16)$$

where

$$\bar{v} = \sqrt{\frac{8 g_c R T}{\pi M}} . \qquad (17)$$

Using this expression for the mean free path of air molecules, Davies has shown that the proper constants for slip factor evaluations are A = 1.257, B = 0.400 and C = 1.10. The temperature used in the above evaluations has been assumed constant at 298° K.

---

[12] Loc. cit.

V. CALCULATION OF THEORETICAL PARTICLE BEHAVIOR

Of the theories that have been proposed to explain the effects of thermal forces on particulates, that of Epstein[13] seems to be supported best by experimental observations. This thermal force equation, based on radiometer theory, was developed for the case of a spherical particulate in a thermal gradient. The mathematical development of the theoretical investigation employs also the equations discussed in the preceding section of this report. The order in which these latter equations are used is essentially reversed, however. In this treatment, a theoretical thermal force for a specific set of conditions is calculated using Epstein's equation,

$$F_t = \frac{9 \pi R \mu^2 k_m D_p \Delta T}{2 M P (2 k_m + k_p) L}. \qquad (18)$$

The gravitational force acting on the particulate under consideration is then evaluated from Equation 14. Finally, the theoretical deposit radius for the particulate is computed from Equation 13 rearranged to the form

$$r_d = \sqrt{r_o^2 + \frac{6 \mu a Q}{\left[1 + \frac{\lambda}{a} (A + Be^{-C a/\lambda})\right] F}} \qquad (19)$$

where

$$F = F_t + F_g . \qquad (20)$$

The computations just described were incorporated in a program for an IBM-650 computer. The program provides for the calculation of (1) the slip factor, (2) the mobility, (3) the thermal force, (4) the gravitational force, (5) the deposit radius, and (6) the terminal verticle velocity of the particulate. It covers a particulate size range from 0.2 to 5 microns, a range of volumetric flow rates from 200 to 1000 cc per minute, and a range of pressures from 0.01 to 1.0 atmosphere.

This program was executed in the Rich Computer Center at Georgia Tech for three materials of markedly different thermal conductivity, i.e.,

---

[13] Epstein, Loc. cit.

magnesium oxide, zinc, and stearic acid. These substances were chosen for theoretical consideration because of their suitability for use in experimental studies. The physical dimensions of the precipitator used in these calculations were also chosen to permit direct comparison of experimental data and theoretical results.

The theoretical data were plotted to show most clearly the effect of operating conditions as well as the effect of the physical properties of the particulate material on thermal precipitation. Results from this investigation, including examples of the plotted data, are presented in the following section of this report.

VI. DISCUSSION OF RESULTS

A. Investigation of Theoretical Particulate Behavior

The theoretical effects of the operating variables of a thermal precipitator upon thermal force are immediately obvious from Equation 19. Also evident are the effects of certain properties of the particulate and of the aerosol carrier medium upon the thermal force. These more direct effects have not been shown in the plots but might be summarized as follows: theoretically thermal force is directly proportional to the thermal gradient, $\Delta T/L$, inversely proportional to the gas pressure, independent of the volumetric flow rate of the aerosol through the precipitator, directly proportional to the square of the viscosity of the carrier medium, inversely proportional to the medium's molecular weight, and directly proportional to the diameter of the particulate.

The term $\frac{k_m}{2\,k_m + k_p}$ relates the thermal conductivity of the particulate material to the thermal force. Where the thermal conductivity is high relative to that of the aerosol carrier medium, the thermal force will be much less than that for a material of relatively low thermal conductivity. The magnitude of this effect is illustrated in Figure 9, a semilog plot of thermal force vs. thermal gradient for stearic acid (k_p = 0.0003 cal/cm-^{o}K-sec), magnesium oxide (k_p = 0.00146 cal/cm-^{o}K-sec), and zinc (k_p = 0.2653 cal/cm-^{o}K-sec). In the case of zinc, for example, the force at any specific condition is approximately 1/170 the force for magnesium oxide, while for stearic acid the force is approximately four times greater. It has been observed that for a typical set of conditions, the forces for stearic acid, magnesium oxide, and zinc are respectively: 3.8×10^{-8}, 1.0×10^{-8}, and 6 X 10 dynes.

Not quite so obvious are the theoretical effects of these same variables upon the radius of a thermal precipitator deposit. Some interesting observations have been obtained, however, by plotting the theoretical data. While the effects have not been conclusively supported by experimentation, the theory appears to predict correctly the general behavior of a given particulate. To that extent, the theoretical data are useful in explaining some of the peculiarities of precipitator operation. Some of the more

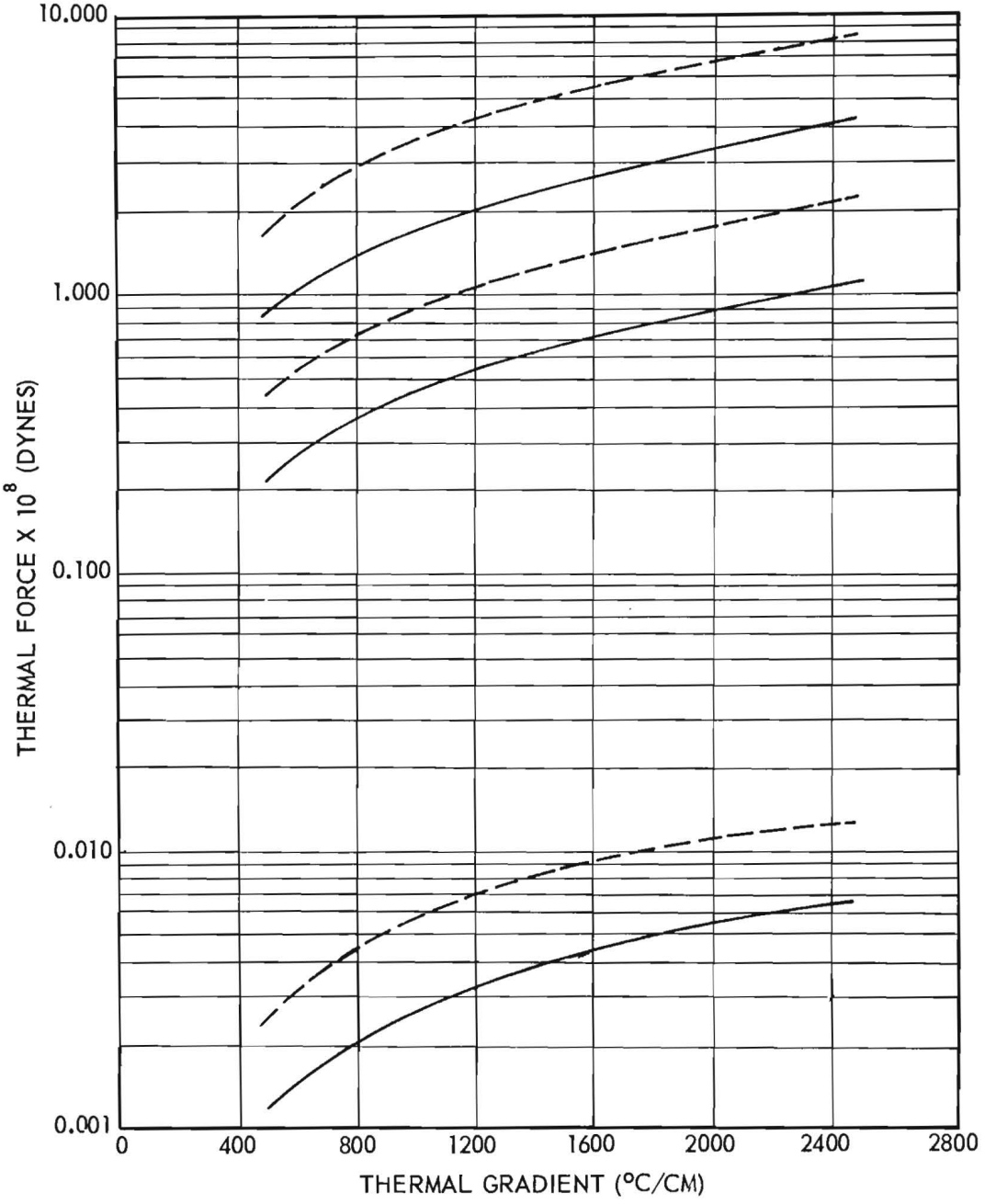

Figure 9. Theoretical Effect of Particulate Thermal Conductivity on Thermal Force. Curves are based on air as carrier medium at pressures of 0.5 atm (broken line) and 1.0 atm (solid line). The uppermost pair of curves apply to stearic acid, k_p = 0.0003 cal/cm-°K-sec; the intermediate pair apply to magnesium oxide, k_p = 0.00146 cal/cm-°K-sec; the lower pair apply to zinc, k_p = 0.265 cal/cm-°k-sec. Thermal forces are for 1.0 micron particles.

interesting and informative relationships are graphically illustrated for discussion. The effect of particulate diameter and pressure on the deposit radius is illustrated in Figure 10, a plot of particulate diameter vs deposit radius with pressure parameters. This plot is based on the behavior of magnesium oxide particles, a thermal gradient of 1970° C, an aerosol flow rate of 600 cc per minute, and a precipitator plate separation of 0.0406 centimeter. It is evident that the deposit radius is a function of pressure, decreasing rapidly as the pressure decreases. Theoretically, for a one-micron particle of magnesium oxide, a decrease in pressure from 1.0 to 0.01 atmosphere results in a decrease in the deposit radius from approximately 6.5 centimeters to 0.5 centimeter. Thus thermal precipitation is theoretically more efficient at lower pressures.

It can be seen in Figure 10 that the deposit radius is a function of particulate diameter and that the deposit radius reaches a maximum value for some critical diameter determined essentially by the operating pressure and by the physical properties of the particulate material. This effect is evident as a "nose" on the curve that is characteristic of the rate of change of deposit radius with respect to particulate diameter. In general, the critical particulate size increases gradually as the pressure decreases, though the overall effect becomes much less pronounced. At very low pressures the "nose" on the curve disappears and, in the case of magnesium oxide, the deposit radius decreases continuously as particulate size decreases below 4 microns at a pressure of 0.01 atmosphere.

The effect of the physical properties of the particulate material on the deposit radius is illustrated in Figure 11, which is also a plot of particle diameter vs deposit radius. In this illustration, curves have been plotted for stearic acid, magnesium oxide, and zinc at pressures of 1.0 and 0.1 atmosphere. The thermal gradient, aerosol flow rate and precipitator plate separation are the same as for Figure 10. Here, it can be seen that the critical particulate size effect is general, but that for any given pressure, the characteristics of the "nose" on the curve (i.e., the rate of change of deposit radius with respect to particle diameter) is highly dependent upon the thermal conductivity and density of the particulate. In particular, the following observations can be made for a pressure

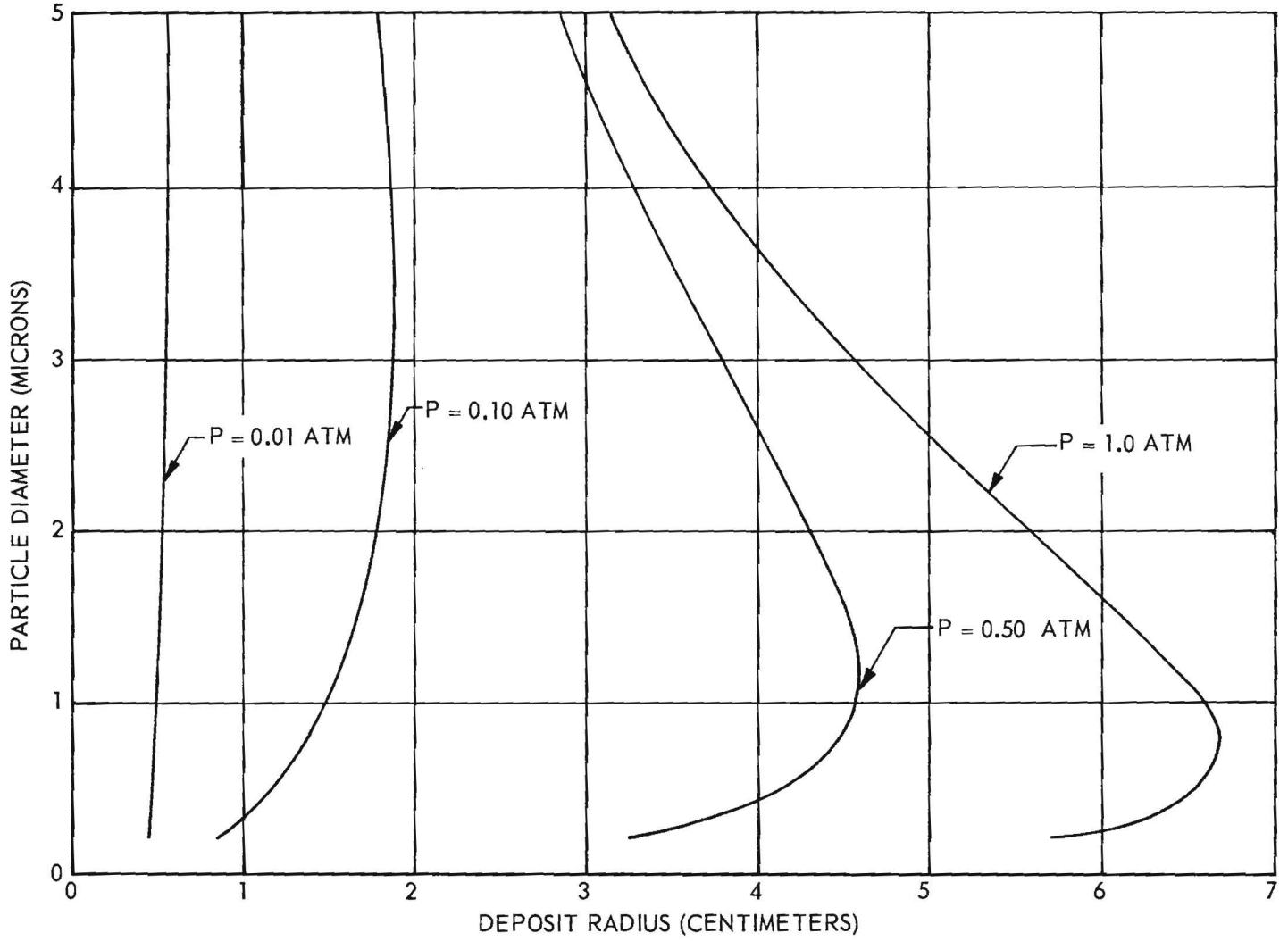

Figure 10. Theoretical Effect of Particle Size and Pressure on the Deposit Radius. Particulate material is magnesium oxide. Aerosol flow rate is constant at 600 cc/min. Thermal gradient is constant at 1970° c/cm. Precipitator plate separation is 0.0406 centimeter.

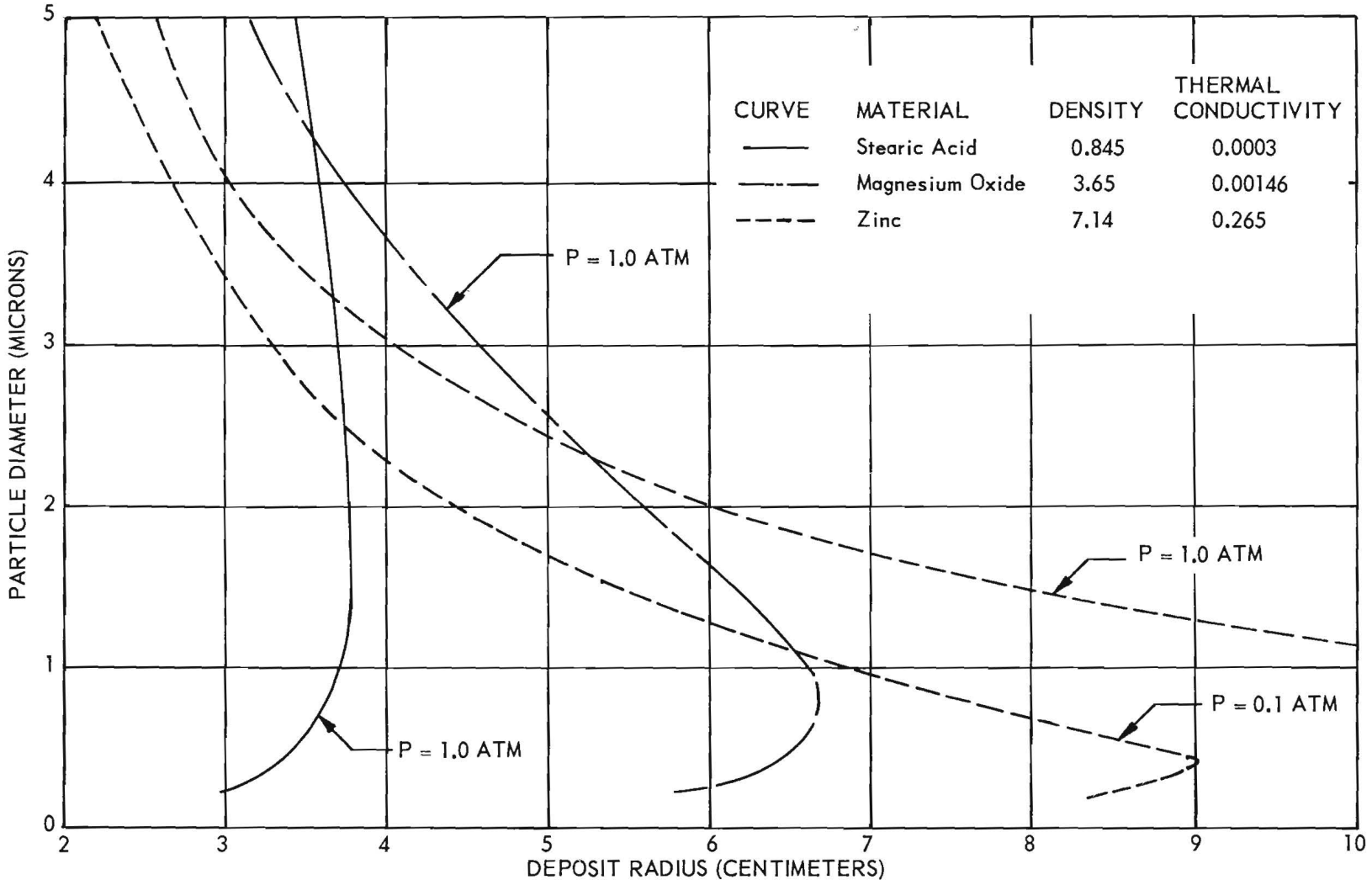

Figure 11. Tehoretical Effect of Thermal Conductivity and Density on Deposit Radius. The base condition are aerosol flow rate = 600 cc/min, thermal gradient = 1970° C/cm, and precipitator plate separation = 0.0406 cm. Thermal conductivity units are cal/cm-°K-sec; density units are gm/cc.

of one atmosphere. For the case of magnesium oxide, the critical particulate size effect is prominent and the critical size is about 0.8 micron. For the case of stearic acid, the critical size effect is less pronounced, and its curvature is similar to that of magnesium oxide at a much lower pressure (i.e., between 0.1 to 0.5 atmosphere). The critical diameter of stearic acid is about 1.7 microns. In the case of zinc, the critical particle diameter is less than 0.2 micron and the deposit radius increases rapidly with decreasing particulate size down to that value. It can be seen, however, from the 0.1-atmosphere curve that the critical particulate size effect is applicable in the case of zinc. Apparently, for a pressure of one atmosphere the maximum deposit radius lies below the particulate size range of these calculations.

Figure 11 also shows that the significance of the effect of particulate size on deposit radius increases as the thermal conductivity increases. In a particulate diameter range from 0.2 to 5 microns and at a pressure of one atmosphere, the deposit radii ranges for stearic acid, magnesium oxide and zinc are, respectively, 2.9 to 3.8 centimeters, 3.1 to 6.6 centimeters, and 2.2 to 38.5 centimeters.

The critical particulate size effect implies a varying particulate size distribution with radius depending upon the operating pressure and the nature of the material. Due to this effect of particulate diameter on the precipitation distance, thermal precipitator deposits can be varied by changing the size of the particulate material being used. Consider particulates ranging from 1.5 micron to 0.2 micron. For stearic acid the critical particulate diameter lies above this size range. Thus the deposit radius decreases as the particulate diameter decreases and the larger particulates would be expected to precipitate near the outer periphery of the deposit. For zinc, on the other hand, the critical particulate diameter is less than the lower limit of the size range being considered. Thus the deposit radius increases as particulate size decreases and the smaller particles would tend to precipitate near outer periphery of the deposit. The critical particulate size for magnesium oxide is about 0.8 micron and lies within the range under consideration. The deposit radius increases with decreasing particulate size to the critical value and then decreases. Thus, at the outer periphery of the deposit, the distribution should contain particulates both greater than and

less than 0.8 micron but approaching that value at the outer extreme. It is further noted that rate of change in particulate diameter with respect to radius for zinc is less than for stearic acid or magnesium oxide and the outer radius of the deposit should not be so sharply defined. Figure 11 indicates further that in the particulate size range for which thermal precipitation is most effective (i.e., below 3 microns), the deposit radius is generally greater for materials of higher thermal conductivity.

The effect of aerosol flow rate on deposit radius is illustrated in Figure 12, where particulate diameter is plotted vs. radius with flow rate and pressure parameters. Again the magnesium oxide particle and the thermal gradient of 1970° C per centimeter are selected as a basis for the illustration. This plot shows, first, the more obvious effect of increasing deposit radius for a given increase in flow rate is greatest for the critical particulate size discussed earlier. Finally, it appears that deposit radius becomes less sensitive to flow rate as the pressure decreases.

B. Experimental Results

Much of the data collected thus far have been for the purpose of testing their significance and reproducibility. Other data were recorded incidental to the establishment of operating procedures and limits. Consequently, the complete tabulation includes some data simply because of their value in supporting statistically the relative magnitude of the experimental thermal forces even though they do not fit into an orderly scheme of analysis. It will be noted that results have been recorded from runs made on two similar precipitators, designated "A" & "B," for two precipitator plate separations, vis., 0.071 and 0.041 centimeter. Tabulated data are presented in Tables I, II, and III, grouped according to precipitator and plate separation. Thermal forces were computed from all experimental data by use of the equations developed in Section III. Also, for each set of operating conditions, a theoretical value of the thermal force and the corresponding theoretical radius have been calculated by following the development in Section IV. Thus a theoretical value is available for direct comparison with the measured value. All data were processed on the IBM-650 computer.

The experimental results are also plotted for graphical presentation presentation. Figure 13 is a plot of thermal force vs. thermal gradient with

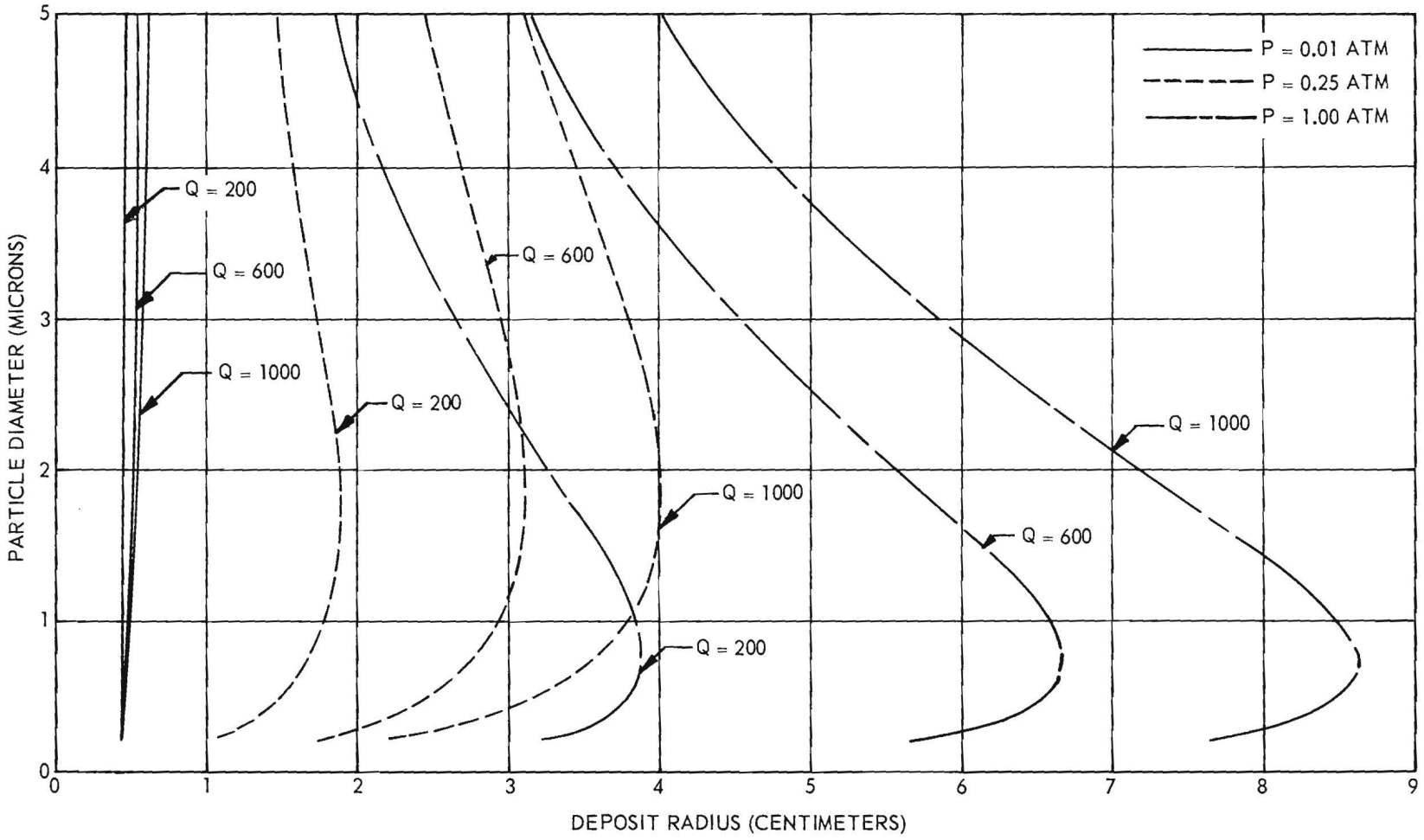

Figure 12. Theoretical Effect of Aerosol Flow Rate on Deposit Radius. This curve also shows the variation in the effect of flow rate with pressure. The curves are based on magnesium oxide particulates, a thermal gradient of 1970° C/cm and a precipitator plate separation of 0.0406 cm. Aerosol flow rate, Q, is in cc/min.

TABLE I

EXPERIMENTAL DATA AND CORRESPONDING COMPUTED VALUES FOR MAGNESIUM OXIDE PARTICLES[a]

(A) Pressure (Atm)	(B) Thermal Gradient (° C/Cm)	(C) Aerosol Flow Rate (CC/Min)	(D) Observed Particle Travel (Cm)	(E) Theoretical[b] Particle Travel (Cm)	(F) Radius Ratio (D/E)	(G) Experimental[b] Thermal Force (Dynes x 10^{-8})	(H) Theoretical[b] Thermal Force (Dynes x 10^{-8})	(I) Force Ratio (G/H)
0.96	841	371.3	2.66	6.59	0.404	2.90	0.404	7.18
0.97	844	396.8	3.06	6.85	0.447	2.40	0.401	5.99
0.96	847	400	3.06	6.83	0.448	2.41	0.407	5.92
1.0	844	425	3.16	7.19	0.439	2.44	0.389	4.27
0.97	871	476	3.37	7.45	0.452	2.42	0.414	5.85
1.0	984	403.2	2.96	6.61	0.448	2.61	0.454	5.75
0.97	1127	420.2	3.01	6.33	0.476	2.63	0.536	4.91
0.96	1110	440.9	2.74	6.50	0.422	3.28	0.533	6.15
0.97	1127	457.4	3.18	6.62	0.480	2.59	0.536	4.83
0.97	1111	460.1	3.04	6.67	0.456	2.84	0.538	5.28
0.96	1409	384.6	2.37	5.48	0.432	3.72	0.677	5.49
0.96	1409	384.6	2.31	5.48	0.421	3.90	0.677	5.76
0.97	1406	402.7	2.49	5.65	0.441	3.58	0.669	5.35
0.97	1406	458.7	2.64	6.06	0.436	3.67	0.669	5.25
0.1	931	612.3	0.60	1.68	0.357	21.7	4.29	5.06
0.5	956	170.5	0.96	2.99	0.321	6.47	0.829	7.80
0.5	1124	491.8	1.74	4.84	0.360	7.24	1.04	7.96
0.5	1118	503.3	1.85	4.91	0.377	6.67	1.03	6.48
0.5	1402	199.0	0.81	2.63	0.307	9.84	1.29	7.63
0.5	1409	217.4	0.91	2.76	0.330	9.02	1.30	6.94
0.5	1411	236.0	0.92	2.89	0.318	9.64	1.30	7.42
0.5	1404	241.0	0.91	2.93	0.311	10.02	1.29	7.77
0.75	880	312.5	1.80	5.25	0.343	4.69	0.541	8.67
0.97	875	135	1.72	3.77	0.456	2.18	0.416	5.24
0.97	882	324	2.94	6.05	0.486	2.08	0.419	4.96
0.96	1062	555	3.24	7.47	0.434	3.07	0.510	6.02
0.97	1132	464.4	2.74	6.66	0.411	3.49	0.538	6.49
0.97	1125	465.8	2.74	6.69	0.410	3.50	0.535	6.54

(Continued)

TABLE I (Continued)

EXPERIMENTAL DATA AND CORRESPONDING COMPUTED VALUES FOR MAGNESIUM OXIDE PARTICLES[a]

(A) Pressure (Atm)	(B) Thermal Gradient (° C/Cm)	(C) Aerosol Flow Rate (CC/Min)	(D) Observed Particle Travel (Cm)	(E) Theoretical[b] Particle Travel (Cm)	(F) Radius Ratio (D/E)	(G) Experimental[b] Thermal Force (Dynes x 10^{-8})	(H) Theoretical[b] Thermal Force (Dynes x 10^{-8})	(I) Force Ratio (G/H)
0.97	1118	467.3	2.86	6.71	0.426	3.18	0.532	5.98
0.97	1115	496.7	2.81	6.94	0.405	3.57	0.530	6.74
0.96	1114	506.8	2.96	6.98	0.424	3.31	0.535	6.19
0.97	1404	376.9	2.46	5.45	0.451	3.40	0.667	5.10
0.96	1409	378.8	2.45	5.43	0.451	3.45	0.667	5.10
0.96	1406	480.8	2.59	2.59	0.419	4.00	0.676	5.92
0.96	1399	493.0	2.59	6.28	0.412	4.10	0.672	6.10
0.96	1399	500.0	2.62	6.32	0.414	4.08	0.672	6.07

[a] Runs made on precipitator "A" with a plate separation of 0.071 centimeter.

[b] All computations based on a particle diameter of 1.0 micron.

TABLE II

EXPERIMENTAL DATA AND CORRESPONDING COMPUTED VALUES FOR MAGNESIUM OXIDE PARTICLES[a]

(A) Pressure (Atm)	(B) Thermal Gradient (° C/Cm)	(C) Aerosol Flow Rate (CC/Min)	(D) Observed Particle Travel (Cm)	(E) Theoretical[b] Particle Travel (Cm)	(F) Radius Ratio (D/E)	(G) Experimental[b] Thermal Force (Dynes x 10^{-8})	(H) Theoretical[b] Thermal Force (Dynes x 10^{-8})	(I) Force Ratio (G/H)
0.5	507	180	2.06	3.93	0.524	1.86	0.468	3.97
0.5	988	166	1.07	2.80	0.382	5.28	0.92	5.74
0.5	1012	169	1.24	2.75	0.451	4.20	0.969	4.33
0.5	1478	184	0.98	2.45	0.400	6.77	1.36	4.98
0.5	2473	194	0.42	1.91	0.220	24.1	2.30	10.48
1.0	503	194	3.11	5.61	0.554	1.04	0.232	4.48
1.0	980	180	1.86	4.29	0.434	2.60	0.452	5.75
1.0	985	188	2.11	4.38	0.482	2.16	0.454	4.76
1.0	988	200	2.16	4.53	0.477	2.21	0.456	4.85
1.0	988	201	2.19	4.54	0.482	2.17	0.456	4.76
1.0	1478	194	1.76	3.78	0.466	3.10	0.682	4.54
1.0	1963	221	1.79	3.58	0.500	3.46	0.905	3.83
1.0	2463	198	1.31	3.02	0.434	5.26	1.13	4.65

[a] Runs made on precipitator "A" with a plate separation of 0.041 centimeter.

[b] All computations based on a particle diameter of 1.0 micron.

TABLE III

EXPERIMENTAL DATA AND CORRESPONDING COMPUTED VALUES FOR MAGNESIUM OXIDE PARTICLES[a]

(A) Pressure (Atm)	(B) Thermal Gradient (° C/Cm)	(C) Aerosol Flow Rate (CC/Min)	(D) Observed Particle Travel (Cm)	(E) Theoretical[b] Particle Travel (Cm)	(F) Radius Ratio (D/E)	(G) Experimental[b] Thermal Force (Dynes x 10^{-8})	(H) Theoretical[b] Thermal Force (Dynes x 10^{-8})	(I) Force Ratio (G/H)
1.0	502	185	2.94	5.57	0.528	1.11	0.232	4.78
1.0	488	193	2.98	5.65	0.527	1.14	0.225	5.07
1.0	488	195	2.78	5.68	0.489	1.32	0.225	5.87
1.0	495	202	2.96	5.76	0.514	1.21	0.228	5.31
1.0	488	203	2.97	5.80	0.512	1.21	0.225	5.38
1.0	493	216	3.05	5.98	0.510	1.23	0.227	5.42
1.0	722	175	2.31	4.73	0.488	1.68	0.333	5.05
1.0	1002	184	1.83	4.30	0.426	2.74	0.462	5.93
1.0	988	190	1.85	4.42	0.419	2.78	0.453	6.14
1.0	1222	238	1.88	4.58	0.410	3.44	0.563	6.11
1.0	1466	210	1.86	3.96	0.470	3.06	0.676	4.53
1.0	1470	227	1.96	4.13	0.475	3.03	0.678	4.47
1.0	1975	198	1.49	3.36	0.443	4.24	0.911	4.65

[a] Runs made on precipitator "B" with a plate separation of 0.041 centimeter.

[b] All computations based on a particle diameter of 1.0 micron.

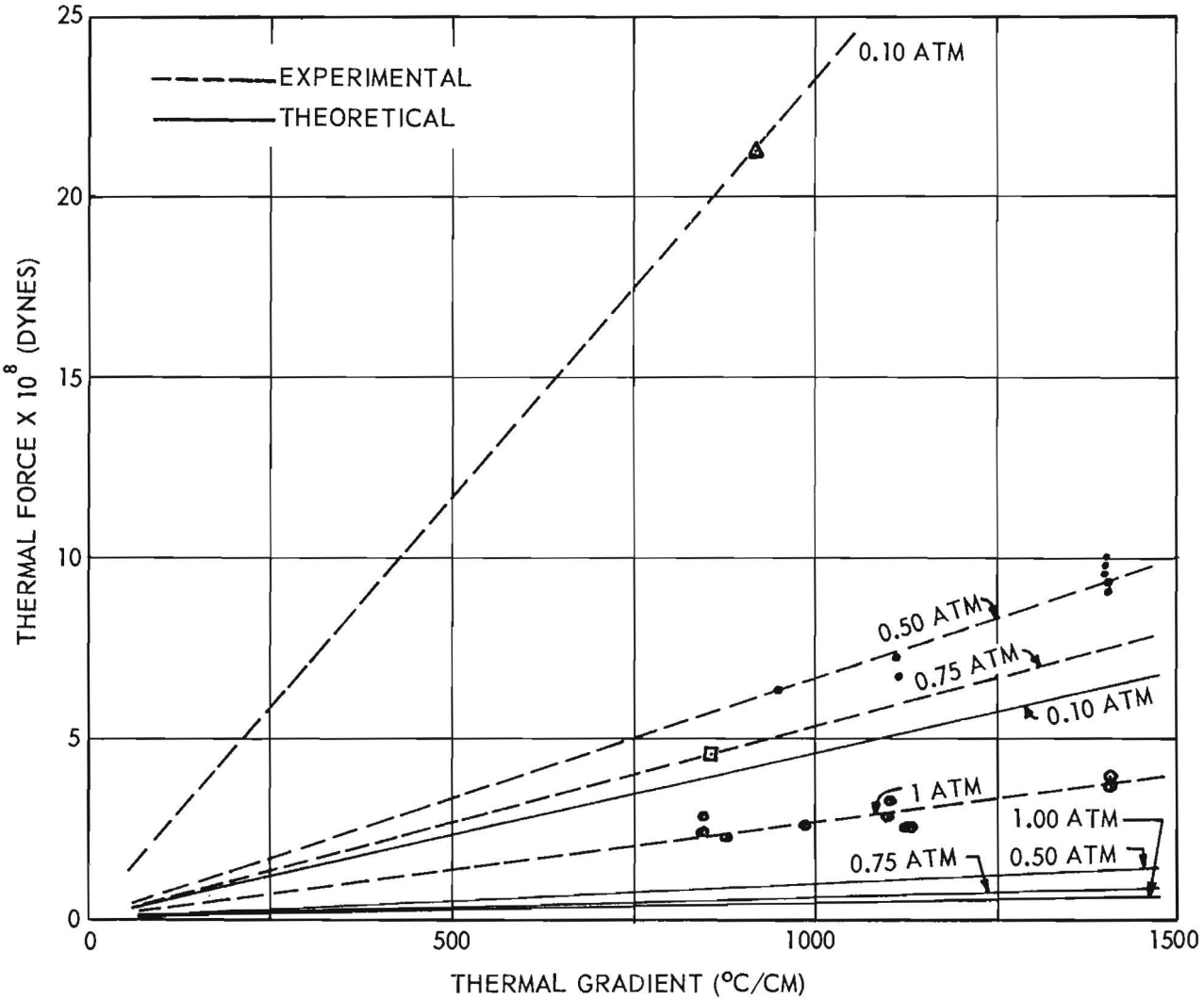

Figure 13. Theoretical and Experimental Effect of Pressure on Thermal Force as a Function of Thermal Gradient. Data are for 1.0 micron magnesium oxide particles, precipitator A; plate separation 0.0711 cm.

pressure parameters of 0.10, 0.50, 0.75 and 1.00 atmosphere. The plot is based on magnesium oxide data from precipitator "A" with a plate separation of 0.071 centimeters (see Table I). Data were collected over a thermal gradient range from 800° to 1400° C per centimeter. An average particulate size of 1.0 micron was used in making the calculations. A series of theoretical curves (solid line) have been included on the graph for comparison with the experimental values (broken line). Because of the limited number of experimental points, considerable reliance has been placed on the theoretical consideration that the thermal force is a linear function of the thermal gradient and that the thermal force is zero when the thermal gradient is zero. It should be noted that for the 0.1 and the 0.75 atmosphere pressure curves only one point on each has been determined. Thus, these curves serve merely to substantiate the magnitude of the ratio of experimental forces to theoretical forces, and there is some doubt as to the accuracy of the absolute value of the force determinations at the lower pressures. Although less data are available than would be desired for conclusive evaluation, a definite disagreement with theoretical results is obvious. The approximate value of the ratio of experimental force to theoretical force has been evaluated for each pressure. These ratio values are 5.1, 6.9, 8.7, and 5.9, respectively, for atmospheric pressures of 0.1, 0.5, 0.75, and 1.0.

The results given in Table I for the thermal force at one atmosphere are adequately supported by the data of two additional series of runs, one, given in Table II, using the same precipitator "A" with a plate separation of 0.041 centimeter and the other, given in Table III, using precipitator "B" with a separation of 0.041 centimeter. A comparison of the three series of runs is made in Figure 14. It may be seen that the results are in general agreement and are consistently higher than accepted theory would predict. The experimental-to-theoretical thermal force ratios range from 4.5 to 6.0.

While all results are within the observed experimental deviation of about 15 per cent, it has been observed that the results given in Table I are consistently higher than those in the other two tables. In this connection, it should be stated that the average flow rate for the first data is on the order of 400 cc per minute while the average flow rates for the second

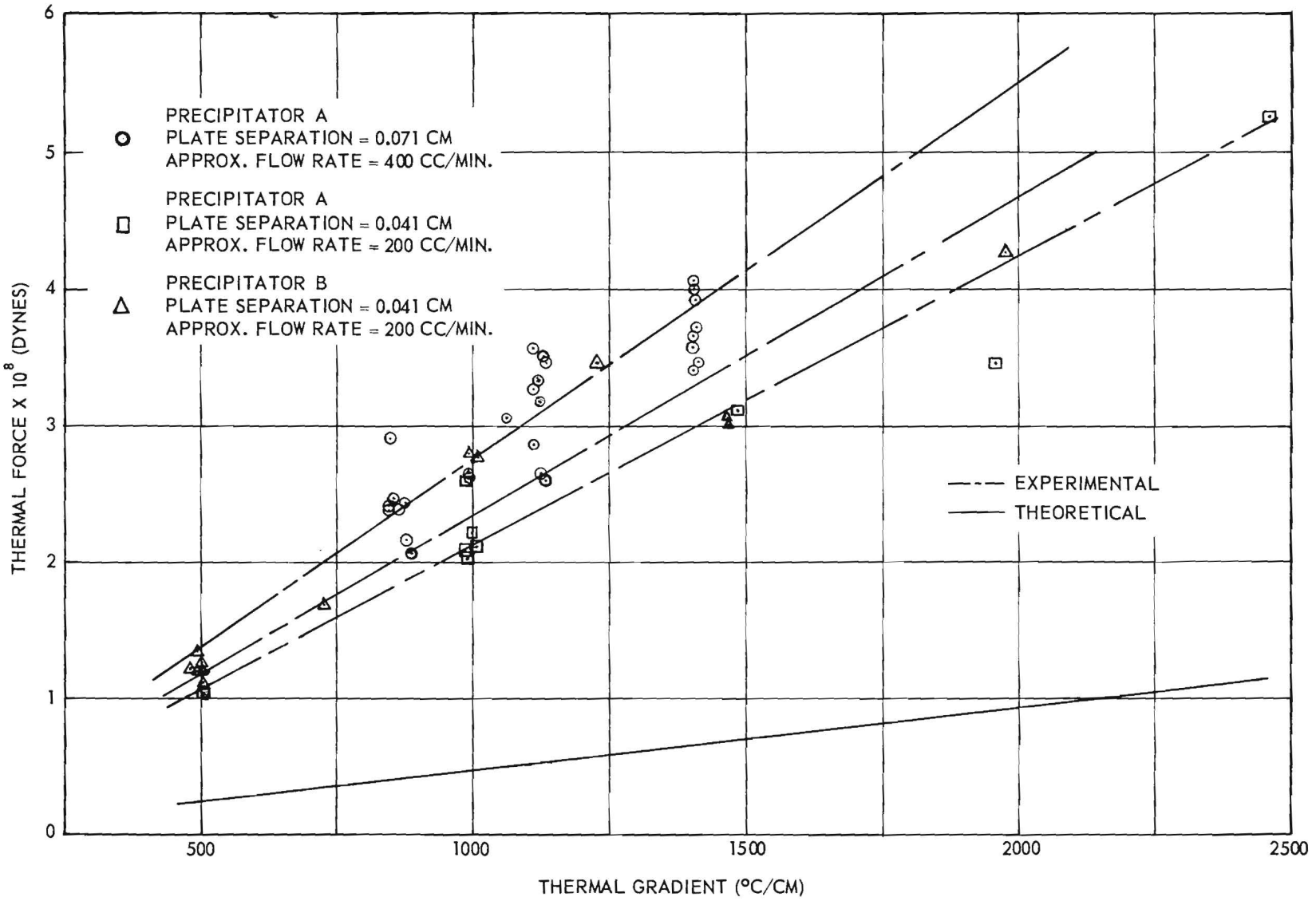

Figure 14. Thermal Force as a Function of Thermal Gradient at 1.0 Atmosphere Pressure. Data are for 1.0 micron magnesium oxide particles.

and third tabulations are less than 200 cc per minute. While the thermal force is theoretically independent of aerosol flow rate, there is thus some indication that this may not be the case. There is not at this time, however, enough experimental evidence to make a conclusive statement.

A look at the tabulated data shows that experimental determinations cover a variety of aerosol flow rates. In order to make a valid estimate of experimental inconsistencies, it has been necessary to adjust the observed deposit radii to a standard flow rate. The adjustment procedure is as follows: Two theoretical deposit radii corresponding to the observed radius are computed, the first based on the experimental flow rate and the second based on the standard flow rate. The first theoretical radius is subtracted from the second value. The difference is then multiplied by the ratio of the observed radius to the theoretical radius that corresponds to the experimental flow rate. This quantity is then added to the observed radius. In this manner all the data in the proximity of a given flow rate may be reduced to the same base flow rate.

Figures 15, 16, and 17 illustrate the consistency of the data for the three series of experimental runs. In each of these graphs, the precipitation distance, $r_d - r_o$, adjusted for constant flow rate, has been plotted against the thermal gradient (broken line curves). In each case a solid line curve has been constructed also to indicate the corresponding theoretical particle travel.

Figure 15 presents the results from Table I. This set of data was obtained using the precipitator "A" with a plate spacing of 0.071 centimeter. Only the data which were obtained at flow rates in the vicinity of the base value of 400 cc per minute have been plotted. The experimental runs were made at a pressure of approximately one atmosphere. It can be seen that all the points lie within an experimental deviation of $\pm$ 10 per cent. Over the limited thermal gradient range, and for the operating conditions of these tests, the relationship between precipitation distance and thermal gradient is essentially linear. The ratio of experimental radius to theoretical radius is approximately 0.47.

Figure 16 presents the results obtained at a pressure of one atmosphere, and a precipitator plate separation of 0.041 centimeter on precipitators "A"

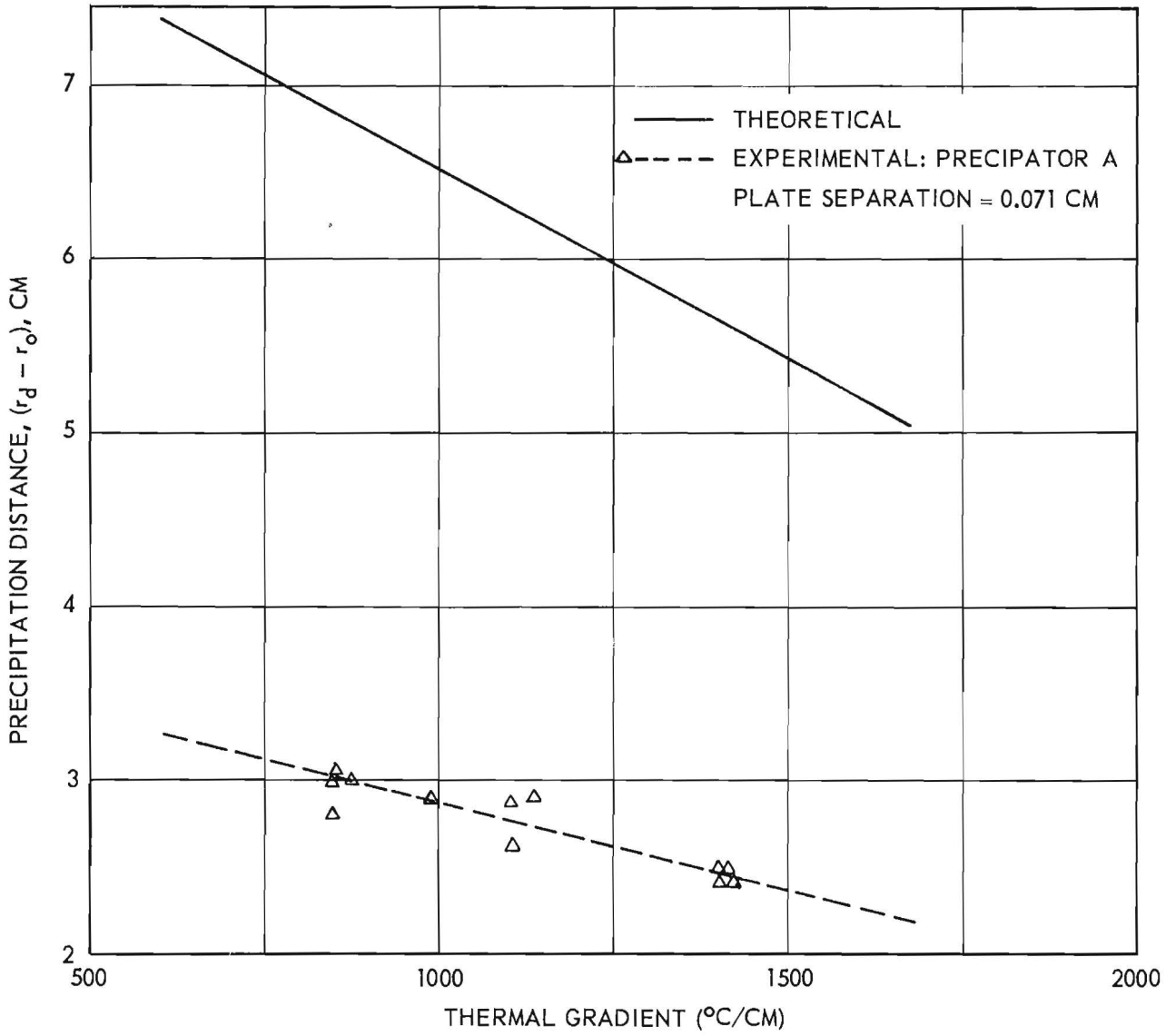

Figure 15. Precipitation Distance as a Function of Thermal Gradient at 1.0 Atmosphere Pressure and an Aerosol Flow Rate of 400 cc/min. Theoretical data are for 1.0 micron magnesium oxide particles.

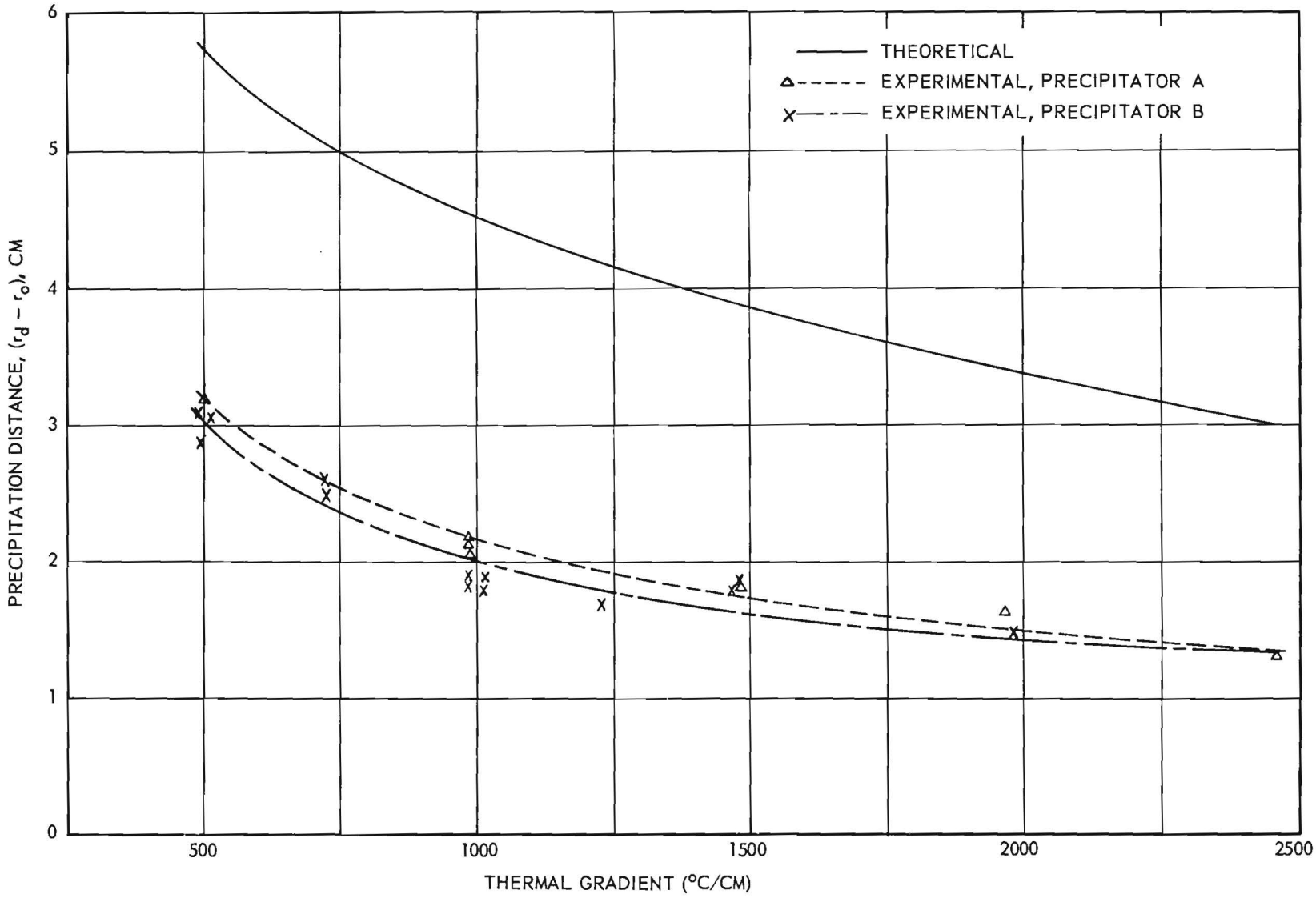

Figure 16. Precipitation Distance as a Function of Thermal Gradient at 1.0 Atmosphere and an Aerosol Flow Rate of 200 cc/min. Theoretical data are for 1.0 micron magnesium oxide particles. Precipitator plate separation is 0.041 cm.

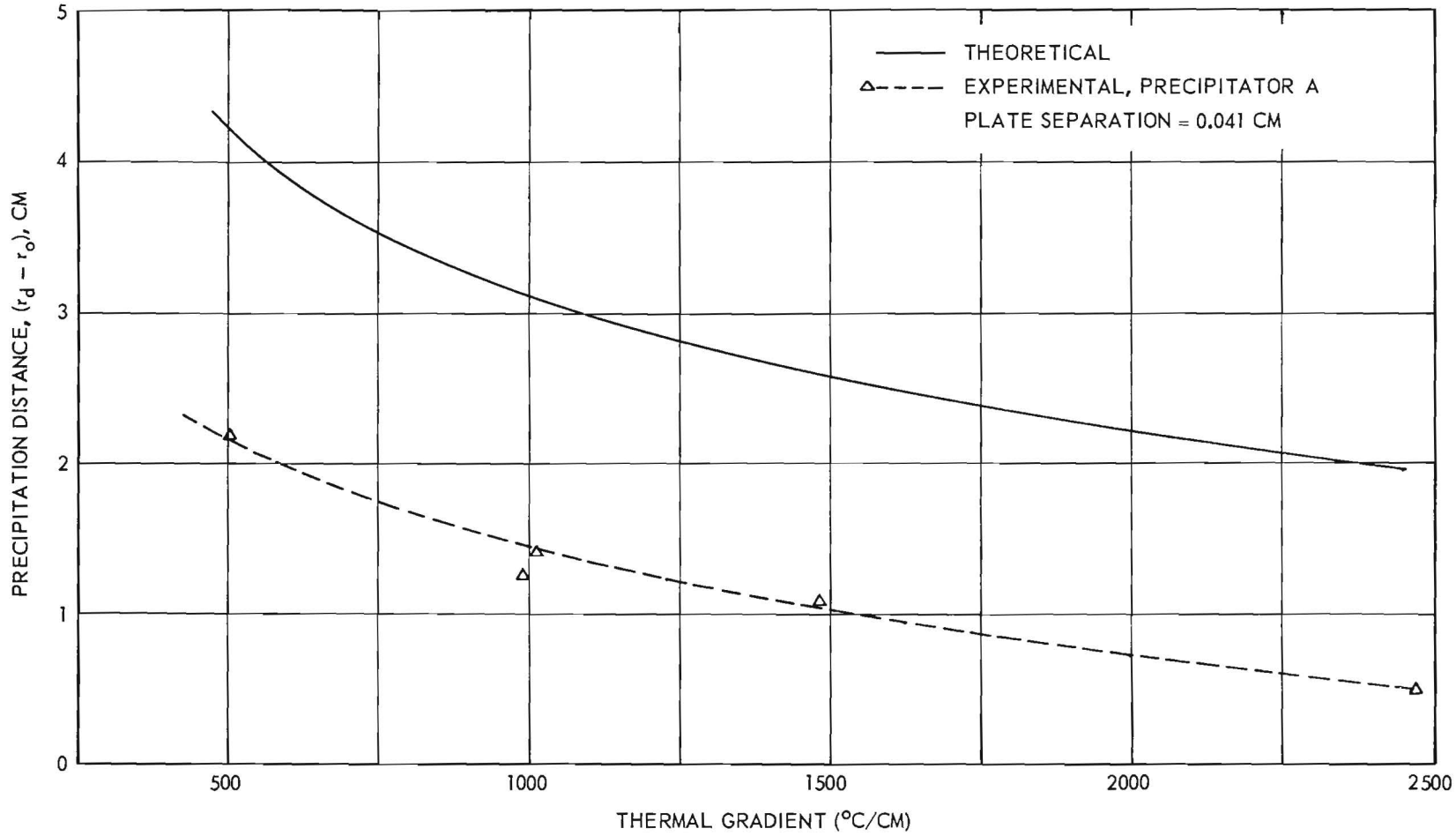

Figure 17. Precipitator Distance as a Function of Thermal Gradient at 0.5 Atmosphere and an Aerosol Flow Rate of 200 cc/min. Theoretical data are for 1.0 micron magnesium oxide particles.

and "B" (Tables II and III). In both cases the precipitation distance, $r_d - r_o$, has been adjusted for a flow of 200 cc per minute and plotted against thermal gradient. From this illustration, it can be seen that the data of both curves lie within an experimental deviation of 15 per cent and for either series the data lie within 10 per cent of the mean curve. It can be seen also that the relationship between precipitation distance and thermal gradient is not linear; instead the rate of change of travel with respect to thermal gradient increases as the thermal gradient decreases. The ratio of observed radius to theoretical radius also varies. For the results of precipitator "A" this ratio varies from about 0.56 for a gradient of 500° C per centimeter to about 0.45 for a gradient of 2500° C per centimeter. For the results of precipitator "B" the ratio decreases from about 0.52 to 0.45 over the same range of thermal gradients.

Figure 17 presents the results obtained at a pressure of 0.5 atmosphere, for a plate separation of 0.041 centimeter in precipitator "A." Again the base flow rate is 200 cc per minute. The curvature of the plot is similar to that of Figure 4. The experimental deviation is within 15 per cent. The experimental radius is again about half the theoretical value. The ratio in this case decreases from a value of 5.2 at 500° C per centimeter to a value of about 2.5 at 2500° C per centimeter. It should be noted that the experimental curve in this case is based on limited data with only a single point above a thermal gradient of 1500° C per centimeter. Thus the low ratio at the upper extreme of the thermal gradient scale is not adequately supported.

A few experimental tests have been made with zinc as the particulate material, but there is not enough significance in the data obtained to warrant its inclusion in this report. Theoretical estimations of the deposit radius for zinc indicate that a complete deposit of the particles in the 0.5- to 1.5-micron range could not be obtained at a pressure of one atmosphere in the experimental precipitator being used. Runs have been attempted at one atmosphere and, while the deposition of particles is not complete, most of the particulate material has been collected within the 4-centimeter radius of the precipitator. The outer periphery of the deposit is not well defined, and precise quantitative measurements of the deposit radius have not yet been made. This degree of precipitation is, however, sufficient to indicate that the thermal force actually exerted upon the zinc particles is many times

greater than the theoretical. With regard to the particle size effect discussed earlier, the anticipated distribution has not been observed. The effect has been confirmed somewhat by the appearance of the zinc deposits, but no conclusive statements can be made at this time.

A major problem area encountered in making experimental measurements still has not been completely resolved. The first problem is that of determining precisely the outer radius of the deposit. Unfortunately, the deposit radius is not sharply defined, even in the case of magnesium oxide. Close examinations of the deposits, both with and without the aid of a microscope, reveal a central area of relatively high density which at some radius, dependent upon the operational conditions, fades rather rapidly into an area of extremely low density. It is the average radius of the band, in which deposition shows a marked decrease, that has been taken as the deposit radius. Thus the width of the circumferential band contributes the greatest experimental error in the results. Fortunately, this band width decreases as the radius of the deposit decreases, so that the percentage error thereby introduced is constant. In this connection, it is noted that the overall density variation is ill defined. Experimental deviations for deposits of this nature are sometimes as high as 15 per cent. A technique for measuring the radii has been developed in which a sharply focused pinpoint of light is traversed radially across the glass collecting disc. The reflected light brightens quite noticeably when it encounters the deposit. A micrometer is used to control the movement of the light and radial measurements are read directly. Measurements made in this way support these made by direct observation. For magnesium oxide this technique works very well, but it is not satisfactory for measurements with zinc deposits. The problem in measuring the radius of a zinc deposit is that of defining the radius. As was mentioned before, the circumferential band is wide and hazy. It appears that some technique based on relative deposit density in conjunction with particle size distribution will have to be developed before a high degree of precision can be attained.

The exact cause of the circumferential band is subject to conjecture. While this effect was predicted by theoretical considerations of the critical particulate size phenomena discussed in part A of this section, the particle

size distribution has not been actually observed. The hazy band might be explained as the result of a slight variation in thermal gradient or aerosol flow rate. The absence of a particle size distribution at the outer periphery of the deposit has introduced an additional complication, vis., that of establishing the particle size which corresponds to an observed radius. The particles of magnesium oxide generated for these experiments range from 0.5 to 1.5 microns in diameter. Within the denser area of the deposit discrete particulate sizes, if indeed any are present, are obscured by a profusion of agglomerates. The agglomerates are large relative to particulate sizes and have been observed, even in deposits of very light overall density. In the circumferential band relatively few agglomerates are observed but individual particles of all sizes are found. Even in the very low density area outside the obvious deposit periphery, all sizes of particles have been observed. There is a conspicuous absence of agglomerates in this region.

For the purpose of calculating thermal forces, an arbitrary particulate diameter of 1.0 micron has therefore been selected. This value is both the average particulate diameter for the aerosol and the theoretical critical size for a pressure of one atmosphere. It has been noted that the size of a particulate greatly influences the theoretical radius and likewise makes a considerable difference in the computed experimental thermal force. More investigation is needed in this area.

VII. CONCLUSIONS

Experimental results thus far may be summarized as follows: For magnesium oxide, the consistency of experimental data is good, deviations generally being less than 10 per cent. The thermal force exerted upon the particles appears to be about five times greater than would be predicted from Epstein's theory. For zinc, the limited data available indicate a force very much greater than predicted. No quantitative results for zinc are available at this time, however. To date, no experimental runs have been made using stearic acid particulates.

VIII. FUTURE WORK

Emphasis will be placed on the immediate continuation of experimental investigations with both zinc and stearic acid particulates by use of present equipment and techniques. These, along with additional experiments on magnesium oxide, will be executed according to an orderly scheme so that definite conclusions can be made about the thermal force on particulates of these materials. Later, two or three other materials will be surveyed to provide a comprehensive coverage of particulate physical properties.

Concurrent with the collection of experimental data, more effort will be directed toward determining the correct particulate size to be used in the calculation of experimental results. Presently, this size can be estimated but further experimental support is necessary for a precise evaluation of results. Work in this area will constitute one of the more important aspects of future investigations. Also, the formulation of relationships and the associated assumptions will be studied and modified to give greater precision in calculations.

The modified Millikan apparatus is presently operable but improvements are needed to ensure reliable data. Efforts with it will be continued in order to supplement the thermal precipitator analyses. It is anticipated also that this experimental apparatus can be used to investigate the effect of particulate temperature on thermal force phenomena. These studies, however, will be attempted only after a thorough investigation of thermal force under normal conditions has been completed.

Respectfully submitted:

Clyde Orr, Jr.
Project Director

Approved:

Wyatt C. Whitley, Chief
Chemical Sciences Division

J. E. Boyd, Director
Engineering Experiment Station

FINAL REPORT

PROJECT NO. B-159

AN INVESTIGATION OF THERMAL FORCE WITH PARTICULAR REFERENCE TO MATERIALS OF HIGH THERMAL CONDUCTIVITY

by

THOMAS W. WILSON, J. ANDREW McALISTER
and CLYDE ORR, Jr.

COVERING THE PERIOD
JANUARY 1, 1959 through JUNE 30, 1961
Printed August 15, 1961

RESEARCH GRANT NSF-G7051
NATIONAL SCIENCE FOUNDATION
WASHINGTON, D. C.

Engineering Experiment Station
Georgia Institute of Technology
Atlanta, Georgia

ENGINEERING EXPERIMENT STATION
of the Georgia Institute of Technology
Atlanta, Georgia

FINAL REPORT

PROJECT NO. B-159

AN INVESTIGATION OF THERMAL FORCE WITH PARTICULAR REFERENCE TO MATERIALS OF HIGH THERMAL CONDUCTIVITY

by

THOMAS W. WILSON, J. ANDREW McALISTER
and CLYDE ORR, JR.

COVERING THE PERIOD
JANUARY 1, 1959 through JUNE 30, 1961
Printed August 15, 1961

RESEARCH GRANT NSF-G7051
NATIONAL SCIENCE FOUNDATION
WASHINGTON, D. C.

ABSTRACT

An experimental investigation of thermal precipitation and of gas-suspended particulate behavior under the influence of a temperature gradient was undertaken in an effort to reconcile conflicts reported from previous studies, specifically those observed with aerosolized solids of high thermal conductivity. An interpretation of results, based on the use of an effective particulate thermal conductivity lower than that of the solid due to agglomeration, permits the qualitative correlation of experimental results with Epstein's theory and provides an explanation of superficial inconsistencies in experimental data.

DEFINITION OF SYMBOLS

A	empirical constant appearing in slip-correction equation.
A_x	cross-sectional area of aerosol stream in precipitator, normal to direction of flow.
a	particulate radius.
a_{rd}	particulate radius evaluated at outer periphery of thermal precipitation deposit.
B	empirical constant appearing in slip-correction equation.
C	empirical constant appearing in slip-correction equation.
C_1	proportionality factor in thermal force-temperature gradient relationship.
C_p	heat capacity at constant pressure.
D	characteristic linear dimension in Reynolds number.
D_p	particulate diameter.
$\frac{dT}{dy}$	temperature gradient in vertical direction.
F	force.
F_d	drag force, resistance of gas to motion of a particle suspended therein.
F_g	gravitational force.
F_t	thermal force.
F_t^o	thermal force value defined by Epstein's equation for particulate thermal conductivity equal to that of the gas.
$(F_t)_{Ep}$	thermal force defined by Epstein.
$(F_t)_W$	thermal force defined by Waldmann.
$f(k)$	thermal force proportionality factor, a function of both particulate and gas thermal conductivity.
g_c	conversion factor (gravitational constant).

DEFINITION OF SYMBOLS (Continued)

K	energy correction factor in parameter of stability in laminar radial flow.
k_g	thermal conductivity of aerosol carrier medium (gas).
$(k_g)_{tr}$	translational constituent of thermal conductivity of gas.
k_p	thermal conductivity of particulate material.
k'	dimensionless reduced thermal conductivity defined as the ratio of particulate to gas thermal conductivity.
L	precipitator plate separation.
M	molecular weight of the aerosol carrier medium (gas).
N_{Pr}	Prandtl number.
N_{Re}	Reynolds number.
P	pressure of the aerosol carrier medium (gas).
Q	volumetric flow rate of the aerosol.
R	universal gas constant.
r	radial coordinate or radial distance.
r_o	precipitor inlet radius.
r_d	deposit radius.
S	slip-correction factor.
T	absolute temperature of aerosol carrier medium (gas).
t	time.
t_f	transit time required for particulate to move from precipitator inlet to cold plate surface.
U	local (or point) fluid velocity.
U_{avg}	average fluid velocity [$U_{avg} = Q/A_x$].
U_{max}	maximum fluid velocity.
V	linear velocity.

DEFINITION OF SYMBOLS (Continued)

V_g	gravitational component of particulate velocity.
V_r	horizontal component of particulate velocity.
V_t	thermal component of particulate velocity.
V_y	vertical component of particulate velocity.
$\bar{v}$	mean molecular speed of gas molecule.
X_e	entrance length.
y	vertical coordinate or vertical distance measured from mid-plane of the precipitation region.
Z	mobility of particulate.
Z_s	particulate mobility corrected for slip effect.
Γ_i	temperature gradient of aerosol particle.
η	viscosity of aerosol carrier medium (gas).
λ	mean free path of aerosol medium (gas).
ρ	density.
ρ_p	particulate density.
σ	stability parameter, a modified Reynolds number for a diverging radial flow system.

TABLE OF CONTENTS

(Continued)

TABLE OF CONTENTS (Continued)

(Continued)

TABLE OF CONTENTS (Continued)

(Continued)

TABLE OF CONTENTS (Continued)

(Continued)

TABLE OF CONTENTS (Continued)

This report contains 144 pages.

LIST OF FIGURES

LIST OF FIGURES (Continued)

LIST OF TABLES

I. SUMMARY

Conflicts between experimental and theoretical results relative to thermal force phenomena have cast doubt upon the validity of both. For this reason a comprehensive experimental investigation was undertaken in an effort to reconcile observations with theory.

Currently accepted theory for systems of low Knudsen number predicts a thermal force which decreases with increasing particulate thermal conductivity. Earlier experimental studies utilizing either thermal precipitation or the direct observation of particulate behavior have produced results which generally support theory when materials of low thermal conductivity have been used. The thermal precipitation of aerosolized solids of high thermal conductivity has indicated forces greater than theoretical. Both of these distinctly different experimental techniques have been employed concurrently in this investigation.

The experimental results reported herein were characterized by inconsistencies similar to those of previous investigations, i.e., forces apparently independent of thermal conductivity and greater than values obtained by theoretical estimates. A detailed study of precipitated deposits and of the individual particulates provided a basis for the concept of an effective particulate thermal conductivity lower than that of the solid material due to the agglomeration of primary aerosol particles.

This observation permits the correlation of experimental observations with theory and provides an explanation of inconsistencies in experimental data which are believed to be superficial. The principal conclusions resulting from this investigation are that agglomerated solid particulate material may be thermally precipitated with an effectiveness much greater than would be predicted by theoretical estimates based on the thermal conductivity of the solid alone and that Epstein's theoretical equation is valid for thermal force estimations provided the effective particulate thermal conductivity is used in computations.

II. INTRODUCTION

There has long been a need for a better understanding of the force exerted on gas-suspended particulates in a nonuniform temperature field. Although a number of investigators have previously studied this force and have suggested mechanisms with which to describe it, experimental results have not been in accord with theory in certain cases, particularly with regard to the influence of particulate thermal conductivity. Whether this is a fault of the theory or of the experiment has not been clearly resolved.

In the past, experimental investigations of thermal force phenomena have pursued four avenues of approach, namely, (1) observations of vane radiometer effects, (2) studies of the dust-free space surrounding hot bodies, (3) analyses of thermal deposits, and (4) the direct observation of particulate behavior in gas suspensions under the influence of a temperature gradient. The first approach was of considerable value in the qualitative confirmation of early theories; but, because of increased interest in aerosols, it has recently given way to the latter approaches. In general, it has been reported that direct observation of particles in nonflowing systems tend to support currently accepted theories while results of experimental techniques involving dynamic or flowing aerosol systems do not. Especially notable discrepancies between theoretical and experimental results have been reported for the precipitation of materials of relatively high thermal conductivity. This suggests that a diminished effective thermal conductivity for a particulate in a dynamic system might bring the thermal precipitator data into agreement with that of static systems which support existing theories. An alternative explanation might lie in the hydrodynamics of a particular system. In view of these possibilities, a comprehensive study of thermal precipitator operation has been undertaken; the results of which are to be compared with observations of particle behavior in a nonflowing gas possessing a thermal gradient. The objective of the present study has been the reconciliation of experimental results and theory, thereby contributing to the elucidation of thermal force phenomena.

III. THEORY OF THERMAL FORCES

The thermal force may be defined as that force which causes a gas-suspended particle in a nonisothermal system to move in the direction of lower temperature. This thermal or radiometric force originates from the interaction of gas molecules with the particle surface, and its mechanism is dependent upon the Knudsen number, the ratio of the mean free path length of the gas to the particle radius. In the case of high Knudsen numbers, i.e., low pressures or very small particles at moderate pressures, the force can be considered due to the momentum impulses of the impinging and departing gas molecules. If one side of the particle is hotter than the other, or if there is a temperature gradient within the surrounding gas, the resulting inequality in a momentum balance over the two hemispheres of the surface defines the force. An alternate approach to the analysis of this thermal force mechanism employs the theory of thermal diffusion, in which very small particles are regarded as oversized gas molecules. On the other hand, when the system is characterized by a low Knudsen number, i.e., $\frac{\lambda}{a} \ll 1.0$, the force may be considered due predominantly to thermal slip streams which flow around the particle. These slip streams arise from a temperature gradient on the surface of the particle itself.

A. Historical Review

The study of thermal forces dates back to 1870 when Tyndall[34] observed the existence of a dust-free space around a heated wire suspended in a dusty atmosphere. He assumed that the dust-free region was caused by the incineration of the dust particles in the vicinity of the heated wire. Shortly thereafter, Lord Rayleigh[25] disproved Tyndall's theory by showing that small temperature differences between the wire and the surrounding air are sufficient to establish the dust-free space. Still later, Osborne Reynolds[26] suggested that a force was the cause of the phenomenon and proceeded to establish means by which it could be calculated. In 1879, Maxwell[21] expanded the theory in studies of stresses developed in nonuniformly heated gases. In 1910, Knudsen[18] developed an acceptable theory for thermal (radiometer) repulsion applicable to systems of very low

pressure. Einstein[10] was the first to produce an equation of qualitative validity. Because of the dual nature of the force mechanism, and of the variety of initial assumptions that may be made regarding the temperature gradients of the particle and the gas, a large number of thermal or radiometer force equations [1,3,10,11, 14, 15, 28, 35] have since appeared. The two which appear to be most accurate are those of Waldmann[35] (1959) and Epstein[11] (1929).

B. Theory of the High Knudsen Number Mechanism (Waldmann)

Waldmann's theoretical treatise deals with the case of high Knudsen number. His analyses, qualitatively simple but mathematically complex, are based on kinetic theory and the principles of thermal diffusion; his general thermal force equation is developed by a rigorous computation of the distribution function of a thermo-conducting gas in accordance with the Enskog-Chapman method.[4] He treats the special cases of thermal forces in a pure gas and in a flowing diffusing gas mixture. His force approximation is reported accurate within one per cent. For practical application in the pure gas suspension the translational constituent of the thermal conductivity of the gas must be known exactly--a requirement which is difficult to fulfill except for pure monatomic gases. The equation, based on the assumptions that the particle does not alter the distribution function of the gas and that its surface temperature corresponds to the local gas temperature, defines a force that is independent of the gas pressure and the nature of the particle. From equation 3.1 below, applicable to the case of the small particle in a nonflowing pure gas, it can be seen that the force is directly proportional to the temperature gradient, the square of the particle radius, and is a function of gas properties, including the translational constituent of thermal conductivity, molecular weight and the absolute temperature.*

$$(F_t)_W = -\frac{16}{15}\,\pi a^2 \sqrt{\frac{M}{2\pi RT}}\,(k_g)_{tr}\,\frac{dT}{dy} \qquad (3.1)$$

Equation 3.1 differs only in the magnitude of the numerical constant from

* Definitions of symbols are listed on pages iii - v.

an equation derived earlier by Einstein.[10]

It should be noted that the theoretical equation implies a temperature gradient not dependent upon internal heat transfer through the particle itself and the equation is thereby restricted to very small aerosol particles and low pressures. Waldmann's analysis is therefore of concern in this investigation only to the extent that it indicates a pressure and particle size limit of maximum thermal force for any specific system independent of the thermal conductivity of the particulate material.

C. Theory of the Low Knudsen Number Mechanism (Epstein)

The mechanism of thermal force for a system characterized by a low Knudsen number is subject to the more complex considerations of thermal creep flow and temperature distribution on the particle surface. Epstein[11] has made a very thorough hydrodynamic analysis of this mechanism. He has assumed a temperature gradient on the particle surface related by thermal transport to that of the gas and thereby has introduced into his force equation the thermal conductivities of both the particle and the gas. Epstein's equation shows a thermal force directly proportional to the particle radius, gas temperature gradient, and gas viscosity; inversely proportional to the molecular weight and pressure of the gas; and markedly dependent upon the relative values of the thermal conductivities involved. The equation is

$$(F_t)_{Ep} = \frac{9\pi R\eta^2 a}{MP} \left[\frac{k_g}{2k_g + k_p} \right] \frac{dT}{dy} \qquad (3.2)$$

Since this is the equation which has been selected as the theoretical standard for comparison with regard to the influence of particulate thermal conductivity, a review of the fundamental assumptions in its derivation is in order. The system has been defined as a spherical particle suspended in a motionless homogeneous gas. It has been stipulated that the radius of the particle is large relative to the mean free path length of the gas molecules so that the fluid may be regarded as a continuum. By assuming no convection, i.e., the temperature gradient increasing upward, and by neglecting

thermal radiation from the particle, the temperature gradient, Γ_i, of the particle may be related to that which exists within the gas, dT/dy, in the following manner:

$$\Gamma_i = \left[\frac{3k_g}{2k_g + k_p} \right] \frac{dT}{dy} \qquad (3.3)$$

This term, $3k_g/(2k_g + k_p)$, may be regarded as a coefficient which adjusts the magnitude of the thermal force according to the relative internal and external heat transfer characteristics. The practical applicability of Epstein's equation hence depends upon the validity of the mathematical model and demands a precise knowledge of the thermal conductivity of the particle.

D. Thermal Force in the Knudsen Number Region Near Unity

Each of the previously discussed mechanisms was selected for mathematical convenience as the most realistic analytical model for the region concerned. In the intermediate Knudsen number region (i.e., near unity) neither alone adequately describes the phenomena of thermal force. Physically, there is no distinct limit to the applicability of either mechanism, but rather a smooth transition between the two, in a sense analogous to the mechanisms of the drag force (i.e., the resistance to the movement of a particle suspended in a fluid). It can be seen by comparison of thermal force and drag force equations (3.1 and 3.2 with 3.4 and 3.5, respectively) that the two forces are dependent upon particle radius functions of the same order in both the high and low Knudsen number region.

Drag Force:

High Knudsen number: $$F_d = \frac{6\pi\eta V a^2}{\lambda(A+B)} \qquad (3.4)$$

Low Knudsen number: $$F_d = 6\pi\eta V a \qquad (3.5)$$

The transition from equation 3.5 to equation 3.4 may be accomplished by the inclusion of a slip correction[19] to give equation 3.6, which accurately describes the drag force in the region of Knudsen numbers near

unity.

$$F_d = \frac{6\pi\eta Va}{1 + \frac{\lambda}{a}\left[A + Be^{-C\frac{a}{\lambda}}\right]} \qquad (3.6)$$

When the Knudsen number, $\frac{\lambda}{a} \gg 1$, equation 3.6 reduces essentially to equation 3.4.

The transition of thermal force equations in the intermediate region is not so easily accomplished. The inclusion of a simple correction factor for slip effect is insufficient because of the complexity of the development of an internal temperature distribution and thermal equilibrium between the gas and the particle which is a basis for the mechanism described by Epstein's equation. A composite correction factor with components which provide separately for viscous slip effects and particulate temperature development might correlate the two analytical concepts; such a factor has not yet been developed.

It is convenient to consider thermal force in the domain of transition Knudsen numbers as an interplay of the individual mechanisms, with the contribution from each diminished to some extent. Hettner[15] has developed a composite equation after this fashion to describe the related phenomenon of photophoresis (discussed below). The expression, being a critical function of the Knudsen number, reduces to an appropriate equation at either extreme. The term in Hettner's equation which becomes more significant in the high Knudsen number region is directly proportional to pressure, in accordance with the observations and theories of several investigators, including Rubinowicz.[28] This pressure influence in photophoresis is basically different from the pressure independence of thermal force defined by Waldmann.[35] The physical validity of the pressure effect upon thermal force has been critically examined by Schmitt,[32] who accepts Waldmann's theoretical conclusion but states that pressure independence is to be expected only when the mean free path of the gas is so great that the molecules in proximity to the particle do not interfere with each other. When the population of molecules becomes sufficiently dense, the distribution function of the gas is changed in such a manner as to

decrease the thermal force. Thus, one must anticipate a force essentially constant for large values of $\frac{\lambda}{a}$, but always increasing with decreasing pressure. An equation suitable for all Knudsen numbers should reduce to Waldmann's equation for $\frac{\lambda}{a} \gg 1$, to Epstein's equation $\frac{\lambda}{a} \ll 1$ and, according to Schmitt, be a rapidly changing inverse function of pressure in the transition region.

E. Photophoresis

Closely related to the thermal force mechanism is the phenomenon of photophoresis, which is the name applied to the motion of particles in the direction of a light beam penetrating the suspension medium. The causitive transport mechanism is identical to that of thermal force. In photophoresis, however, the temperature distribution on the particle surface is the result of unidirectional thermal irradiation. Due to refraction in a transparent particle, it is possible for the side opposite the light source to be subjected to irradiation more intense than that impinging upon the front surface. It has been observed that photophoretic migration may be either positive or negative, i.e., directed toward or away from the radiation source, depending upon the orientation of the temperature gradient. Hence more properties of the system, including the radiation-focusing properties of the particle, are involved in photophoresis; and its analysis is proportionally more complex. This investigation is not directly concerned with photophoresis, however.

IV. EXPERIMENTAL OBSERVATIONS OF OTHER INVESTIGATORS

Experimental observations independent of this investigation are reviewed briefly herein to establish (1) the validity of theoretical analyses and (2) the quantitative inconsistencies which have been reported. With this purpose in mind, the review is restricted primarily to the investigations of particulate behavior, omitting much of the earlier work on vane radiometers.

A. Observations on the Dust-Free Space Phenomena

Prior to 1945 thermal force studies had dealt with clouds of particles. With regard to the influence of particulate thermal conductivity, the only experimental contribution was made by Watson[36] in his study of the dust-free space surrounding hot bodies. He observed that the nature of the particulate cloud did not affect the thickness of the dust-free space, reporting a variation in its width of less than 3 per cent (within his experimental error) for aerosols of different substances such as magnesium oxide, flint dust, carbon black, tobacco smoke and sulfur "smoke." His observations suggest a thermal force independent of particulate thermal conductivity, at least for the range investigated. The suggested independence is conjectural however and will be discussed later. Zernik,[37] in a theoretical analysis of the dust-free space phenomena, derived an equation for computing the width of the dust-free space. By assuming a zero conductivity for the particulate material, he obtained a magnitude supported by the data of Watson.

B. Direct Observation of Particulate Behavior by Rosenblatt and LaMer

In 1945, Rosenblatt and LaMer[27] introduced a new technique into the study of thermal forces by using an adaptation of the Millikan oil drop experiment to observe directly the behavior of a particle in a thermal field. By measuring the difference in the velocities of a free-falling particle and of the same particle under an imposed temperature gradient, the thermal force was deduced. Experimental results covering a Knudsen number range from 0.04 to 1.5 have been reported in terms of thermal velocity dependence upon temperature gradient, gas pressure, and particle radius. The conclusions may be summarized as follows. The thermal velocity and, hence the force, were found directly proportional to the temperature

gradient. Both the thermal velocity and force were approximately inversely proportional to pressure for Knudsen numbers less than 0.5. The thermal velocity for constant pressure increased with decreasing particle radius to a maximum for $\frac{\lambda}{a} \approx 1.5$ and thereafter decreased. The direct proportionality of thermal force to particle radius was confirmed indirectly for Knudsen numbers less than 0.5 by the experimental observation of a linear relationship between particle size and the thermal velocity divided by the slip factor. The fundamental properties of Epstein's equation were therefore substantiated. Experimental and theoretical force magnitudes were reported different by a factor of two, which the authors considered satisfactory agreement in view of the uncertainty in the thermal conductivity of the tricresyl phosphate droplets (estimated from an empirical equation to be 4.8×10^{-4} cal/cm sec ^{o}K) and the approximations in theoretical derivations.

C. Direct Observation of Particulate Behavior by Saxton and Ranz

The available data on thermal forces were extended in 1952 by Saxton and Ranz,[29] who also employed an adaptation of the Millikan experiment with the specific objective of investigating the effect of particle size, temperature gradient and aerosol material. These experiments, conducted with castor oil and paraffin oil droplets (thermal conductivities of 4.3×10^{-4} and 2.95×10^{-4} cal/cm sec ^{o}K, respectively) at atmospheric pressure, were characterized by Knudsen numbers ranging from 0.0615 to 0.277. Their results, in agreement with those of Rosenblatt and LaMer,[27] indicated a thermal force directly proportional to both temperature gradient and particle radius. In addition, the force was found to be an inverse function of the thermal conductivity of the aerosol material. The agreement between experimental data and Epstein's theory was satisfactory, with average deviations within a probable experimental error of 20 per cent.

D. Investigation of Thermal Precipitation by Schadt and Cadle

In 1956 Schadt and Cadle[30] conducted an experimental investigation of thermal precipitation, using particulate materials of widely varying thermal conductivity. The investigation was prompted by the conspicuous absence of published reports that confirmed the difficulty of collecting

aerosol particles having high thermal conductivity as suggested by Epstein's equation. The experimental results, based on measurements of the precipitated deposit, essentially confirmed the theoretical effect of particle size and temperature gradient on thermal forces. Also, a decrease in thermal force associated with higher particulate thermal conductivity was observed in accordance with theoretical concepts. However, the apparent magnitude of the forces on sodium chloride and iron particles were reported on the average 30 to 40 times the value predicted for their conductivities of 1.55×10^{-2} and 0.16 cal/cm sec $^{\circ}$K, respectively. On the other hand, quantitative agreement between experimental results and Epstein's theoretical value was reported for stearic acid, which has a very low thermal conductivity (3.0×10^{-4} cal/cm sec $^{\circ}$K). The average apparent magnitude of the thermal forces in this case ranged from 76 to 96 per cent of the theoretical value, depending upon the particle size, with closest agreement being reported for the smallest particles (radius = 0.3 micron). Maximum deviations from the average experimental data were sometimes as high as 90 per cent. Precipitation was effected at atmospheric pressure in all cases, and the characteristic Knudsen number ranges were 0.026 to 0.435, 0.326 to 0.653 and 0.131 for the stearic acid, sodium chloride and iron aerosols, respectively.

E. Direct Observation of Particulate Behavior by Schmitt

An experimental investigation by K. Schmitt,[32] specifically oriented toward the confirmation of Waldmann's theory (equation 3.1), produced excellent quantitative agreement (5 per cent deviation) between experimental and theoretical results for small particles in a static pure monatomic gas. However, experimental force magnitudes for particles in pure polyatomic gases were found less than Waldmann's theoretical values by as much as 20 per cent--a discrepancy attributed to inaccurate approximations of the translational constituent of thermal conductivity. Schmitt was particularly concerned with force and velocity dependence upon the gas pressure, the particle radius, and the nature of both the particle and the gas. He concurs with Waldmann's theoretical concept of a pressure independent thermal force in the high Knudsen number region and, in fact, shows experimentally that the force approaches a constant value with decreasing pressure when $\frac{\lambda}{a} > 2.0$. Schmitt further presents a hypothesis

based on alteration of the distribution function explaining an observed exponential decrease in thermal force as the pressure increases into the transition region. The linear dependence of thermal force on surface area, i.e., a^2, also has been supported by his experimental observations over a relatively narrow particle size range. Furthermore, he has concluded from observations in the high Knudsen number region that this thermal force is, in fact, independent of the thermal conductivity and the accommodation of the particle; while the thermal velocity, as theorized, is dependent upon both the accommodation coefficient and pressure.

Schmitt's investigation was extended to include the domain of mean free path lengths small relative to particle radius, supplementary to his study of the high Knudsen number region. Experimental results in this case tended to support the theory of Epstein. That is, the data indicated the proper qualitative relationships between thermal force, the associated thermal velocity, and the variables of pressure, particle radius, and particulate thermal conductivity. The quantitative agreement of experimental and theoretical values was generally not so close as in the case of high Knudsen numbers. Schmitt's experimental velocities for a given material suspended in a number of gases exhibited deviations from theoretical velocities, sometimes positive and sometimes negative, by as much as 45 per cent. In the case of an oil droplet suspended in argon however, his experimental thermal velocity was only 3 per cent below the theoretical value. Thermal velocity data for four different materials in argon, while qualitatively consistent with theory, indicated an extreme velocity variation due to particulate thermal conductivity about 30 per cent less than would be expected from quantitative application of Epstein's equation.

The data accumulated by Schmitt also defined the transition region of the thermal force mechanism, at least for the aerosols investigated. The experimental relationships between thermal force, velocity, pressure, and particle radius indicate that the transition occurs within the range $0.05 < \frac{\lambda}{a} < 0.2$, but that the force in the region of $\frac{\lambda}{a} > 0.2$ is still somewhat diminished by the altered distribution function and becomes essentially constant only for $\frac{\lambda}{a} > 3.0$. Furthermore, it appears that the influence of particulate thermal conductivity decreases as $\frac{\lambda}{a}$ increases beyond 0.12.

F. Review of Independent Experimental Observations

In retrospect, all data obtained by direct observation utilizing a Millikan-type thermal cell, including that of Schmitt, Rosenblatt and LaMer, and Saxton and Ranz, pertain to a static (nonflowing) aerosol system and are limited to some extent by the following considerations: (1) Particle behavior was observed under conditions of a relatively low temperature gradient ($\frac{dT}{dy} < 150^{\circ}C/cm$) where the thermal component of velocity is small compared to the gravitational component. (2) A narrow range of relatively low thermal conductivities was studied. The observations of Schadt and Cadle, on the other hand, pertain to a dynamic (flowing aerosol) system with relatively high temperature gradients (1600° to $9800^{\circ}K/cm$). Also, only Schadt and Cadle have investigated the force on materials outside the limited thermal conductivity range from 2.9×10^{-4} to 6.0×10^{-4} cal/cm sec $^{\circ}K$.

Schmitt alone has dealt extensively with the high Knudsen number mechanism; however, his results provide substantial evidence of the validity of Waldmann's equation. As far as the low Knudsen region is concerned, there is consistent confirmation of Epstein's theory in respect to the effect of temperature gradient, particle radius, and gas pressure except insofar as Rosenblatt and LaMer have reported a maximum in the thermal velocity versus particle radius curve for low pressures. With regard to the influence of particulate thermal conductivity, most investigators, with the notable exception of Watson, have obtainded data which provide qualitative support of the relationship proposed by Epstein. Furthermore, in the case of particulates of very low thermal conductivity, agreement between experiment and theory is quantitatively satisfactory. The greatest inconsistency appears in the thermal precipitation of sodium chloride and iron where the experimental forces seem to be many times greater than theoretical values. In evaluating this observation several facts should be kept in mind: (1) The system involved a flowing aerosol in which hydrodynamic considerations complicate the resolution of thermal forces; (2) these were the only thermal force data reported for materials of high thermal conductivity; (3) the Knudsen numbers for these forces are characteristic of a region in which thermal conductivity influence may not be

fully developed, if Schmitt's observation may be extrapolated to this extent; and (4) the particulate material was a solid.

The considerations previously discussed give rise to speculation concerning the apparent inconsistency between theory and experiment. Does Epstein's relationship fail in the case of aerosols of high particulate thermal conductivity, or have superficial factors, such as inaccurate hydrodynamic or heat transfer assumptions, in the analytical interpretation of data led to erroneous thermal force values? With this question in mind, this investigation of thermal forces was undertaken utilizing the experimental techniques of both direct particle observation and analysis of thermal precipitation. Conclusions were then to be based on comparison of the results obtained in each case for several aerosolized materials of widely varying physical properties.

V. EXPERIMENTAL METHODS AND EQUIPMENT

A. General Approach

The general experimental approach is easily visualized. An aerosol is generated and subjected to a thermal field. The resulting thermal force causes migration of the suspended material. In the direct observation experiment the velocity of particulate migration is measured and the magnitude of the force deduced. In thermal precipitation the particulate material is deposited upon a cold surface. From measurements of the radius of the deposit, the velocity component in the direction of the temperature gradient is computed and the force is subsequently evaluated.

While the approach in either case is similar, there are distinct limitations on each which make difficult a direct comparison of results. These limitations can be more clearly defined after the details of the equipment and procedures have been discussed.

B. Direct Observation of Particulate Behavior (Modified Millikan Experiment)

For the direct observation of particulate behavior the adaptation of the Millikan method was used. This method employs an electrostatic field for the manipulation of a charged particle. The particle is observed through the technique of dark field illumination. The adaptation provides for the establishment of a temperature gradient in the gas surrounding the particle through controlled heating and cooling of the electrodes.

1. Modified Millikan Apparatus

The modified Millikan apparatus is shown in Figure 1. The essential elements of the device which provide for optical viewing and electrostatic field control are schematically illustrated in Figure 2. The central cell in this apparatus was specially designed for thermal force determinations as shown in Figure 3. Two cylindrical brass electrodes, one inch in diameter, were positioned concentrically, one above the other, with a separation of 0.075 cm. The upper electrode contained a resistance coil for electrical heating, and the lower one was equipped for cooling with an internal water jet. A small centering electrode was installed in the surface of the lower principal electrode to prevent the loss of the particle being observed through lateral drifting. Copper-constantan thermocouples

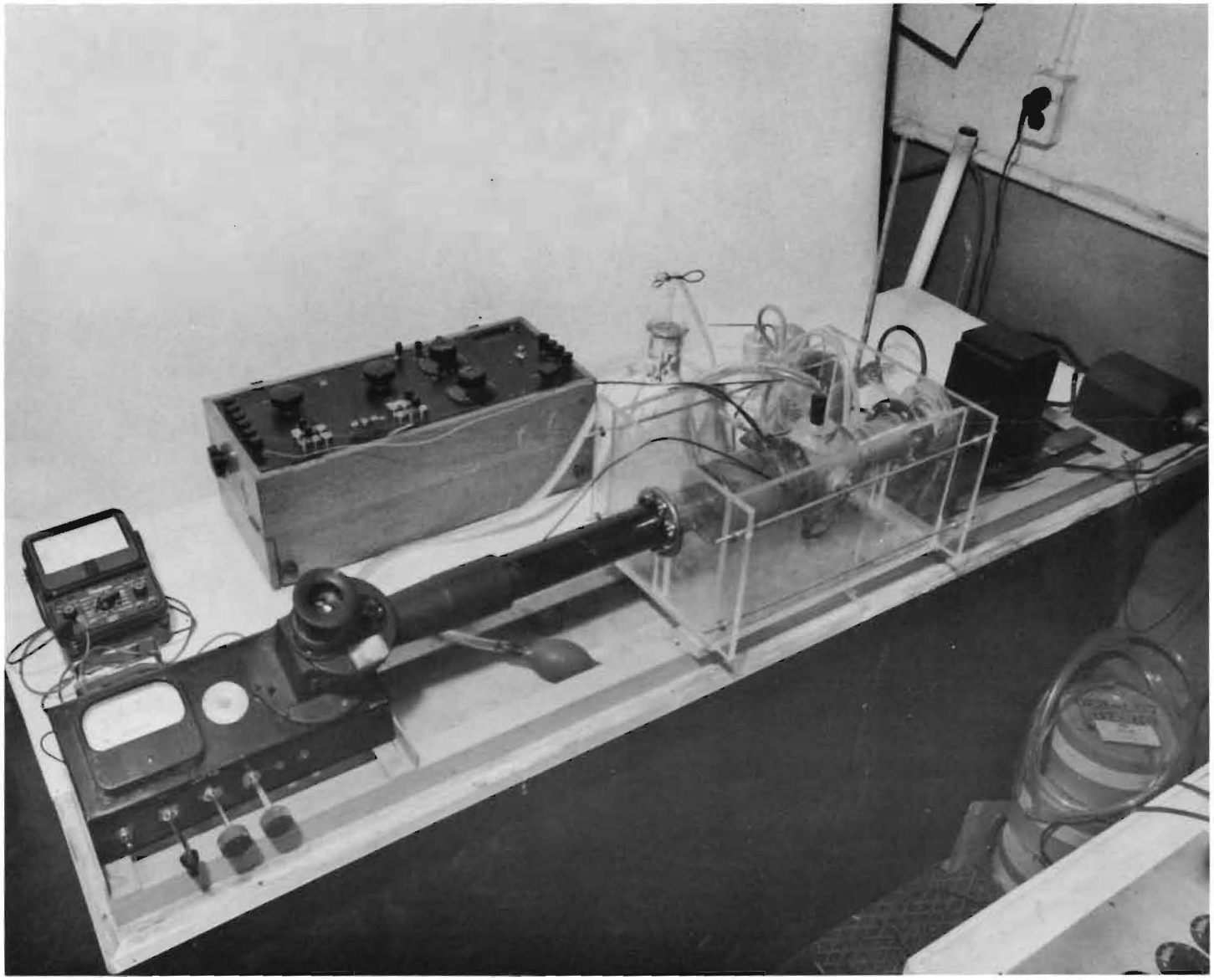

Figure 1. Modified Millikan Apparatus. This device, designed for the direct observation of suspended particulates, has been adapted for thermal force studies by the installation of a central thermal cell.

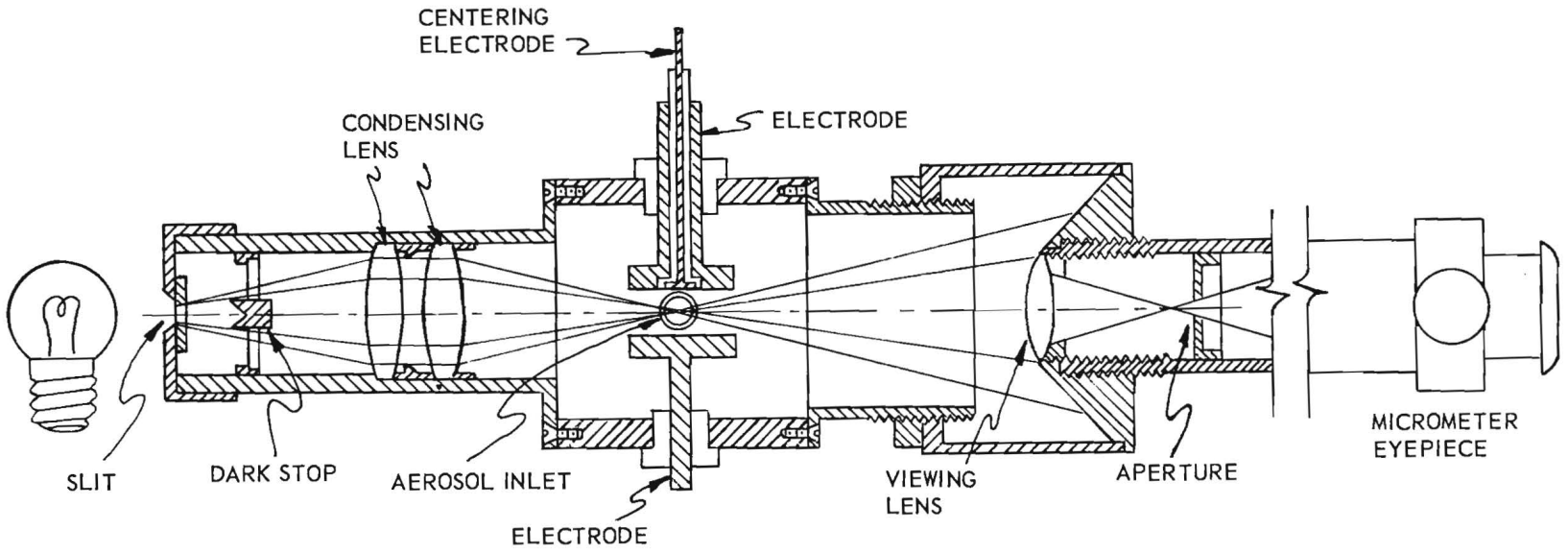

Figure 2. Essential Elements of Modified Millikan Device. Shown above is a schematic diagram of the optical system providing dark field illumination of suspended particulates.

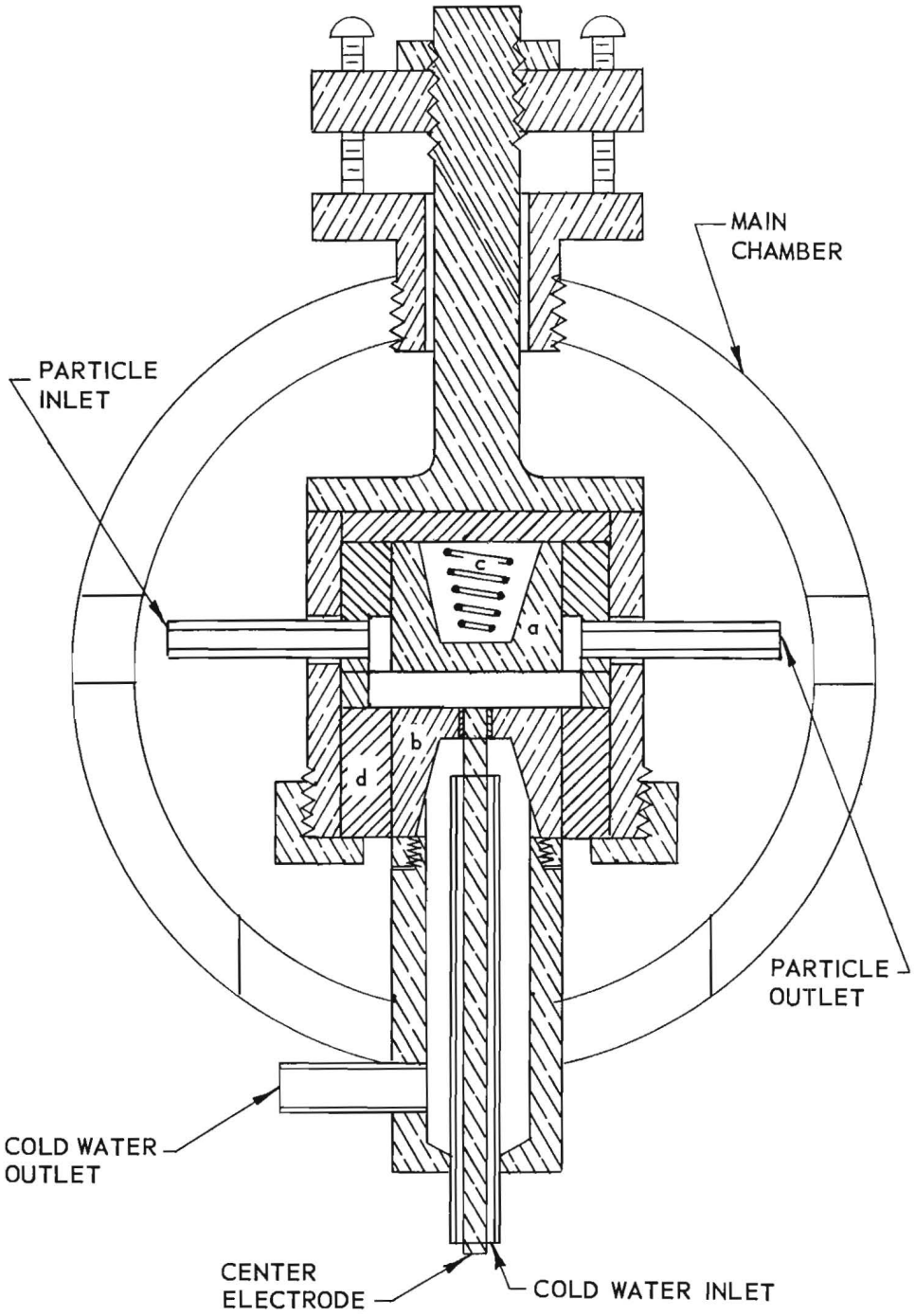

a – UPPER ELECTRODE
b – LOWER ELECTRODE
c – HEATER
d – BAKELITE INSULATION

Figure 3. Detail of Central Cell of Modified Millikan Apparatus. This thermal cell, containing electrodes and temperature control elements, was installed in the objective section of a conventional Millikan apparatus.

were inserted near the inner surfaces of both electrodes for temperature measurement. The electrodes were encased in Bakelite shells and the unit was rigidly mounted in a brass case. The complete assembly was suspended in the main chamber of the Millikan apparatus. A water bath was provided for shielding the main chamber from ambient room temperature changes.

2. Experimental Procedure

Charged aerosol particles to be studied in this apparatus were introduced into the central cell in very dilute concentration. A single particle was snared in the electrostatic field and suspended between the principal electrodes. In this position the particle, observed through the optical system, could be raised or lowered by altering the electrical field strength. The effective diameter of the suspended particle was determined from repeated measurements of its terminal velocity under the influence of gravity in the absence of a temperature gradient. This was accomplished by turning off the current to the electrodes and timing the vertical descent of the particle between the calibrated cross-hairs of the micrometer eyepiece. In this manner particulate behavior could be observed as many times as desired by reapplying the electrical field to reposition the particle and to avoid its contact with the electrode surface. After the diameter of the particle had been determined, a thermal field was established and another series of velocity measurements was obtained. From this second series of measurements the thermal velocity component was resolved.

Under usual operating conditions, the upper electrode was grounded and the lower principal electrode voltage was adjusted to provide a potential difference in the range from 0 to 300 volts as required for particle suspension. The small centering electrode was maintained within $\pm$ 5 volts of the lower electrode potential. Temperature differences between hot and cold surfaces ranged up to $7^{\circ}C$. A series of eight to ten measurements were ample for particle size determination and as many measurements as possible were obtained under the influence of the thermal field. The optical system had a relatively short depth of field and the series of thermal velocity data was usually terminated after four or five measurements by the particle's escape from the zone in focus due to the excessive

lateral drift which occurred in the nonisothermal system.

C. Thermal Precipitation

For thermal precipitation studies, a number of precipitator designs are available, including models of various geometric configurations with heating elements consisting of wires, ribbons, or plates. Regardless of the design, the operating principle is the same in all cases. A thermal field, i.e., a temperature gradient in the gas, is established by flowing an aerosol between surfaces of different temperatures. Thermal forces cause the gas-suspended particles to move toward, and ultimately to precipitate upon, the cooler surface.

1. Radial Flow Thermal Precipitator (Model I)

The thermal precipitator initially selected for the experimental phase of this investigation (Model I shown in Figure 4) was a radial flow type consisting essentially of two horizontal circular plates concentrically mounted in such a way that the separation between plates could be varied by the insertion of shims. General construction details are presented in Figure 5. The uppermost plate was electrically heated. The lower plate, recessed to accommodate a removable glass collecting disk, was water cooled. The hot plate temperature was controlled by a variable transformer and was continuously monitored with an assembly consisting of a thermocouple, an automatic potentiometer, and an ammeter. The cold plate temperature was regulated by cooling water.

2. Precipitator Operation and Experimental Procedure

In operation, an aerosol was introduced through an inlet in the center of the hot plate; it flowed radially between the hot and cold surfaces; the particulate matter was precipitated upon the cold plate (glass disk); and the gas was subsequently exhausted from the system. Typical particulate paths are shown in the schematic diagram of Figure 6.

The precipitator was prepared for operation by inserting a clean glass collecting-plate moistened on both sides with Kel-F 3 (fluorocarbon oil, M. W. Kellog Company) to insure adequate thermal contact and retention of impinged particles. The temperatures of the hot and cold plates were set for the desired thermal gradient, and the system was allowed to come to thermal equilibrium. In collecting experimental data, the

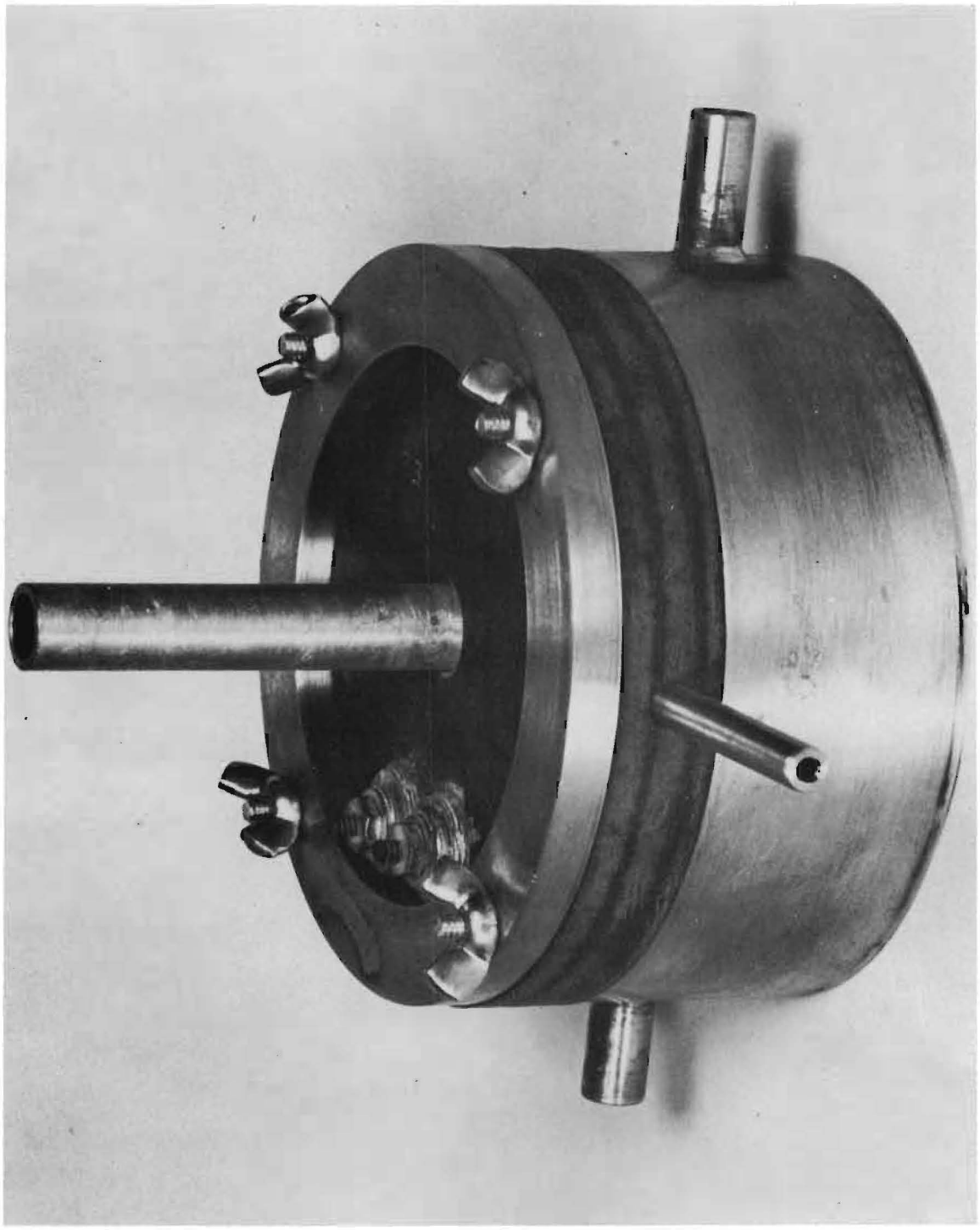

Figure 4. Radial Flow Thermal Precipitator (Model I).

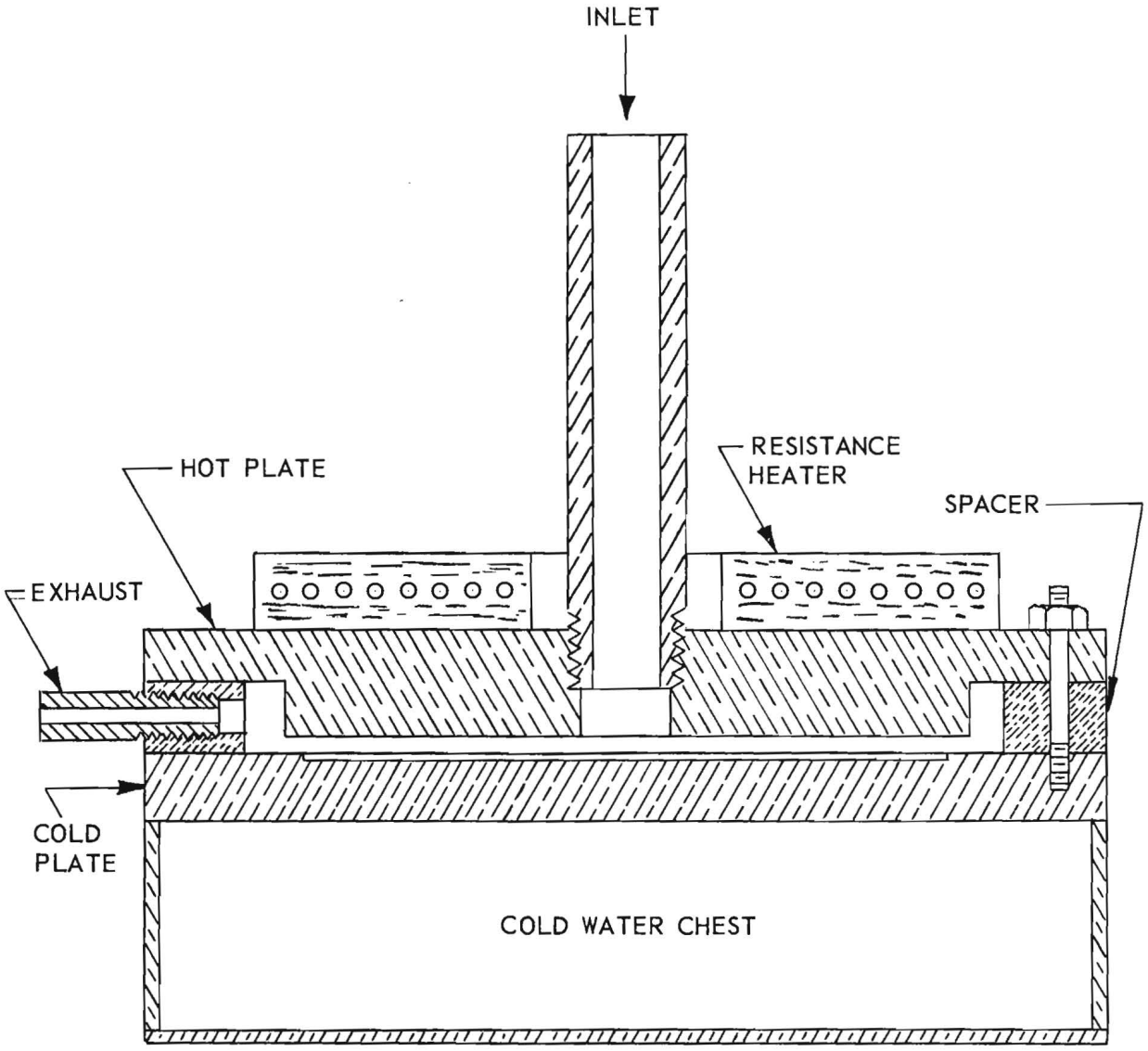

Figure 5. Thermal Precipitator Detail (Model I).

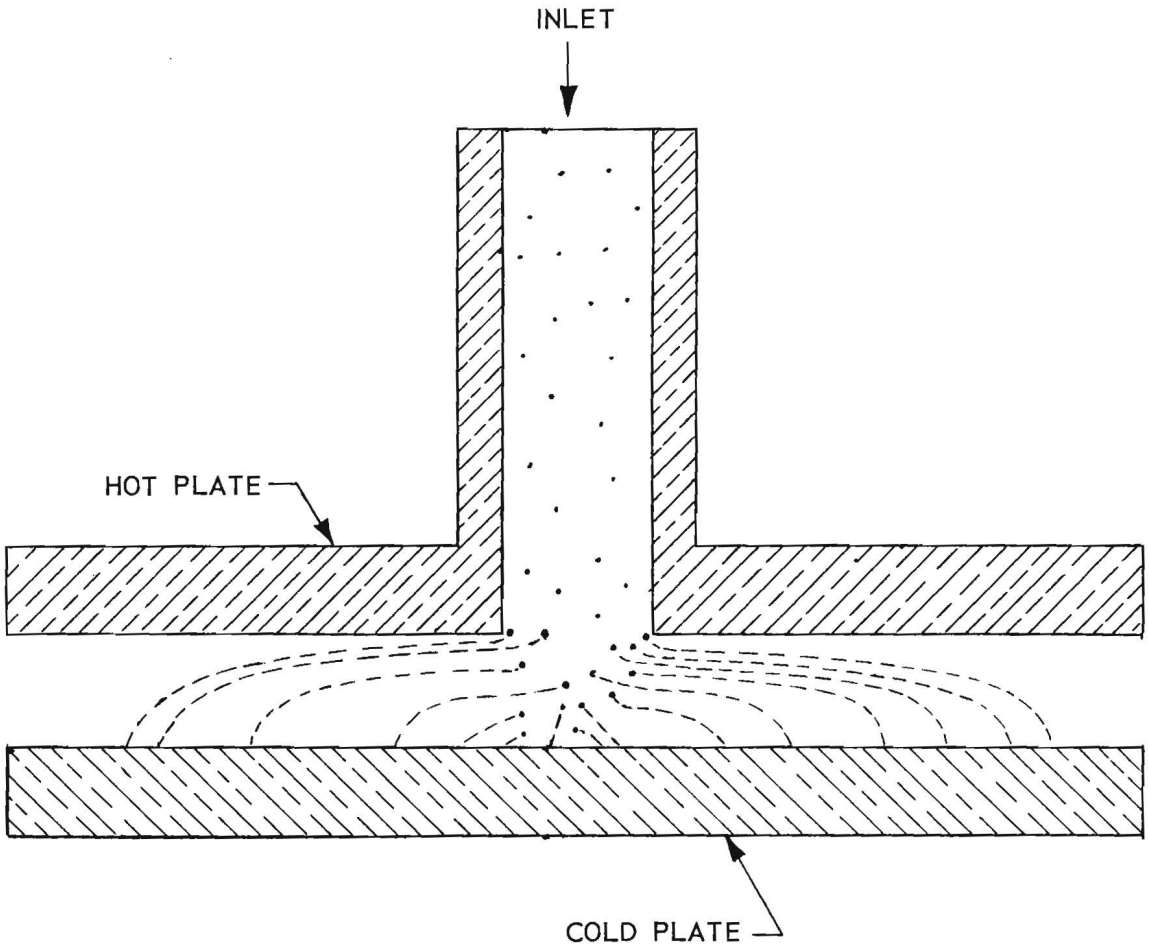

Figure 6. Schematic Diagram of Thermal Precipitator Showing Typical Particulate Paths.

following procedure was employed. An aerosol of the test material was generated and metered through the precipitator at a constant flow rate. The particulate material was deposited, and the collecting disk was subsequently removed for analysis. Figure 7 is a photograph of the glass collecting-disk showing a typical deposit. Experimental results, i.e., thermal velocities and forces, were then computed from the maximum deposit width. This width, measured radially from the point of particulate entry to the point of precipitation, is established by those particulates traveling the greatest distance.

3. Radial Flow Thermal Precipitator (Model II)

As can be seen in Figure 6, particulates traveling the maximum distance must have entered the precipitation zone nearest the heated surface at the outer radius of the inlet. Particulates entering at other points are precipitated at shorter radii. This means that only the outer extremity of the deposit has significance. Also, it is evident that the temperature gradient does not begin abruptly at the point of entry between precipitator plates; rather, the entire inlet tube becomes heated and, due to the dust-free space effect, particulates are limited in their approach to the heated surface. Thus there is reason to suspect that those observed at the outer periphery of the deposit may have entered the region between precipitator plates at some point below the hot plate. To avoid this uncertainty, and further, to utilize deposit measurements obtained at radial distances other than that of the outer periphery, another radial flow precipitator, Model II, shown partially disassembled in Figure 8, was designed to restrict the variation in entrance conditions.

Figure 9 is a cross-sectional view of the modified precipitator, which is similar to Model I except that the inlet stream is composed of two parts. One portion of the stream containing particulates enters around the side of the inlet valve and emerges into the precipitation zone between the valve lip and the hot plate. A second phase of particle-free gas enters the precipitation zone from within the valve stem. This stream prevents the development of turbulence at the valve lip. By adjusting the micrometer, the valve lip is brought near the hot plate surface, forcing all particulates to enter the precipitation zone essentially at the same level. Experiments

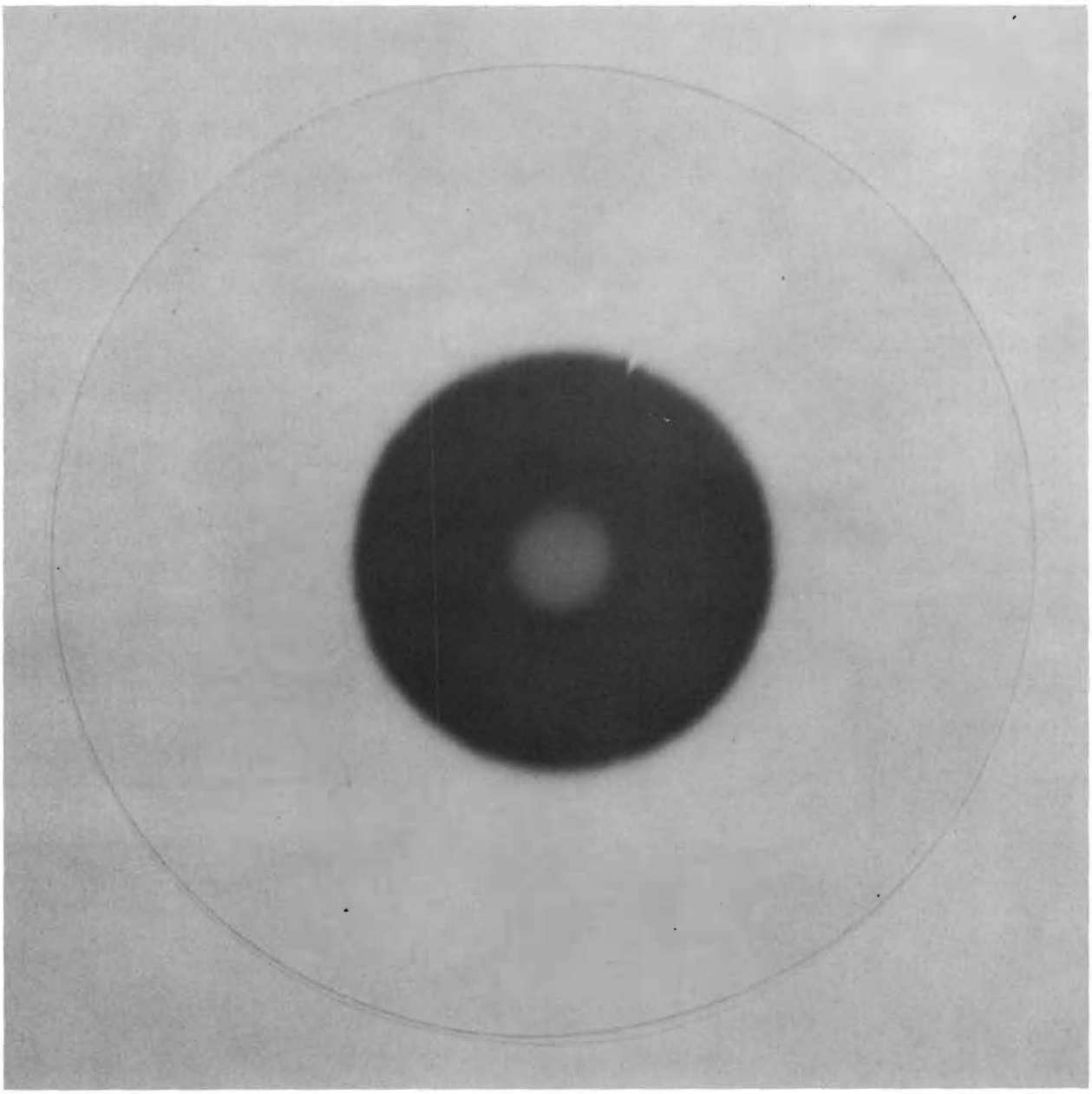

Figure 7. Collecting Plate from a Thermal Precipitator Showing Particle Deposit in the Center.

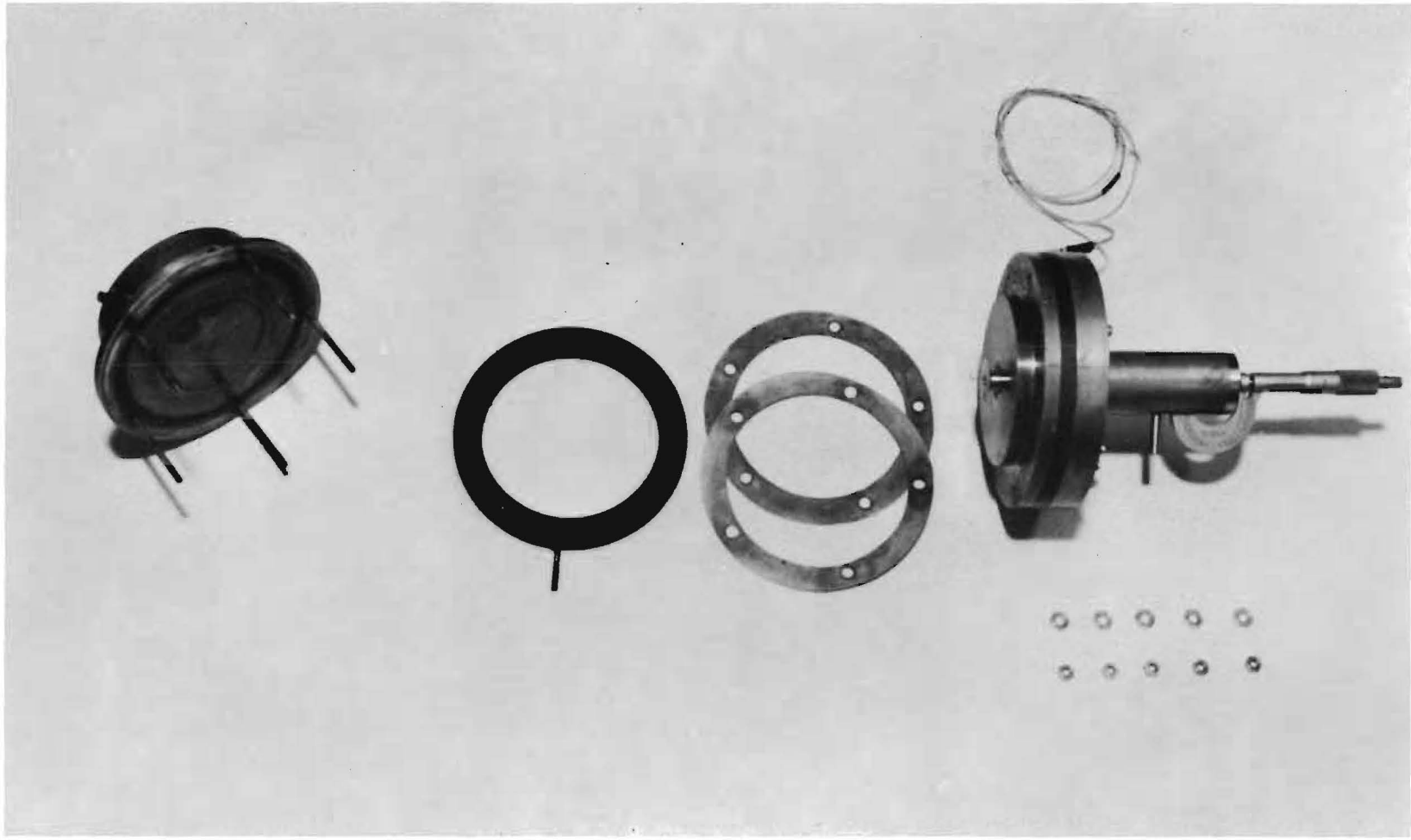

Figure 8. Modified Radial Flow Thermal Precipitator Partially Disassembled (Model II).

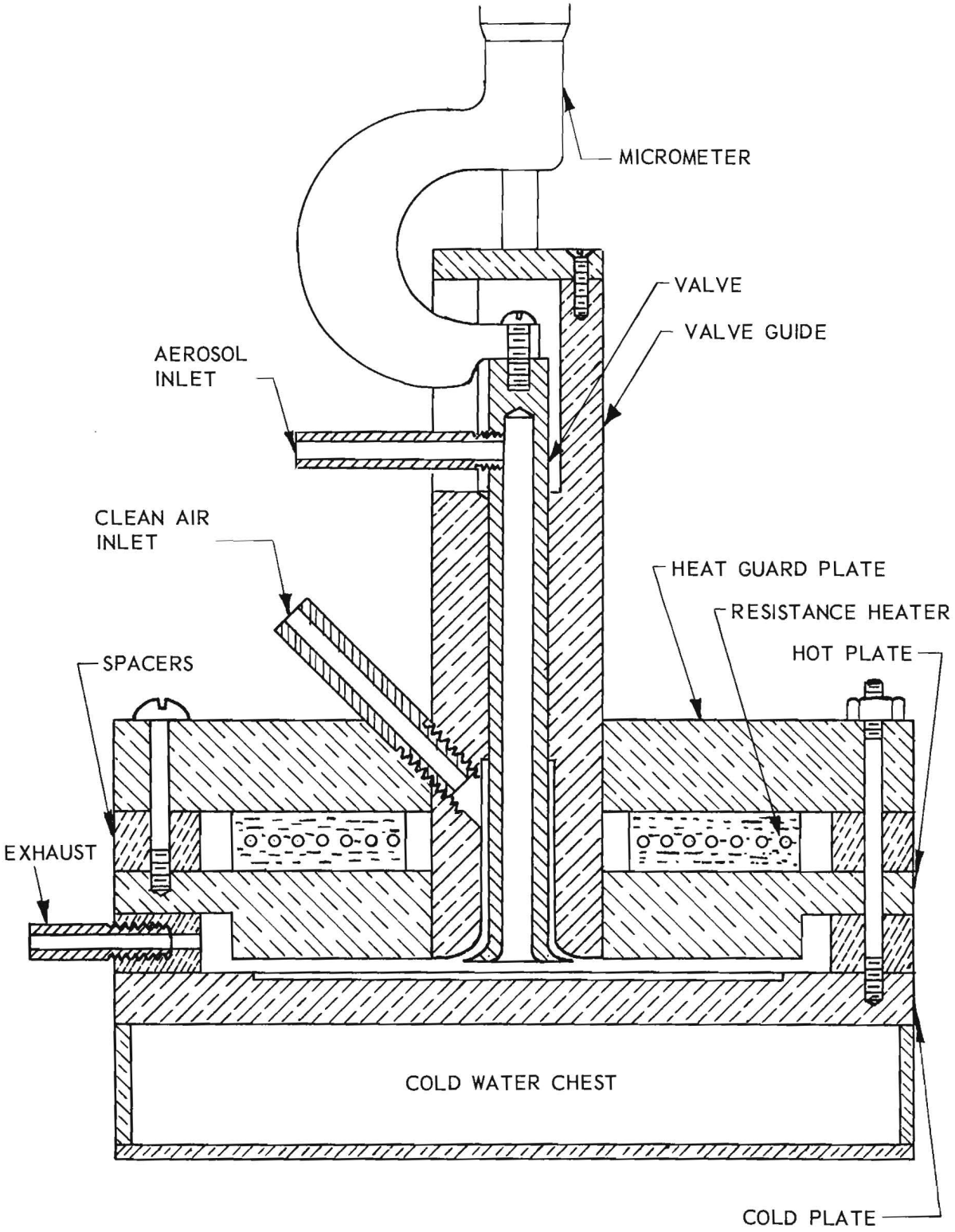

Figure 9. Modified Thermal Precipitator Detail (Model II).

showed that it was possible to limit the particle entrance to 0.005 cm from the upper surface. Other than for the adjustment of the inlet stream, operation of Model II thermal precipitator is identical to that of Model I.

4. Linear Flow Thermal Precipitator (Model III)

As will be shown in the next section, the computations of thermal velocity and force from precipitation data involve a number of simplifying assumptions due to the complexity of a precise mathematical analysis of the fluid flow and heat transfer in the radial flow system. In an effort to facilitate the mathematical analysis, a rectilinear flow thermal precipitator, Model III, was designed and constructed. A schematic diagram of this unit is shown in Figure 10. However, the deposits obtained with this precipitator were not amenable to precise physical analysis, and the data obtained with it were of little additional value.

D. Auxiliary Equipment

In addition to the principal experimental devices described above, auxiliary equipment was needed for the generation of aerosols and for the control of aerosol flow rates. Four techniques were utilized in the generation of aerosols. Magnesium oxide aerosols were prepared by burning magnesium in air or oxygen. Powdered materials, including aluminum oxide, zinc, aluminum, iron, and graphite were atomized with compressed air using a Holmspray Powder Atomizer No. 520-1. Sodium chloride aerosols were formed by the evaporation of finely dispersed solution droplets generated with a DeVilbis Nebulizer No. 180. Finally, aerosols of very finely divided materials, including platinum, silver, sodium chloride, and the oxides of magnesium, aluminum, iron and bismuth were produced by an exploding wire technique.

The exploding wire device, constructed for use in another investigation, made possible the generation of metallic aerosols by vaporizing electro-conducting materials and condensing the product. A sudden release of electrical energy provides the heat of vaporization and, also, the explosive force which disperses the particulate material. The essential elements of this aerosol generator are a high voltage power supply, a capacitor bank and an explosion chamber. The system is capable of delivering

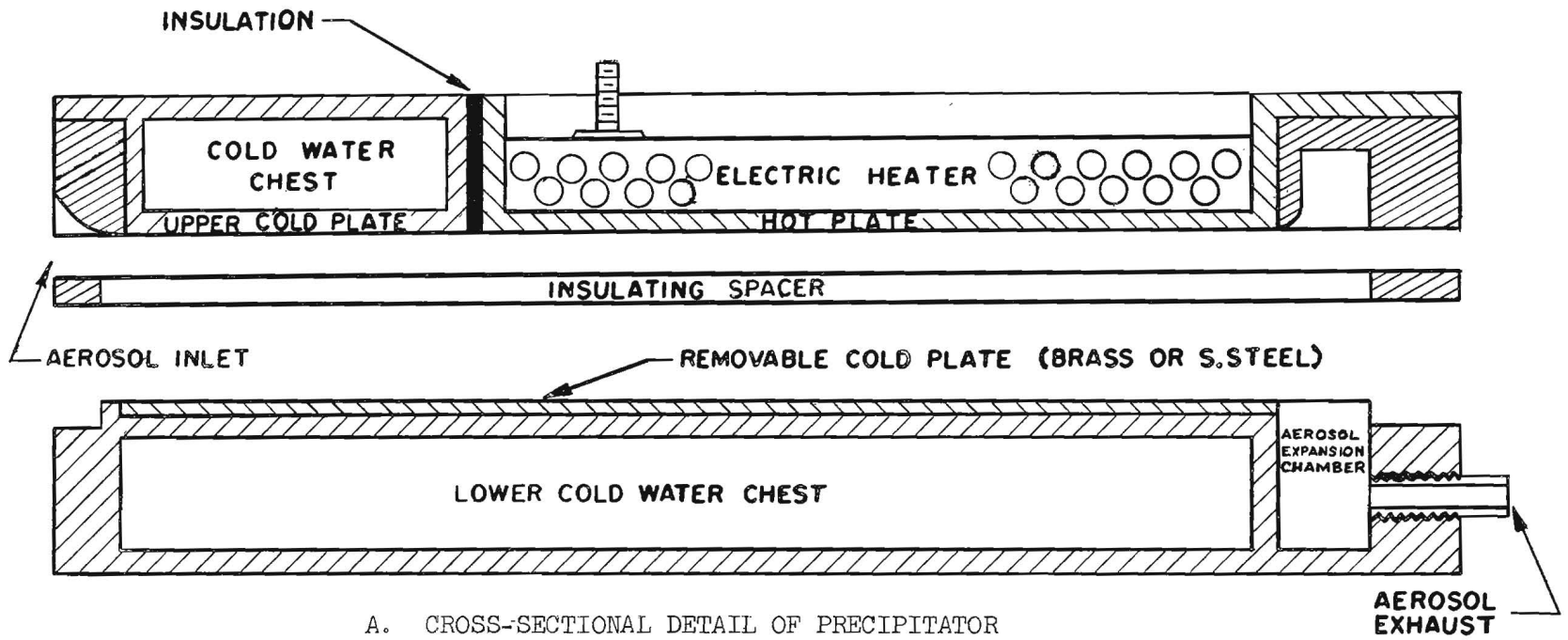

A. CROSS-SECTIONAL DETAIL OF PRECIPITATOR

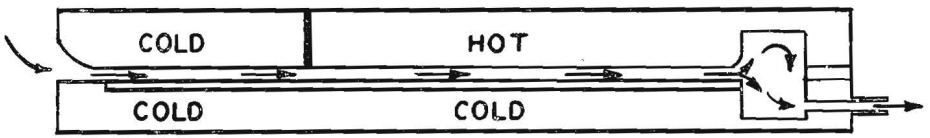

B. FLOW DIAGRAM

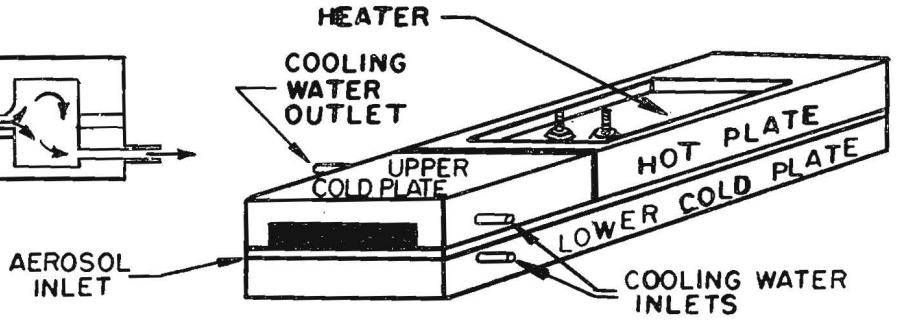

C. PICTORIAL VIEW

Figure 10. Schematic Diagram of Linear Flow Precipitator (Model III).

an almost instantaneous discharge of 1600 joules (32 microfarads at 10,000 volts) of electrical energy into the material to be aerosolized. The dispersion of most metals in air usually yields an aerosol of metallic oxides. If the noble metals are exploded in air, or if more reactive materials are vaporized in an inert atmosphere, the aerosol product consists essentially of very small spherical metallic particles. The particle size distribution resulting from such a detonation is somewhat dependent upon the energy of the electrical discharge and the physical properties, including the size and shape, of the exploded element.

Preliminary investigations showed clearly that precipitator deposit dimensions were particularly sensitive to aerosol flow rates and that these rates were difficult to control and measure under the conditions encountered. A positive displacement mechanism utilizing calibrated reservoirs and a flowing fluid was developed to insure constant aerosol flow and precise measurement. This aerosol flow system made it possible to maintain control at very low flow rates needed for reliable experimental results.

E. Measurement of Deposit Radii

The evaluation of the deposit radii in thermal precipitation studies where the deposits were dense and sharply defined was accomplished by direct visual observation. The glass collecting-disk, after having been removed from the precipitator, was placed on a rectilinear graph paper grid having one-millimeter divisions. The deposit was oriented with its center at the grid origin, and a series of eight radial measurements of the periphery of the deposit were made at 45° increments under 30x magnification. The average of these individual measurements was then recorded as the deposit radius. The peripheries of less dense deposits were not so easily detected, however, and radial measurements were difficult to make with precision. An alternate technique, which employed a traversing mechanism and a sharply focused pinpoint of light, was developed. The pinpoint of light, in traversing the surface of the glass collecting-disk, brightened noticeably when it encountered even a faint deposit. Radial measurements therefore could be read directly from the vernier scale of the calibrated traversing mechanism. For more accurate work, examinations

were made using an optical microscope at magnifications up to 800x and measurements were obtained with a micrometer attachment. In obtaining average radial distances under the microscope, a series of four diametric measurements were recorded at two or more magnifications.

F. Particle Size Determination (in Precipitated Deposits)

The particle size was generally determined by optical microscope examination of the precipitated deposits. In the later stages of the investigation, it became apparent that these evaluations were sometimes misleading, and electron micrographs were then made for detailed study of precipitated particulate materials.

All of the above-mentioned measurements, in conjunction with the data recorded on precipitator operating conditions, were used to compute experimental values for the particulate velocities and thermal forces.

G. Limitations of Experimental Methods

The general limitations of the two experimental methods may now be examined in the light of equipment and procedures. First, in both techniques, the element of higher temperature must be uppermost to avoid convection effects in the aerosol. This requirement means that the thermal forces must be directed toward the lower surface and the particulate velocity is therefore the sum of both thermal and gravitational components. For reliable thermal force evaluations, the thermal velocity component must be sufficiently large relative to the gravitational velocity component to overcome experimental errors. By application of Epstein's thermal force theory and Stoke's law, the relative magnitudes of the thermal and gravitational velocity components have been evaluated as a function of temperature gradient and particulate thermal conductivity for a hypothetical particle of one micron diameter and unit density. If the thermal velocity component should be as much as 20 per cent of the gravitational component for significant experimental observations, then reliable data should be obtainable only for particles of thermal conductivity less than about 4×10^{-3} cal/cm sec $^{\circ}K$ for a temperature of $50^{\circ}C/cm$, which is the usual gradient for Millikan type observations. Since the density of most particulate materials is greater than unity, the limiting

thermal conductivity value is actually somewhat less than that given above. On the other hand, decreasing the particle diameter to 0.5 micron raises this conductivity limit to about 1.5×10^{-2} cal/cm sec ^{o}K and by so doing there is introduced the possibility mentioned above that hydrodynamic and thermal equilibrium considerations of the system on which Epstein's equation is based may not apply.

Since the thermal velocity component is directly proportional to temperature gradient, and much higher temperature gradients are permissible in precipitators, thermal precipitation is more readily adaptable to the study of thermal forces for aerosols of higher particulate conductivity. In this case, the geometry and operating conditions of the device as well as the properties of the particulate material determine the limiting particulate velocity. For a temperature gradient of $1500^{o}C$/cm in the precipitators used in this investigation, it can be shown that significant results can be expected only for materials of conductivity lower than 0.01 cal/cm sec ^{o}K if the particle diameter is as large as 1.0 micron. Theoretically, this investigation is therefore still limited to materials of relatively low thermal conductivity. On the other hand, if thermal forces are as much as 40 times greater than Epstein's equation predicts (as was suggested by Schadt and Cadle[30]), the investigation could be extended to particulate materials of high conductivity, perhaps including even copper and silver.

The idea of making a direct comparison of the data of both experimental approaches is appealing but such a comparison can be made only in terms of forces observed per unit temperature gradient. This also stems from the physical limitations of the experimental equipment. Precise velocity measurements in the Millikan-type thermal cell can be made only for relatively low velocities which, for most particulates (i.e., relatively low thermal conductivites), restricts the temperature gradient to the order of magnitude of $100^{o}C$/cm or less. On the other hand, complete deposition of particulate material in a precipitator of practical dimensions requires temperature gradients at least on the order of several hundred degrees per centimeter. It is therefore not practicable to obtain data from the two studies in the same range of temperature gradients.

VI. CALCULATION OF EXPERIMENTAL THERMAL VELOCITY AND FORCE

Thermal force phenomena in thermal precipitation are deduced from the path which a particle describes in moving through the precipitation zone. As a particle falls under the influence of both gravitational and thermal forces, it is moved horizontally by the ambient airstream. Hence the particulate path is a function of both vertical precipitating forces and the radial movement of the air in which the particle is suspended. By joint application of Stoke's law and the principles of laminar fluid flow, the particulate behavior and the motivating forces can be resolved. This treatment is presented in the following derivations.

A. Calculation of Particulate Velocity

Aerosol flow through a thermal precipitator must be laminar for the analysis of results. If the parabolic velocity profile for laminar flow between parallel plates is assumed not to be significantly altered by the temperature gradient, the relationship between the point velocity, U, and the maximum velocity, U_{max}, of the flowing fluid may be expressed in the nomenclature of Figure 11 by

$$U = U_{max}\left[1 - \left(\frac{4}{L^2}\right) y^2\right] \tag{6.1}$$

For the parabolic velocity profile, the maximum velocity and the average fluid velocity are related through

$$U_{max} = \frac{3}{2} U_{avg} \tag{6.2}$$

Direct substitution of U_{max} in equation 6.1 yields

$$U = \frac{3}{2} U_{avg}\left[1 - \frac{4y^2}{L^2}\right] \tag{6.3}$$

The average fluid velocity is defined as

$$U_{avg} = \frac{Q}{A_x} = \frac{Q}{2\pi rL} \tag{6.4}$$

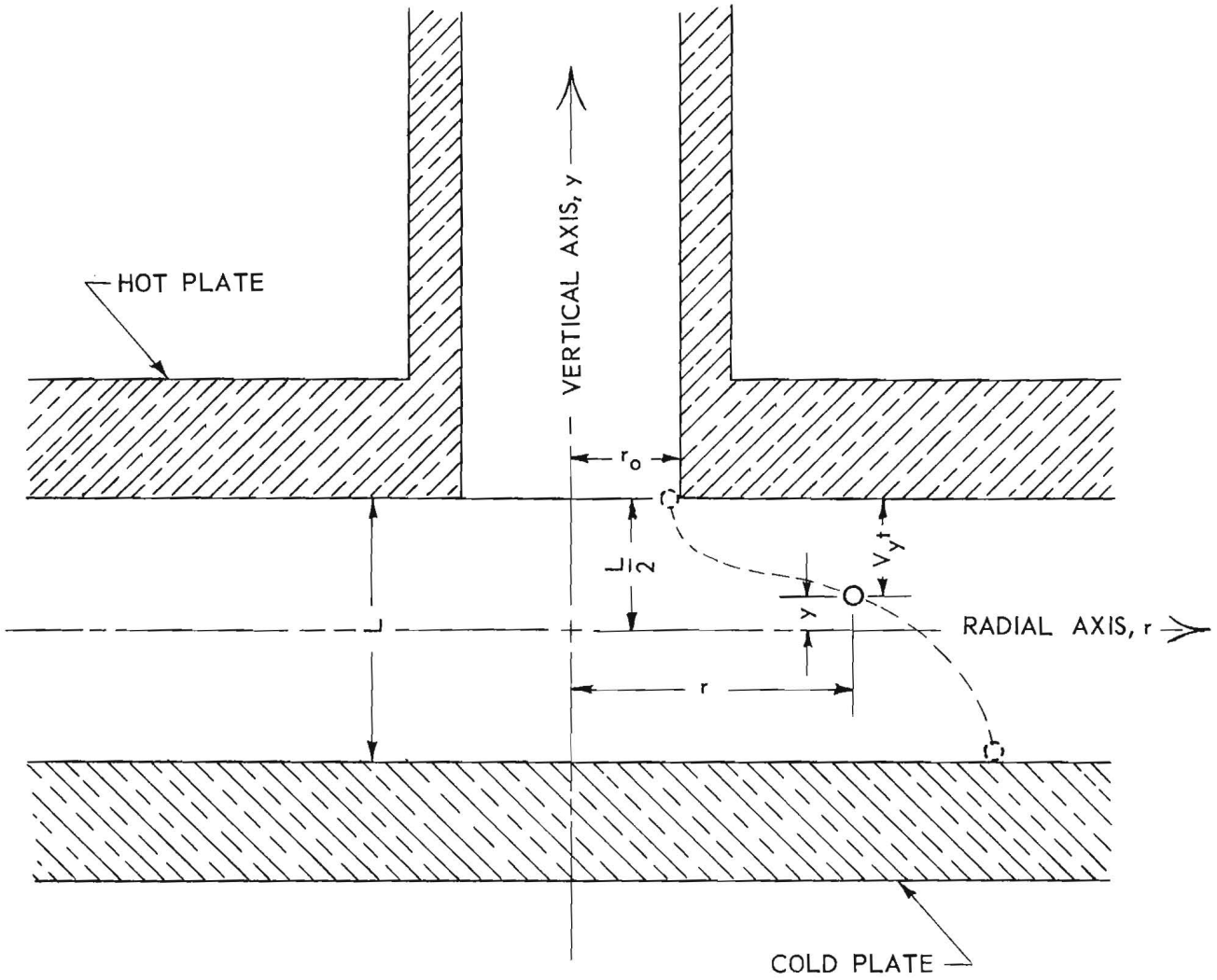

Figure 11. Coordinate System for Defining Particulate Trajectory.

where Q is the volumetric flow rate of the aerosol and A_x is the cross-sectional area of the aerosol stream normal to the direction of flow. Thus,

$$U = \frac{3Q}{4\pi rL}\left[1 - \frac{4y^2}{L^2}\right] \tag{6.5}$$

The relationship between the point velocity of the fluid and the horizontal velocity component, V_r, of a particle suspended in the fluid at that point may now be considered. The time required for a one-micron particle of unit density initially at rest to be accelerated to 95 per cent of the flowing fluid velocity is on the order of 10 microseconds.* This time is very small relative to the residence time of the aerosol in the precipitator. It may therefore be assumed that the particulate velocity and the fluid velocity are identical. Thus, the horizontal velocity component of the particle may be expressed by

$$V_r = \frac{dr}{dt} = \frac{3Q}{4\pi rL}\left[1 - \frac{4y^2}{L^2}\right] \tag{6.6a}$$

or, rearranging, by

$$r\,dr = \frac{3Q}{4\pi L}\left[1 - \left(\frac{4}{L^2}\right)y^2\right]dt \tag{6.6b}$$

Integration of equation 6.6b requires knowledge of the vertical coordinate of the particulate position, y, as a function of time. In the absence of precise information regarding y = y(t), the simplest case has been

---

*This calculation was made by equating the particulate drag force to the inertial force:

$$\frac{(U - V_r)}{Z} = \frac{\rho_p \pi D_p^{\,3}}{6}\frac{dV_r}{dt}$$

Integration of this differential equation yields

$$t = \frac{\rho_p \pi D_p^{\,3} Z}{6} \ln\left[1 - (V_r/U)\right]$$

assumed, namely, a constant vertical velocity, V_y, defined as follows:

$$V_y = \frac{L}{t_f} \tag{6.7}$$

where t_f is the total time in transit. It follows then, from Figure 11, that

$$y = \frac{L}{2} - V_y t = \frac{L}{2} - \left(\frac{L}{t_f}\right) t \tag{6.8}$$

Substituting this expression for y in equation 6.6b, and integrating between limits gives

$$\int_{r_o}^{r_d} r dr = \frac{3Q}{4\pi L} \int_{o}^{t_f} \left[1 - \left(\frac{4}{L^2}\right) \left(\frac{L}{2} - \frac{Lt}{t_f}\right)^2 \right] dt \tag{6.9}$$

for a particle starting at r_o and moving to r_d. Performing the indicated integration and simplifying gives

$$t_f = \frac{\pi L}{Q} \left(r_d^2 - r_o^2 \right) \tag{6.10}$$

in which precipitation time, t_f, is a function of plate spacing, aerosol flow rate, and the precipitation radius. The vertical component of particulate velocity, V_y, may then be expressed in terms of the aerosol flow rate and the deposit radius (both of which are experimentally determined quantities) by substitution of the above result for t_f in equation 6.7.

$$V_y = \frac{Q}{\pi(r_d^2 - r_o^2)} \tag{6.11}$$

B. Calculation of Thermal Force and Thermal Velocity

After the vertical component of particulate velocity has been determined, either by direct observation or by the computation indicated above, the thermal force and thermal velocity may be evaluated in the following manner.

A particulate moving in a viscous medium under the influence of a constant force attains a constant velocity, V, that is indicative of the force. The relationship may be expressed by

$$V = FZ \tag{6.12}$$

where Z, the mobility [20] of the particulate, depends on its size and shape and on the properties of the fluid medium. For a sphere in a homogeneous medium, the definition of mobility is analogous to Stoke's law,[24]

$$Z = \frac{1}{6\pi\eta a} \tag{6.13}$$

where η is the viscosity of the fluid and a is the radius of the particle. As the inhomogeneity, i.e., mean free path length, of the fluid becomes comparable in size with the particle, equation 6.13 must be modified by the inclusion of a slip-correction factor, S, and the mobility is then defined by

$$Z_s = \frac{S}{6\pi\eta a} \tag{6.14}$$

The slip correction, a function of $\frac{\lambda}{a}$, accounts for the tendency of the particle to slip between the molecules of the fluid medium.[5,6,23] By rearranging equation 6.12 and making the appropriate substitutions for V_y and Z (equations 6.11 and 6.14) the total precipitating force may be computed from experimental quantities.

$$F = \frac{V_y}{Z_s} = \left[\frac{6\pi\eta a}{S}\right] V_y \tag{6.15a}$$

or, for thermal precipitation, the total precipitating force is

$$F = \frac{6\eta a Q}{[r_d^2 - r_o^2]\, S} \tag{6.15b}$$

It should be noted that in the usual experimental operating position, i.e., hot plate above cold plate, the precipitating force defined above is

the resultant of both gravitational and thermal forces. The gravitational force may be easily resolved according to the following equation from a knowledge of the particle radius, a, and density, ρ_p,

$$F_g = \frac{4}{3} \pi g_c a^3 \rho_p \tag{6.16}$$

where g_c is the gravitational constant.

It is therefore possible to compute the thermal force acting on the particle from experimental data by

$$F_t = \frac{6\pi\eta a V_y}{S} - F_g \tag{6.17a}$$

Again, the equivalent expression applicable to thermal precipitation reduces to

$$F_t = \frac{6\eta a Q}{[r_d^2 - r_o^2]\, S} - F_g \tag{6.17b}$$

The thermal velocity, V_t, can be computed by substituting the thermal force obtained from equation 6.17 for the force in equation 6.12.

$$V_t = F_t Z_s \tag{6.18}$$

Tantamount to the preceding development is the following analysis. Since the particulate velocity also is a vector quantity, it may be resolved into its thermal and gravitational components.

Thus,

$$V = V_t + V_g \tag{6.19a}$$

If the gravitational component has been observed in the absence of a temperature gradient, the thermal component may be obtained directly by

$$V_t = V_y - V_g \tag{6.19b}$$

Otherwise, the gravitational component must be computed from the relationship

of equation 6.12

$$V_g = F_g Z_s = \left[\frac{4}{3}\pi g_c a^3 \rho_p\right]\left[\frac{S}{6\pi\eta a}\right] = \frac{2g_c a^2 \rho_p S}{9\eta} \qquad (6.20)$$

Then the thermal velocity component is obtained from

$$V_t = V_y - \frac{2g_c a^2 \rho_p S}{9\eta} \qquad (6.21)$$

Finally, the thermal force is computed from equation 6.18.

This latter treatment has the slight advantage that its application in thermal velocity evaluation from a Millikan-type experiment makes a knowledge of the particle size and density unnecessary. Thermal force evaluations, on the other hand, are equivalent.

C. Evaluation of Mean Free Path Length and Slip-Correction Factor

In order to apply the equations developed in the preceding treatment, it is necessary to evaluate the mean free path length of the carrier gas molecules and, in turn, the slip-correction factor. The mean free path length, λ, from the pressure-independent viscosity concept of kinetic theory, is defined such that the pressure-mean free path product, $P\lambda$, for a given gas is a function of temperature, T, only. The proper relationship is given by

$$\lambda = \frac{\eta RT}{0.499\ MP\bar{v}} \qquad (6.22)$$

where $\bar{v}$, the mean molecular speed, is defined as

$$\bar{v} = \sqrt{\frac{8g_c RT}{\pi M}} \qquad (6.23)$$

where R is the universal gas constant and M is the molecular weight of the gas.

The slip effect mentioned above was investigated by Knudsen and Weber[19] who deduced an empirical equation which defines a correction factor of

the form

$$S = 1 + \frac{\lambda}{a}\left[A + Be^{-C\frac{a}{\lambda}}\right] \qquad (6.24)$$

The empirical constants, A, B, and C, have been evaluated for several systems. According to Davies,[6] the proper values consistent with the above definition of the mean free path length of air are A = 1.257, B = 0.400, and C = 1.10.

D. Review of Simplifying Assumptions

It should be noted that in the preceding development of equations several simplifying assumptions have been made. These are enumerated below. First, in the evaluation of the horizontal velocity component for thermal precipitation, it has been assumed (1) that fluid flow is laminar, (2) that entrance effects are negligible, (3) that fluid properties, including viscosity and density, are constant (i.e., temperature independent), and (4) that the horizontal particulate velocity component at any time is equal to that of the flowing fluid at the same point. Second, in the derivation of precipitation time and vertical particulate velocity, it has been assumed (5) that the thermal force is constant, implying (6) a linear temperature gradient in the fluid and (7) a force directly proportional to temperature gradient, (8) that the vertical velocity is constant, implying a negligible acceleration time for the particle in beginning its descent, (9) and that the particle of concern originated at the hot plate inlet, r_o. Finally, in the computation of thermal velocity and thermal force, it has been assumed (10) that the particle is spherical and (11) that its mobility is independent of the temperature of the system and the nature of the particle. These assumptions were made in order to facilitate mathematical analysis. The complexity of a more rigorous treatment is hardly justifiable in view of the precision of the experimental techniques. An evaluation of the inaccuracy introduced by these assumptions is included in the analysis of errors.

VII. CALCULATION OF THEORETICAL PARTICLE BEHAVIOR

An extensive theoretical investigation of particle behavior was made, based on Epstein's analysis of thermal force. The mathematical development of the theoretical investigation employed also the equations discussed in the preceding section of this report. The order in which these equations were used was essentially reversed, however, for theoretical considerations. In this treatment, the theoretical force, F_t, was computed in accordance with equation 3.2. The corresponding thermal velocity, V_t, was then evaluated from equation 6.18. The theoretical gravitational force, F_g, was computed from equation 6.16. Finally, the theoretical deposit radius for the particulate was calculated from equation 6.15b rearranged to the form

$$r_d = \sqrt{r_o^2 + \frac{6\eta a Q}{SF}} \qquad (7.1)$$

where

$$F = F_t + F_g \qquad (7.2)$$

The computations just described were incorporated in a program for an IBM 650 computer. The program provided for the calculation of (1) the slip factor, (2) the mobility, (3) the thermal force, (4) the gravitational force, (5) the deposit radius, and (6) the terminal vertical velocity of the particle. It covered a particulate diameter range from 0.2 to 5 microns, a range of volumetric flow rates from 200 to 1000 cc/min and a range of pressures from 0.01 to 1.0 atmosphere.

This program was executed in the Computer Center at Georgia Tech for three materials of markedly different thermal conductivity, i.e., magnesium oxide, zinc, and stearic acid. The physical dimensions of the precipitator and the temperature gradients used in these calculations were chosen to permit direct comparison of experimental data and theoretical results.

The theoretical data were plotted to show most clearly the effect of operating conditions as well as the effect of the physical properties of the particulate material on thermal precipitation. Results from this investigation, including examples of the plotted data, are presented in

the following section of this report. The results of this theoretical investigation have been most useful in programming experimental work, in comparing experimental results, and in explaining some of the pecularities of thermal precipitator operation.

VIII. THEORETICAL PARTICULATE BEHAVIOR

A. Magnitude of Thermal Forces

The theoretical effects of pertinent variables on thermal force are immediately obvious from the equations which have been presented and discussed in Section III. Of interest in this respect, however, are the magnitudes of thermal forces for specific systems and the magnitudes of changes in this force resulting from finite changes in the independent variables. Just how large is the thermal force on a one-micron magnesium oxide particle suspended in air, and how much greater is this force than that which would be expected under the same conditions for a particle such as zinc where the thermal conductivity is 175 times greater? These questions are answered in Figure 12 where pressure and thermal conductivity effects are illustrated in a semilog plot of thermal force versus temperature gradient for stearic acid (k_p = 0.0003 cal/cm sec ^{o}K), magnesium oxide (k_p = 0.00146 cal/cm sec ^{o}K) and zinc (k_p = 0.265 cal/cm sec ^{o}K). For example, the force at any specific condition for zinc is approximately 1/170 the force for magnesium oxide, while for stearic acid the force is approximately four times greater. It has been observed that for a one-micron-diameter particle at atmospheric pressure the thermal forces predicted for stearic acid, magnesium oxide, and zinc are respectively 1.7×10^{-11}, 4.5×10^{-12} and 2.7×10^{-14} dynes per unit temperature gradient. The thermal forces then are comparable to the force of gravity on the respective particles at temperature gradients of about 25^{o}, 415^{o} and 136,000^{o} C/cm. It should be noted that the gravitational force decreases much more rapidly with decreasing particle size than does thermal force. For a 0.5-micron particle, the temperature gradients at which thermal and gravitational forces are approximately equal are then 3^{o}, 52^{o} and 17,000^{o} C/cm, respectively.

B. Influence of Particulate Thermal Conductivity on Thermal Force

The theoretical effect of thermal conductivity is perhaps illustrated most clearly in Figure 13 where the thermal force proportionality factor, f(k), defined in accordance with Epstein's thermal force equation (3.2) as

$$f(k) = 3k_g/(2k_g + k_p), \qquad (8.1)$$

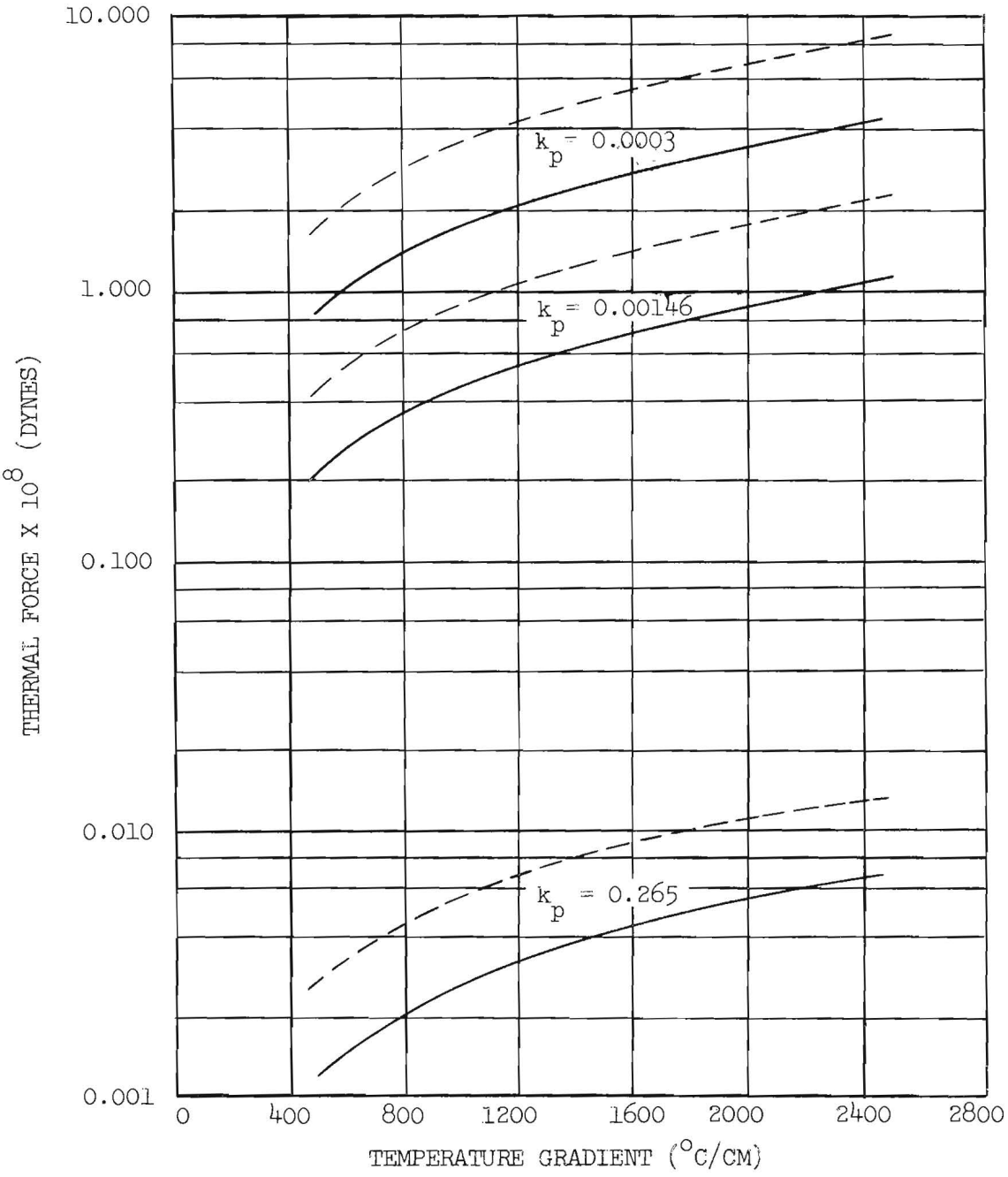

Figure 12. Relative Theoretical Magnitudes of Thermal Forces. Thermal forces are for 1.0 micron particles. Curves are based on air as the carrier medium at pressures of 0.5 atm (broken line) and 1.0 atm (solid line). The uppermost pair of curves apply to stearic acid; the intermediate pair apply to magnesium oxide; the lower pair apply to zinc. The units of thermal conductivity are cal/cm sec °K.

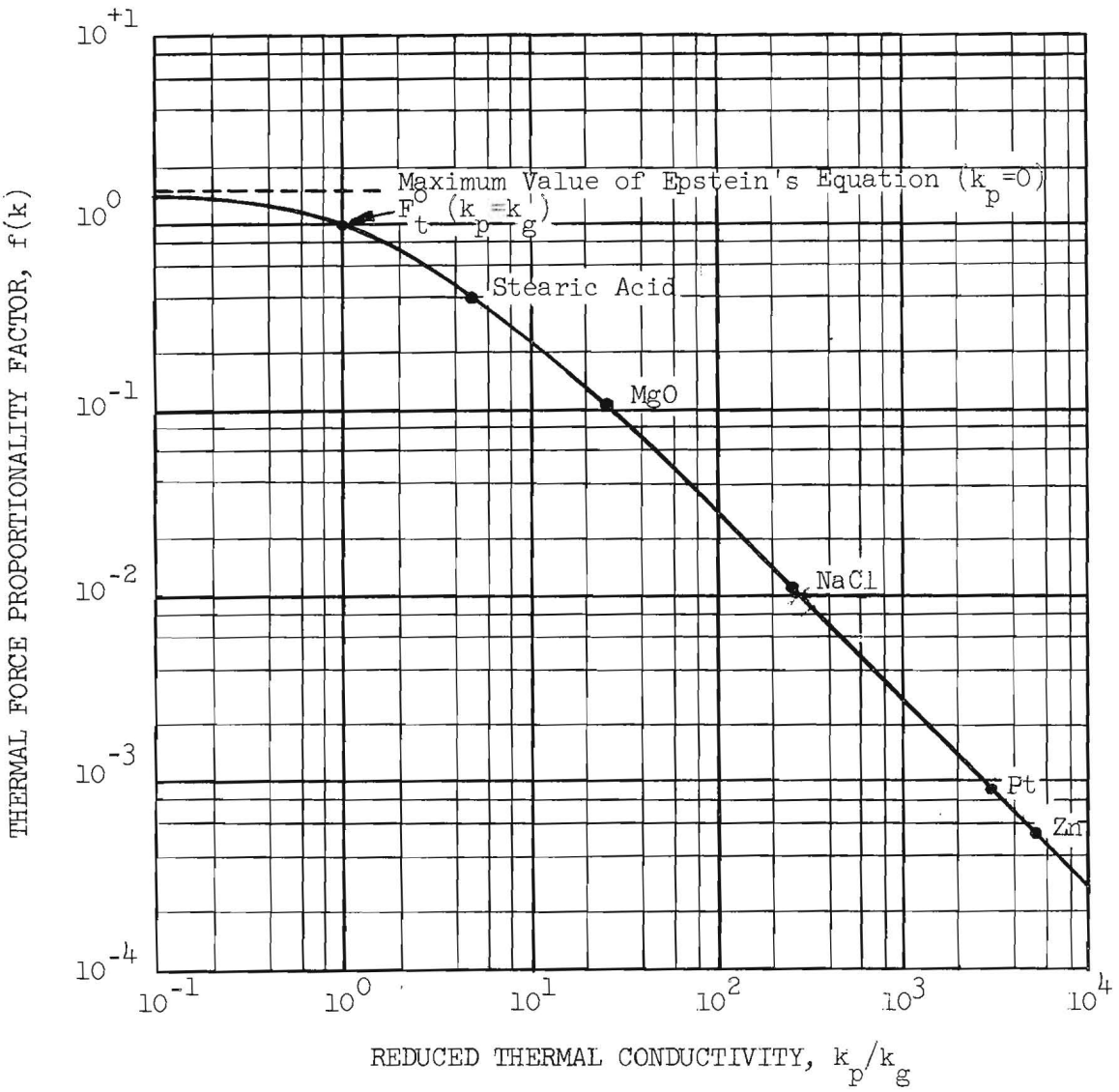

Figure 13. Theoretical Effect of Particulate Thermal Conductivity on Thermal Force. The curve is based on Epstein's thermal force theory and is applicable to any gas suspension of particulate material. Point values are designated for the specific particulate suspension in air.

has been plotted against a reduced thermal conductivity, k′, defined by

$$k' = k_p/k_g \tag{8.2}$$

The theoretical effective thermal force is given by the relationship

$$F_t = [f(k)]\, F_t^o \tag{8.3}$$

where F_t^o is the thermal force value for a particulate material of conductivity exactly equal to that of the gas in which it is suspended, i.e., the circumstance under which f(k) reduces to unity. It is immediately evident that for $k_p \gg 2k_g$ the thermal force is essentially inversely proportional to the particulate thermal conductivity. At the other extreme, i.e., $k_p \ll 2k_g$, it would appear from the above relationship that the thermal force approaches a limiting value, $(F_t)_{max} = 3/2\ F_t^o$, as the particulate conductivity approaches zero. In fact, for any value of $k_p < k_g$ (which is conceivable, for example, in the case of an agglomerated particulate mass) the proportionality factor has a value greater than unity. This implies a temperature gradient within the particle greater than that which exists within the gas at some distance from the particle. Such a situation seems unlikely in view of the basic stipulation that the particulate temperature gradient originates through thermal conduction from the gas. In other words, it is inconceivable with heat transfer from the gas to the particle, that the maximum surface temperature of the particle could be higher than the corresponding gas temperature. A larger particulate gradient then would require the lowest surface temperature to be less than the gas temperature at that point. This seems improbable if the rate of heat transfer is more rapid in the gas than in the particle. In fact, Epstein's equation, from which the proportionality factor was defined, was obtained under the boundary condition of equal surface and gas temperatures. A more reasonable limiting value would be $(F_t)_{max} = F_t^o$, which occurs when $k_p = k_g$. For any lower particulate thermal conductivity, the internal transfer of heat is negligible and the assumption that the temperature at any point on the particle's

surface is equal to the local gas temperature is logical. This conclusion is consistent with the concept of a reduction in particulate temperature gradient, and therefore in thermal force as well, resulting from a more rapid internal heat transfer rate due to higher particulate conductivity.

C. Influence of Independent Variables on Precipitation Deposit Radius

The influence of the independent variables upon the radius of a thermal precipitator deposit is not quite so obvious as is their effect upon the thermal force. This obscurity stems from the fact that the effectiveness of thermal precipitation is determined primarily by thermal velocity, not thermal force alone. Both the thermal force and the drag resistance offered by the gas to the movement of the particle are intimately related in thermal velocity. Furthermore, both thermal and gravitational force components contribute to the precipitation of particulate material and must be jointly considered in an analysis, as was shown in the preceding sections.

From the results of previous experimental studies the theory appears to predict reliably the general behavior of a given particulate. To that extent, the theoretical data have been useful as a guide to precipitator operation. Some of the more interesting and informative relationships are graphically illustrated for discussion.

1. The Effect of Particle Diameter and Pressure

The effect of particle diameter and pressure on the deposit radius is illustrated in Figure 14, a plot of particulate diameter versus deposit radius with pressure parameters. This curve is based on theoretical values and shows the behavior of particles with a thermal conductivity of 0.00146 cal/cm sec ^{o}K, a thermal gradient of 1970^{o} C/cm, an aerosol flow rate of 600 cc/min, and a precipitator plate separation of 0.041 cm. It is evident that the deposit radius is a function of pressure, decreasing rapidly as the pressure decreases. Theoretically, for a one-micron particle a decrease in pressure from 1.0 to 0.01 atmosphere results in a decrease in the deposit radius from approximately 6.5 cm to 0.5 cm under the above conditions. Thus thermal precipitation is expected to be more efficient at lower pressures.

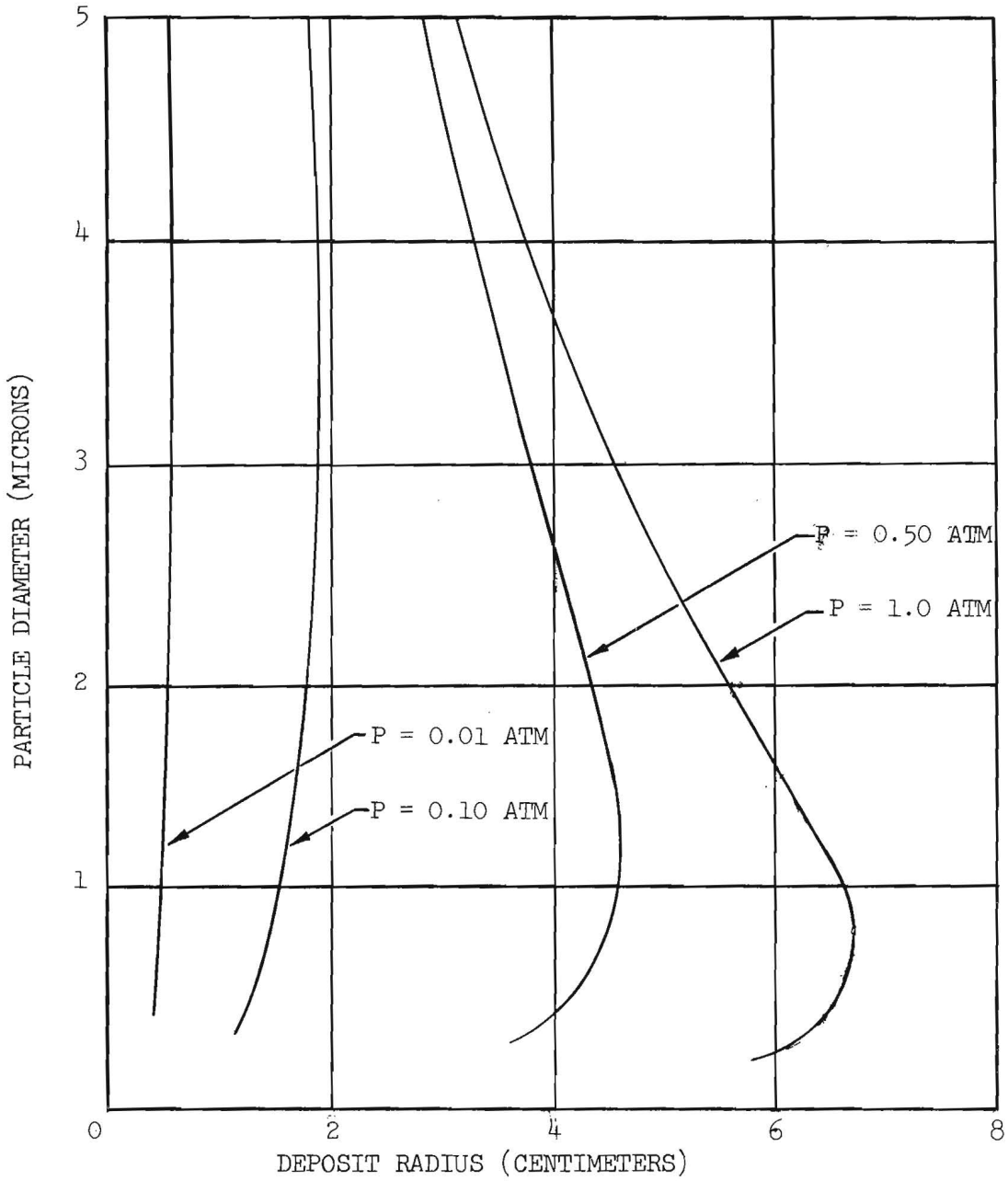

Figure 14. Theoretical Effect of Particulate Size and Pressure on the Deposit Radius. Curves have been plotted for magnesium oxide particles with k_p = 0.00146 cal/cm sec ^{o}K. Aerosol flow rate is constant at 600 cc/min. Temperature gradient is constant at 1970^{o}C/cm.

It can be seen also in Figure 14, that the deposit radius is a function of particulate diameter and that the deposit radius reaches a maximum value for some critical diameter determined essentially by the physical properties of the particulate material and the gas. This effect can be interpreted as the interplay of thermal and gravitational velocity components, which is illustrated in Figure 15, a log-log plot of particulate velocity versus particle size. The thermal velocity component increases, while the gravitational velocity component decreases with decreasing particle diameter. It is evident that there will always be a minimum in the composite velocity curve which corresponds to the critical particle size. The value of the critical particle diameter thus depends upon the relative magnitudes of the gravitational and thermal velocity components. Referring again to Figure 14, the decreasing deposit radius associated with increasing particle size above the critical value is easily understood as the gravitational influence which becomes predominant in that region at higher pressures. Furthermore, this effect is minimized at lower pressures where the thermal component is larger relative to the gravitational component of velocity.

2. The Effect of Particulate Properties on Deposit Radius

The effect of the physical properties of the particulate material on the deposit radius is illustrated in Figure 16, which is also a plot of particle diameter versus deposit radius. In this illustration, curves have been plotted for stearic acid, magnesium oxide, and zinc at pressures of 1.0 and 0.1 atmosphere. The thermal gradient, aerosol flow rate, and precipitator plate separation are the same as for Figure 14. Here the dependence of deposit radius upon the combined effect of thermal conductivity and density is emphasized. In particular, the following observations can be made for a pressure of one atmosphere. For the case of magnesium oxide, the prominent critical particle size effect indicates that both gravitational and thermal velocity contributions are significant. In the case of stearic acid the critical size effect is much less pronounced due to a higher thermal velocity contribution (i.e., lower thermal conductivity) and the lower gravitational velocity contribution

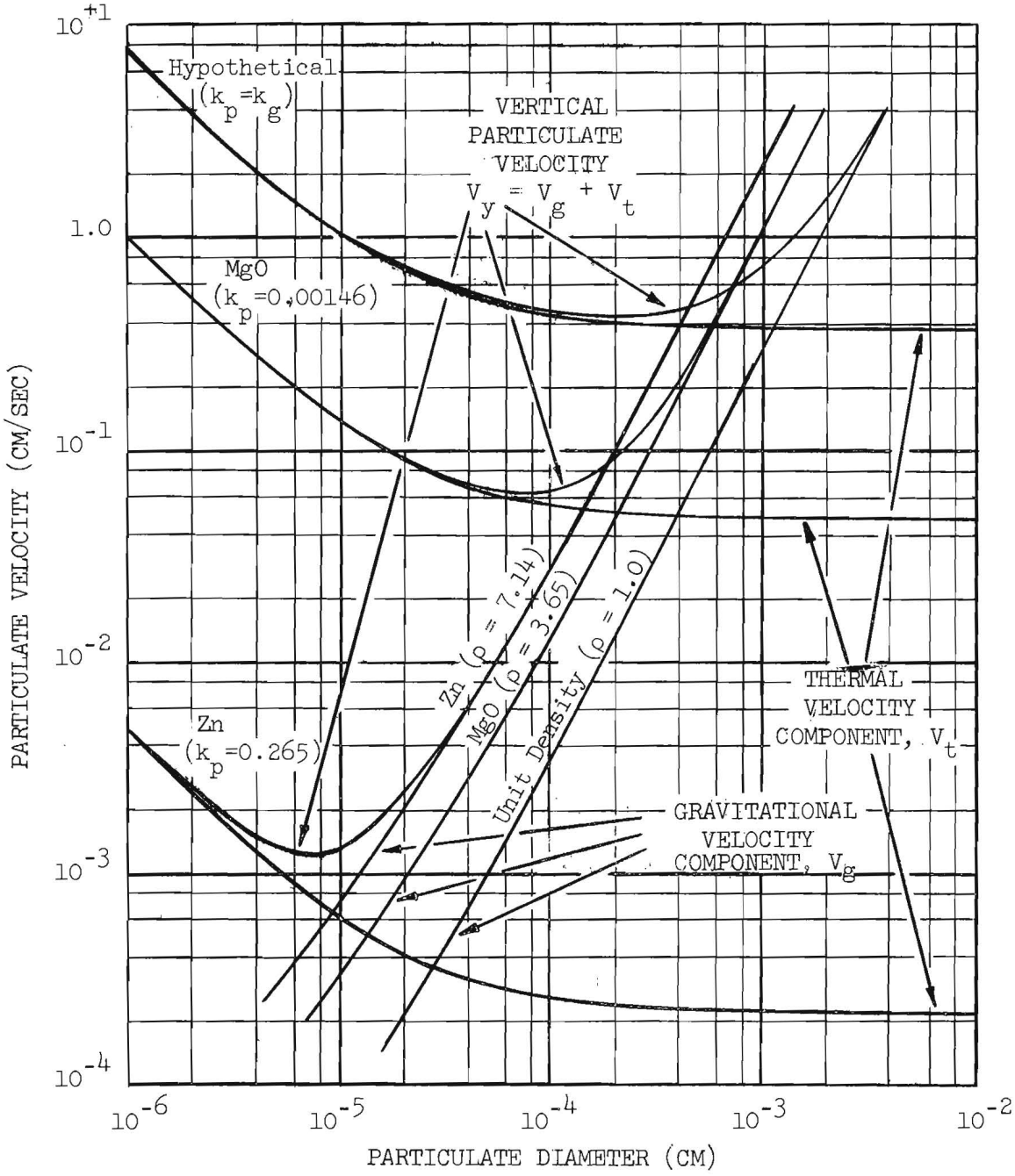

Figure 15. Theoretical Effect of Particle Diameter on Particulate Velocity. Thermal velocity component curves are based on a temperature gradient of 1500°C/cm and a pressure of 1.0 atmosphere. Units of thermal conductivity are cal/cm sec °K. Units of density are gm/cc.

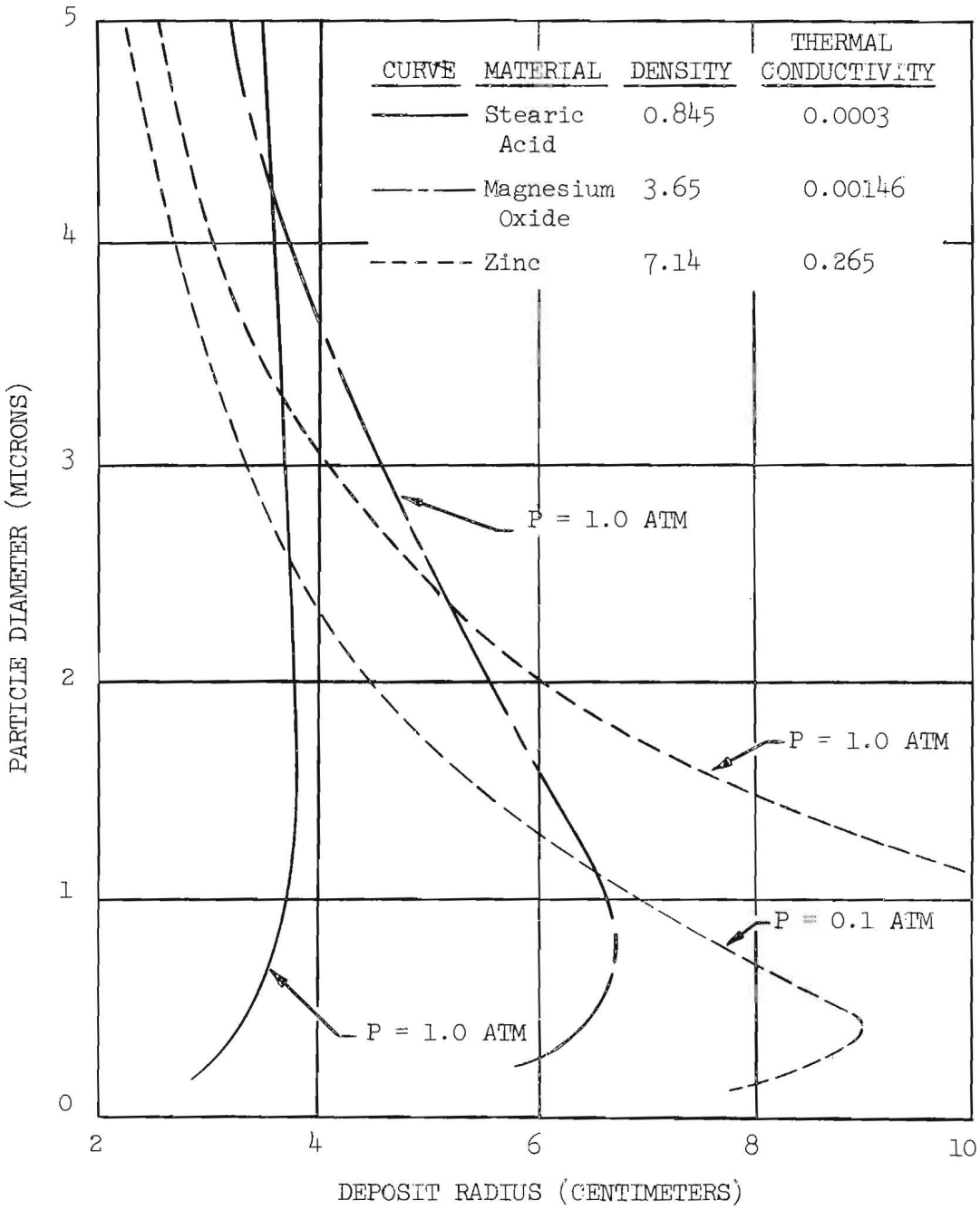

Figure 16. Theoretical Effect of Thermal Conductivity and Density on Deposit Radius. The base conditions are aerosol flow rate = 600 cc/min, temperature gradient = 1970°C/cm, and precipitator plate separation = 0.041 cm. Thermal conductivity units are cal/cm sec °K; density units are gm/cc.

which results from the lower particulate density. In the case of zinc, the curve is practically that for gravitational settling since the thermal velocity contribution is very small. At 0.1 atmosphere, however, the thermal velocity contribution becomes significant, even for zinc.

3. Implications of the Critical Particle Size Effect

The critical particle size effect implies a varying particulate size distribution with radius depending upon the operating pressure and the nature of the material. Consider aerosols containing particles in the diameter range from 0.5 to 1.5 microns. For stearic acid the critical diameter lies above this size range. Thus the deposit radius decreases as the particulate diameter decreases and only the larger particles would be expected to precipitate at the outer periphery of the deposit. For zinc the critical particulate diameter is less than the lower limit of the hypothetical aerosol. Thus, the deposit radius increases as the particle size decreases, and only the smaller particles would precipitate at the outer periphery. The critical particle size for magnesium oxide is about 0.8 micron and lies within the range under consideration. The deposit radius increases with decreasing particulate diameter to the critical value and then decreases. Thus, near the outer periphery of the deposit, the distribution should contain particulates both larger and smaller than 0.8 micron but approaching that value at the outer extreme. It is to be noted further, that the greater the gravitational contribution to particulate velocity, the more sharply defined should be the particle distribution.

4. The Effect of Aerosol Flow Rate

The effect of aerosol flow rate on deposit radius is illustrated in Figure 17, where particulate diameter is plotted versus flow rate with pressure parameters. Again the magnesium oxide particle and the thermal gradient of 1970°C/cm are selected as a basis for the illustration. This plot shows the more obvious effect of increasing deposit radius with increasing flow rate. In view of the magnitude of deposit variation due to changes in this variable compared with the variation due to thermal

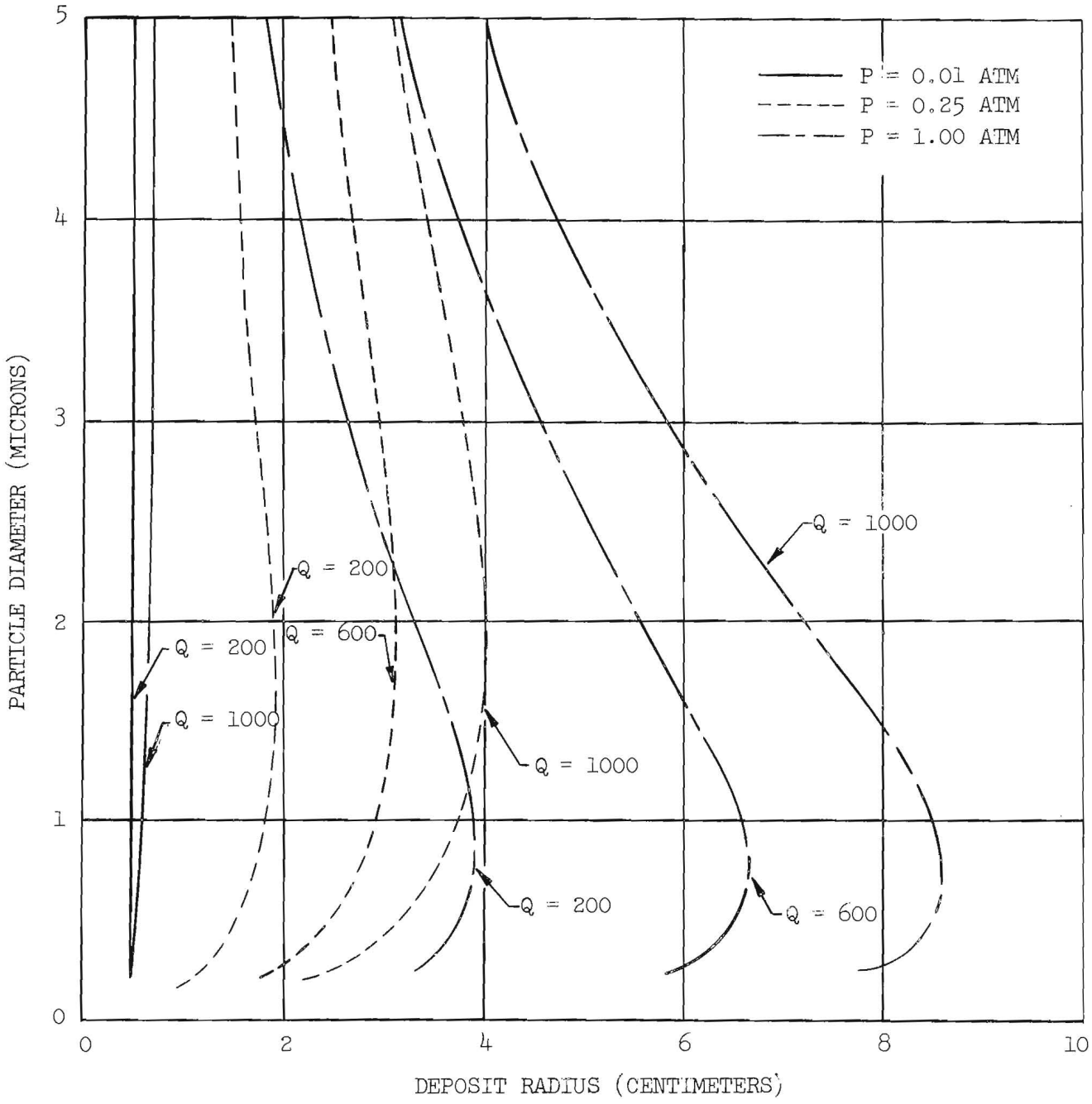

Figure 17. Theoretical Effect of Aerosol Flow Rate on Deposit Radius. This illustration also shows the variation in the effect of flow rate with pressure. The curves are for the precipitation of magnesium oxide particulates at a temperature gradient of 1970°C/cm. Aerosol flow rate, Q, is expressed in cc/min.

conductivity, it is clear that precise flow control is essential.

D. Derivation of Linear Relationships between Deposit Radius and Independent Variables

It was found in a preliminary experimental investigation of thermal precipitation that rigorous duplication of operating conditions for each experimental observation was time consuming and sometimes impossible with available equipment. While precise measurement is essential for reproducibility, it is not necessary to establish identical aerosol flow rates and temperature gradients for each run. It can be shown from theoretical considerations that relationships suitable for interpolation can be established between those variables and the magnitude of the deposit radius. Rearranging equation 6.15b yields

$$(r_d^2 - r_o^2) = \left[\frac{6\eta a}{FS}\right] Q \qquad (8.4)$$

which indicates that the quantity $(r_d^2 - r_o^2)$ should be directly proportional to the aerosol flow rate, Q. This relationship provides a means of adjusting observed deposit radii to a standard flow rate basis for comparision of experimental data. A similar rearrangement of equation 6.17b predicts an essentially linear relationship between the reciprocal of $(r_d^2 - r_o^2)$ and the temperature gradient, that is

$$(r_d^2 - r_o^2)^{-1} = \left[\frac{5}{6\eta a_{rd} Q}\right] F_t + \left[\frac{S}{6\eta a_{rd} Q}\right] F_g \qquad (8.5)$$

where the symbol, a_{rd}, represents the critical particle radius evaluated at the periphery of the deposit Since the thermal force is directly proportional to the temperature gradient, $\frac{dT}{dy}$, the equation may be rewritten

$$(r_d^2 - r_o^2)^{-1} = \left[\frac{C_1 S}{6\eta a_{rd} Q}\right] \frac{dT}{dy} + \left[\frac{S}{6\eta a_{rd} Q}\right] F_g \qquad (8.6)$$

where C_1, the proportionality factor for the thermal force-temperature

gradient relationship, is a function of all the other related variables of Epstein's basic force equation (3.2). Equation 8.6 expresses the quantity $(r_d^2 - r_o^2)^{-1}$ as a linear function of temperature gradient if the coefficients of $\frac{dT}{dy}$ and F_g may be assumed constant. This assumption is precisely valid only for the case of constant particle radius. As was mentioned above, the critical particle size, i.e., that which would be observed at the maximum deposit radius, is dependent upon the relative magnitudes of the thermal and gravitational forces and is therefore subject to slight variation with changing temperature gradient. The assumption of constant coefficients is sufficiently valid, however, to permit linear interpolation of experimental data over a limited temperature gradient range. This is tantamount to linear interpolation of precipitation velocities and is permissible only as long as the gravitational component is negligible.

It should be noted that in this theoretical discussion, the thermal conductivity of magnesium oxide powder has been arbitrarily assigned to the magnesium oxide particulate. This has been done in order to cover a suitable range of thermal conductivity for the purpose of comparative illustrations. The suitability of this choice will be discussed further in Section XI, Discussion of Results.

IX. EXPERIMENTAL OBSERVATIONS

A. Scheme of Analysis

In the course of this experimental investigation, data were accumulated according to the following scheme of analysis. First, the thermal precipitation of a standard particulate material was thoroughly studied to establish the degree of reproducibility of data and the reliability of the experimental and analytical procedures. Next, precipitation studies were conducted with a number of particulate materials with various physical properties in an effort to deduce the effect of thermal conductivity. In some instances, the data obtained appeared inconsistent, not only in regard to theory, but with respect to other observations as well. In an attempt to resolve these apparent inconsistencies, other devices and techniques were employed in the preparation of aerosols and the precipitation of particulate materials. Finally, a detailed study of the precipitated deposits and the individual particulates was undertaken. In conjunction with the accumulation of thermal precipitation data, observations were obtained with the modified Millikan apparatus for comparison with the results of thermal precipitation.

B. Thermal Precipitation Experiments

1. Precipitation of Magnesium Oxide Using Model I Precipitator

Magnesium oxide was selected as the standard particulate material because of the characteristics of the aerosol and the ease with which it could be generated. By burning a strip of magnesium ribbon in air or oxygen an aerosol with a particle size distribution apparently ranging from 0.5 to 1.5 microns in diameter could be produced. The individual particles so generated are generally of a cubic configuration, such that the assumption of a spherical particulate form in the mathematical treatment is statistically sound. Furthermore, theoretical considerations suggested that the relative magnitudes of thermal force and gravitational force would be optimized from the point of view of analysis of results by the particulate size, density, and effective thermal conductivity peculiar to magnesium oxide.

a. Experimental Data. In this initial phase of the experimental work, a substantial quantity of data was accumulated for the magnesium oxide aerosol in the pressure range from 0.1 to 1.0 atmosphere. Experiments were performed at a variety of aerosol flow rates and for a range of temperature gradients from 500° to 2500° C/cm. Results were recorded from runs made on two Model I thermal precipitators, designated IA and IB, at two precipitator plate separations, viz., 0.07 and 0.04 cm. Tabulated data are presented in Tables I, II, and III grouped according to precipitator and plate separation. Experimental thermal forces were computed from all experimental data using the equations developed in Section VI. Also, for each set of operating conditions, a theoretical value of the thermal force and the corresponding theoretical deposit radius have been calculated according to the development in Section VII. Thus a theoretical value is available for direct comparison with each measured value. All data were processed on the IBM-650 computer.

b. Experimental Confirmation of Linear Relationships between Deposit Radius and Independent Variables. The tabulated data cover a variety of aerosol flow rates and temperature gradients. In order to make a valid estimate of experimental deviations, it has been necessary to adjust the observed deposit radii to standard conditions. The relationships for the interpolation of experimental data, which were developed theoretically in the preceding section, have been confirmed for this application. The linear relationship of equation 8.4 between the aerosol flow rate, Q, and the quantity $(r_d^2 - r_o^2)$ is experimentally verfied in Figure 18. Also, the approximate linearity between the temperature gradient, $\frac{dT}{dy}$, and the quantity $(r_d^2 - r_o^2)^{-1}$ suggested by equation 8.6 is shown in Figure 19 to be adequate for extrapolation over the temperature gradient range of 500° to 2500° C/cm.

c. Thermal Force Dependence upon Temperature Gradient and Pressure. The experimental results have been plotted to illustrate in Figure 20 the dependence of thermal force on temperature gradient and pressure. The plot has been based on magnesium oxide data from precipitator IA with a plate separation of 0.07 cm (see Table I). Data were

TABLE I

EXPERIMENTAL DATA FOR THE PRECIPITATION OF MAGNESIUM OXIDE PARTICLES USING RADIAL FLOW PRECIPITATOR IA WITH PLATE SEPARATION OF 0.07 CENTIMETER

(A)	(B)	(C)	(D)	(E)	(F)	(G)	(H)	(I)
Pressure (Atm)	Temperature Gradient (°C/Cm)	Aerosol Flow Rate (CC/Min)	Observed Particle Travel (Cm)	Theoretical* Particle Travel (Cm)	Radius Ratio (D/E)	Experimental* Thermal Force (Dynes x 10^{-8})	Theoretical* Thermal Force (Dynes x 10^{-8})	Force Ratio (G/H)
0.96	841	371.3	2.66	6.59	0.404	2.90	0.404	7.18
0.97	844	396.8	3.06	6.85	0.447	2.40	0.401	5.99
0.96	847	400	3.06	6.83	0.448	2.41	0.407	5.92
1.0	844	425	3.16	7.19	0.439	2.44	0.389	4.27
0.97	871	476	3.37	7.45	0.452	2.42	0.414	5.85
1.0	984	403.2	2.96	6.61	0.448	2.61	0.454	5.75
0.97	1127	420.2	3.01	6.33	0.476	2.63	0.536	4.91
0.96	1110	440.9	2.74	6.50	0.422	3.28	0.533	6.15
0.97	1127	457.4	3.18	6.62	0.480	2.59	0.536	4.83
0.97	1111	460.1	3.04	6.67	0.456	2.84	0.538	5.28
0.96	1409	384.6	2.37	5.48	0.432	3.72	0.677	5.49
0.96	1409	384.6	2.31	5.48	0.421	3.90	0.677	5.76
0.97	1406	402.7	2.49	5.65	0.441	3.58	0.669	5.35
0.97	1406	458.7	2.64	6.06	0.436	3.67	0.669	5.25
0.1	931	612.3	0.60	1.68	0.357	21.7	4.29	5.06
0.5	956	170.5	0.96	2.99	0.321	6.47	0.829	7.80
0.5	1124	491.8	1.74	4.84	0.360	7.24	1.04	7.96
0.5	1118	503.3	1.85	4.91	0.377	6.67	1.03	6.48
0.5	1402	199	0.81	2.63	0.307	9.84	1.29	7.63
0.5	1409	217.4	0.91	2.76	0.330	9.02	1.30	6.94
0.5	1411	236	0.92	2.89	0.318	9.64	1.30	7.42
0.5	1404	241	0.91	2.93	0.311	10.02	1.29	7.77
0.75	880	312.5	1.80	5.25	0.343	4.69	0.541	8.67

(Continued)

TABLE I (Continued)

EXPERIMENTAL DATA FOR THE PRECIPITATION OF MAGNESIUM OXIDE PARTICLES USING RADIAL FLOW PRECIPITATOR IA WITH PLATE SEPARATION OF 0.07 CENTIMETER

(A) Pressure (Atm)	(B) Temperature Gradient (°C/Cm)	(C) Aerosol Flow Rate (CC/Min)	(D) Observed Particle Travel (Cm)	(E) Theoretical* Particle Travel (Cm)	(F) Radius Ratio (D/E)	(G) Experimental* Thermal Force (Dynes x 10^{-8})	(H) Theoretical* Thermal Force (Dynes x 10^{-8})	(I) Force Ratio (G/H)
0.97	875	135	1.72	3.77	0.456	2.18	0.416	5.24
0.97	882	324	2.94	6.05	0.486	2.08	0.419	4.96
0.96	1062	555	3.24	7.47	0.434	3.07	0.510	6.02
0.97	1132	464.4	2.74	6.66	0.411	3.49	0.538	6.49
0.97	1125	465.8	2.74	6.69	0.410	3.50	0.535	6.54
0.97	1118	467.3	2.86	6.71	0.426	3.18	0.532	5.98
0.97	1115	496.7	2.81	6.94	0.405	3.57	0.530	6.74
0.96	1114	506.8	2.96	6.98	0.424	3.31	0.535	6.19
0.97	1404	376.9	2.46	5.45	0.451	3.40	0.667	5.10
0.96	1409	378.8	2.45	5.43	0.451	3.45	0.667	5.10
0.96	1406	480.8	2.59	6.18	0.419	4.00	0.676	5.92
0.96	1399	493.0	2.59	6.28	0.412	4.10	0.672	6.10
0.96	1399	500.0	2.62	6.32	0.414	4.08	0.672	6.07

* All Computations are based on a particle ~~diameter~~ of 1.0 micron.

TABLE II

EXPERIMENTAL DATA FOR THE PRECIPITATION OF MAGNESIUM OXIDE PARTICLES USING RADIAL FLOW PRECIPITATOR IA WITH PLATE SEPARATION OF 0.04 CENTIMETER

(A)	(B)	(C)	(D)	(E)	(F)	(G)	(H)	(I)
Pressure (Atm)	Temperature Gradient (°C/Cm)	Aerosol Flow Rate (CC/Min)	Observed Particle Travel (Cm)	Theoretical* Particle Travel (Cm)	Radius Ratio (D/E)	Experimental* Thermal Force (Dynes x 10^{-8})	Theoretical* Thermal Force (Dynes x 10^{-8})	Force Ratio (G/H)
0.5	507	180	2.06	3.93	0.524	1.86	0.468	3.97
0.5	988	166	1.07	2.80	0.382	5.28	0.92	5.74
0.5	1012	169	1.24	2.75	0.451	4.20	0.969	4.33
0.5	1478	184	0.98	2.45	0.400	6.77	1.36	4.98
0.5	2473	194	0.42	1.91	0.220	24.1	2.30	10.48
1.0	503	194	3.11	5.61	0.554	1.04	0.232	4.48
1.0	980	180	1.86	4.29	0.434	2.60	0.452	5.75
1.0	985	188	2.11	4.38	0.482	2.16	0.454	4.76
1.0	988	200	2.16	4.53	0.477	2.21	0.456	4.85
1.0	988	201	2.19	4.54	0.482	2.17	0.456	4.76
1.0	1478	194	1.76	3.78	0.466	3.10	0.682	4.54
1.0	1963	221	1.79	3.58	0.500	3.46	0.905	3.83
1.0	2463	198	1.31	3.02	0.434	5.26	1.13	4.65

*All computations are based on a particle diameter of 1.0 micron.

TABLE III

EXPERIMENTAL DATA FOR THE PRECIPITATION OF MAGNESIUM OXIDE PARTICLES USING RADIAL FLOW PRECIPITATOR IB WITH PLATE SEPARATION OF 0.04 CENTIMETER

(A)	(B)	(C)	(D)	(E)	(F)	(G)	(H)	(I)
Pressure (Atm)	Temperature Gradient (°C/Cm)	Aerosol Flow Rate (CC/Min)	Observed Particle Travel (Cm)	Theoretical* Particle Travel (Cm)	Radius Ratio (D/E)	Experimental* Thermal Force (Dynes x 10^{-8})	Theoretical* Thermal Force (Dynes x 10^{-8})	Force Ratio (G/H)
1.0	502	185	2.94	5.57	0.528	1.11	0.232	4.78
1.0	488	193	2.98	5.65	0.527	1.14	0.225	5.07
1.0	488	195	2.78	5.68	0.489	1.32	0.225	5.87
1.0	495	202	2.96	5.76	0.514	1.21	0.228	5.31
1.0	488	203	2.97	5.80	0.512	1.21	0.225	5.38
1.0	493	216	3.05	5.98	0.510	1.23	0.227	5.42
1.0	722	175	2.31	4.73	0.488	1.68	0.333	5.05
1.0	1002	184	1.83	4.30	0.426	2.74	0.462	5.93
1.0	988	190	1.85	4.42	0.419	2.78	0.453	6.14
1.0	1222	238	1.88	4.58	0.410	3.44	0.563	6.11
1.0	1466	210	1.86	3.96	0.470	3.06	0.676	4.53
1.0	1470	227	1.96	4.13	0.475	3.03	0.678	4.47
1.0	1975	198	1.49	3.36	0.443	4.24	0.911	4.65

*All computations are based on a particle diameter of 1.0 micron.

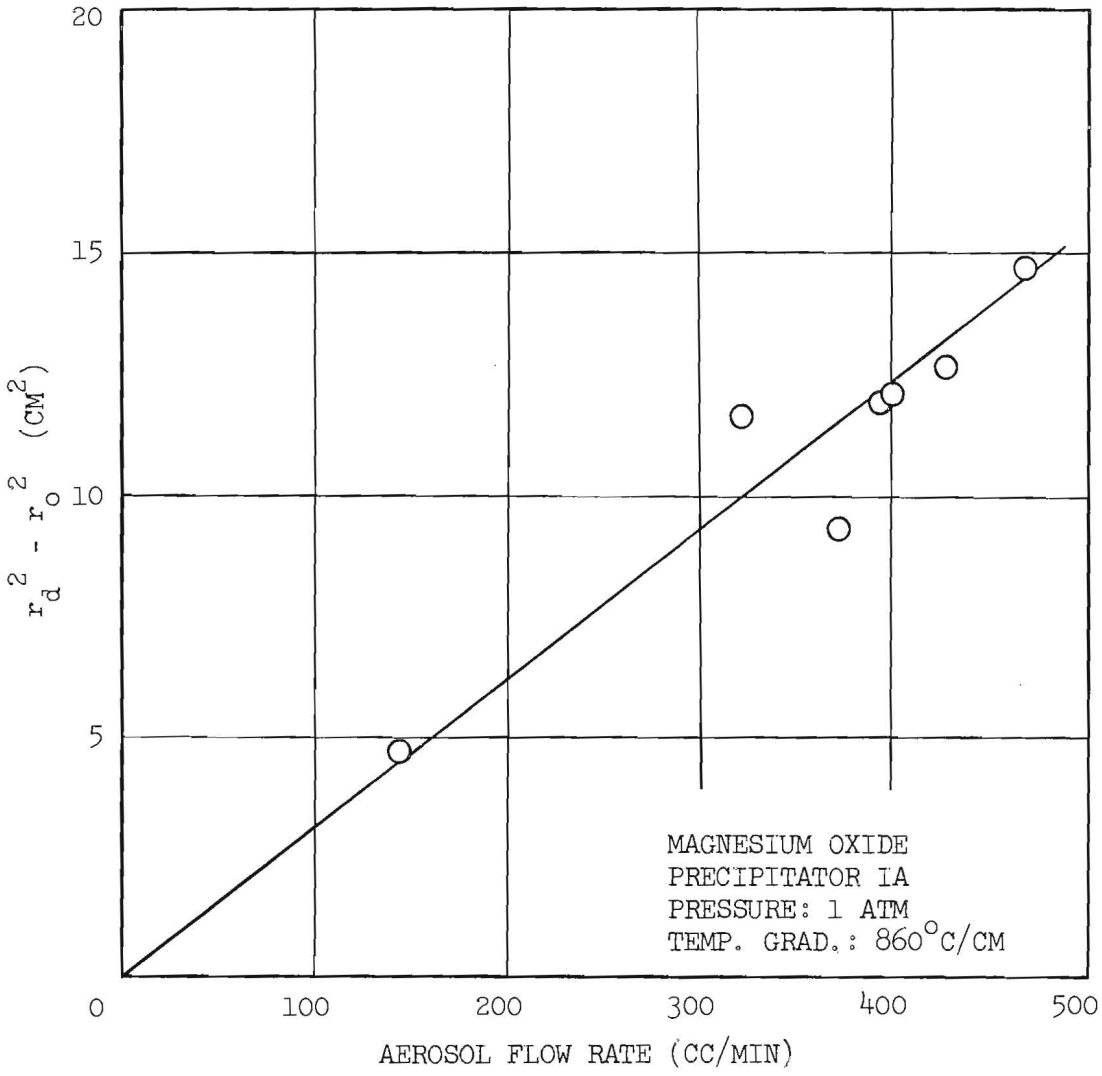

Figure 18. Linear Dependence of $(r_d^2 - r_o^2)$ on Aerosol Flow Rate.

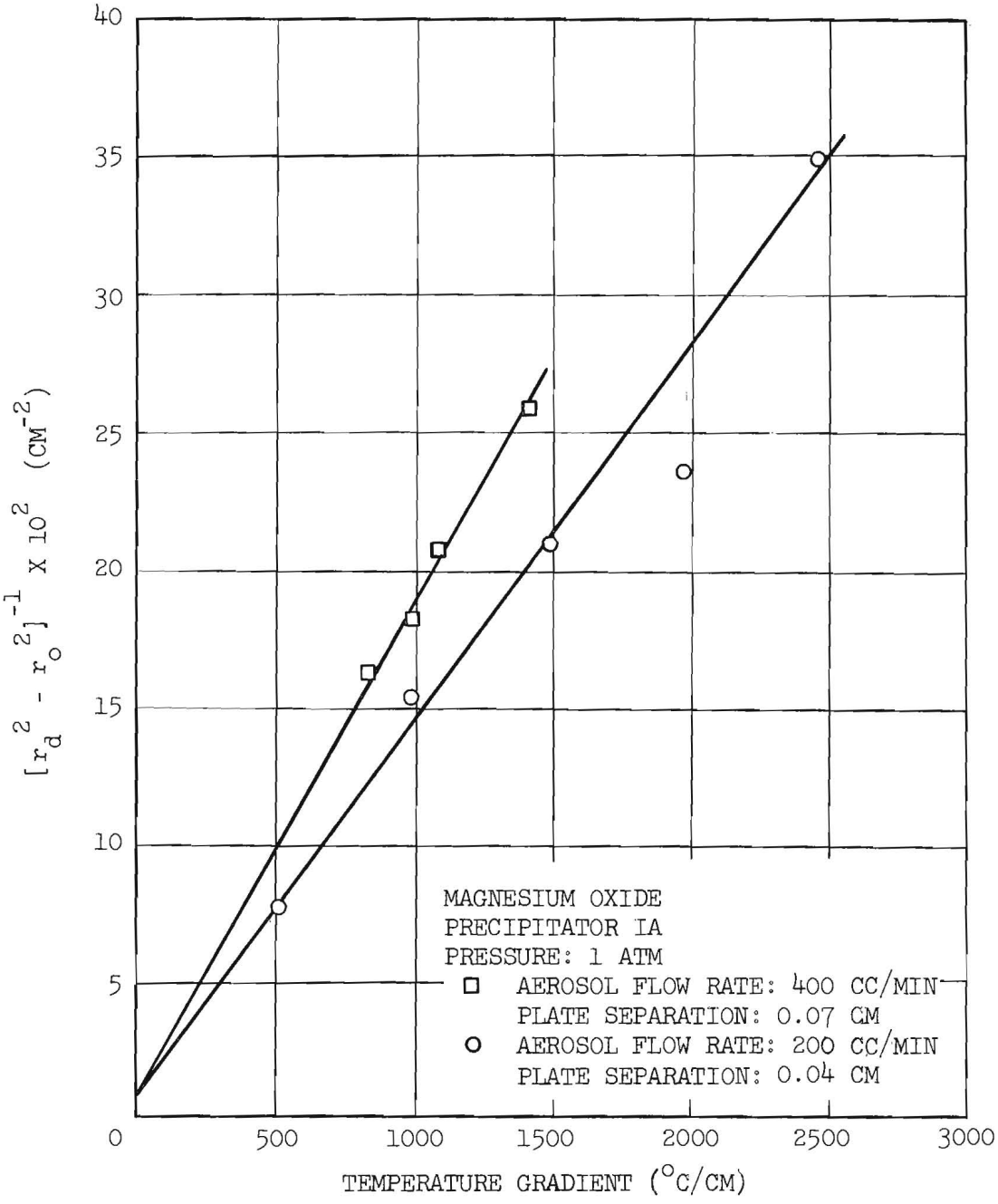

Figure 19. Linear Dependence of $(r_d^2 - r_o^2)^{-1}$ on Temperature Gradient.

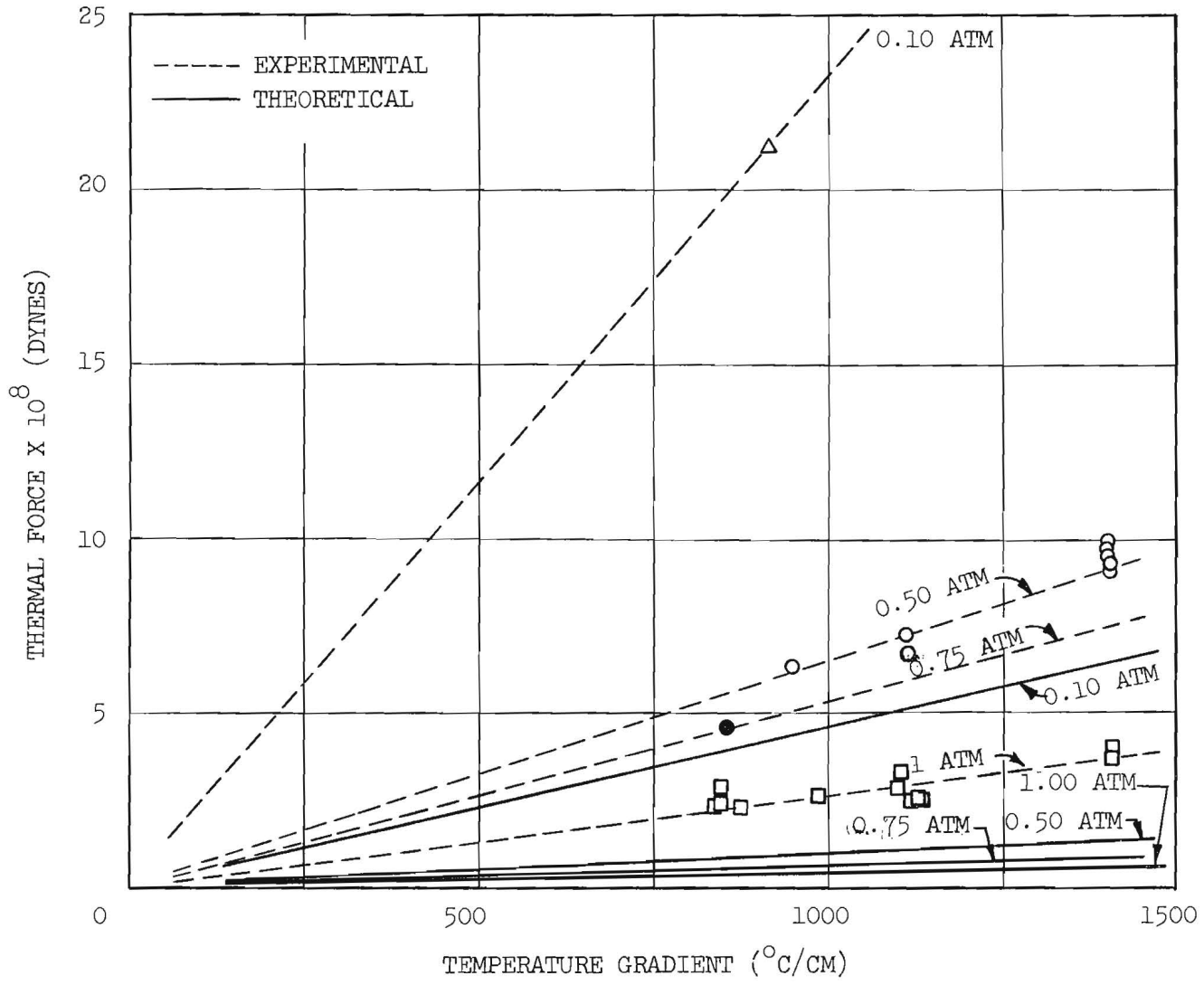

Figure 20. Effect of Pressure on Thermal Force. Data are for 1.0 micron magnesium oxide particles; Precipitator IA; plate separation 0.07 cm.

collected over a thermal gradient range from 800° to 1400° C/cm. An average particulate diameter of 1.0 micron was used in making the calculations. Theoretical curves (solid line) have been included on the graph for comparison with the experimental values (broken line). It should be noted that the 0.1 and 0.75 atmosphere pressure curves have been drawn through a single experimental point with an intercept at the origin. Thus these curves serve merely to substantiate the magnitude of the absolute value of the force determinations at the lower pressures. At all pressures a definite disagreement with theoretical results has been indicated. The ratio of experimental force to theoretical force appeared to be on the order of six to one.

d. Consistency of Experimental Data. The results given in Table I for the thermal force at one atmosphere are adequately supported by those of two additional series of experiments. The data presented in Table II were obtained using the same precipitator, IA, with a plate separation of 0.04 cm. The data of Table III were obtained using another precipitator at the same design, IB, with a plate separation of 0.04 cm. A comparison of the three series of runs is made in Figure 21. It may be seen that the results are in general agreement and are consistently higher than Epstein's theory would predict. The experimental-to-theoretical thermal force ratios range from about 4 to 7.

Figures 22 and 23 illustrate the consistency of the data for the three series of experiments. In each illustration, the particle travel, $r_d - r_o$, adjusted for constant flow rate, has been plotted against the temperature gradient (broken line curves). In each case a solid line curve has also been constructed to indicate the corresponding theoretical particle travel.

Figure 22 presents the results from Table I. Only the data obtained at atmospheric pressure and with flow rates in the vicinity of the base value of 400 cc/min have been plotted. It can be seen that all the points lie within an experimental deviation of ± 10 per cent. Over the limited temperature gradient range, and for the operating conditions of these tests, the relationship between particle travel and temperature gradient is essentially linear. The ratio of experimental radius to

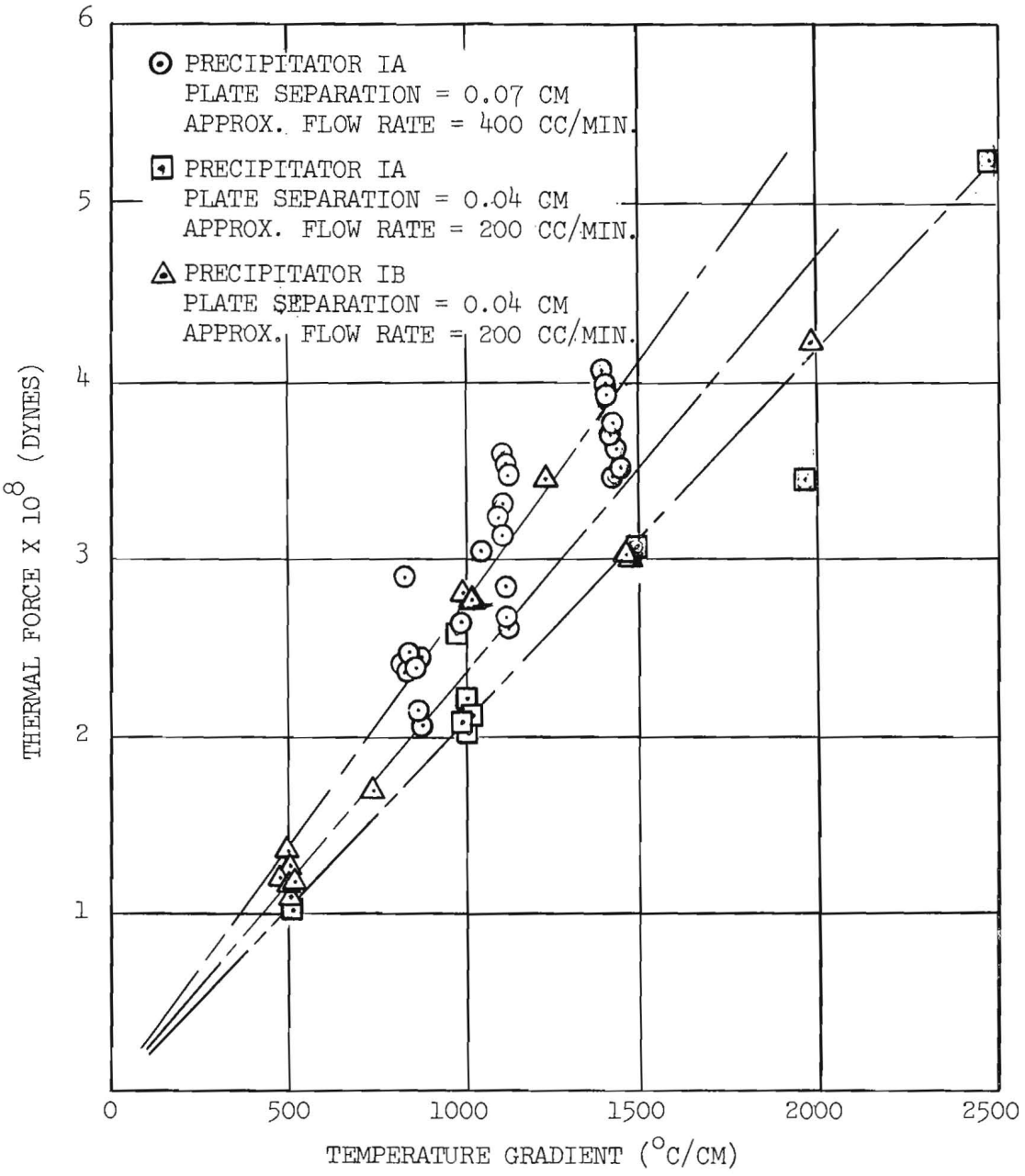

Figure 21. Thermal Force as a Function of Temperature Gradient at 1.0 Atmosphere Pressure. Data are for 1.0 micron magnesium oxide particles.

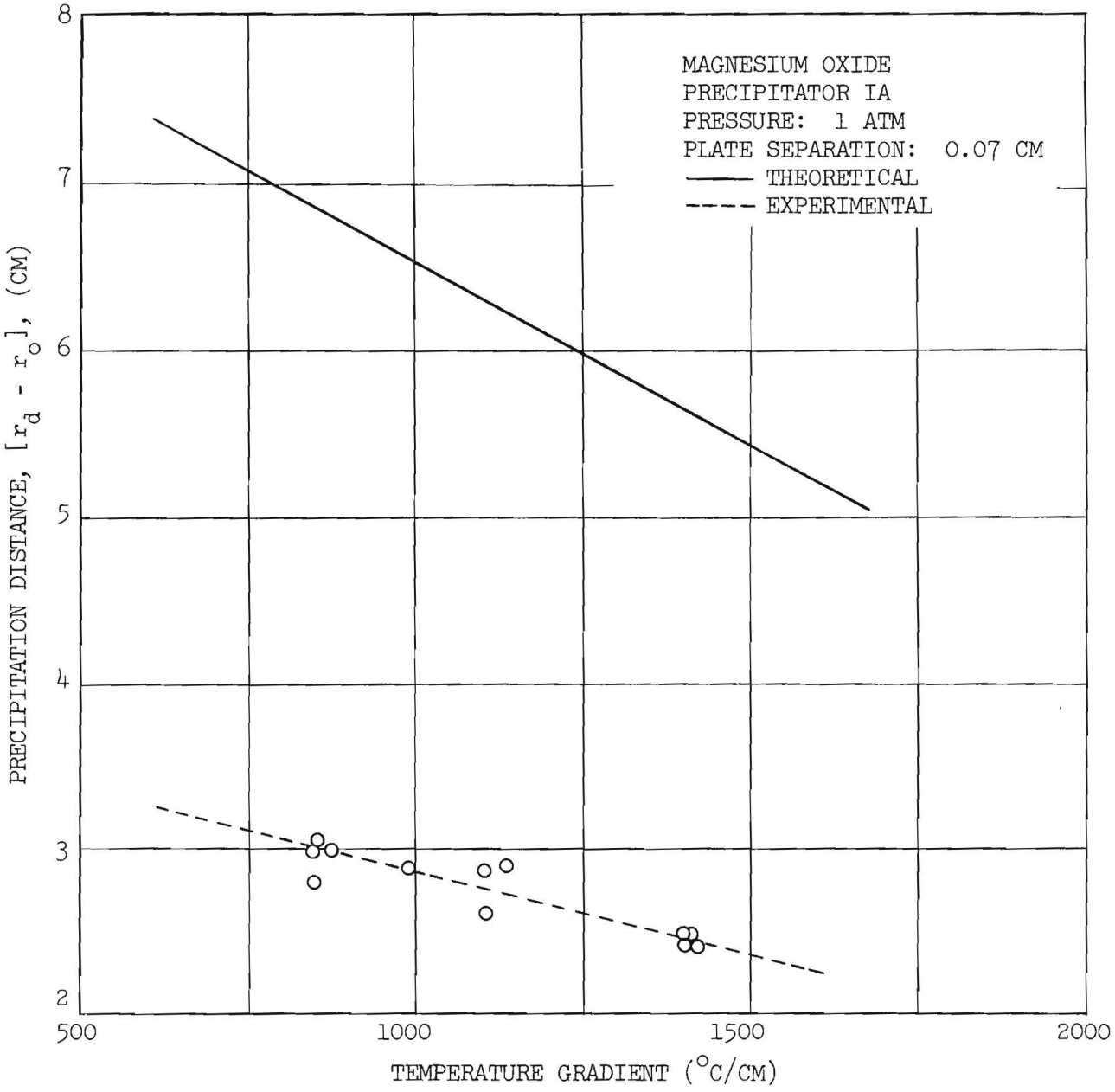

Figure 22. Precipitation Distance as a Function of Temperature Gradient at 1.0 Atmosphere Pressure and an Aerosol Flow Rate of 400 CC/Min. Theoretical data are for 1.0 micron particles.

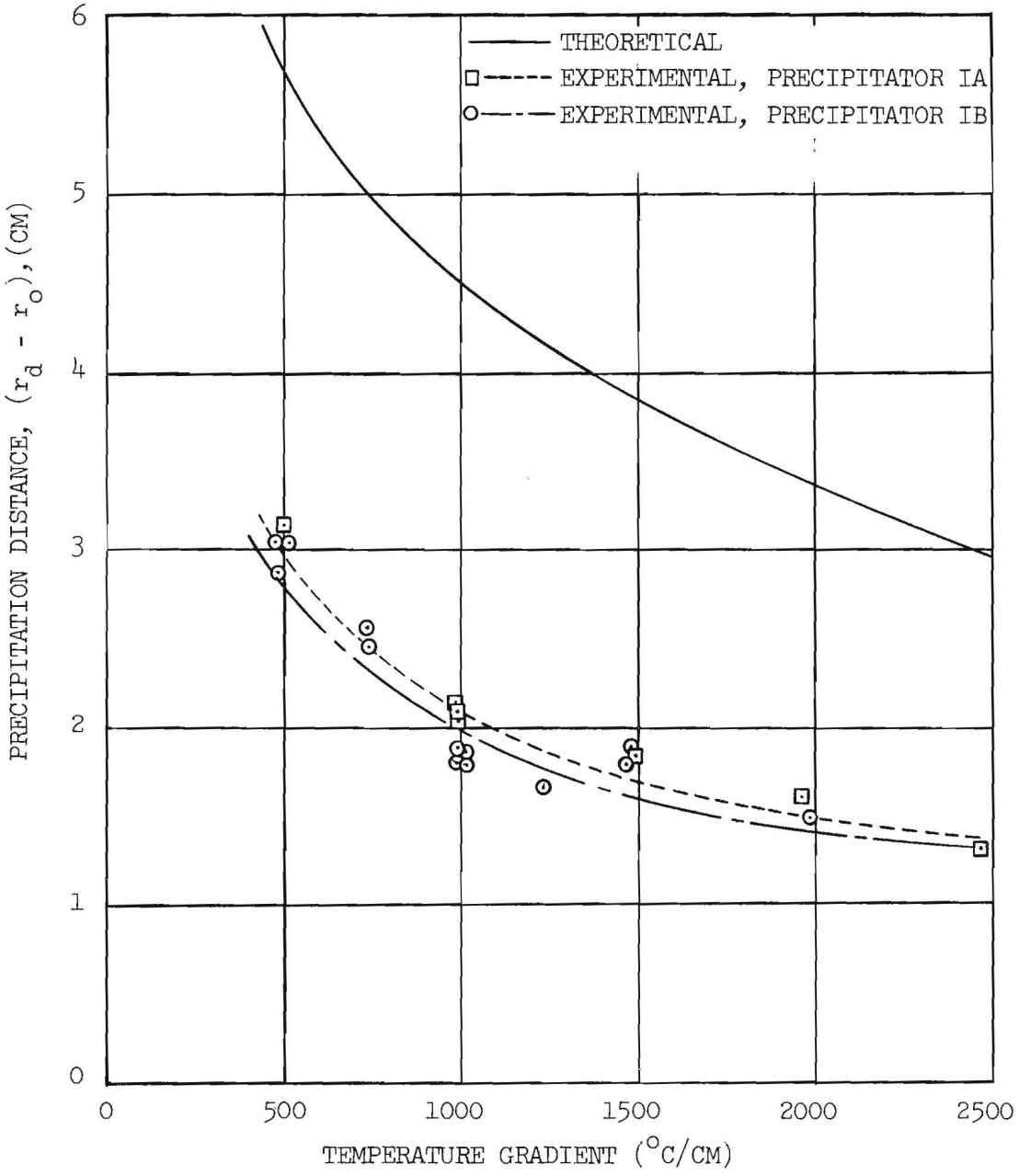

Figure 23. Precipitation Distance as a Function of Temperature Gradient at 1.0 Atmosphere Pressure and at an Aerosol Flow Rate of 200 CC/Min. Theoretical curve is for 1.0 micron magnesium oxide particles. Precipitator plate separation is 0.04 cm.

theoretical radius is approximately 0.47.

Figure 23 presents the results obtained at a pressure of one atmosphere and a precipitator plate separation of 0.04 cm on precipitators IA and IB. In both cases the particle travel, $r_d - r_o$, has been adjusted for a flow of 200 cc/min and plotted against temperature gradient. From this illustration, it can be seen that the data of both curves lie within an experimental deviation of ± 15 per cent and for either series the average values lie within ± 10 per cent of the mean curve. It can be seen also that the relationship between precipitation distance and temperature gradient is actually not of the linear character indicated in Figure 22. Instead, the rate of change of travel with respect to temperature gradient increases as the thermal gradient decreases. The ratio of observed radius to theoretical radius also varies. For the results of Table II (Precipitator IA) this ratio varies from about 0.56 for a gradient range of 500°C/cm to about 0.45 for a gradient of 2500°C/cm. For the results of Table III (Precipitator IB) the ratio decreases from about 0.52 to 0.45 over the same range of thermal gradients.

The data of all three series of experiments generally fall within an observed experimental deviation of about 15 per cent (see Figure 21). It has been noted however that the forces given in Table I are consistently higher than those presented in Tables II and III. In this connection, it should be noted that the average flow rate for the first set of data was on the order of 400 cc/min while the average flow rate for the second and third tabulations are less than 200 cc/min. According to the simplified theoretical development, the thermal force is independent of the aerosol flow rate which therefore should have no bearing on these results. However, this conclusion is based on the assumption of negligible entrance effects and a linear temperature profile.

2. Precipitation of Magnesium Oxide Using Model II Precipitator

From the results presented above, it is clear that the apparatus and techniques initially employed would produce acceptable data. However, as was mentioned earlier, it seemed that a radial flow precipitator with a restricted aerosol inlet might yield more revealing deposits. Such a precipitator (Model II) was designed, constructed, and put into operation.

Considerable difficulty was encountered with aerosol flow control in this apparatus due primarily to the split gas stream at the aerosol inlet. Data were obtained for the precipitation of magnesium oxide, but the results were of little additional value. Significant deductions regarding the thermal forces still could not be made from the deposit interior. The deposit radii, measured to the outer periphery, were of value, however, in supporting the results of Model I experiments. The data obtained from a typical series of experiments with Precipitator II are presented in Table IV.

TABLE IV

EXPERIMENTAL DATA FOR THE PRECIPITATION OF MAGNESIUM OXIDE PARTICLES USING RADIAL FLOW PRECIPITATOR II WITH PLATE SEPARATION OF 0.04 CENTIMETER

Pressure (Atm)	Thermal Gradient (°C/Cm)	Aerosol Flow Rate (CC/Min)	Deposit Radius (Cm)	Experimental* Thermal Force (Dynes x 10^{-8})	Theoretical* Thermal Force (Dynes x 10^{-8})	Force Ratio
0.98	670	245	3.54	1.56	0.309	5.05
0.97	990	115	2.18	2.69	0.457	5.89
0.97	1475	150	1.85	6.28	0.681	9.21
0.96	1480	99	1.88	3.75	0.683	5.50
0.97	1560	100	1.96	3.31	0.720	4.60

* All computations based on a particle diameter of 1.0 micron.

It is evident that the data of line 3 are inconsistent with the remainder of the tabulation. It has been noted that this particular observation was made from a very faint deposit which may have been larger than the measurements indicate. With this single exception, the experimental forces are comparable to those determined by experiments with Precipitators IA and IB, as shown in Figure 24, and fall within the previously observed deviation. The fact that the same thermal force values were obtained with precipitators of different design lends considerable support to the reliability of experimental results.

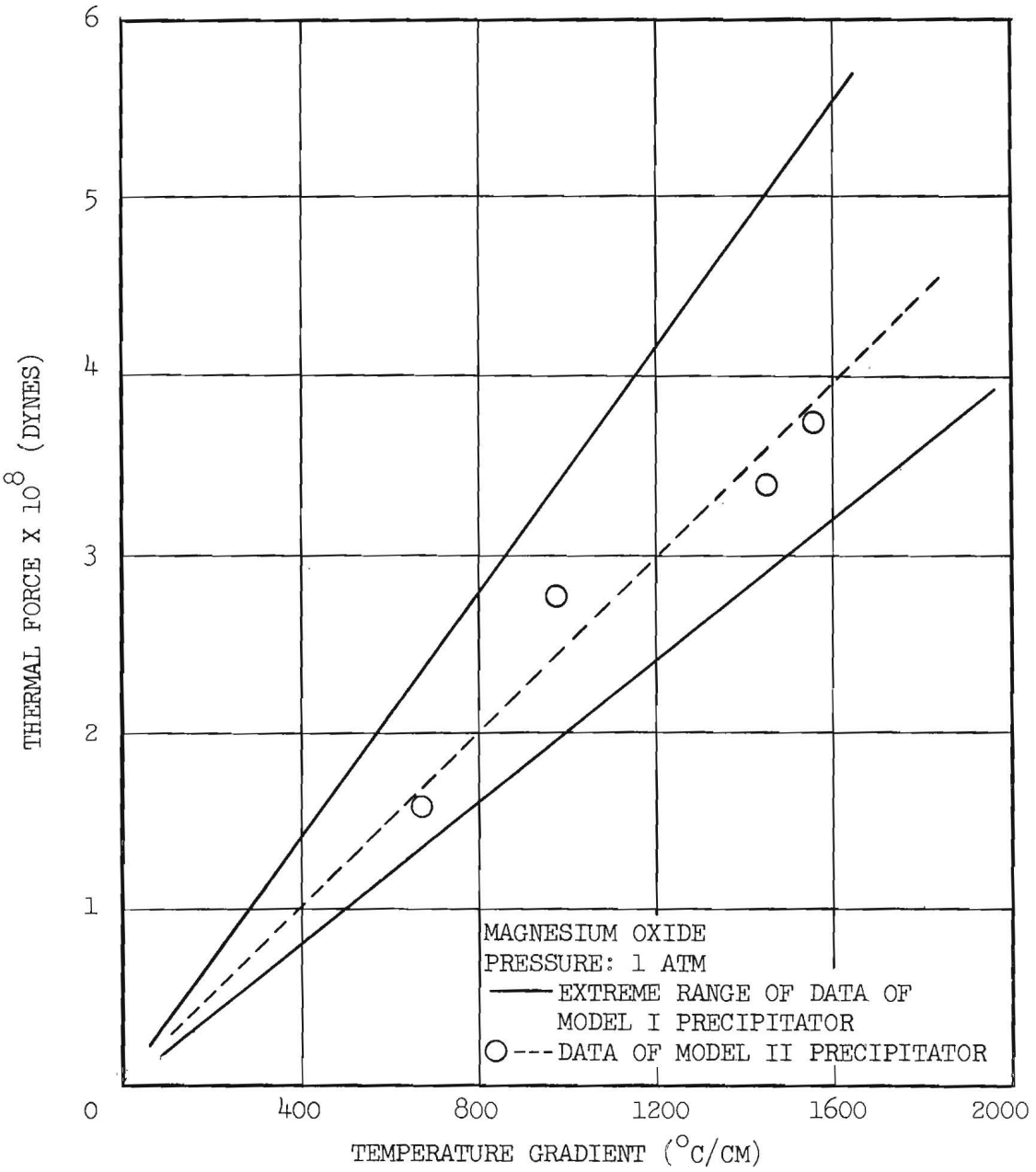

Figure 24. Comparison of Experimental Force Evaluations from Data of Radial Flow Precipitator Models I and II.

The Model II precipitator was larger and more complicated than Model I, and the time required for it to reach thermal steady state was about four times greater. This factor, in conjunction with the flow control difficulties attendant to the operation of Precipitator II and the fact that the experimental data obtained with it were in no sense superior, led to its abandonment. Experimental studies were resumed using the original radial flow precipitator.

3. Precipitation of Metallic Aerosols Using Model I Precipitator

The accumulation of data for a number of materials of various thermal conductivities was next undertaken. The choice of particulate materials for this investigation is severely limited. If the particles are too small relative to the mean free path of the carrier gas, the thermal force mechanism is not dependent upon thermal conductivity of the particulate material and the aerosols would be unsuitable for this investigation. If the particles are too large, the gravitational component outweighs the thermal component of velocity and significant deductions could not be made from experimental observations. Therefore, the particulate diameter is restricted to a lower limit of about 0.1 micron for atmospheric observations and to an upper limit ranging from 0.5 to 5 microns, depending upon the density of the material. Further, it is necessary that the thermal conductivity of the subject material be known accurately. Liquid droplets would seem ideal for numerous reasons, namely, (1) droplet size is easily controlled by standard aerosolization techniques, (2) the particulate thermal conductivity may safely be assumed equal to the bulk conductivity, (3) liquid densities are usually low, (4) a spherical particulate is assured, and (5) a wide range of relatively low thermal conductivities is available. Unfortunately, the analysis of a fluid deposit is unreliable due to the uncertainty in droplet size at the time of precipitation because of agglomeration of the primary droplets and to its tendency to flow after deposition on the usual collecting surface. Also, the range of thermal conductivity for suitable liquids is severely limited. Hence, liquid aerosols were disqualified. A number of powders thought to meet the requirements for experimental study were obtained, including aluminum oxide, carbon, zinc, iron, and aluminum.

Because of the pronounced conflict of theoretical and previous experimental observations which had been reported for materials of high thermal conductivity, the next precipitation experiments were conducted with metallic aerosols. Numerous attempts to obtain deposits suitable for analysis invariably produced the following results. The deposits were characterized by a dense central zone with a radius comparable to that of the magnesium oxide deposits. The outer periphery was not well defined, but it appeared that most of the particulate material had been deposited in the central region. Close examination of the deposits under an optical microscope revealed a central core of relatively high density which at some radius, dependent upon the operating conditions, faded rather rapidly into an area of extremely low density. The circumferential band between the regions of high and low density was wide and hazy. It was difficult to obtain data of quantitative value from such deposits. However, the following qualitative observations were recorded, specifically for zinc deposits, but applicable to deposits of aluminum, carbon, and iron as well. Particle diameters, ranging from 0.5 to 2 microns, were observed in the circumferential band. Within the more dense area of the deposit, discrete particulate sizes were obscured by a profusion of agglomerates. The agglomerates appeared large relative to the primary particle size and were observed even in deposits of very light overall density. In the circumferential band relatively few agglomerates were observed. Beyond the band which marks the apparent deposit periphery there was a conspicuous absence of agglomerates, but a background of uniform low particulate density extending over the entire surface of the collecting disc was always observed. Similar observations were made on deposits of magnesium oxide, with one notable exception. The background of scattered particles was not observed. Thus the deposit periphery was clearly defined by the circumferential band which was always much more narrow in the case of the oxide.

These observations suggested a premature conclusion that metallic particles, while not so effectively precipitated as materials of lower thermal conductivity, are subjected to thermal forces much greater than Epstein's equation predicts.

4. Precipitation of Aluminum Oxide Using Model I Precipitator

In order to obtain data of quantitative significance, attention was once again focused on materials of low thermal conductivity. Precipitators IA and IB, each with a plate separation of 0.04 cm, were used to collect deposits from aluminum oxide aerosols at atmospheric pressure. The data collected from these experiments are presented in Table V. The data of Series A were obtained with Precipitator IA over a range of temperature gradients from 988° to 1980° C/cm, and that of Series B were obtained with Precipitator IB over a range of aerosol flow rates from 182 to 670 cc/min. Extravagant precautions were taken during this series of experiments to maintain constant control and precise measurement of operating conditions. The resulting decrease in experimental deviations is evident in the tabulated force ratios, particularly for Series B. The consistency of individual experimental determinations of Series B has been graphically illustrated in Figure 25 where the quantity $(r_d^2 - r_o^2)$ has been plotted versus aerosol flow rate. This curve also supports the theoretical linear relationship predicted by equation 8.4, even more substantially, in fact, than does Figure 18. The departure from linearity indicated by the two points for flow rates of 595 and 670 cc/min are easily explained. These flow rates approach the upper limit of precipitator throughput capacity at the operating conditions of these experiments. A portion of the precipitated deposit overlapped the periphery of the removable collecting disk due to a slight eccentricity in its positioning in the precipitator. Hence, the average deposit radii recorded for these runs has been slightly underestimated. These two points have been shown because of their additional weight in supporting the precision of the measurements but have not been considered in evaluating average force measurements or experimental deviations. The individual deviations for Series A and B were found to be within 11 and 6 per cent, respectively. As in the study of magnesium oxide, the experimental forces were apparently higher than the values obtained from Epstein's equation using the thermal conductivity reported for the powder, this time by a factor in the range from 3.5 to 7.0. The average results for each series, while different, were within ± 15 per cent of the median value.

TABLE V

EXPERIMENTAL DATA FOR THE PRECIPITATION OF ALUMINUM OXIDE PARTICLES USING RADIAL FLOW PRECIPITATOR MODEL I[a]

Series	Pressure (Atm)	Temperature Gradient (°C/Cm)	Aerosol Flow Rate (CC/Cm)	Deposit Radius (Cm)	Experimental[b] Thermal Force (Dynes x 10^{-8})	Theoretical[b] Thermal Force (Dynes x 10^{-9})	Force Ratio
A	1.0	988	200	2.8	1.84	4.08	4.51
A	1.0	1003	330	3.44	2.00	4.14	4.83
A	1.0	1450	267	2.9	2.34	5.98	3.92
A	1.0	1488	265	2.40	2.41	6.14	3.93
A	1.0	1980	200	1.60	3.69	8.17	4.52
B	1.0	1480	182	1.94	3.78	6.12	6.18
B	1.0	1492	321	2.67	3.41	6.17	5.53
B	1.0	1488	358	2.79	3.50	6.15	5.69
B	1.0	1490	400	2.84	3.76	6.16	6.11
B	1.0	1485	467	3.18	3.47	6.14	5.65
B	1.0	1480	595	3.37	3.96	6.12	6.48
B	1.0	1485	670	3.5+	4.13	6.14	6.73

[a] Runs made with a plate separation of 0.04 centimeter.

[b] All computations based on a particle diameter of 1.0 micron.

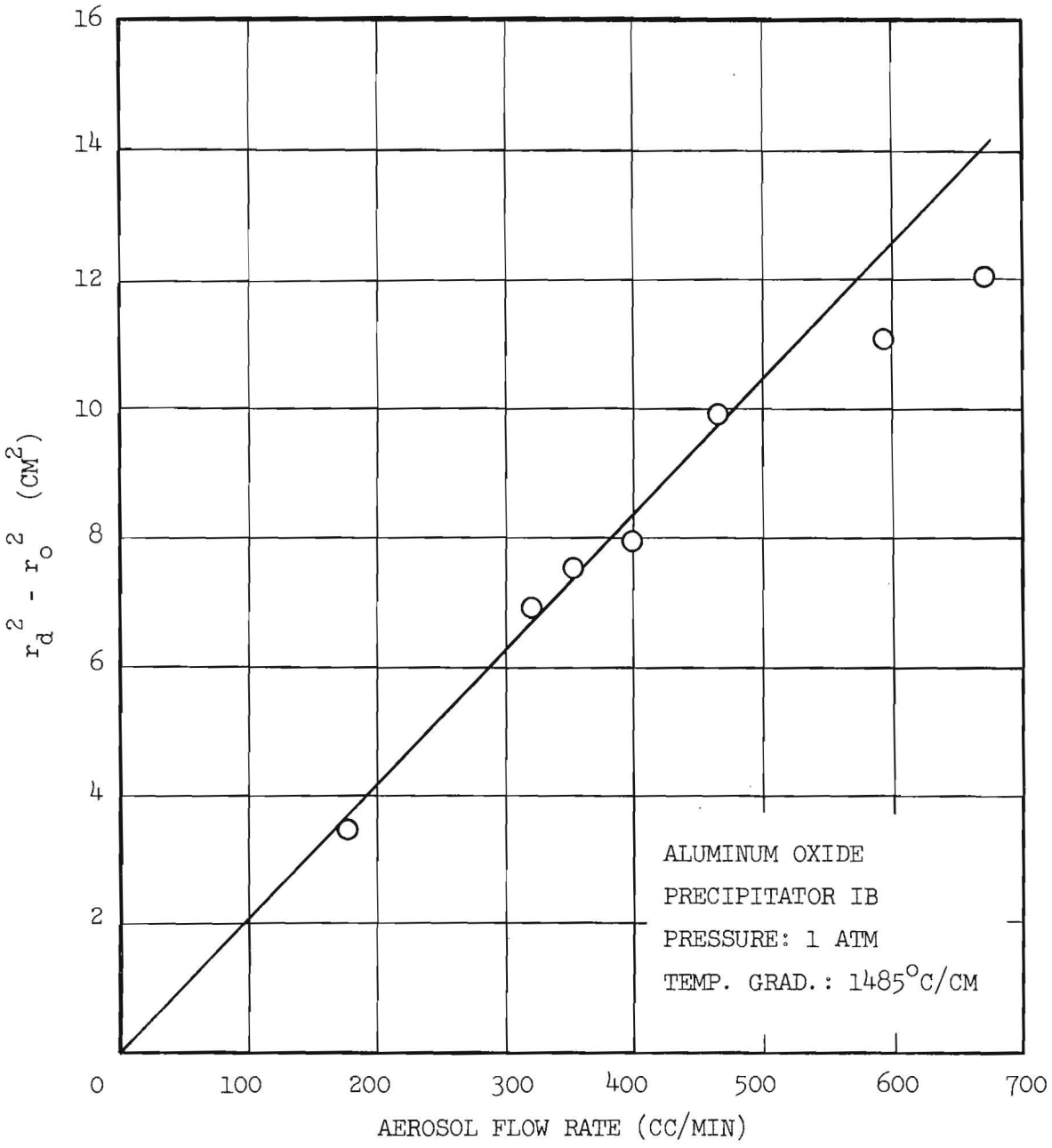

Figure 25. Consistency of Experimental Observations in the Precipitation of Aluminum Oxide.

5. Precipitation of Aluminum Oxide Using Model III Precipitator

The fact that experimental forces observed for both magnesium oxide and aluminum oxide were consistently higher than theoretical values led to speculation concerning the validity of the hydrodynamic analysis of data obtained with the radial flow precipitator. As was pointed out in Section VI, a number of simplifying assumptions were made in the derivation of the equations used for computation. Especially uncertain were entrance effects which had been assumed negligible. This assumption could be justified only through rough estimation by analogy to flowing systems less complex mathematically than the radial flow precipitator. A more rigorous hydrodynamic analysis could be made for a rectilinear flow precipitator with many of the assumptions eliminated. In an effort to establish the quantitative validity of thermal force and velocity values computed from experimental observations, such a precipitator, Model III, was constructed and used in this investigation. Unfortunately, the gain in the mathematical simplicity of the analysis of results was offset by a lack of precision in the physical control and measurement of temperature gradient and deposit dimensions in particular. This lack of precision was due primarily to the large surface area required for complete deposition and to edge effects induced by the precipitator plate spacer. The results of the experimental precipitation of aluminum oxide particles with Precipitator III are presented in Table VI. It is apparent that the experimental deviations between individual experiments were greater than in the case of radial flow precipitation, and Precipitator III was therefore less suitable for this experimental investigation. Still, the data of Table VI are valuable in establishing the credibility of earlier force measurements, since the entrance effects in the establishment of temperature and velocity profiles in Precipitator III are thought to be less significant, and the position of the uppermost particles at the entrance to the precipitation zone is more certain. The general agreement of these data with those of the radial flow precipitator is illustrated in Figure 26.

6. Precipitation of Solids of Various Thermal Conductivities Using Model I Precipitator

In view of the experimental results which had been obtained up

TABLE VI

EXPERIMENTAL DATA FOR THE PRECIPITATION OF ALUMINUM OXIDE PARTICLES USING LINEAR FLOW PRECIPITATOR III

Series[a]	Temperature Gradient ($^{\circ}$C/Cm)	Aerosol Flow Rate (CC/Min)	Deposit Length (Cm)	Experimental Thermal Force[b] (Dynes x 10^{-8})	Theroretical Thermal Force[b] (Dynes x 10^{-8})	Force Ratio
A	560	454	8.5	1.49	0.242	6.15
A	544	520	9.4	1.54	0.235	6.55
A	571	690	13.2	1.44	0.246	5.86
B	552	460	3.6	3.85	0.238	16.17
B	1395	533	3.5	4.64	0.601	7.73
B	1408	280	1.3	6.48	0.606	10.68
B	1597	1172	5.5	6.53	0.688	9.50

[a] Data classified as series A or B according to precipitator plate separation. For series A, plate separation = 0.127 cm; for series B, plate separation = 0.038 cm.

[b] All computations based on a particle diameter of 1.0 micron.

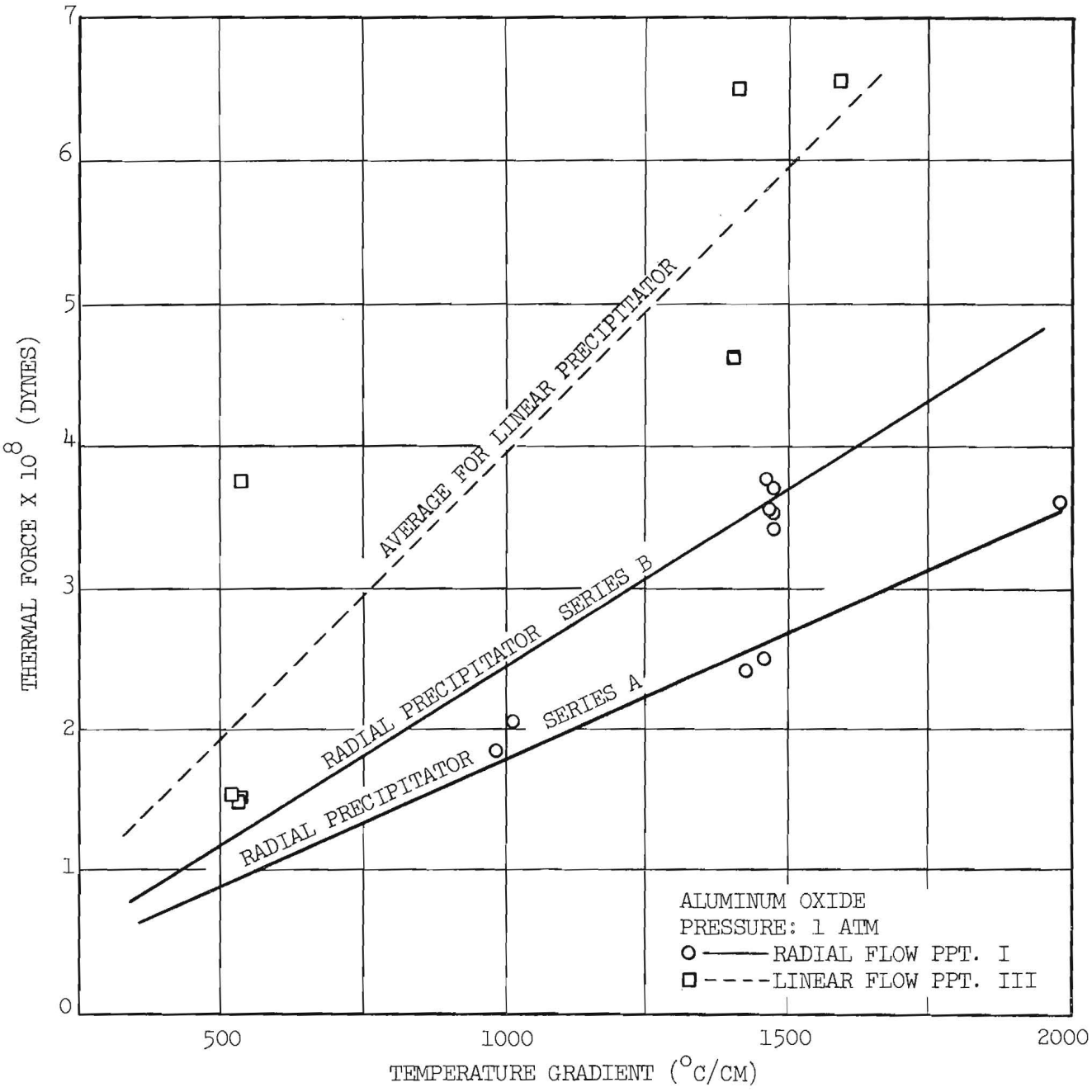

Figure 26. Comparison of Experimental Force Evaluations from Data of Radial and Linear Flow Precipitators, Models I and III.

to this point, the original Model I radial flow precipitator was selected for further studies. One additional refinement was made in an effort to increase the precision of the data. The average discrepancy which had been observed in the experimental results using Precipitators IA and IB could be accounted for by an error of less than 0.002 inch in the evaluation of precipitator plate separation. For this reason the hot plate face and the plate spacer of Precipitator IB were remachined and the plate separation was recalibrated. The experimental investigation of thermal precipitation was then resumed with added confidence. Observations were made for several airborne particulate materials precipitated at atmospheric pressure under temperature gradients ranging from 1100° to 1700° C/cm. Plate separation was maintained on the order of 0.04 cm. The average results which were obtained are presented in Table VII. Magnesium oxide and aluminum oxide aerosols were precipitated as standards for comparison with previous results. The data for these materials (lines 1 and 2) are in agreement with those of initial experiments.

a. Aerosols Produced by the Dispersion of Powders. Aerosols of gas carbon, zinc, aluminum pigment and iron were generated by atomization. The deposits obtained with each of these materials were of the nature of the zinc deposits previously described. That is, to the naked eye precipitation appeared to be complete, but under microscopic examination a dense central deposit was observed against a light background of fine particulate material. Measurements of the radii of the dense central core were recorded and thermal forces computed therefrom. The average results are presented in lines 3 through 6 of Table VII. These observations seem to be in complete disagreement with theory. Not only are the values many times greater than theoretical forces based on the bulk conductivity of particulate material, but the qualitative theoretical influence of thermal conductivity is not evident. For example, the maximum force on aluminum pigment particulates is apparently greater than the average force on aluminum oxide particulates, yet the thermal conductivity of aluminum is many times that of its oxide.

b. Aerosols Produced by the Exploding Wire Technique. Since it appeared that thermal precipitation of materials of relatively high

TABLE VII

EXPERIMENTAL DATA ON THE PRECIPITATION OF VARIOUS PARTICULATE MATERIALS USING RADIAL FLOW PRECIPITATOR MODEL I

Line No.	(A) Particulate Material	(B) Aerosolization Techniques	(C) Thermal Conductivity of the Solid (Cal/Cm Sec ^{o}K)	(D) Experimental Thermal Force Per Unit Temp. Gradient x 10^{11} (Dyne Cm/^{o}C)	(E) Theoretical Thermal Force Per Unit Temp. Gradient x 10^{11} (Dyne Cm/^{o}C)	(F) Force Ratio (D/E)	(G) Reduced Thermal Force x 10^{7} $[F_t \div a\frac{dT}{dy}]$ (Dynes/^{o}C)
1	MgO	Mg burned in air	0.00146[a]	2.30	0.475	4.85	4.60
2	Al_2O_3	Atomized	0.00163[a]	1.89	0.432	4.38	3.78
3	Gas Carbon	Atomized	0.00826	3.27[b]	0.086	38	6.54
4	Al	Atomized	0.504	2.17[b]	0.00142	1530	4.34
5	Zn	Atomized	0.265	2.19[b]	0.00270	812	4.38
6	Fe	Atomized	0.11 - 0.14	2.14[b]	0.006	357	4.28
7	Ag	Exploded	0.963	2.86	0.0007	4080	5.72
8	Pt	Exploded	0.167	3.35	0.0043	778	6.70
9	Al_2O_3	Aluminum exploded in air	0.00163[a]	3.45	0.432	7.99	6.90
10	Bi_2O_3	Bismuth exploded in air	--	2.73	--	--	5.46
11	NaCl	Aqueous solution exploded	0.0155	3.22	0.046	70	6.44
12	Iron Oxides	Iron Exploded in air	0.00135[a]	3.70	0.49	7.55	7.40

[a] Thermal conductivity of powder.

[b] Force computation on central core deposit radius, i.e., precipitation not complete.

thermal conductivity is effective (though not necessarily complete), additional experiments were conducted using aerosols generated by the exploding element technique. In this way, deposits were obtained with particulate materials including silver, platinum, sodium chloride, and the oxides of aluminum, iron, and bismuth. The average data of these materials are presented in lines 7 through 12 of Table VII. The first deposits obtained from aerosols generated by this technique were of metallic materials. Exceptionally large thermal forces were indicated by the deposit dimensions (see Table VII, lines 7 and 8). Furthermore, it appeared that the deposition of silver and platinum particulates was essentially complete, i.e., no background of particulates was observed beyond the outer periphery of the dense deposit. Aerosols of aluminum oxide were then generated by exploding the metal wires in oxygen. Again, complete deposition was obtained by precipitation with deposit radii which indicated a force considerably greater than that deduced from precipitated deposits of aerosols generated by atomization (Table VII, line 9). Further experimentation indicated exceptionally large forces for all aerosols generated by this technique, usually in the range from 3 to 4 x 10^{-11} dynes per unit temperature gradient for a 1.0-micron-diameter. Furthermore the magnitudes of the apparent thermal force seem to be independent of the thermal conductivity of the particulate material.

7. Precipitation of Solids of Various Thermal Conductivities Using Model I Precipitator in Inverted Position

A question arises in examination of the results of Table VII. Is it possible that thermal forces are obscured by some overriding influence such as gravitational or inertial force? If the particulate size evaluation by use of the optical micrometer is even moderately accurate (i.e., primary particle diameters less than 2 microns), then such factors could hardly be significant. In order to eliminate the remote possibility that the gravitational component might be excessive, a series of experimental observations was made with the thermal precipitator inverted during operation. In this way, the precipitating force was directly opposed to the gravitational force and must therefore have been significantly greater than the gravitational force in order for complete precipitation to take

place. The average results of these runs are presented in Table VIII. The data of the first line were obtained by the precipitation of magnesium oxide from an aerosol generated by burning. The thermal force value deduced in this case is essentially the same as that for normal precipitator operation. In the case of zinc (line 2) the aerosol was generated by dispersing the powder in air. Again, the precipitation of particulate material was not perfectly efficient. The force value deduced from the dense deposit core radius is only slightly higher than that of normal precipitator operation. In all other cases, including particulate materials of magnesium oxide, aluminum oxide, silver, platinum, graphite, and the oxides of iron, bismuth, lead, tin and antimony (lines 3 through 12) the aerosols were generated by the exploding element technique. In general, the forces deduced from inverted precipitator operation were slightly higher than the corresponding forces for normal precipitator operation. The greater precipitating force for these particulates was confirmed, and the effects of gravity and inertia discounted.

C. Detailed Study of Precipitator Deposits

If the foregoing observations are to be of any quantitative value in the study of thermal forces, then an acceptable interpretation of the apparent inconsistancy must be found. In view of the general support of Epstein's theory provided by Millikan type observations of other investigations, it seems most likely that the apparent discrepancy might be attributed to inaccuracies in the effective particulate thermal conductivity. In any event, it was decided that a detailed study of the deposit and of the individual particulates might be helpful in this analysis.

1. Characteristic Appearance of Deposits

The qualitative observations on the nature of deposition reported earlier were made from deposits which had been obtained primarily for the purpose of determining deposit radii. The deposits were deliberately made very dense for sharp definition of the outer periphery (see Figure 7). It was in such deposits that the heavier background for materials of high thermal conductivity was most obvious. Less dense deposits are preferable for detailed study specifically to permit particle counting and electron

TABLE VIII

EXPERIMENTAL DATA ON THE PRECIPITATION OF VARIOUS PARTICULATE MATERIALS USING RADIAL FLOW PRECIPITATOR MODEL I IN INVERTED POSITION

Line No.	(A) Particulate Material	(B) Aerosolization Techniques	(C) Thermal Conductivity of the Solid (Cal/Cm Sec ^{o}K)	(D) Experimental Thermal Force Per Unit Temp. Gradient x 10^{11} (Dyne Cm/^{o}C)	(E) Theoretical Thermal Force Per Unit Temp. Gradient x 10^{11} (Dyne Cm/^{o}C)	(F) Force Ratio (D/E)	(G) Reduced Thermal Force $[F_t \div a\frac{dT}{dy}]$ (Dynes/^{o}C)
1	MgO	Mg burned in air	0.00146[a]	2.36	0.475	4.97	4.72
2	Zn	Dispersed powder	0.265	2.60[b]	0.00270	963	5.20
3	MgO	Metal exploded in air	0.00146[a]	3.21	0.475	6.76	6.42
4	Al_2O_3	Metal exploded in air	0.00163[a]	3.53	0.432	8.17	7.30
5	Ag	Exploded	0.963	3.71	0.0007	5300	7.41
6	Pt	Exploded	0.167	3.68	0.0043	855	7.36
7	Graphite	Exploded	0.105	3.81	0.0068	560	7.62
8	Iron Oxides	Metal exploded in air	0.00135[a]	4.03	0.49	8.23	8.06
9	Bi_2O_3	Metal exploded in air	--	2.26	--	--	4.52
10	PbO	Metal exploded in air	--	3.72	--	--	7.44
11	SnO	Metal exploded in air	--	4.39	--	--	8.78
12	SbO	Metal exploded in air	--	3.26	--	--	6.52

[a] Thermal conductivity of powder.

[b] Force computation based on central core deposit radius, i.e., precipitation not complete.

microscope evaluation. Many of these less dense deposits of several different particulate materials were examined as a basis for the discussion which follows.

a. Deposit Density Variation with Radial Distance (Optical Micrographs). In general, the observations pertinent to dense deposits were found true for sparse deposits also. The characteristic appearance of these deposits is illustrated in a series of micrographs of an aluminum oxide deposit. The micrographs were taken at 390x magnification at strategic positions relative to the deposit and location in the precipitator as indicated in Figure 27. The sequence of micrographs (Figure 28) shows the nature and relative density of the deposit at (A) the central region beneath the precipitator inlet where deposition is the result of gravitational settling, (B) the beginning of the controlled thermal field, (C) the interior region of uniform high density, (D) the periphery of the dense central core, (E) an intermediate position in the circumferential band which was considered the average periphery, (F) a point immediately beyond the average periphery where scattered deposition occurs, and (G) outside the deposit boundary. It is evident that the deposition of particulate material was essentially complete. The interior of the deposit (micrographs A through D) is characterized by a dense deposit of particulates ranging from submicron diameter to several microns; many of the particulates are agglomerated. The predominant primary particle diameter appears to be on the order of 0.5 to 1.5 microns with agglomerated particulates much larger. Furthermore, the extent of agglomeration, with respect to both frequency and composite diameter, decreases with increasing deposit radius. Only an occasional particle (micrograph G) was observed beyond the circumferential band which marks the deposit boundary. Deposits of other particulate materials were of similar appearance, with the notable exception of atomized powders of high thermal conductivity for which the light background scattering of small particles was always observed.

b. Deposit Density Variation with Radial Distance (Particle Count). A particle count of the aluminum oxide deposit has been made corresponding to the micrographs of Figure 28. The results are shown in Table IX along with counts for zinc and aluminum deposits. From this

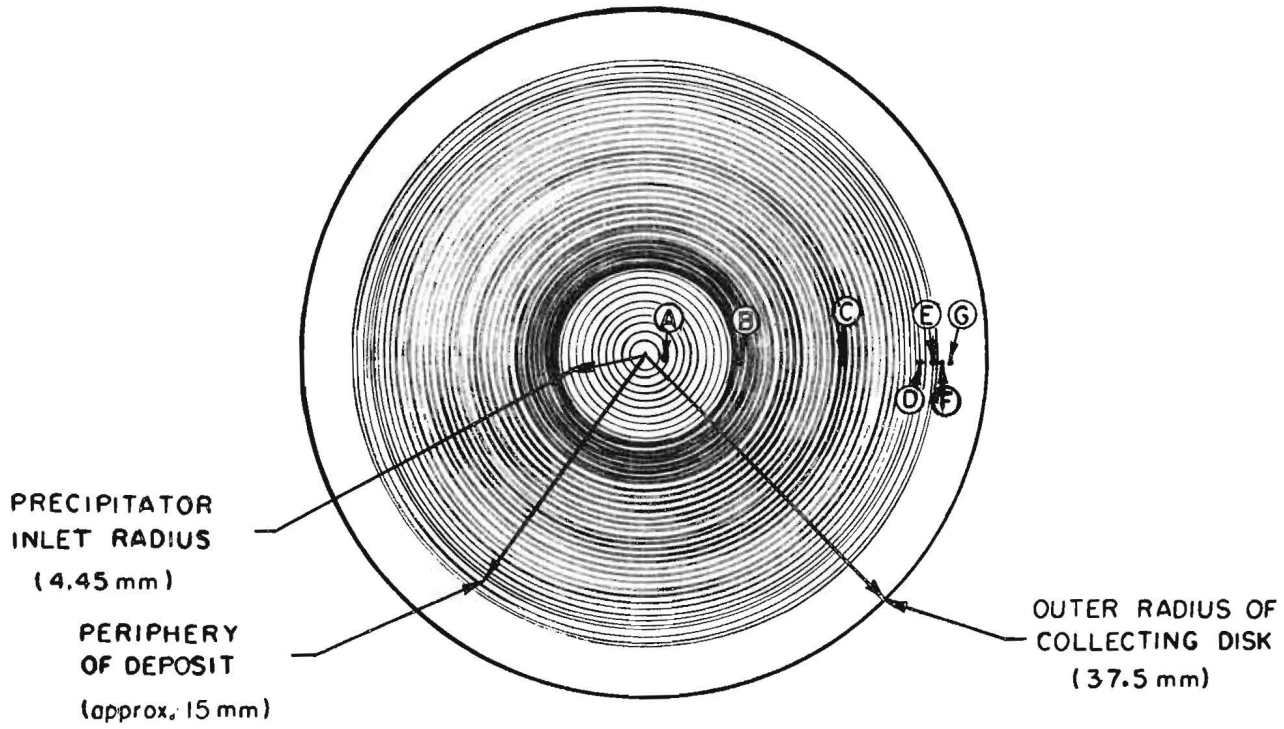

POSITION:	A	B	C	D	E	F	G
RADIAL DISTANCE FROM DEPOSIT CENTER (mm):	1.0	5.0	10.0	14.0	15.0	15.5	15.9

27A. Collecting Disk and Deposit.

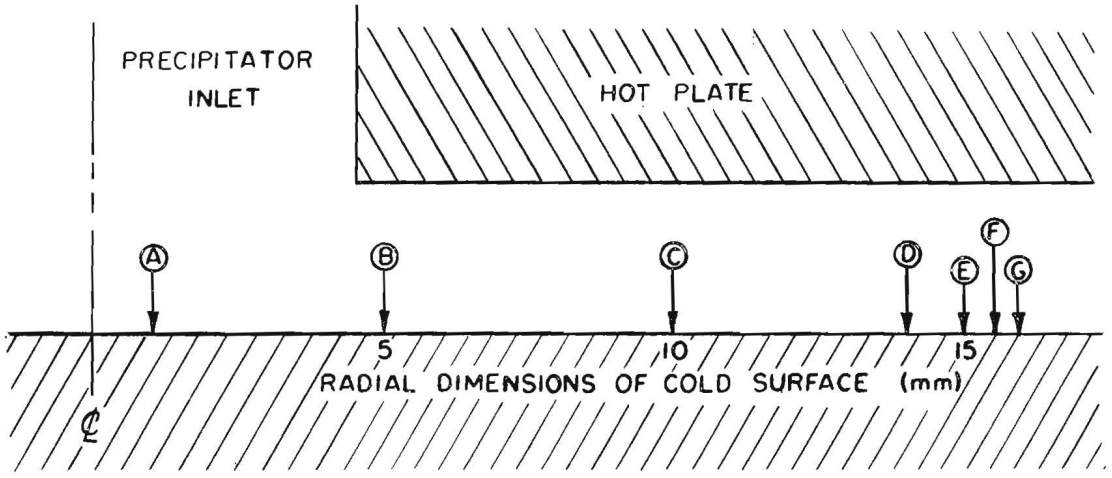

27B. Schematic View of Precipitator.

Figure 27. Location of Points at Which Micrographs of Figure 28 Were Taken. Corresponding positions are indicated by encircled alphabetical symbols.

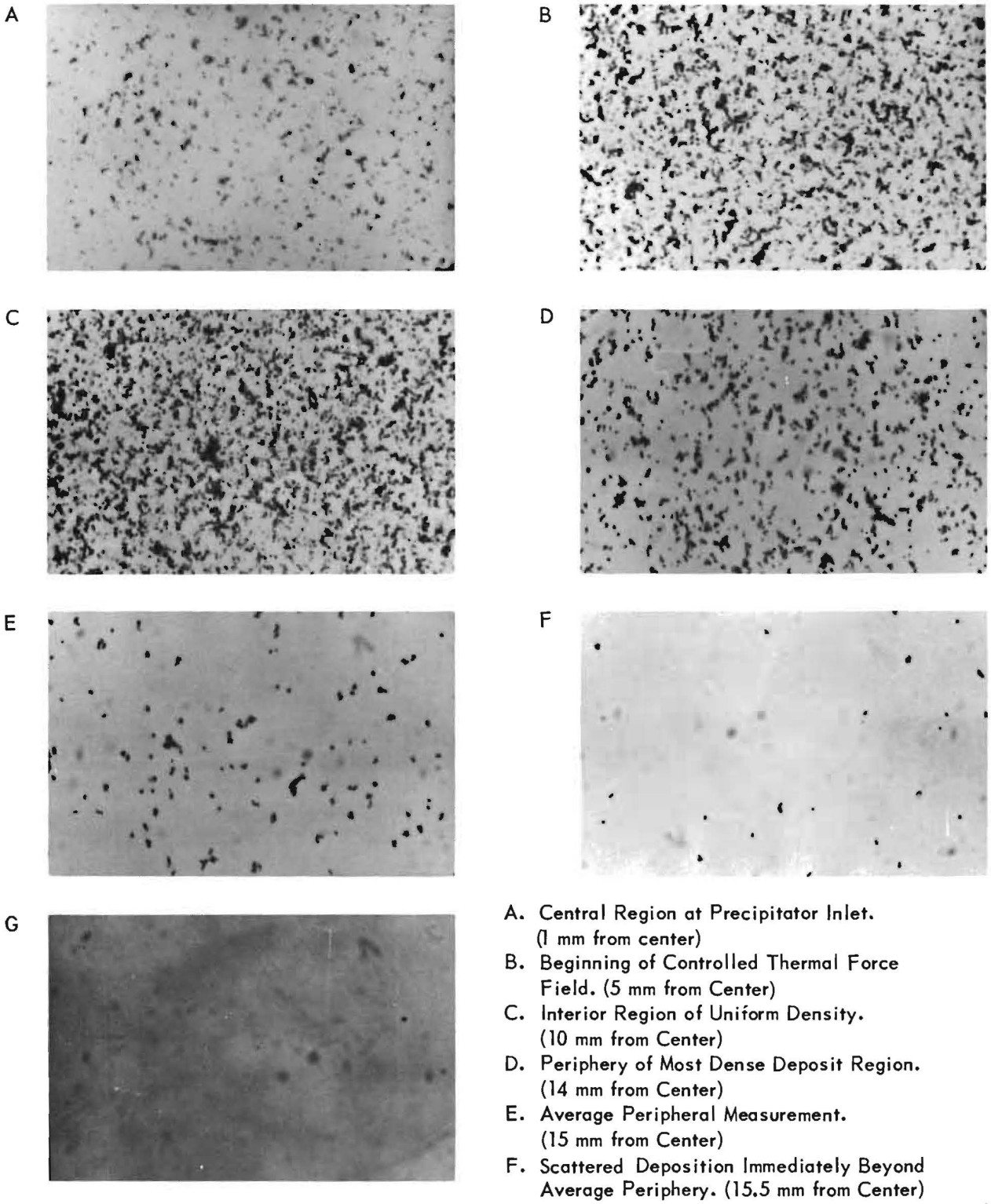

A. Central Region at Precipitator Inlet. (1 mm from center)
B. Beginning of Controlled Thermal Force Field. (5 mm from Center)
C. Interior Region of Uniform Density. (10 mm from Center)
D. Periphery of Most Dense Deposit Region. (14 mm from Center)
E. Average Peripheral Measurement. (15 mm from Center)
F. Scattered Deposition Immediately Beyond Average Periphery. (15.5 mm from Center)
G. Beyond Deposit Boundary. (15.9 mm from Center)
AEROSOL: Aluminum Oxide (Dispersed Powder)
MAGNIFICATION: 390X

Figure 28. Optical Micrographs of Aluminum Oxide Deposit.

TABLE IX

NUMBER OF PARTICLES AT VARIOUS RADIAL DISTANCES FOR THERMAL PRECIPITATION DEPOSITS[a]

Aluminum Oxide		Zinc		Aluminum	
Radial Distance[b] (Mm)	Particle Count[c]	Radial Distance (Mm)	Particle Count	Radial Distance (Mm)	Particle Count
1.0	864	0	128	0.0	280
5.0	1194	5.0	434	5.0	450
10.0	1268	10.0	373	10.0	430
14.0	672	12.0	401	15.0	386
15.0	130	13.0	266	20.0	220
15.5	25	14.0	27	25.0	56
15.9	2	14.5	7	30.0	3
16+	negligible	15 to 30	5 to 15		

[a] Precipitation from aerosols generated by dispersion of powder.

[b] Distance measured from center of deposit.

[c] Number of particles per unit area, counting agglomerates as single unit. (Unit area is not identical for all three materials.)

tabulation the different degrees of deposit definition are evident. The circumferential band may be identified with the decreasing particle count at the deposit periphery. Its width then is determined by the radial distance between the point of maximum deposit density and the point which marks either the termination of the deposit or the beginning of the scattered background. The circumferential band width in the case of aluminum oxide was on the order of 1.5 millimeters with a 15-millimeter deposit radius. This is congruous with the band width of 10 to 15 per cent of the total deposit radius which was typically observed with deposits of atomized oxides. In general, the deposit band width for atomized materials of high thermal conductivity was somewhat wider than this, while that for aerosols produced by the exploding wire technique was usually much narrower. That is, the deposits obtained from the exploded aerosol materials were more sharply defined and the background of scattered particles was not found. In additional test cases, aerosols were generated by exploding a cartridge of metallic powder, namely, zinc, aluminum, iron or graphite. Usually, the deposit possessed a very dense central core area with the scattered background characteristic of deposits of the atomized material.

2. Nature of Particulates

a. Optical Microscopy. From observations with the optical microscope, it appeared that deposited material consisted always of a mixture of primary particles and agglomerated masses. The usual distribution seemed to be on the order of 20 to 40 per cent agglomerates (see Figure 28). A particle size distribution for a zinc deposit at a point in the hazy circumferential band indicated visible particulates which appeared to be primary (i.e., unagglomerated) in the diameter range from < 0.4 to 3 microns with a preponderance of particles on the order of 0.4 to 0.8 micron. Agglomerates apparently ranged from 2 to 10 microns with occasional masses as large as 30 microns.

b. Electron Microscopy

(1) Deposit of Atomized Zinc Powder. Electron microscopy was more revealing than optical microscopy. Figure 29 shows the extent of true agglomeration in the zinc deposit discussed above. Figure 29A,

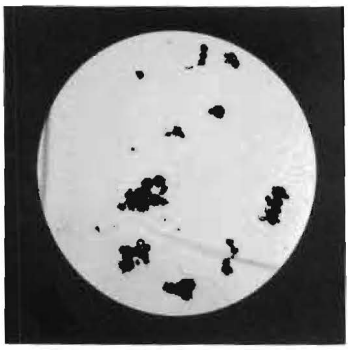

10 μ
A. 1100X

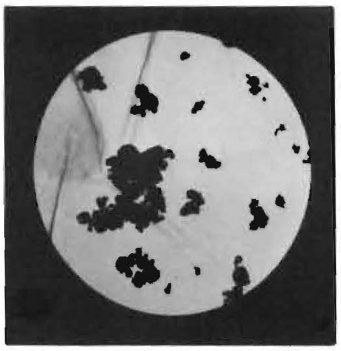

10 μ
B. 1100X

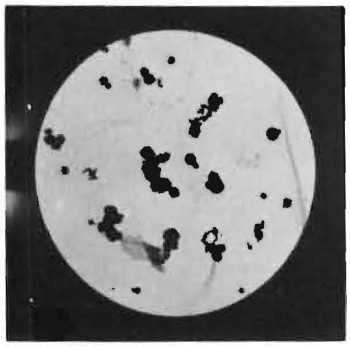

10 μ
C. 1100X

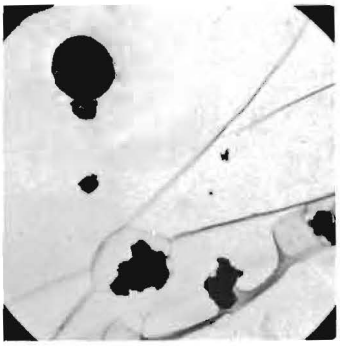

10 μ
D. 2300X

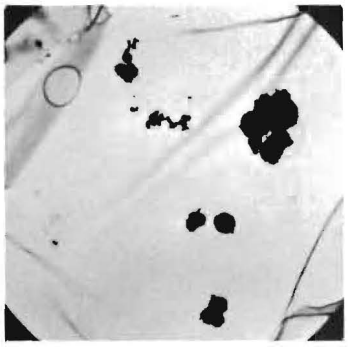

10 μ
E. 2300X

A, B & C: Taken in Circumferential Band Defining Dense Core Deposit.
D & E: Taken in Scattered Background Beyond Dense Central Core.
AEROSOL: Atomized Zinc Powder.

Figure 29. Electron Micrographs of Zinc Deposit.

B, and C were taken in the circumferential band at 1100x magnification. These micrographs show that essentially all particulates consist of an agglomeration of fine primary particles (much more frequent than the estimate of 20 to 40 per cent of the optical microscopy study). Even those small particles (0.5 to 2 microns) appear to be agglomerates. It was noted in scanning the deposit sample with the electron microscope that very few true primary particles on the order of one micron were observed in the region of dense deposition. On the other hand, most of the particulates observed in the lightly scattered background outside the central core of the deposit were not agglomerates (Figure 29D). A very few small agglomerates were observed in this region (Figure 29E). There was a conspicuous absence of large agglomerates. Furthermore, it can be seen that the agglomerates of Figure 29E are of a more simple character, consisting of fewer and larger primary constituents.

(2) Deposit of Atomized Aluminum Oxide Powder. An electron micrograph sequence, corresponding to the optical micrograph sequence of Figure 28, is presented in Figure 30. The same aluminum oxide deposit was used in both studies. The sequence of micrographs A, B, C and D, shown here at a magnification of 2300x, were taken at the respective radial distances (measured from the center of the deposit) of 1, 10, 14 and 15.5 millimeters. The comparative density of the deposit at each point, and the size, frequency, and complexity of agglomerates is immediately obvious. The agglomerates of the outer periphery of the deposit (micrograph D) are generally smaller and less complex than those in the more dense deposit region. This is illustrated clearly in micrograph E taken at 15.5 millimeters at a magnification of 5500x. An attempt to obtain micrographs of the few particles beyond the 15.5 millimeter radius was unsuccessful because of the scarcity of particulate material.

(3) Deposit of Magnesium Oxide Produced by Burning Magnesium. In view of the extent of agglomeration heretofore unsuspected, a deposit of magnesium oxide particles generated by burning magnesium ribbon was studied. The results are shown in Figure 31. All micrographs were taken of particulate material stripped from the outer periphery of

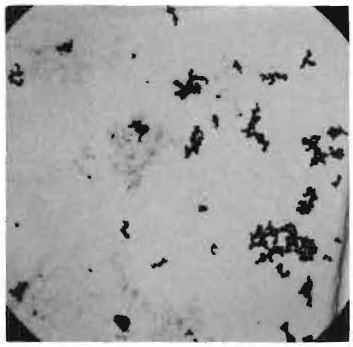

10 μ
A. 2300X

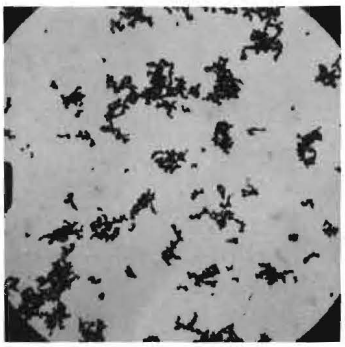

10 μ
B. 2300X

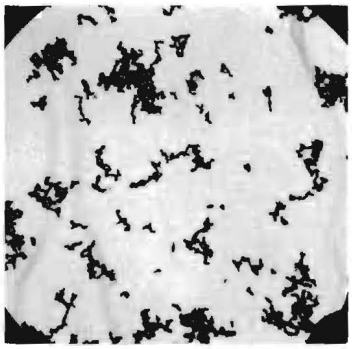

10 μ
C. 2300X

10 μ
D. 2300X

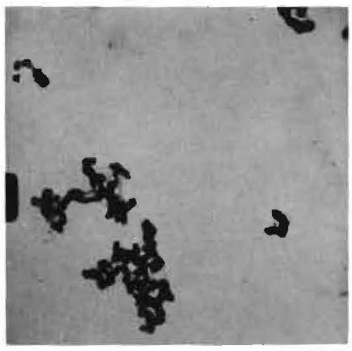

1μ
E. 5500X

NOTE: This Sequence Corresponds to the Optical Micrograph Sequence Of Figure 27. Micrographs were taken at the Radial Distances Indicated Below.

A. 1.0 mm
B. 10.0 mm
C. 14.0 mm
D. 15.5 mm
E. 15.5 mm

AEROSOL: Aluminum Oxide (Dispersed Powder)

Figure 30. Electron Micrographs of Atomized Aluminum Oxide Deposit.

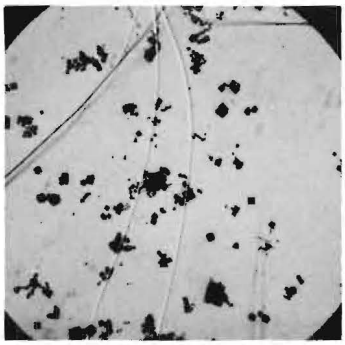

10 μ
A. 2300X

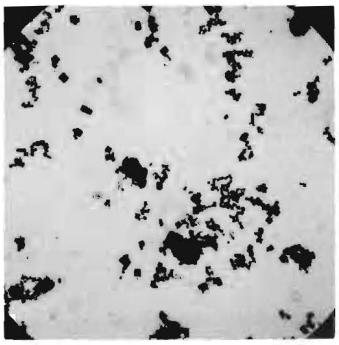

10 μ
B. 2300X

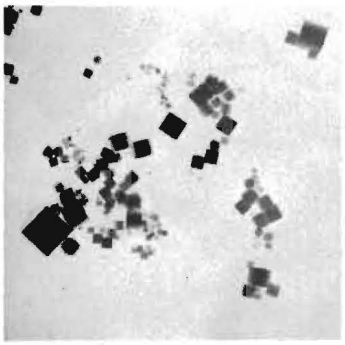

1 μ
C. 8000X

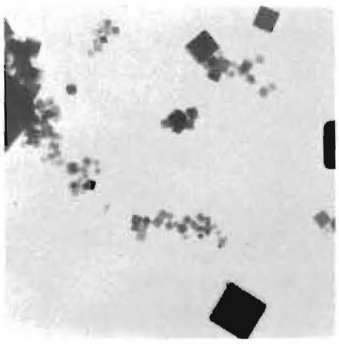

1 μ
D. 8000X

Figure 31. Electron Micrographs of Magnesium Oxide Deposit. All micrographs taken at the outer periphery of the deposit. Aerosol produced by burning magnesium ribbon in air.

the deposit. Shots A and B are shown at a magnification of 2300x where the relative extent of agglomeration is evident. The predominant primary particle size was considerably less than one micron; however, most agglomerated masses are on the order of one to two microns. A large number of unagglomerated primary particles on the order of 0.5 micron were observed. Shots C and D are at 8000x magnification where the cubic configuration of the primary particles as well as the relative simplicity of agglomeration is emphasized.

(4) Deposits from Silver and Platinum Aerosols Produced by Exploding Wire Technique. Very interesting results were obtained in the electron microscopy of aerosols generated by the exploding element technique. Figure 32 shows particulate material precipitated from aerosols of metallic silver (micrographs A, B and C) and platinum (micrographs D, E and F). Figure 32A at a magnification of 8000x shows essentially all the material highly agglomerated with complex particulates ranging from less than 0.1 to about 2 microns in diameter. The predominant agglomerate diameter seems to be about one micron. Micrographs B and C show the complex silver agglomerates at a magnification of 23,000x. A range in primary particle sizes may be observed in the micrographs from 0.01 to 0.15 micron. Figure 32D shows a deposit of platinum particulates at 12,900x. Again the material is highly agglomerated and most of the complex deposits, while not clearly distinguishable, appear to be less than 0.5 micron in diameter. Figure 32E shows the extremely complex agglomeration at 18,900x and Figure 32F at 22,800x shows the primary particle range from less than 0.005 to 0.10 micron in diameter.

(5) Deposit from Aluminum Oxide Aerosol Produced by Exploding Wire Technique. The results of a study of aluminum oxide deposits from an aerosol generated by exploding aluminum foil in air are presented in Figure 33. The relative deposit densities at the extremes of the circumferential band defining the deposit are shown in micrographs A and B at a magnification of 10,200x. Shot A was taken at the edge of the dense core, and shot B was taken at a radial distance one centimeter beyond this point. The individual agglomerates from another deposit are shown more clearly in Figure 33C at 12,900x. These agglomerates are similar to those

SILVER

1 μ
A. 8000X

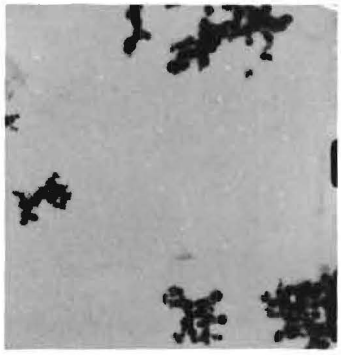

1 μ
B. 23,000X

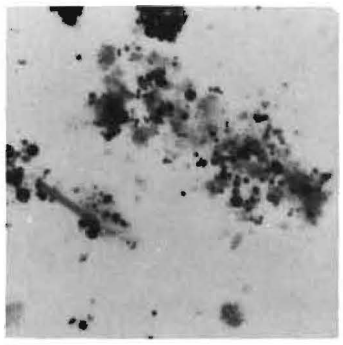

1 μ
C. 23,000X

PLATINUM

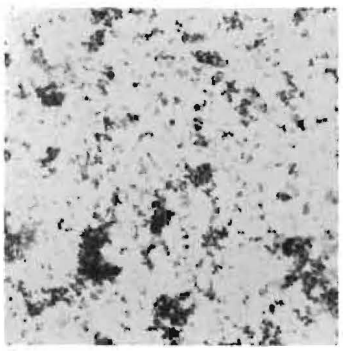

1 μ
D. 12,900X

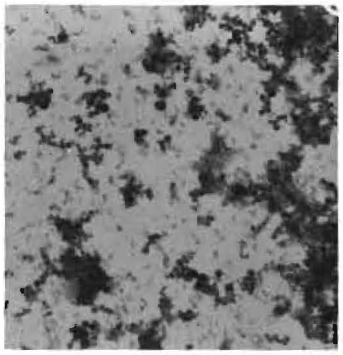

1 μ
E. 18,900X

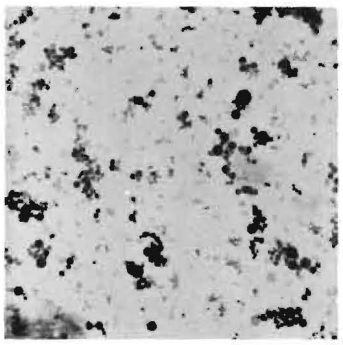

1 μ
F. 22,800X

Figure 32. Electron Micrographs of Silver and Platinum Deposits. Micrographs A, B and C are of Silver Deposit. Micrographs D, E and F are of Platinum Deposit. Both Metallic Aerosols Produced by Exploding Wire Technique.

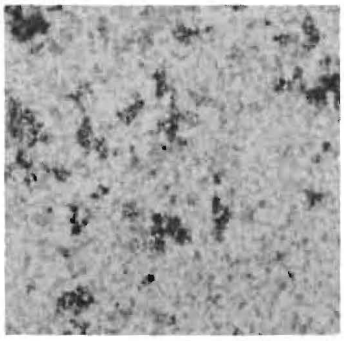

1 μ
A. 10,200X

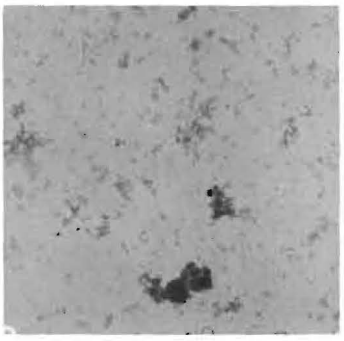

1 μ
B. 10,200X

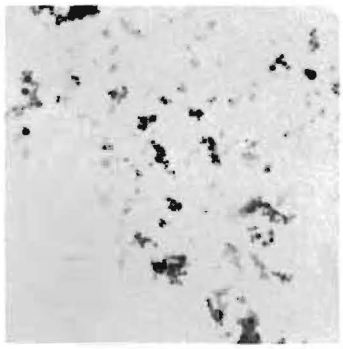

1 μ
C. 12,900X

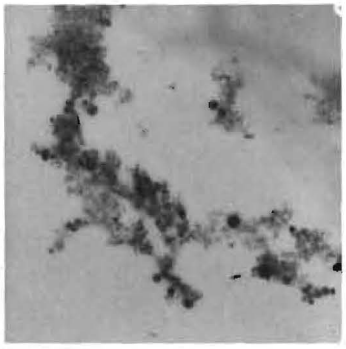

1 μ
D. 18,900X

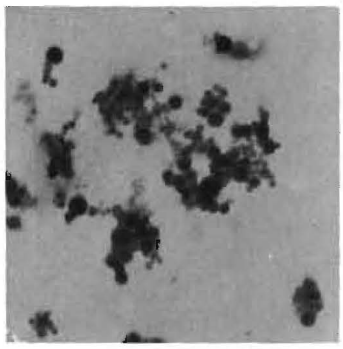

1 μ
E. 23,000X

1 μ
F. 23,000X

Figure 33. Electron Micrographs of Exploded Aluminum Oxide Deposit. Aluminum oxide aerosol produced by exploding aluminum foil in air.

of the metallic aerosols, both in complexity and size. The extremes in primary particle diameter (from less than 0.01 to 0.1 micron) as well as the complex structure of the large agglomerated mass is illustrated in micrograph D. The perfectly spherical configuration of the primary particles is shown clearly in Figures 33E and F at a magnification of 23,000x.

(6) Deposit from Composite Sodium Chloride Aerosol. In an effort to compare directly the thermal force on large primary particles (i.e., diameter on the order of one micron) with that on agglomerates of the same diameter composed of very small primary particles, a composite aerosol of sodium chloride was prepared. The agglomerates of fine particles were produced by exploding a concentrated sodium chloride solution. The large primary particle component was produced by dispersing the particulate material in the fine particle aerosol. The deposit which was obtained consisted of a central core deposit of relatively high density fading into a scattered deposit of low density. Figure 34A is an optical micrograph taken at the periphery of the central core area at a magnification of 640x. A few of the larger particles (diameter range from 1 to 5 microns) are visible in the center. These particles were observed in random scattering over the entire collecting disk surface. The irregular particles and those not so well resolved in the optical micrograph are shown more clearly in the electron micrograph of 34B at 2300x. Still more detail is visible in Figure 34C at 13,000x magnification and in Figures 34D and E at a magnification of 23,000x.

3. Significance of Observations

As will be shown in the discussion of results, the information on the properties of the aerosol particles presented above has provided a basis for the interpretation of several of the apparent anomalies of thermal force phenomena. This detailed knowledge of agglomerate composition is only qualitatively applicable to aerosols which consist of agglomerated clouds (including a wide range in size and complexity) as well as primary particles. The difficulties associated with a quantitative analysis of the macroscopic precipitation phenomena are obvious, and the problem could not be further resolved within the time limit of this investigation.

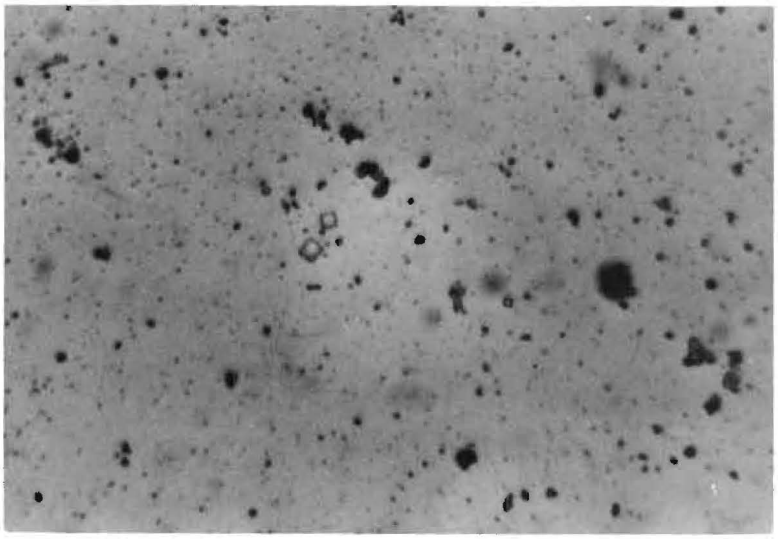

10 μ
A. 640X

OPTICAL MICROGRAPH

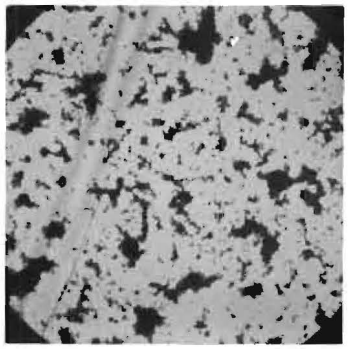

1 μ
B. 2300X

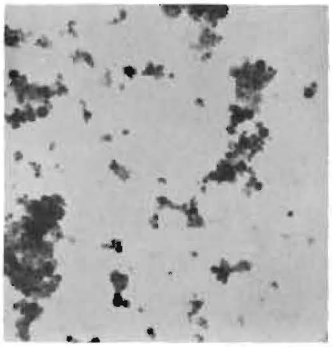

1 μ
C. 13,000X

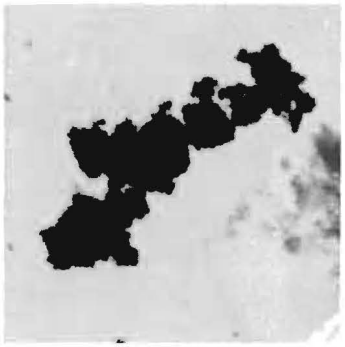

1 μ
D. 23,000X

ELECTRON MICROGRAPHS

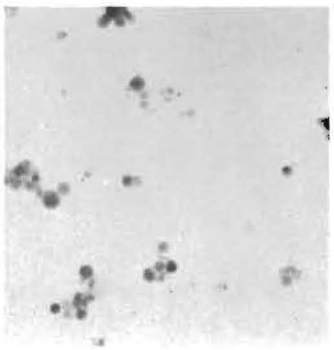

1 μ
E. 23,000X

Figure 34. Micrographs of Sodium Chloride Deposit. Composite aerosol was produced by both exploding wire technique and dispersion of solid power.

D. Direct Observation of Particulate Behavior

1. General Observations

For comparison with the results of the thermal precipitation study, thermal force data were collected also with the modified Millikan apparatus. The data were obtained by the direct observation of particle behavior using the experimental procedure outlined in Section V. The thermal components of velocity and force were computed in accordance with the equations 6.18 and 6.19b. Experiments were conducted with a number of aerosols, including magnesium oxide, aluminum oxide, carbon, zinc, aluminum, copper, and tobacco smoke. Quantitative results were obtained only with the first three particulate materials. In experiments using zinc, no measurable difference in terminal velocities was observed for a given particle falling with and without the imposed temperature gradient. Apparently, the thermal velocity component was negligible relative to the gravitational component in accordance with the theory of Epstein. In the case of aluminum and copper aerosols, the dispersed material consisted of particles too large for accurate observations, i.e., the terminal velocity of gravitational settling was too great for precise velocity measurements. The individual tobacco smoke particles, on the other hand, proved to be too small for observations, i.e., the excessive translational drift prevented continuous observation in the limited depth of field of the optical system. Atomization of magnesium oxide, aluminum oxide, and carbon (Cabot Carbon, Sterling 92) produced particles suitable for experimental observation. Several particles with apparent diameters in the range from 0.5 to 5 microns were observed in each case at two or three different temperature gradients. In all cases the observations were made at atmospheric pressure.

2. Experimental Data

The significant results are presented in Table X where the most consistent data have been included to illustrate the typical magnitudes and particle size dependence of experimental forces for the various materials. These data were compiled by the selection of only the reproducible velocity components for particles observed at the indicated temperature

TABLE X

EXPERIMENTAL DATA FROM THE DIRECT OBSERVATION OF PARTICLES USING THE MODIFIED MILLIKAN APPARATUS

(A)	(B)	(C)	(D)	(E)	(F)	(G)	(H)
Particulate Material	Particulate Diameter	Temperature Gradient	Experimental Thermal Velocity x 10^4	Experimental Thermal Force x 10^{10}	Theoretical[a] Thermal Force x 10^{10}	Force Ratio E/F	Reduced Thermal Force x 10^8 $[F_t \div a\frac{dT}{dy}]$
	(Microns)	($^\circ$C/Cm)	(Cm/Sec)	(Dynes)	(Dynes)		(Dynes/$^\circ$C)
MgO	0.95	15.3	2.40	0.331	0.370	0.895	4.51
MgO	0.95	15.3	2.63	0.362	0.370	0.979	4.93
MgO	0.95	15.3	2.86	0.395	0.370	1.068	5.38
MgO	0.95	29.4	4.93	0.680	0.712	0.956	4.82
MgO	0.95	29.4	4.84	0.668	0.712	0.940	4.73
MgO	2.32	22.9	3.41	1.29	1.35	0.955	4.86
MgO	2.32	22.9	3.49	1.32	1.35	0.977	4.97
MgO	2.32	40.1	5.98	2.26	2.37	0.953	4.86
MgO	2.32	40.1	5.90	2.23	2.37	0.941	4.79
MgO	3.69	12.1	1.25	0.76	1.14	0.667	3.39
MgO	3.69	12.1	1.68	1.02	1.14	0.894	4.56
MgO	3.69	12.1	1.86	1.13	1.14	0.991	5.05
MgO	3.69	31.5	4.59	2.78	2.96	0.939	4.77
MgO	3.69	31.5	4.47	2.71	2.96	0.916	4.65
Gas Carbon	0.651	17.1	0.72	0.0642	0.095	0.676	1.15
Gas Carbon	0.651	17.1	0.57	0.0508	0.095	0.535	0.91
Gas Carbon	0.651	17.1	0.16	0.0143	0.095	0.160	0.26
Gas Carbon	0.651	38.4	1.34	0.119	0.213	0.559	0.95
Gas Carbon	0.651	38.4	1.16	0.103	0.213	0.484	0.82
Gas Carbon	2.94	22.9	0.88	0.415	0.576	0.721	1.23
Gas Carbon	2.94	22.9	0.67	0.316	0.576	0.549	0.94
Gas Carbon	2.94	43.9	1.07	0.505	1.103	0.458	0.78

Continued

TABLE X (Concluded)

EXPERIMENTAL DATA FROM THE DIRECT OBSERVATION OF PARTICLES USING THE MODIFIED MILLIKAN APPARATUS

(A)	(B)	(C)	(D)	(E)	(F)	(G)	(H)
Particulate Material	Particulate Diameter (Microns)	Temperature Gradient ($^{\circ}C/Cm$)	Experimental Thermal Velocity x 10^4 (Cm/Sec)	Experimental Thermal Force x 10^{10} (Dynes)	Theoretical[a] Thermal Force x 10^{10} (Dynes)	Force Ratio E/F	Reduced Thermal Force x 10^8 $[F_t + a\frac{dT}{dy}]$ (Dynes)
Al_2O_3	0.743	18.5	4.99	0.517	0.576	0.898	7.53
Al_2O_3	0.743	18.5	4.87	0.505	0.576	0.877	7.35
Al_2O_3	0.743	33.1	8.63	0.896	1.012	0.885	7.29
Al_2O_3	0.743	33.1	8.90	0.922	1.012	0.910	7.50
Al_2O_3	1.68	12.5	3.08	0.799	0.865	0.923	7.61
Al_2O_3	1.68	12.5	3.21	0.833	0.865	0.963	7.94
Al_2O_3	1.68	43.5	10.63	2.76	3.01	0.917	7.56
Al_2O_3	1.68	43.5	11.06	2.87	3.01	0.955	7.86
Al_2O_3	2.12	22.1	5.28	1.82	1.93	0.943	7.76
Al_2O_3	2.12	22.1	5.15	1.78	1.93	0.923	7.59
Al_2O_3	2.12	31.3	7.63	2.63	2.73	0.964	7.93
Al_2O_3	2.12	31.3	7.33	2.52	2.73	0.924	7.59
Al_2O_3	2.12	40.9	9.65	3.33	3.57	0.933	7.69

[a] Theoretical value for MgO based on thermal conductivity of the pressed brick, $k_p = 0.00271$ cal/cm sec $^{\circ}K$. That for Al_2O_3 and gas carbon based on thermal conductivity of the powder.

gradients. Where reproducibility could not be achieved, the data were discarded. This technique of selecting data was essential because of the excessive experimental deviations sometimes observed. The indirectly measured thermal velocity component was occasionally lower than the reproducible value by a factor of three and sometimes higher by a factor of ten. Such extreme deviations are not surprising in view of the fact that thermal velocity components were typically 5 to 20 per cent of the total velocity. For example, a decrease in the time of descent on the order of 0.2 second was recorded for an observed gravitational settling time of about 2 seconds. The reliability of experimental results is considered much more acceptable than the extreme deviations suggest. The reliability is indicated by the consistency of reproducible measurements for a given particle at different temperature gradients and by the consistency of force evaluations for particles of various diameters.

The experimental thermal velocities are presented in Figure 35 where the thermal velocity component has been plotted against temperature gradient. The dependence of thermal velocity on particle size, due primarily to the slip effect, is illustrated here also.

The typical experimental thermal forces observed for magnesium oxide, aluminum oxide, and gas carbon are illustrated in Figures 36, 37 and 38, respectively. Again, the temperature gradient scale is the abcissa. Theoretical force curves (solid lines) have been included for comparison. Close correlation between experimental and theoretical results for aluminum oxide was obtained by using the thermal conductivity of the pressed powder in computations. Closest correlation in the case of magnesium oxide was obtained by using the thermal conductivity of magnesia brick. Fair agreement between experimental and theoretical values for gas carbon was obtained by using the value reported for the powder.

The results which have been presented are thus somewhat incongruous and the correlation with theoretical values seems dependent upon the almost arbitrary assignment of thermal conductivity. Furthermore, this experimental technique was apparently restricted (by the physical limitations of the apparatus) to the study of particulate materials of low

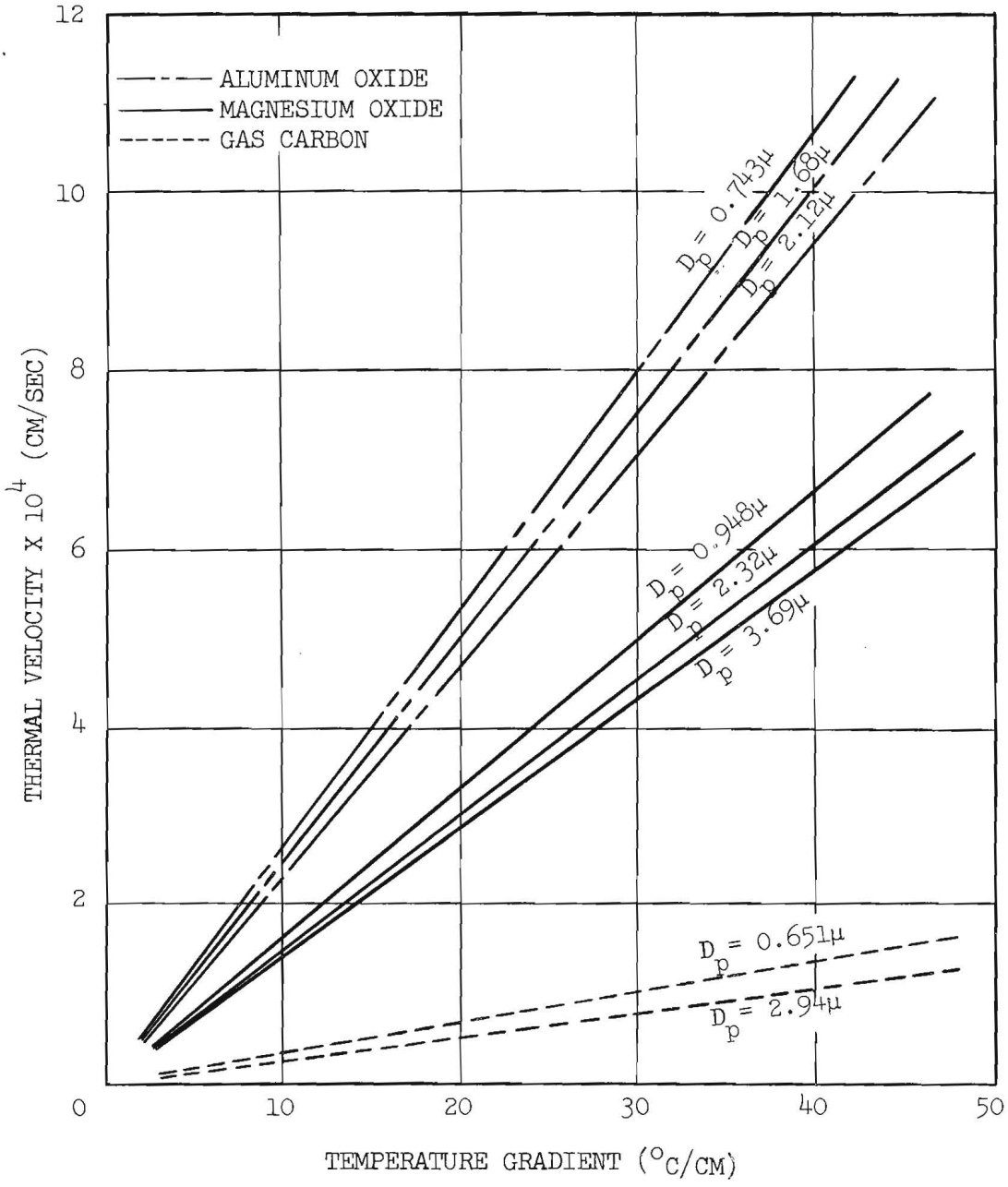

Figure 35. Observed Thermal Velocity Dependence Upon Temperature Gradient, Particle Size and Particulate Material.

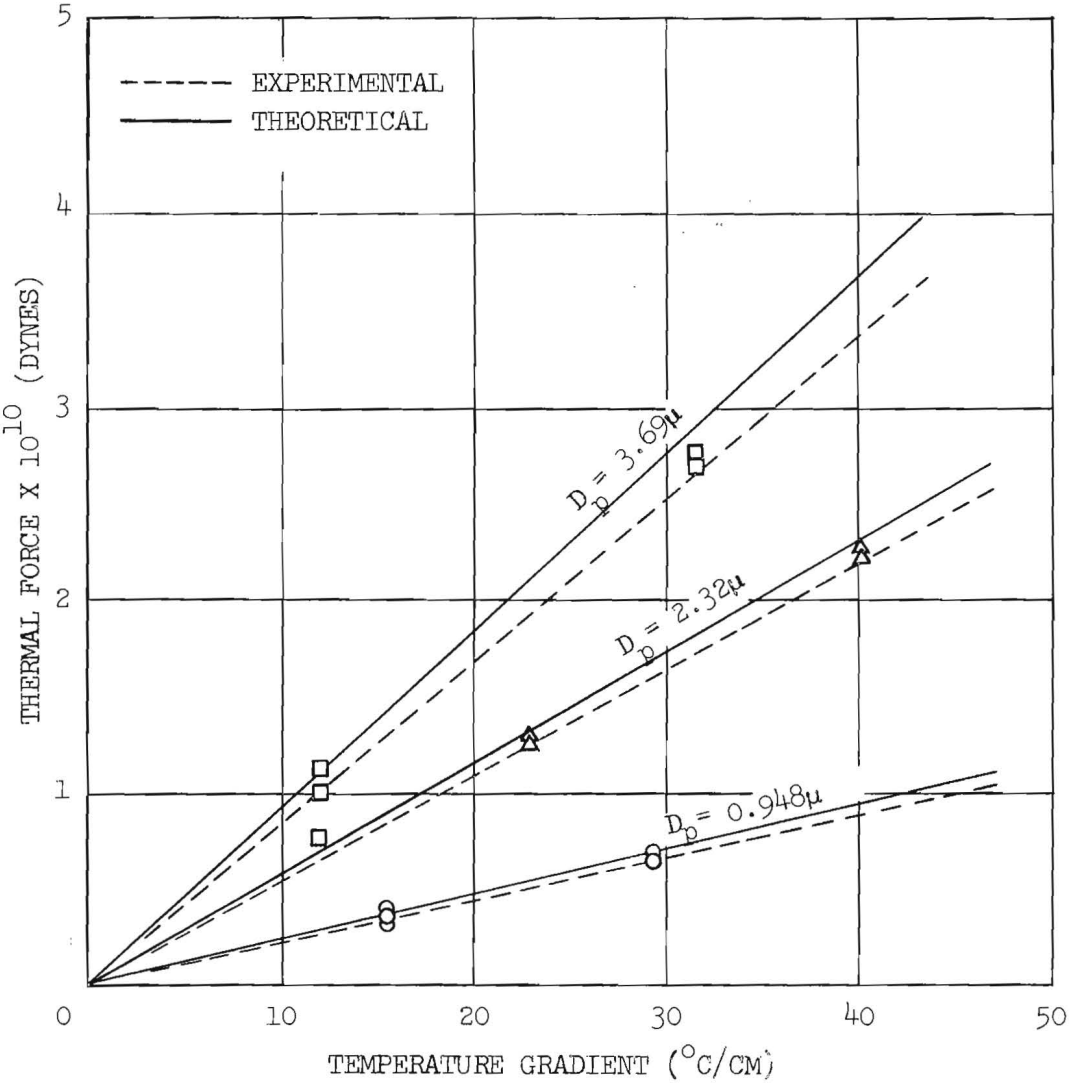

Figure 36. Experimental Thermal Forces for Magnesium Oxide Based on Direct Observation of Particulate Behavior.

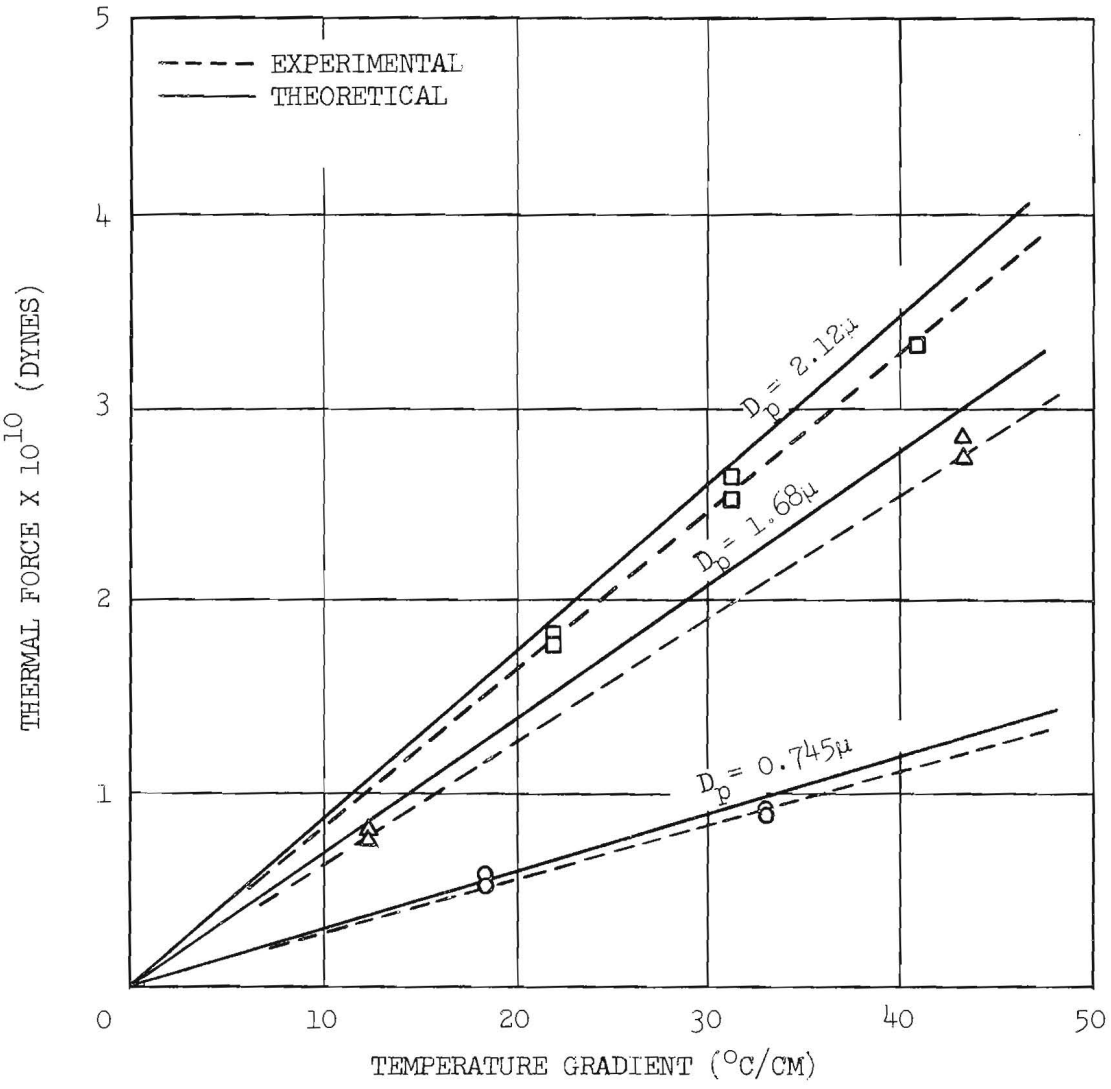

Figure 37. Experimental Thermal Forces for Aluminum Oxide Based on Direct Observation of Particulate Behavior.

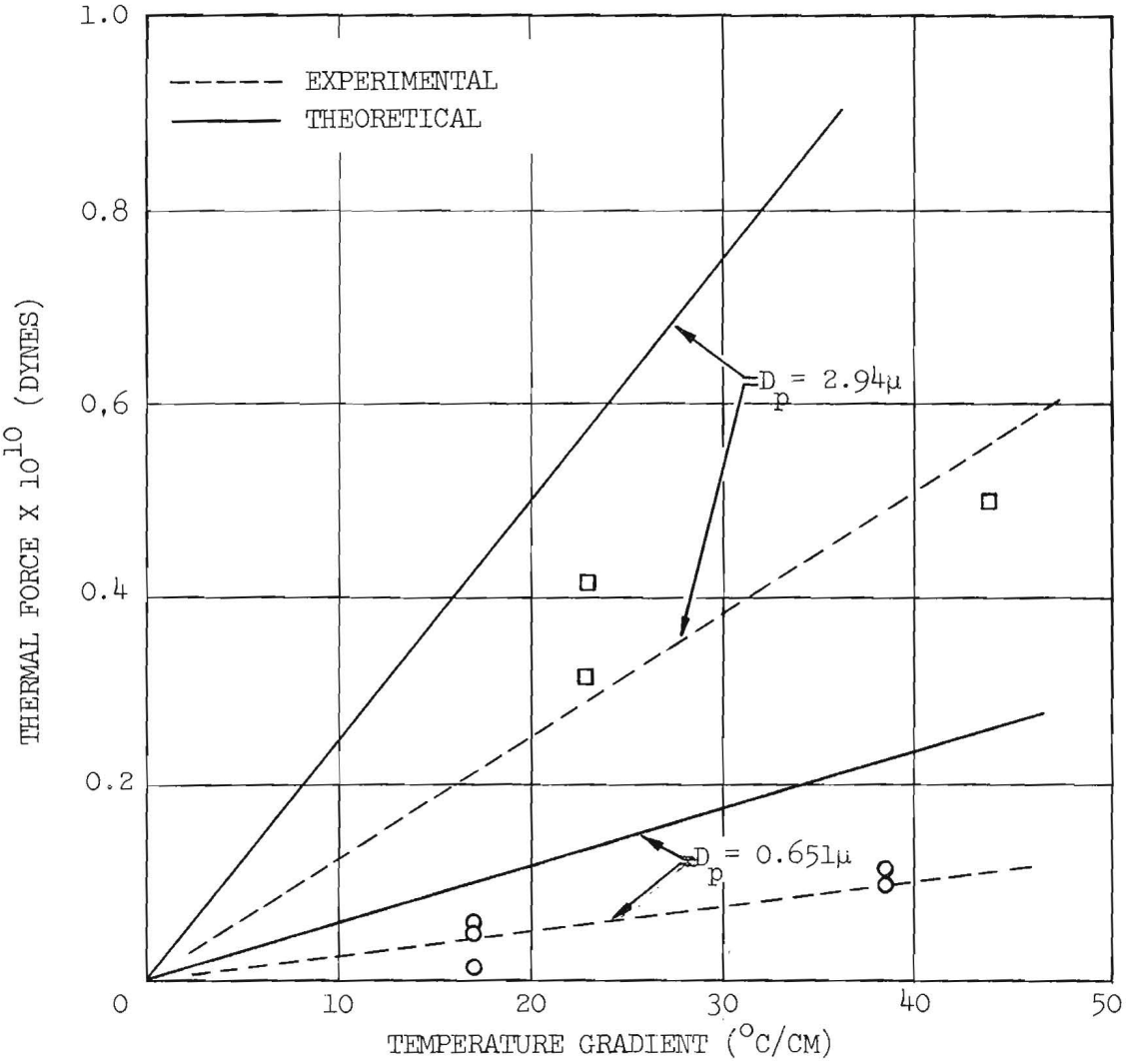

Figure 38. Experimental Thermal Forces for Gas Carbon Based on Direct Observation of Particulate Behavior.

thermal conductivity. Since some data had been obtained for comparison with the results of the precipitation study, the modified Millikan cell investigation was discontinued.

X. ANALYSIS OF ERRORS

A. Errors Inherent in Thermal Precipitation Evaluation

The evaluation of experimental data involves errors inherent in both mathematical simplifications and experimental measurements. Before any true correlation of these results with theory is made, the establishment of reasonable confidence limits is desirable.

1. Errors of Method

a. The Assumptions Involved in the Derivation of Horizontal Velocity Components. In Section VI, dealing with the calculation of experimental thermal velocities and forces, the key simplifying assumptions involved in the derivation of the equations have been enumerated. The related errors of method will be considered briefly. In deriving the horizontal velocity component of the airborne particle as it moves radially between the parallel plates of the precipitator, the following assumptions were made: (1) fluid flow is laminar, (2) entrance effects are negligible, (3) fluid properties are constant, and (4) the horizontal particulate velocity component at any time is equal to that of the flowing fluid at the same point.

(1) The Assumption of Laminar Fluid Flow. With regard to the first assumption, the stability criterion for a flowing system is established by a critical Reynolds number, or its equivalent, that defines a maximum tolerable velocity. The Reynolds number, N_{Re}, can be written in any of several dimensionless forms, e.g., as

$$N_{Re} = \frac{Dv\rho}{\eta} \qquad (10.1)$$

where D is a characteristic linear dimension of the flow channel, V is the linear velocity of the flowing fluid, ρ is the fluid density, and η is the absolute viscosity of the fluid. It has been found that the critical Reynolds number for transition to turbulent flow in tubes is about 2300, and that, under usual conditions, flow in tubes is turbulent when the Reynolds number exceeds 3000. By using the hydraulic radius definition to ascertain the characteristic linear dimension, a maximum value,

$N_{Re} < 100$, was computed for the radial flow precipitators used in this investigation. The usual form of the Reynolds number, computed in this fashion, is not strictly applicable to the radial system; but the value obtained suggests laminar flow.

It is well known that the transition Reynolds number depends, in addition to other factors, on the variation of pressure and velocity along a surface. Specifically, it has been observed that a flow deceleration lowers the critical Reynolds number.[9] Hence diverging radial flow may be expected to be less stable than rectilinear flow. An expression for the stability criterion has been derived by McGinn[22] in a study of the radial flow of water between fixed parallel plates. He developed a dimensionless parameter

$$\sigma = \frac{K\rho QL}{24\pi\eta r_o^2} < 1 \qquad (10.2)$$

which is essentially a Reynolds number multiplied by the ratio of two characteristic lengths. In the above, K is an energy correction factor, the value of which depends on the shape of the velocity profile; L is the distance between plates; and r_o is the inlet radius. The remaining symbols were defined previously. The value of σ computed for the experimental system is on the order of 0.5. Thus the requirements for laminar flow are fulfilled. It should be noted that the use of the inequality, equation 10.2, as a stability criterion has been justified only by its successful application to limited experimental data for liquid flow. Still, it appears that the assumption of laminar flow is well justified.

(2) The Evaluation of Entrance Effects. The entrance effects on thermal precipitation cannot be readily evaluated. Neither has a study of entrance effects for the radial flow system been found in the literature, but, due to the similarity between the parabolic velocity profiles of both radial and tube flow, some qualitative conclusions can be reach by analogy. It has been found that an entrance length, X_e, on the order of

$$X_e = 0.035\ DN_{Re} \qquad (10.3)$$

is required for the build-up to the parabolic profiles.[2] In equation 10.3, D is the diameter of a tube and N_{Re} is the customary Reynolds number. The application of this empirical relationship to a radial flow system is somewhat ambiguous since the plate separation is not directly equivalent to tube diameter. A Reynolds number should be defined specifically for the system. Generally, however, for small Reynolds numbers the ratio, X_e/D, is small, and for close plate separations, the entrance length required for the establishment of a parabolic velocity profile is also small. If equation 10.3 is even roughly applicable to the radial flow precipitator then the velocity profile is probably established within the first 2 or 3 millimeters of radial distance. While this entrance length is on the order of 20 per cent of the typical deposit radius, this percentage is not indicative of the error introduced by neglecting the entrance effects. This is apparent, when one considers the development of the momentum boundary layer from the wall out, realizing that the particles of concern are those which begin their trajectory nearest the hot plate surface. The air enters the zone between plates with a linear (vertical) velocity profile, but the layers adjacent to the plates are quickly decelerated as the momentum is redistributed. Thus the air close to the plates assumes a velocity consistent with the parabolic profile in a short time relative to that required for its complete development. Furthermore, there is a mass flux directed toward the center of the flowing stream associated with its acceleration. A similar approach may be used in evaluating the entrance effect in the establishment of a temperature profile. By boundary layer theory[31] it can be shown that the rate of development of a temperature profile can be related to the rate of momentum boundary layer development; and that the relative rate is dependent upon the Prandtl number, N_{Pr}, a property of the fluid defined by

$$N_{Pr} = \frac{C_p \eta}{k} \qquad (10.4)$$

where C_p is the heat transfer capacity at constant pressure,
k is the thermal conductivity, and
η is the viscosity.

Where gases are concerned, the Prandtl number is near unity and the rate of development of both temperature and velocity profiles is essentially the same. This leads to the conclusion that entrance lengths are no greater for the establishment of temperature profiles than for velocity profiles. A consideration of the development of the temperature profile from the hot plate outward does not simplify the evaluation of entrance effects. If the aerosol enters the precipitator at some temperature near that of the cold plate, then the temperature gradient near the hot plate is initially very great and it seems that an aerosol particle in this region might be subjected to a proportionally large thermal force.

In order to evaluate the total entrance effect one must consider three factors which act simultaneously during the development of the profiles to influence the motion of a suspended particle. These are (1) an initial horizontal velocity component higher than that defined by the established profile, (2) a thermal gradient greater than that of the linear steady state profile, and (3) a mass flux component in the vertical direction. The first of these factors tends to increase the deposit radius while the second and third tend to decrease it.

It would be presumptuous to assign a value to the error of entrance effects without a more thorough analysis. Still, some logical limits of this error may be estimated in the following manner. If the particles' horizontal velocity is initially equal to that of the incoming gas, then the deposit radius will be greater than that for a trajectory defined by a parabolic profile by an increment which must be less than the entrance length. The force in turn is inversely proportional to the difference between the squares of the inlet radius and the deposit radius. If the rough estimate for the entrance length given above is used to evaluate the force error, it turns out that the apparent force (computed from an observed deposit radius) would be about 30 per cent low.

The last two factors listed above can be considered jointly. It may be recalled that the mass flux and the temperature gradient are associated with the development of boundary layers. The greatest conceivable influence of these factors upon a particle would be manifest

in keeping it at the surface of the boundary layer. It is possible to visualize a boundary layer surface originating at the inlet in the hot plate and sloping downward to a midplane at which it encounters the boundary layer from the lower plate. The intercept marks the full development of the profile. The particle which enters the precipitation zone nearest the hot plate surface then may be visualized as sliding down the boundary layer surface until it reaches the point of fully developed temperature profile; whereupon it begins to follow a trajectory described by equations 6.8 and 6.9. This conception is admittedly oversimplified, but it is analogous to the idea of a dust-free space existing about the hot plate surface. An approaching particle, being unable to penetrate its hypothetical boundary, would then be deflected along its surface. In the extreme, for a perfectly parabolic velocity profile, the particle traveling the greatest distance would have originated near the midpoint between the plates. The deduced force would have been overestimated by a factor of about 2. Therefore, a reasonable error in the deduced force value due to entrance effects falls in the range from +30 to -50 per cent.

(3) The Assumption of Constant Fluid Properties. Now, in consideration of the assumption of constant fluid properties, the viscosity and density are of primary concern. The maximum difference between hot and cold plate temperatures for these experiments was on the order of 130°C. The viscosity of air increases from about 180 to 238 micropoises over this temperature interval, which gives a deviation of about ± 15 per cent from the median value. The density decreases from about 12.05×10^{-4} to 8.34×10^{-4} gm/cc over this temperature interval, which gives a deviation of about ± 20 per cent. The influences are cumulative, and the overall effect is manifest in a skewed velocity profile, i.e., the assumption of a parabolic velocity profile is not correct. The general form of this profile will be retained, however, and the value of its maximum velocity, occurring at some point nearer the cold plate that the maximum of a true parabolic profile, will not be very different from that of the simplified case. Furthermore, the temperature gradient existing in the flowing fluid causes its thermal conductivity to increase nearer the hot

plate. The result is a nonlinear temperature profile with the temperature gradient decreasing with increasing temperature toward the hot plate. As in the analysis of entrance effects, an accurate evaluation of error associated with the assumption of constant fluid properties calls for a more thorough mathematical analysis, and the solution of the problem is not immediately available. It appears that the error involved would be a low percentage.

(4) The Assumptions Regarding the Horizontal Velocity Component. The assumption that the horizontal velocity component of the particle is equal to that of the flowing fluid at the same point is sound. As was shown by the simple calculation in section VIA, Calculation of Particulate Velocity, the time required for the particle to adjust to 95 per cent of the velocity of the flowing fluid is negligible. The error introduced is certainly less than 5 per cent.

b. The Assumptions Involved in the Derivation of Precipitation Time and Vertical Particulate Velocity. The basic assumptions introduced in the derivation of precipitation time and vertical particle velocity are that the thermal force is constant and that the particle of concern originated at the hot plate inlet. The latter was considered in the discussion of entrance effects. The former implies a linear temperature gradient and a force directly proportional to temperature gradient. The nonlinearity of the temperature gradient was mentioned above. For the entire plate separation the linear assumption holds very well since the deviations from the average gradient, being positive in one extreme and negative in the other, tend to compensate for each other. However, if the particle trajectory originates at some point significantly below the hot plate surface, the observed force may be in error by as much as a factor of two.

The direct proportionality between thermal force and temperature gradient has been experimentally demonstrated many times and may be stipulated without the introduction of error. An additional assumption introduced in this derivation was that of a negligible acceleration time for the particle in beginning its descent. An inertial force evaluation has shown this time to be negligible in comparison to the total transit time.

c. Other Assumptions. The remaining assumptions introduced in the computation of velocities and forces are that the particle is spherical and that its mobility is independent of the temperature of the system and the nature of the particle. The actual deviation of particle geometry from a spherical form has been illustrated in the micrographs of the preceding section. The dependence of thermal force on particulate shape cannot be evaluated mathematically. Conclusions regarding this error can only be based on the observation that the particulate material at the periphery of a deposit included numerous forms; all apparently were precipitated with comparable velocities. Hence, it is deduced that both thermal and drag forces are dependent upon shape, as well as size, in such a way as to balance the effect.

Finally, in regard to the assumptions concerning the mobility of the particle, reference is made to its definition (equation 6.14). It is evident from the presence of the viscosity term in the denominator of the equation that the mobility is temperature dependent. Furthermore, the inclusion of the slip factor indicates that it is also dependent upon the nature of the particle since the slip factor coefficients may be related to the accommodation coefficient. In the Knudsen number region of concern, the slip correction is not very much different from unity and the nature of the material is unimportant. Likewise, it appears that the assumption of constant mobility is acceptable if a mean temperature is chosen for its evaluation.

d. Confidence Limits. In placing confidence limits upon the equations used for analysis of data, the combined error associated with the individual assumptions must be considered. The two most significant factors involved are the entrance effects and the nonlinearity of the temperature profile. For the former a reasonable estimate of error was +30 to -50 per cent, the lower limit occurring when the particle enters the precipitation zone at midpoint. It is under this condition that the error due to a nonlinear temperature profile is greatest. The probable error of these two effects combined may be included reasonably in a range from +30 to -75 per cent. With the nominal errors which might be ascribed to all other simplifications included, it seems most unlikely

that the actual force could be more than twice the deduced force or less than one fifth its value.

2. Experimental Errors

a. Direct Measurements. In thermal force evaluation from precipitation experiments, the following physical measurements were obtained: precipitator plate separation, hot and cold plate temperature, aerosol flow rate, deposit radius, particle size and operating pressure. Limits for experimental errors have been assigned where possible for both the random (or accidental) errors in measurement and the systematic or constant errors which have a bearing on the accuracy of experimental observations.

(1) Plate Separation. For any given series of experiments, i.e., for a single precipitator, the plate separation measurements were subject to a precision error of ± 7 per cent due to variations in collecting disk thickness, surface irregularities, and variable film thickness in the wetted heat transfer seal between collecting disk and cold plate. The systematic error, which includes the machining tolerances in the fabrication of the precipitator, introduces an additional uncertainty in the accuracy of the measurement on the order of ± 10 per cent, which is reflected in experimental deviations observed when different precipitators are used. Efforts were always made to minimize the precision error by measuring the collecting disks before insertion, by positioning them in such a way that surface irregularities in both disk and precipitator were mated, and by using as few disks as practicable for a given series of experiments.

(2) Plate Temperatures. Plate temperatures were measured with a copper-constantan thermocouple and potentiometer assembly calibrated for ± 0.5°C accuracy. The thermocouples were imbedded in the brass plates. The temperature of the cold plate surface was estimated by a steady state heat transfer calculation which indicated a temperature drop in the range from 1° to 3° C across the fluid film and the glass collecting-disk. In some of the earlier observations, this temperature drop was neglected and the maximum error associated with the temperature drop across the flowing aerosol may have been as large as ± 20 per cent. For most observations the maximum precision error which allows for temperature

fluctuation during the experiment was on the order of ± 5 per cent, giving a maximum uncertainty in the accuracy of the measurement on the order of ± 10 per cent.

(3) Aerosol Flow Rate. The aerosol flow rate was measured by timing the rate of descent of a liquid miniscus in a calibrated cylinder. The cylinder was graduated in 100 cubic centimeter increments for a capacity of 2.5 liters. Constant flow control was maintained and the random error in the precision of measurement has been estimated less than ± 5 per cent. The accuracy of flow rate measurements, allowing for the systematic error associated with the calibration of the cylinders, has been estimated uncertain by ± 7 per cent.

(4) Deposit Radius. The method of measuring deposit radii and the nature of deposits have been discussed in detail in preceding sections. Since the periphery of a deposit was defined by a circumferential band of rapidly decreasing density, rather than by abrupt discontinuity, a certain error of observer judgment is introduced into the measurement of deposit radii. Still, in the cases of complete deposition, there was always a finite limit to this uncertainty, defined by the radial distance between the points of maximum density and complete absence of particulate matter. This maximum uncertainty, characteristic of the accuracy of the measurement, has been evaluated at ± 20 per cent. The precision error, associated with the reproducibility of results, is considerably less as indicated by the consistency of measurements and has been estimated less than ± 10 per cent. The precision error stems from variation in overall deposit density and variation in deposit radius around its circumference. The accuracy of radial measurements is partially dependent upon the nature of the particulate material. Where deposits are sharply defined, as in the case of magnesium oxide, aluminum oxide, or exploded materials, the foregoing analysis is applicable, though deviations were frequently less than indicated above. On the other hand, in the case of atomized metallic powders, the definition of the dense central core region was largely guesswork with estimates which might have been inaccurate by a factor of two. Such measurements have not been given as much significance as those which are more definite

however, and therefore do not warrant quantitative consideration in the evaluation of experimental error. In fact, it is possible that the indefinite deposit boundary reflects a variation in the nature of the individual particles (e.g., variable particulate thermal conductivity due to agglomeration and/or compactness) and, in that sense, is not actually an experimental error. This factor will be discussed more thoroughly later.

(5) Particle Size. Particle sizes were usually measured with an optical micrometer. Electronmicroscopy has revealed the fallacy of these measurements, but the error thereby introduced into thermal velocity and force evaluations is generally not serious. It has been shown, both theoretically and experimentally, that thermal velocity is essentially independent of particle diameter; an effect substantiated by the observation of a range of particle sizes in the periphery of a deposit. Therefore, the radius of a precipitated deposit is dependent on particle size only to the degree of significance of the gravitational velocity component. For small particles or materials of low density, this error in thermal velocity component is usually less than ± 10 per cent. A thermal force evaluation for any specific particle diameter in the observed range possesses an error of comparable percentage due to this source. For more dense particulate materials, such as platinum or silver, the value of thermal velocity may be in error by as much as a factor of two.

(6) Pressure. The pressure of the aerosol entering the precipitator was measured with a mercury manometer. The slight pressure differential imposed to induce aerosol flow has been considered negligible and the measured value has therefore been taken as the pressure under which precipitation occurs. The precision of pressure measurement has been assigned a liberal error of ± 0.5 per cent. The inaccuracy of assigning the observed value to the precipitation pressure is probably less than ± 2 per cent, however the influence of pressure on precipitator deposition is magnified, due to its contribution to both thermal force and drag resistance. It has been estimated that the maximum error from this source could be no more than ± 10 per cent.

b. Propagation of Experimental Errors in Computation of Thermal Velocities and Forces. In the estimation of overall precision and accuracy, it is necessary to consider not only the errors of method and the errors of measurement, but also the propagation of errors. It is evident that the error in a calculated value which is a function of directly measured quantities depends upon the nature of the function and the magnitudes of the individual quantities and errors. Thus, the reliability of the thermal force and velocity values obtained from experimental observations varies with the operating conditions of the precipitator and aerosol used. Typical thermal force evaluations have been examined as a guide in the establishment of confidence limits.

An evaluation of error propagation based on the precipitation of magnesium oxide under moderate operating conditions gave the following results. The vertical particulate velocity, $V_y = 0.248$ cm/sec, computed from equation 6.11, involves measurements of aerosol flow rate and deposit radius. The accuracy errors of ± 7 per cent and ± 20 per cent associated respectively with the individual measurements of these variables gives rise to a maximum uncertainty in the velocity of +72 to -36 per cent. If the vertical particulate velocity is resolved into its thermal and gravitational components in accordance with equation 6.19a, the uncertainty in the thermal velocity is seen to be dependent upon the relative magnitude of the gravitational velocity component (equation 6.20). The gravitational component may range from about 1 to 25 per cent of the total vertical velocity, its value being determined by the particulate radius, a, chosen as a basis for computation from the observed range of particle sizes, i.e., $0.25 < a < 0.75$ micron. The maximum deviation introduced in thermal velocity attributable to the arbitrary assignment of particle radius is on the order of +5 to -10 per cent, and the overall experimental uncertainity in its evaluation falls within the range from -46 to +78 per cent. Its magnitude must then be in the range $0.126 < V_t < 0.418$ cm/sec. The magnitude of the thermal force (equation 6.18) will vary considerably, $0.94 \times 10^{-8} < F_t < 9.17 \times 10^{-8}$ dynes, depending upon the chosen particle radius; however, the uncertainty in its evaluation is only slightly dependent upon this factor. It can be shown that the evaluation for a 0.5-micron diameter gives $F_t = 1.50 \times 10^{-8}$ dynes

with an uncertainty of +75 to -37 per cent. The evaluation for a 1.5 micron diameter gives $F_t = 5.03 \times 10^{-8}$ dynes with an uncertainty of +82 to -42 per cent. Furthermore, it can be seen that regardless of the particle size, the ratio of thermal force to particle radius, F_t/a, is given by the computed value, 6.92×10^{-4} dynes/cm, with an uncertainty of +78 to -46 per cent. The use of this ratio instead of force alone can relieve the uncertainty in particle size. Hence, it is evident that the inaccuracy in the experimental observation is not significantly increased in going from particulate velocity to thermal force.

It should be noted that the foregoing evaluation involves only those experimental measurements used in the computation of thermal force. The magnitude of this experimental force is dependent upon the operating conditions of the precipitator and has been evaluated for a given pressure, temperature gradient, and absolute temperature. The uncertainty in the measurement of these conditions results in additional inaccuracy which becomes important when a comparison of experimental and theoretical values is made. It can be shown that the individual errors in the measurement of these operating variables are such that the proper value for the experimental force may exceed the range indicated above by a factor of 1.5 or may be lower by a factor of 0.7. Thus an adequate allowance for the maximum error of experimental measurements places the indirectly observed force somewhere in the range from about 0.38 to 2.7 times the computed value.

c. Estimate of Probable Experimental Error. The range of inaccuracy given above is based upon a very generous assignment of errors, and the liklihood of an overall error of the magnitude indicated by the above limits is most improbable since it could exist only if all the individual errors extremes occurred simultaneously in such a way as to maximize or minimize the computed force. A more probable and useful evaluation of experimental uncertainty may be based on observed experimental deviations, even though the data available are inadequate for a reliable statistical analysis. The following evalution is therefore of the nature of an estimate and should be regarded as such. However, the data are sufficiently abundant so that confidence may be placed in the relative observations.

Individual series of experiments employing a single precipitator produced data of consistency such that observed deviations in the quantity $(r_d^2 - r_o^2)$ were generally within ± 5 per cent of the median value for linear dependence upon aerosol flow rate (c.f., Figure 24, noting discussion regarding the excessive deviation of the two points at the upper extreme). This deviation, indicative of the reproducibility of the experiment, includes the composite contribution of the individual precision errors associated with the measurements of temperature drop, aerosol flow rate, plate separation, pressure, and deposit radius.

There remains the question of the accuracy of the measurements, and the additional inaccuracy of systematic errors must be estimated as before. Since the precision error in the deposit radius measurement has been included above, the additional inaccuracy ascribed to the somewhat arbitrary observer's definition of deposit boundary, is probably on the order of ± 10 per cent. The additional uncertainties in the measurements of aerosol flow rate, temperature gradient, and pressure are probably less than ± 2, ± 5, and ± 2 per cent, respectively. The range in error of measurement associated with the computation of the vertical particulate velocity then drops between +33 and -25 per cent. The maximum deviation introduced in the thermal velocity attributable to the assignment of particle size remains on the order of +5 to -10 per cent, and the overall uncertainty in this velocity component ranges from +38 to -35 per cent. As before, no significant increase in error is introduced in the calculation of thermal force from thermal velocity and the uncertainty in the thermal force calculation due to the propagation of measurement error remains between +38 and -35 per cent. The inaccuracy may exceed this range due to the uncertain measurements of temperature gradient, absolute temperature, and pressure. The appropriate expansion of the above range indicates that the indirectly observed thermal force value is probably included between 0.5 to 1.8 times the computed value.

3. Final Estimate of Experimental Uncertainty

The above evaluation does not provide for the errors of method introduced through the simplifications and approximations in the derivation

of the equations which were employed. The estimation of maximum inaccuracy is greatly increased by their consideration. The above range of uncertainty must again be extended and it is concluded that the actual experimental thermal force might be different from the computed value by a factor as large as 3.5 or as small as 0.1.

Again, attention is called to the facts that generous limits of inaccuracy have been assigned and that the occurrence of the extreme error is highly improbable. The greatest uncertainty is interjected through the error of method; however, any substantial reduction in this uncertainty calls for a rigorous analysis which, at the present time, is not feasible. The foregoing treatment has been presented primarily to emphasize the fact that caution must be exercised in drawing conclusions from thermal precipitation data regarding the validity of theoretical thermal force equations.

While the method may be inaccurate to the extent indicated above, the results thereby obtained are reliable for many purposes. The errors of method, as well as the systematic experimental inaccuracies, are inherently identical for similar observations on the precipitation of various materials. The limits of precision are fairly well indicated by the scattering of data. It is evident that sound conclusions may be based on the relative effectiveness observed in the precipitation of various aerosols.

B. Errors Inherent in Direct Observation Experiments

1. Experimental Errors

Discussion of error so far has been restricted to thermal precipitation experiments. Now, turning attention to the Millikan type experiments, it becomes immediately evident that there are fewer sources of uncertainty in the direct observation of particulate behavior. The vertical particulate velocity and the gravitational velocity component are directly measurable. The thermal velocity component is computed as the difference between the two measured quantities, each of which possesses experimental uncertainty, so that the propagated error in the indirect measurement is highly dependent upon the relative magnitudes of the velocity components. No matter how precise the individual direct measurements, the error in the thermal velocity becomes very large as the gravitational component approaches

the total vertical velocity. In the extreme, such observations lose their significance, as was experienced in the futile experiments with zinc powder.

2. Scattering of Data as a Guide in Evalution of Error in Thermal Velocity

The scattering of data may be considered as the best guide in the evaluation of error. The deviations in the indirectly measured thermal velocities for a given material were sometimes very large, as was mentioned in presentation of experimental observations. They indicate maximum limits of error for any one particular observation which are comparably large. On the other hand, confidence limits may be based on the consistency of the reproducible velocity measurements for a given particle at different temperature gradients and on the consistency of force evaluations for particles of different diameters (see Table IX). A reasonable precision error associated with the average value obtained from the selected data seems to be on the order of ± 15 per cent. As in the precipitation experiments, the thermal velocity has been determined for a given pressure, temperature gradient, and absolute temperature. The uncertainty in their measurement, as well as in the determination of particle radius, introduces additional inaccuracy which must be taken into consideration for a comparison of experimental and theoretical values. Confidence limits, which allow for these inaccuracies and for the reasonable precision error, have been estimated such that the correct thermal velocity is probably not different from the indirectly observed value by more than ± 50 per cent. It should be noted that in the computation of these results, there is no error of method comparable to that introduced in the derivation of equations for the analysis of thermal precipitation.

3. Confidence Limits for Thermal Force Evaluations

The subsequent evaluation of the experimental thermal force requires an estimate of the mobility of the particle and, hence, a knowledge of its size. The diameter of the particle may be deduced from its observed gravitational settling velocity, assuming that the particle is a sphere and that its density is known. The particle size determination is therefore subject to considerable error. An underestimation of particle

size (which is likely when the theoretical density values are used) is reflected in the evaluation of the experimental thermal force. This error may be reduced to the magnitude of the error associated with the slip correction (usually less than ± 10 per cent) by dividing the experimental force by the particle radius. In the comparison of theoretical and experimental values for either thermal velocity or force, cancellation of the error due to particle size discrepancies occurs and the above stated confidence limits remain essentially unchanged.

XI. DISCUSSION OF RESULTS

A. Review of Experimental Observations

From the presentation of experimental observations it is apparent that the results are not always in close agreement with values which are computed by Epstein's force equation. In fact, there is evidence of internal inconsistency within these observations, which seems paradoxical in view of the reproducibility generally obtained. In reviewing experimental results, the following observations are noteworthy: (1) Materials such as oxides (presumably of low thermal conductivity) were easily precipitated. (2) Metallic aerosols produced by the dispersion (atomization) of powders were not completely precipitated, which indicates low thermal forces in accordance with theory. (3) The deposits of atomized metallic aerosols were characterized by dense central regions that suggest exceptionally great forces on much of the suspended particulate material. (4) Particulate matter was always precipitated completely from aerosols generated by the exploding wire technique. (5) The experimental forces calculated from the precipitation of these aerosols always appeared very great and seemed to be independent of bulk thermal conductivity. (6) Detailed examination of precipitated deposits and of individual particles indicated extensive agglomeration where effective precipitation of materials of high bulk thermal conductivity occurred. (7) Direct observations of particulate behavior (modified Millikan experiment) were generally in agreement with theory provided an effective particulate thermal conductivity was assumed close to the values reported for the bulk powder.

While experimental error may account for the slightly high thermal force observed in the precipitation of nonmetallic particles, it cannot explain the efficient precipitation sometimes observed with metallic aerosols. It has been suggested that the inconsistent observations might be correlated with currently accepted theory by using an effective particulate thermal conductivity lower than that of the bulk material. The observed agglomeration of primary particles provides the basis for such an explanation. Before pursuing this interpretation further, the matter of particulate thermal conductivity and its role in thermal force needs to be considered.

B. Significance of Thermal Conductivity in Theory

The essential element in the derivation of Epstein's equation is the consideration of internal heat transfer. A proper thermal force evaluation therefore, demands an accurate value for the particulate conductivity. Otherwise, the magnitude of the computed theoretical force is not of quantitative validity and cannot properly be referred to as Epstein's theoretical value. If the particle is a solid mass or a liquid droplet, its thermal conductivity may reasonably be assumed equivalent to that of the bulk material. On the other hand, if the particulate is a porous solid or an agglomerated mass of primary particles, the rate of internal heat transfer may be markedly decreased. The same thermal force equation seems still applicable as long as an effective thermal conductivity is used. Of course, the shape of an agglomerated particulate is probably not spherical and the thermal slip stream is undoubtedly disrupted by the discontinuity of its surface. In this case, however, the equation probably holds as well as for a rough irregular primary particle (one with a shape other than spherical). Some disagreement between experimental and theoretical results should be anticipated, therefore, because of the deviation of the real particles from the mathematical model. But, the major problem in the correlation of results lies in an accurate determination of the effective thermal conductivity. Heretofore, the thermal conductivity of the solid, the fused brick, or the pressed powder has been used arbitrarily in theoretical thermal force evaluations.

C. Effective Thermal Conductivity of Solids Possessing Void Space

The thermal conductivity of a solid possessing voids is actually less than that of the homogeneous solid. This effect has been subjected to investigation in its application to porous polycrystalline materials[12] and to powders.[7,8,33] Simple correlations based on the porosity of the material, the conductivity of the solid, and the conductivity of the gas have been successfully applied to packed beds and porous solids, but have not been developed to the extent that predictions are certain, particularly for the large void fractions which may be encountered with very fine particles. Hence, the existing correlations are not strictly applicable to

agglomerates, but their use in the interpretation of thermal force phenomena is interesting and informative.

1. Porous Solids

The effect of void space upon the thermal conductivity of a solid depends upon whether the solid is a porous mass or an agglomerate of individual primary particles. In the former case, the conductivity of the solid is reduced by the decrease in cross-sectional area due to porosity. At low temperatures, thermal transport across the pore volume by radiation is negligible. It has been theorized that under this condition the effective thermal conductivity is a linear function of the void fraction, and usually is not very much different from that of the solid of theoretical density.

2. Powders

A bed of powder, and likewise an agglomerated particle, is characterized by small regions or points of contact between the solid particles of the powder. Most of the conduction of heat takes place in the vicinity of the contacts. Hence, the effective thermal conductivity is dependent upon the size, shape, and arrangement of particles. In general, the solid contact area is very small and the effective conductivity is strongly dependent upon that of the gas. Furthermore, the thermal conductivity of the gas phase is reduced when the effective gas spaces have dimensions of the same order as the mean free path of the gas molecules. Since most of the conduction, even in the gas phase, occurs near points of contact, this reduction becomes significant when the particle diameter is many times the length of the mean free path. Deissler and Eian[8] have determined a critical Knudsen number on the order of 0.00072 defining the "breakaway pressure" for a powder of rather large particles of magnesium oxide. Below this point the effective thermal conductivity decreases rapidly with pressure. Schotte[33] has developed a correlation for predicting the thermal conductivity of packed beds for various conditions of pressure, temperature, and particle size which indicates that the effective conductivity of a powder may approach that of the gas. Schotte stresses the fact that the given correlation has

definite limits of tested applicability which exclude large void fractions and ratios of solid-to-gas thermal conductivities greater than 6,000. It is probable, however, that agglomerates such as those observed in thermal precipitation could have effective thermal conductivities much lower than that of the bulk solid. Also, it is clearly conceivable that their effective conductivities might approach that of the gas. If this is the case, the thermal force exerted upon agglomerated particulates might be expected to approach the limiting value given by Epstein's equation under the condition that the particulate conductivity is equal to the gas phase conductivity.

As was mentioned above, the effective thermal conductivity may be dependent upon the shape and arrangement of the primary particles. It will also be sensitive to the manner of particle contact and to surface irregularities, particularly for solids of high thermal conductivity. These factors have not been accounted for in the referenced correlations. Therefore, the evaluation of the effective particulate conductivity would be uncertain, even if the range of applicability for the correlations were extended to include fine particle agglomerates.

D. Estimates of Effective Particulate Thermal Conductivity

1. Evidence of Agglomeration

With the foregoing discussion in mind, some evaluations of effective particulate thermal conductivity have been attempted for the purpose of drawing qualitative conclusions regarding the experimental observations. In making an evaluation, it is necessary to decide whether the particulate of concern is porous, nonporous, or agglomerated. This decision may be based on either or both of two sources of information, viz., electron micrographs and a knowledge of the apparent density of the particle. The electron micrographs of Section IX indicate complex agglomeration with large void fractions for all aerosolized materials produced by the exploding wire technique. Where unagglomerated primary particles were observed, their diameters were in the range from 0.005 to 0.1 micron. Electron micrographs of deposited particulates generated by other techniques indicated both agglomerates and individual

primary particles in the diameter range near one micron. As for the knowledge of apparent density, Fuks[13] quotes values for certain smokes including two materials of particular interest. He reports the apparent density of magnesium oxide particles produced by burning metallic magnesium in a range from 0.24 to 3.48 against the actual value of 3.6, and that of silver particles produced by condensation from electric arc vaporization in a range from 0.64 to 4.22 compared with the actual value of 10.5. These values, as well as the data for other aerosol particles cited by Fuks, indicate that a relatively high degree of agglomeration with a wide range of void fractions may generally be anticipated.

2. Evaluation Based on Correlations for Powders

The evaluations of effective thermal conductivity have been based on the correlations of Deissler and Eian[8] and of Schotte.[33] It has been pointed out that due to the large void fractions associated with agglomeration, the correlation cannot properly be applied to fine dusts. However, the nature of the correlation indicates that increasing the void fraction merely decreases the effective conductivity. By assuming any void fraction greater than 0.6 and any solid conductivity up to that of silver, it has been estimated that the effective conductivity of an agglomerate from an aerosol produced by the exploding wire technique must be equal to or less than that of the gas. Similar evaluations for void fractions in the range from 0.2 to 0.6 and primary particle diameters between 0.1 and 1.0 micron indicate effective conductivities in the range from 1 to 20 times that of the gas, depending upon the ratio of solid-to-gas thermal conductivity. The higher value corresponds to a metallic powder of low void fraction. These evaluations lead to the conclusion that even a slight degree of agglomeration will result in a marked lowering of effective particulate conductivity. However, it is essentially impossible to make an evaluation for the simple agglomerate composed of few primary particles or for the chain type of coagulation since the analogy to a powder obviously breaks down and the nature of interfacial contact becomes most important.

3. Experimental Observations Supporting Evaluation

The above estimates of effective conductivity of fine powders are substantiated by the results of Smoluchowski's experimental study. These results, according to Jakob,[16] show that the thermal conductivity of a number of granular powders (including quartz, zinc, soot, and diatomacious earth) becomes smaller than that of air at low pressures, and that decreasing the particle size permits this substantial lowering of conductivity to occur at much higher pressures. For example, a zinc dust consisting of 0.028 mm grains was found to have the conductivity of air at a pressure slightly below 10 mm Hg. The same conductivity was observed for a powder consisting of 0.0062 mm grains at a pressure slightly below 50 mm Hg. Soot was observed to have an effective conductivity near that of air at atmospheric pressure. Thermal conductivities 3 to 10 times smaller than that of air have been obtained, even with metallic powders, at a pressure of 1.0 mm Hg. Also, a very fine silica aerogel (94 per cent air) apparently has a conductivity smaller than that of air at atmospheric pressure. Furthermore, the effective conductivities of all powders approached the same value at sufficiently low pressures.

E. Interpretation of Circumferential Band Observed in Thermal Precipitation Deposits

It seems likely that a given aerosol possesses a wide range of effective thermal conductivities between that of the gas (for complex agglomeration) and that of the primary particles. It is possible that the decrease in precipitated deposit density at the boundary (the hazy band) merely reflects the corresponding range of effective particulate conductivities and is not indicative of fluctuating operating conditions. Since the thermal conductivites of most complex agglomerates might be very much lower than that of the primary particle, they probably would determine the boundary of the dense central core of a deposit. Assuming that most of the particulate material is present in the aerosol in the form of complex agglomerates, the following results would be anticipated. If the unagglomerated primary particles are very small, as in the case of exploded aerosolized matter, they would not be observed

beyond the periphery of the deposit, which would be sharply defined. If the primary particles have a high thermal conductivity, they would pass through the precipitator and might be exhausted from the system without precipitation. If the primary particles have a low thermal conductivity, they would be precipitated at some finite distance beyond the central core boundary to give a definite band width representing the extremes of particulate conductivity. If the unagglomerated primary particles possess a high thermal conductivity and represent a large fraction of airborne material, the central core comprised of deposited agglomerates would be visible; however, the remainder of the collecting disk would be covered with particles due to gravitational settling or to relatively weak thermal forces. These hypothetical results very nearly fit the experimental observations.

A simple check on this concept was made by computing the experimental velocities and forces associated with the maximum and minimum (light and dense) deposit radii for a typical aluminum oxide deposit. It was found that the range of thermal force values defined by these extremes almost bridged the gap between the modified Millikan cell results and the maximum theoretical thermal force based on equal gas and particulate thermal conductivities. This range, and other average results of this investigation, can be compared most readily by discussing them in terms of a reduced thermal force defined by dividing the thermal force by both the particle radius and the temperature gradient. The results of this investigation, along with theoretical values, are tabulated in Table XI.

F. Correlation of Experimental Results with Theory

A correlation of experimental results with theoretical values has been graphically illustrated in Figure 39. In this illustration the reduced thermal force based on Epstein's equation has been plotted against thermal conductivity. Theoretical points representing the forces on certain materials have been indicated in their appropriate positions on the curve. The ranges of experimentally observed forces, not including estimated errors, have been indicated on a graph to the left of the theoretical curve. It is evident that results can be satisfactorily

TABLE XI

TABULATED SUMMARY OF THERMAL FORCE VALUES

Source of Data	Particulate Material	Aerosolization Technique	Thermal Conductivity of Solid $\times 10^3$ (Cal/Cm Sec $^\circ$K)	Reduced Thermal Force $\times 10^7$ (Dynes/$^\circ$C)
Epstein's theory	Hypothetical particle	--	0.0533 ($k_p = k_g$)	8.95
Epstein's theory	MgO powder	--	1.46	0.913
Epstein's theory	MgO pressed brick	--	2.71	0.509
Epstein's theory	MgO solid	--	90	0.016
Epstein's theory	Al_2O_3 powder	--	1.63	0.823
Epstein's theory	Al_2O_3 fused brick	--	8	0.176
Epstein's theory	Al_2O_3 solid	--	80	0.018
Epstein's theory	Gas Carbon	--	8.26	0.171
Epstein's theory	Aluminum	--	504	0.00286
Epstein's theory	Iron	--	130	0.0011
Epstein's theory	Zinc	--	265	0.00540
Epstein's theory	Pt	--	167	0.00865
Epstein's theory	Silver	--	963	0.00149
Direct observation of particle	MgO	Mg burned in air	--	0.34 - 0.54
Direct observation of particle	Al_2O_3	Dispersed powder	--	0.73 - 0.79
Direct observation of particle	Gas Carbon	Dispersed powder	--	0.03 - 0.12

(Continued)

TABLE XI (Continued)

TABULATED SUMMARY OF THERMAL FORCE VALUES

Source of Data	Particulate Material	Aerosolization Technique	Thermal Conductivity of Solid x 10^3 (Cal/Cm Sec ^oK)	Reduced Thermal Force x 10^7
Thermal Precipitation:				
Linear III	Al_2O_3	Dispersed powder	--	7.0 (avg.)
Radial II	MgO	Mg burned in air	--	4.8 (avg.)
Radial I	MgO	Mg burned in air	--	4.6 (avg.)
Radial I	Al_2O_3	Dispersed powder	--	7.0 (max.)
Radial I	Al_2O_3	Dispersed powder	--	4.0 (avg.)
Radial I	Al_2O_3	Dispersed powder	--	1.5 (min.)
Radial I	Carbon	Dispersed powder	--	6.5 (max.)
Radial I	Carbon	Dispersed powder	--	<0.0065 (min.)
Radial I	Zinc, Iron & Aluminum	Dispersed powder	--	4.2 (max.) <0.0065 (min.)
Radial I	All Solids	Exploded	--	8.88 (max.) 5.5 (min.)

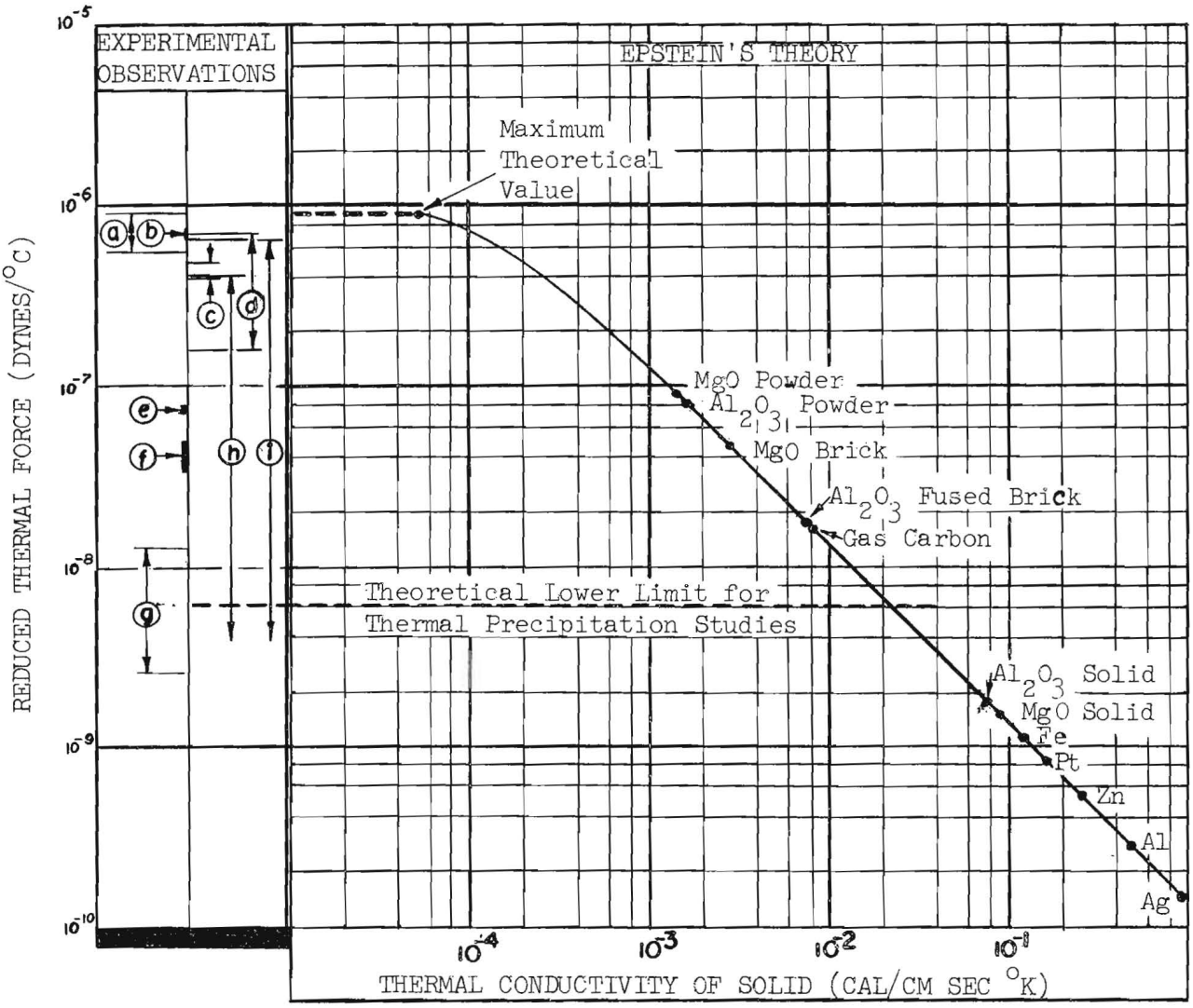

RANGES OF EXPERIMENTAL OBSERVATIONS:

(a) Precipitation of exploded materials.
(b) Average value for precipitation of Al_2O_3 with Linear Precipitator III
(c) Precipitation of Al_2O_3 and MgO with Precipitators I and II.
(d) Based on circumferential band width observed in the precipitation of Al_2O_3.
(e) Direct particulate observations, Al_2O_3.
(f) Direct particulate observations, MgO.
(g) Direct particulate observations, gas carbon.
(h) Precipitation of atomized metals.
(i) Precipitation of atomized carbon.

Figure 39. Correlation of Experimental and Theoretical Thermal Force Values. The points which have been labeled on the curve are theoretical values for specific materials. Experimental values are indicated by alphabetical symbols.

correlated with the hypothesis outlined above. Most discrepancies are understandable in terms of experimental errors. A review of experimental observations in the light of this theory shows qualitative coherence.

1. The range of forces observed with the precipitation of particulate materials produced by the exploding wire technique extends from the maximum theoretical value of 8.8×10^{-7} dynes/°C down to the level of 5.5×10^{-7} dynes/°C. This observation is consistent with the concept of a complex of very fine particles and large void fraction possessing a thermal conductivity close to that of the gas in which it is suspended. The fact that precipitation appeared to be complete is attributed to the very large thermal velocities predicted by Waldmann's high Knudsen number mechanism which would effectively precipitate the very fine primary particles. The fact that the deposit is sharply defined indicates that essentially all agglomerates have the same effective thermal conductivity.

2. The average experimental values for the precipitation of the oxides of aluminum and magnesium (aerosolized by powder dispersion and burning) lie between 4.0 and 4.8×10^{-7} dynes/°C, just below the range for exploded materials. It is supposed that the forces are representative of a median thermal conductivity in the range defined by the deposit radii corresponding to the extremes of the circumferential band. This range, for a typical deposit, overlaps that of the exploded materials and its upper limit falls only 30 per cent below the theoretical maximum at 7×10^{-7} dynes/°C. Its lower limit (not sharply defined) extends to 1.5×10^{-7} dynes/°C.

3. The central core deposit radii, comparable for most materials, give an average force value on the order of 4×10^{-7} dynes, even for aerosols of dispersed metallic powders. The observations again indicate a range of forces with an upper limit corresponding to that for the oxides. This supports the estimations of a high effective conductivity for more complex agglomerates independent of the bulk value. A notable exception in this case was the precipitation of atomized gas carbon, where the central core area indicated a reduced force value of 6.5×10^{-7}, which is very close to the maximum.

4. The metallic aerosols (including gas carbon and sodium chloride) produced by the dispersion of powder were not completely precipitated. Thus the lower extremity of the reduced thermal force range lies below 6×10^{-9} dynes/°C, which is the minimum detectable with the precipitator used in the investigation. It appears that the effective particulate conductivity was above 2×10^{-2} cal/cm sec °K, which is consistent with bulk conductivities. It is therefore surmised that primary particles or very simple agglomerates constitute a substantial portion of the aerosolized material.

5. The average reduced force values obtained from Millikan type observations with magnesium and aluminum oxide are respectively 4.8×10^{-8} and 7.5×10^{-8} dynes/°C. Herein some inconsistency arises with the question of appropriate thermal conductivity for the primary particles. It has been observed that these values correspond very closely to the theoretical values obtained by using the thermal conductivities reported for the pressed brick and for the powder. It has also been observed that this force magnitude, in the case of aluminum oxide, is only 50 per cent below the value corresponding to the maximum deposit radius in the thermal precipitation experiment. Thus the two experimental observations are in agreement (certainly within the range of experimental errors) if the particles observed in the modified Millikan cell correspond to the precipitated particulates of greatest thermal conductivity. This situation is probable since larger, more complex agglomerates would be expected to fall out before reaching the central cell of the Millikan apparatus and smaller particles are more likely to be ensnared in the electrostatic field. Why then would the effective particulate thermal conductivity not be that of the nonporous polycrystaline oxide reported by Kingerly, et.al.,[17] i.e., on the order of 0.06 to 0.08 cal/cm sec °K? It seems that this would be the proper value for magnesium oxide, in view of the maximum apparent density reported by Fuks[13] and the cubic form of the primary particles seen in the electron micrographs. If the effective particulate conductivities for the oxides were as great as these values, both types of experiments might be expected on a theoretical basis, to respond with indications of lesser forces. It may then be

assumed that the nature of the particles was basically different from the nonporous polycrystalline solid; that is, the particles were highly porous or consisted of very simple agglomerates. If the latter assumption is accepted, an effective thermal conductivity in the range indicated is not unreasonable. That such might be the case is suggested by the estimated diameters of the particles observed directly. For both materials, particulate diameters as large as 2 to 3 microns have been reported. Since underestimation of particle diameters is likely, and no primary particles as large as two microns were seen in the electron micrographs; the observations were probably made for simple agglomerates. Furthermore, the cubic structure of the primary particles of magnesium oxide would result in more effective interparticle contact than would be expected for the irregular primary particles of alpha-alumina. Since both materials possess comparable bulk conductivities it is not surprising that Millikan type observations indicated a greater force (and hence a lower effective particulate conductivity) for the aluminum oxide. Still, the uncertainty introduced by the apparent inconsistency remains. If primary particles of metallic aerosols are not completely precipitated, it seems reasonable that primary particles of the oxides also would be precipitated ineffectively

6. The Millikan type observations with gas carbon indicate reduced forces on the order of 1.0×10^{-8} dynes/^{o}C; this value is slightly lower than the theoretical value based on the bulk conductivity of the powder. Again, the concept of a simple agglomerate with an effective conductivity much lower than that of polycrystalline solid is suggested. As before, a quantitative evaluation is out of the question.

7. Finally, a specific example is cited. The composite aerosol of primary salt particles, including diameters in a range from a few hundredths to several microns produced a deposit which showed complete deposition of the fine agglomerated material but ineffective precipitation of the large unagglomerated material. This deposit indicated the force range extending from the maximum value to less than 6.5×10^{-9} dynes/C^{o}. Thus there is strong support for the hypothesis, but its quantitative testing is inadequate.

G. Interpretation of Earlier Observations

With the hypothesized concept it is also possible to explain some of the apparent anomalies in thermal force phenomena which have been reported prior to this investigation. For example, the thermal precipitation of most materials can be accomplished, regardless of thermal conductivity of the solid, because of the low effective particulate conductivity ascribed to agglomeration. It is probable that most of the visible particulates in a smoke or dust are complex agglomerates. Since a very large fraction of the airborne matter would be collected it is understandable that precipitation would have been considered totally effective. Also, the dust-free space observed around a heated element would be essentially of constant width (this width being characteristic of the limiting force value). In cases where thermal precipitation of materials of high solid conductivity has been observed, it has been reported that deposits of all materials have been of essentially the same width. It should be noted that in some cases with solids of very high conductivity Epstein's equation has been qualitatively correct. While the Schotte correlation may not be quantitatively accurate, it does indicate that the effective conductivity is dependent upon the solid conductivity, particularly when its value is large.

H. Applicability of Experimental Observations as Test of Theory

There is one other point which should be emphasized in the discussion of results. It may be recalled from the theoretical discussion that the force mechanism is dependent upon the Knudsen number. In going from the concept of molecular theory (where the distribution function is not influenced by intermolecular collisions in the vicinity of the particle) to the hydrodynamic-thermal creep analysis (where the fluid is regarded as a continuum) a situation is encountered where neither theory is adequate. In this situation of Knudsen number near unity, the thermal slip streams develop progressively as the population density of the molecules increases in the vicinity of the particle. It is in this realm that the particulate thermal conductivity begins to exert its influence. There is some uncertainty as to the inception of this influence and to the Knudsen number at which it is fully developed. From the observations of Schmitt,[32]

discussed in Section IV, Experimental Observations of Other Investigators, the effect of thermal conductivity does not seem to be fully established even at a Knudsen number as low as 0.15. Most of the experimental observations of thermal forces, particularly those for materials of relatively high thermal conductivity, have been made for systems characterized by Knudsen numbers near this value or greater. Hence, there exists a possibility that the observations are characterisitic of a transition region in which Epstein's equation might not be expected to apply quantitatively. If this is the case, experimental forces would be expected to be greater than predicted and less dependent upon thermal conductivity. The existence of this possibility is a major weakness of most thermal force investigations. It is not possible to say at this point whether the above mentioned factor is reflected in the reported observations.

XII. CONCLUSIONS AND RECOMMENDATIONS

In view of the discussion of results, it is inevitable that conclusions drawn from this investigation are qualitative. They may be summarized as follows:

1. The thermal precipitation of solid particulate material when agglomerated will be accomplished with an effectiveness generally much greater than would be predicted by theoretical estimates based upon the thermal conductivity of the massive solid.

2. Experimental thermal forces in a system characterized by low Knudsen numbers may be correlated with Epstein's equation by using an effective thermal conductivity for the particulates.

3. The thermal precipitation of solid particulate material is most effective if the aerosol consists of very fine primary particles or of large primary particles of low solid thermal conductivity.

4. Complex agglomerates of primary particles of high solid conductivity may be subjected to a thermal force characteristic of a low effective particulate conductivity.

5. Large unagglomerated primary particles of high thermal conductivity will be subject to relatively low thermal forces and their precipitation is ineffective.

6. The effective thermal conductivity of a complex agglomerate will approach that of the gas in which it is suspended, regardless of the solid conductivity, and the thermal force acting upon it will approach a maximum value defined by Epstein's equation.

7. In accordance with Epstein's equation the thermal force is directly proportional to the temperature gradient and the particle diameter. The pressure dependence of thermal force was found in qualitative agreement with Epstein's theory, but the data collected were not sufficient for a quantitative conclusion regarding this effect.

The correlation of experimental results and theory has been accomplished with a concept of effective particulate conductivity. This interpretation is hypothetical and, while it is based upon stong experimental evidence, additional investigation is needed for quantitative

confirmation. The techniques which have been employed in this investigation are adaptable for experimental testing of the hypothesis, but they are subject to the limitations discussed previously. Also, the study of solid particulate aerosols is further complicated by the tendency toward agglomeration. With a significant degree of agglomeration the uncertainty in effective particulate conductivity remains a serious obstacle. An exact knowledge of particulate thermal conductivity is essential for quantitative testing of theory. In this respect, an aerosol of dispersed liquid droplets seems ideal. Unfortunately, the use of liquids has major drawbacks. Specifically, most liquids fall into a narrow range of relatively low thermal conductivity. A comprehensive experimental study must include aerosolized materials of high thermal conductivity since Epstein's theory is significantly different from others only under this condition. Mercury would fulfill this requirement. However, particularly with mercury, a disadvantage becomes significant. Except with special aerosolization techniques, mercury droplets may be coated with an oxide film which prevents their fusion into a single sphere upon contact and results in the formation of agglomerated units similar to those of solid particles. The apparent density of the particulates of mercury is sometimes only one tenth the theoretical density.[13] It is obvious that a satisfactory experimental investigation will require a most careful selection of particulate materials and aerosolization techniques and a precise knowledge of the nature of the particulates produced.

Section X, Analysis of Errors, of this report included a discussion of the errors associated with thermal precipitation studies. The confidence limits for precipitation data must be narrowed considerably for accurate thermal force evaluations to be obtained. Hence, it is generally recommended that emphasis in future studies be placed on direct observations of particulate behavior.

Finally, it seems that more valid testing of Epstein's theory should be made under conditions of very low Knudsen number. This condition would be achieved by increasing particle size or by decreasing the free path length of the gas molecules. Increasing the particle size would lead to larger gravitational components and inaccuracies in thermal component

measurement. Hence, pressure variation is the preferable approach. A comprehensive study that includes a pressure range adequate for testing theories of both high and low Knudsen number mechanisms is recommended. For this study, a reasonable upper limit might be around ten atmospheres pressure for particle diameters on the order of one micron.

Respectfully submitted:

Clyde Orr, Jr.
Project Director

Wyatt C. Whitley, Chief
Chemical Sciences Division

Robert E. Stiemke, Director
Engineering Experiment Station

XIII. BIBLIOGRAPHY

1. S. P. Bakanov and B. V. Deryagin, "Theory of Thermal Precipitation of Highly Disperse Aerosol Systems," Colloid Journal (Kolloidny Zhurnal 21, No. 4, 365-372 (1959).

2. R. B. Byrd, W. E. Stewart, and E. N. Lightfoot, Transport Phenomena, 1st. Ed., John Wiley and Sons, Inc., New York (1960) p. 47.

3. W. Cawood, "The Movement of Dust or Smoke Particles in a Temperature Gradient," Transactions of the Faraday Society 32, 1068-1073 (1936).

4. S. Chapman and T. G. Cowling, Mathematical Theory of Non-Uniform Gases, Cambridge Press, Cambridge (1939).

5. E. Cunningham, "On the Velocity of Steady Fall of Spherical Particles Through Fluid Medium," Proceedings of the Royal Society 83A, 357-365 (1910).

6. C. N. Davies, "Definitive Equations for the Fluid Resistence of Spheres," Proceedings of the Physical Society 57, 259-270 (1945).

7. R. G. Deissler and J. S. Boegli, "An Investigation of Effective Thermal Conductivities of Powders in Various Gases," Transactions of the American Society of Mechanical Engineers 80, 1417-23 (1958).

8. R. G. Deissler and C. S. Eian, "Investigation of Effective Thermal Conductivities of Powders," National Advisory Committee on Aeronautics, RM E52C05 (1952).

9. E. R. G. Eckert and R. M. Drake, Jr., Heat and Mass Transfer, 2nd Ed., McGraw Hill Book Company, Inc., New York (1959) p. 129.

10. A. Einstein, "Zur Theorie der Radiometer-krafte," Zeitschrift für Physik 54, 1-6 (1924).

11. P. S. Epstein, "Zur Theorie der Radiometers," Zeitschrift für Physik 54, 537-563 (1929).

12. J. Francl and W. D. Kingery, "Thermal Conductivity: IX, Experimental Investigation of Effect of Porosity on Thermal Conductivity," Journal of the American Ceramic Society 37, No. 2, 99-107 (1954).

13. N. A. Fuks (Academy of Sciences of the U.S.S.R. Institute of Scientific Information), The Mechanics of Aerosols, CWS Special Publication 4-12, U. S. Army Chemical Warfare Laboratories, Army Chemical Center, Maryland (1955) pp. 31, 34, 82-92.

14. G. Hettner, "Zur Theorie des Radiometers: Thermal Repulsion as a Radiometer Phenomenon," Zeitschrift für Physik 27, 12-22 (1924).

15. G. Hettner, "Zur Theorie der Photophorese," Zeitschrift für Physik 37, 179-192 (1926).

16. M. Jakob, Heat Transfer, Vol. I, John Wiley and Sons, Inc., New York (1949) pp. 90-1.

17. W. D. Kingery, J. Francl, R. L. Coble, and T. Vasilos, "Thermal Conductivity: X, Data for Several Pure Oxide Materials Corrected to Zero Porosity," Journal of the American Ceramic Society 37, No. 2, 107-110 (1954).

18. M. Knudsen, "Eine Revision der Gleichgewitchtsbedingung der Gase Thermische Molekulartromung," Annalen der Physik 31, 205-229 (1910).

19. M. Knudsen and S. Weber, "Luftwiderstand gegen die langsame Bewegung kleiner Kugeln," Annalen der Physik 36, 981-994 (1911).

20. J. Mattauch, "Eine experimentelle Ermittlung des Widerstandsgesetzes kleiner Kugeln in Gasen," Zeitschrift für Physik 32, 439-472 (1925).

21. J. C. Maxwell, "On Stresses in Rarified Gases Arising from Inequalities of Temperature," Philosophical Transactions of the Royal Society (London) 170, 231-256 (1879).

22. J. H. McGinn, "Observations on the Radial Flow of Water Between Parallel Plates," Applied Scientific Research 5A, 255-264 (1956).

23. R. A. Millikan, "Coefficients of Slip in Gases and the Law of Reflection of Molecules from the Surfaces of Solids and Liquids," Physical Reviews 21, 217-238 (1923).

24. R. A. Millikan, Electron (+ and -), University of Chicago Press, Chicago (1935) p. 95.

25. Lord Rayleigh, "On the Dark Plane Which is Formed Over A Heated Wire in Dusty Air," Proceedings of the Royal Society (London) 34, 414-418 (1882).

26. O. Reynolds, "On Forces Caused by the Communication of Heat Between a Surface and a Gas," Philosophical Transactions of the Royal Society (London) 166, 725-735 (1876).

27. P. Rosenblatt and V. K. LaMer, "Motion of a Particle in a Temperature Gradient; Thermal Repulsion as a Radiometer Phenomenon," Physical Review 70, 385-395 (1946).

28. A. Rubinowicz, "Radiometerkräfte and Ehrenhaftsche Photophorese," Annalen Der Physik 62, 695-737 (1920).

29. R. L. Saxton and W. E. Ranz," Thermal Force on an Aerosol Particle in a Temperature Gradient," Journal of Applied Physics 23, 917-922 (1952).

30. C. F. Schadt and R. D. Cadle, "Thermal Forces on Aerosol Particles in a Thermal Precipitator," Journal of Colloid Science 12, No. 4, 356-362 (1957).

31. H. Schlicting, Boundary Layer Theory, 4th Ed., McGraw - Hill Book Company, Inc., New York (1960).

32. K. Schmitt, "Untersuchungen an Schwebstoffteilchen im Temperatufeld," Zeitschrift fur Naturforschung 14A, 870-881 (1959).

33. W. Schotte, "Thermal Conductivity of Packed Beds," Journal of the American Institute of Chemical Engineers 6, No. 1, 63-67 (1960).

34. J. Tyndall, "On Dust and Diseases," Proceedings of the Royal Institution of Great Britain 6, 3 (1870).

35. L. Waldmann, "Uber die Kraft eines inhomogenen Gases and Kleine suspendierte Kugeln," Zeitschrift für Naturforschung 14A, 870-881 (1959).

36. H. H. Watson, "The Dust-free Space Surrounding Hot Bodies," Transactions of the Faraday Society 32, 1073-1081 (1936).

37. W. Zernik, "The Dust-free Space Surrounding Hot Bodies," British Journal of Applied Physics 8, 117-120 (1957).